2012

ACID-BASE CATALYSIS IN PROTON-COUPLED ELECTRON TRANSFER REACTIONS (PCET): THE EFFECTS OF BRÖNSTED BASES ON THE OXIDATION OF GLUTATHIONE AND HYDROQUINONE

Ramos Jonnathan Medina
Virginia Commonwealth University

Acid-Base Catalysis in Proton-Coupled Electron Transfer Reactions (PCET): the Effects of Brönsted Bases on the Oxidation of Glutathione and Hydroquinone

A thesis submitted in partial fulfillment of the requirements for the degree of Doctor of Philosophy in the Department of Chemistry at Virginia Commonwealth University.

By
Jonnathan Medina-Ramos
B.S. Universidad del Valle-Colombia 2006
PhD. Virginia Commonwealth University-USA-2012

Director: Julio C. Alvarez, PhD
Department of Chemistry

Virginia Commonwealth University
Richmond, Virginia
December, 2012

Acknowledgements

I want to thank the Department of Chemistry at Virginia Commonwealth University for giving me the opportunity to come here and work on my post-graduate education. This has been an invaluable experience and I am thankful with all the staff, faculty and fellow students that have made this possible. Also, I want to thank my advisor Dr. Julio Alvarez for believing in me and letting me be part of his research group. Every project we have worked on has been a challenge and I keep learning every day as they evolve.

To the members of my graduation committee thanks a lot for allowing me to continue on the Ph.D. track two years ago and I hope the work I am presenting to you is worth the trust you put in me.

To my colleagues Dr. Olufemi Oyesanya, Dr. Fernando Luna, Trang Nguyen MSc., Dr. Marwa Elazazy, Dr. Timothy Alligrant, Kenji Nokura, Daniel Gerard and Dr. Michael Dcona, thank you all for your friendship and support.

To the students that worked with me on the projects that lead to this thesis; Mary Olagunju, Amy Clingenpeel, Jendai Robinson, Emnet Ashenafi, Andrew Walsh and Vitaly Kisurin, thanks a lot.

To my family and friends back in Colombia; to my mom Marlen, my sister Diana and my dad Yesid for taking care of me unconditionally.

Finally, I want to thank the NSF and the Jeffress Memorial Trust for funding this research and the James V. Quagliano Fellowship in Chemistry for honoring me with their award in 2011.

Table of Contents

List of Tables

List of Figures

Chapter 1:

Chapter 2:

Chapter 3:

Chapter 4:

List of Schemes

Chapter 1:

List of Symbols and Abbreviations

GSH	Reduced glutathione
GS^-	Glutathione in the thiolate form
$GS^\bullet$	Glutathione radical
$GSH^{\bullet+}$	Glutathione radical cation
GSSG	Glutathione disulfide
^1H NMR	Proton Nuclear Magnetic Resonance
A	Ampere
mA	Mili-ampere
μA	Micro-ampere
AC	Acetate
4-APA	4-aminophthalic acid
ΔG	Free energy
Ag/ AgCl	Silver/ Silver Chloride reference electrode
B	Base form of buffer
BH^+	Acid form of buffer
BZ	Benzoate
CEPT	Concerted proton coupled electron transfer
CV	Cyclic voltammetry
CVs	Cyclic voltammograms
D	Diffusion coefficient
DEA	Diethylaniline
DI	Deionized water
D_2O	Deuterium oxide
DNA	Deoxyribonucleic acid
E	Electrode potential
e^-	Electron
eV	Electron-volts
$E_{1/2}$	Midpoint potential

ET	Electron transfer
EPT	Electron Proton Transfer
ETPT	Stepwise electron transfer followed by proton transfer
F	Faraday Constant
Fe	Iron
Fc/Fc^{+}	Ferrocene/ Ferrocenium
$Fe(CN)_6^{4-/3-}$	Hexacyanoferrate
$Fe(bpy)_3^{3+/2+}$	Tris-(2,2'-bipyridine)iron (III)/(II)
$Fe(phen)_3^{3+/2+}$	Tris-(1,10-orthophenanthroline)iron (III)/(II)
GC	Glassy carbon
GCE	Glassy carbon electrode
H^{+}	Proton
$H_2PO_4^{-}$	Monobasic hydrogen phosphate
H_3O^{+}	Hydronium ion
HCl	Hydrochloric acid
His	Histidine
HPO_4^{2-}	Dibasic hydrogen phosphate
H_2Q or 1,4-H_2Q	Hydroquinone
H_2P	Phthalic acid
HP^{-}	Hydrogen phthalate
I	Electrode current
Ir	Iridium
$[IrCl_6]^{3-/2-}$	Hexachloroiridate (III)/(IV)
k_{ET}	Electron transfer rate constant
k_f	Forward rate constant
k_b	Reverse rate constant
k_{obs}	Observed rate constant
k_s	Heterogeneous electron transfer rate constant
K	Equilibrium constant
KCl	Potassium chloride
λ	Reorganizational energy

M	Molarity; Molar
MeCN	Acetonitrile
mM	Milimolar
MESNA	2-mercaptoethanesulfonic acid
Mo	Molybdenum
$Mo(CN)_8^{4-/3-}$	Octacyanomolibdate (IV)/(V)
mPa•s	Milipascals times seconds
NaCl	Sodium chloride
NaOD	Sodium Deuteroxide
NaOH	Sodium Hydroxide
NP	Nitrophenyl
OH^-	Hydroxide ion
Os	Osmium
$Os(bpy)_3^{3+/2+}$	Tris-(2,2'-bipyridine)osmium (III)/(II)
$Os(dpbpy)_3^{3+/2+}$	Tris-(4,4'-(bisphosphonic acid)-2,2'-bipyridine)osmium (III)/(II)
P^{2-}	Phthalate
PCET	Proton Coupled Electron Transfer
PT	Proton transfer
pH	$-\log[H^+]$
pK_a	$-\log K_a$
PTET	Stepwise proton transfer followed by electron transfer
PGE-^{1}H NMR	Pulse gradient echo-proton nuclear magnetic resonance
R	Universal gas constant
RDS	Rate determining step
Ru	Ruthenium
$Ru(NH_3)_6^{3+/2+}$	Hexaammineruthenium (III)/(II)
$Ru(bpy)_3^{3+/2+}$	Tris-(2,2'-bipyridine)ruthenium (III)/(II)
SHE	Standard hydrogen electrode
SFM	Scan force microscopy
TBAOH or TBAH	Tetrabutylammonium hydroxide
$TBAPF_6$	Tetrabutylammonium hexafluorophosphate

TFAC	Trifluoroacetate
TFMP	(Trifluoromethyl)phenyl
V	Volts
V/s	Volts per second
XPS	X-ray photoelectron spectroscopy
α	Symmetry factor
β	Brönsted coefficient for a general base catalysis process
δ	Chemical shift
η	Viscosity

Abstract

ACID-BASE CATALYSIS IN PROTON-COUPLED ELECTRON TRANSFER REACTIONS (PCET): THE EFFECTS OF BRÖNSTED BASES ON THE OXIDATION OF GLUTATHIONE AND HYDROQUINONE

By Jonnathan Medina-Ramos, Ph.D. in Chemistry

A dissertation submitted in partial fulfillment of the requirement fro the degree of Doctor of Philosophy at Virginia Commonwealth University.

Virginia Commonwealth University, 2012

Thesis Director: Julio C. Alvarez, Ph.D., Department of Chemistry at VCU

This thesis presents the results and discussion of the investigation of the effects of Brönsted bases on the kinetics and thermodynamics of two proton-coupled electron transfer processes: the mediated oxidation of glutathione and the electrochemical oxidation of hydroquinone. Proton-coupled electron transfer (PCET) is the name given to reactions that involve the transfer of electron(s) accompanied by the exchange of proton(s). PCETs are found in many chemical and biological processes, some of current technological relevance such as the oxygen reduction reaction in fuel cells, which involves the transfer of four electrons and four protons ($4e^-$, $4H^+$); or the splitting of water into protons ($4H^+$), electrons ($4e^-$) and oxygen (O_2) efficiently achieved in photosynthesis. The study of PCET mechanisms is imperative to understanding biological processes as well as to developing more efficient technological applications. However, there are still many unanswered questions regarding the kinetic and thermodynamic performance of PCETs, and especially about the effect of different proton acceptors on the rate and mechanism of PCET reactions. This study aimed to investigate the effect of Brönsted bases as proton acceptors on the kinetics and thermodynamics of two model PCET processes, the oxidation of

glutathione and hydroquinone. The analysis presented in this thesis provides insight into the influence of different proton acceptors on the mechanism of PCET and it does so by studying these reactions from a different angle, that one of the acid-base catalysis theory which has been successfully applied to the investigation of numerous chemical reactions coupled to proton transfer. We hope future research of PCETs can benefit from the knowledge of acid-base catalysis to better understand these reactions at a molecular level.

Chapter 1:

Introduction and background

1.1 Proton Coupled Electron Transfer Reactions (PCET): what they are and their relevance.

This thesis deals with the study of reactions that involve electron transfer(s) accompanied by proton (H^+) transfer(s). Reactions of this type are abundant in chemistry and fundamental to numerous biological processes, hence the great interest in investigating their mechanisms and physicochemical intricacy. [1-12] The present work describes an investigation of the electrochemical oxidation of glutathione in aqueous solutions as well as the voltammetry of hydroquinone in non-aqueous media, both of them in the presence of weak Brönsted bases.[13]

These electrochemical processes are examples of reactions that involve the transfer of electrons intimately associated with the transfer of protons and their study allowed for a deeper understanding of the kinetic and thermodynamic behavior of such type of reactions in the presence of Brönsted species, at conditions of variable free energy, pH, Brönsted base structure and concentration. The knowledge gathered from researching glutathione's and hydroquinone's electrochemistry supports the conclusions from studies done by other authors and, in some cases, it challenges the arguments proposed by others in the discussion of similar systems. This introduction will provide some basic definitions and a brief presentation of the most relevant work done in the field of proton-coupled electron transfer reactions (PCETs) in order to lay down the context for the work that will be discussed in the following chapters of this thesis.

1.2 Proton-coupled electron transfer versus stepwise proton-electron transfer mechanisms.

Numerous chemical reactions which involve transferring of electrons are also accompanied by the transfer of protons. Examples are the $2e^-$, $2H^+$ oxidation of hydroquinone, and its counterpart the $2e^-$, $-2H^+$ reduction of benzoquinone (Eq. 1.1)[1,13,14]; the $4e^-$, $4H^+$ reduction of oxygen (Eq. 1.2)[12]; the $1e^-$, $1H^+$ oxidation of tyrosine by the $P680^+$ cofactor in the photosystem II (Eq. 1.3)[7]; and the $1e^-$, $1H^+$ oxidation of biological thiols like cysteine, glutathione and homocysteine (Eq. 1.4)[12,15-18]. However, transfer of proton(s) and electron(s) are not always intimately related in redox reactions where both species are involved; in some cases the proton exchange is completed before the electron transfer occurs or vice versa, while in some reactions proton and electron are transferred in a single step without formation of a stable intermediate.[5-11]

The two scenarios where proton and electron transfer occur in a separate fashion in the same redox reaction are usually known as stepwise pathways ETPT or PTET to indicate an electron transfer (ET) followed by proton transfer (PT) or a proton transfer followed by an electron transfer, respectively. A third scenario where proton and electron transfer occur in a single step is called a *concerted* proton-coupled electron transfer, commonly represented by the acronym CPCET. Some authors replace the notation CPCET by CEP, which also stands for 'concerted proton-electron transfer'. The term 'concerted' implies that proton and electron are both transferred in such a way that no intermediate species is detectable.[5-8]

Scheme 1.1A is typically used to illustrate stepwise and concerted pathways for proton-coupled electron transfer reactions, where the diagonal pathway represents the concerted reaction (CPCET) and the vertical-horizontal (ET-PT) and horizontal-vertical (PT-ET) routes correspond to the stepwise mechanisms.[7]

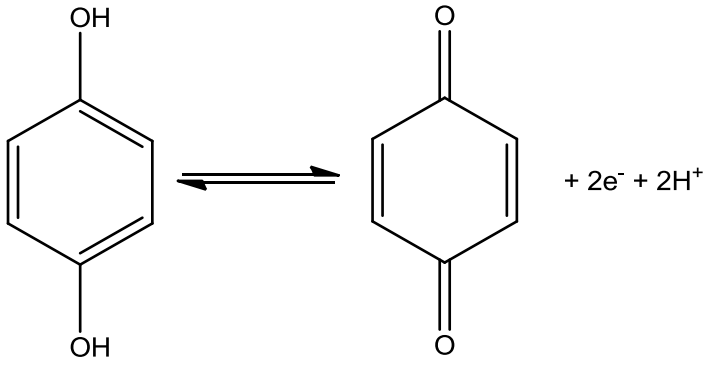

1,4-hydroquinone benzoquinone

Eq. 1.1

$$O_2 + 4H^+ + 4e^- \rightleftharpoons 2H_2O$$

Eq. 1.2

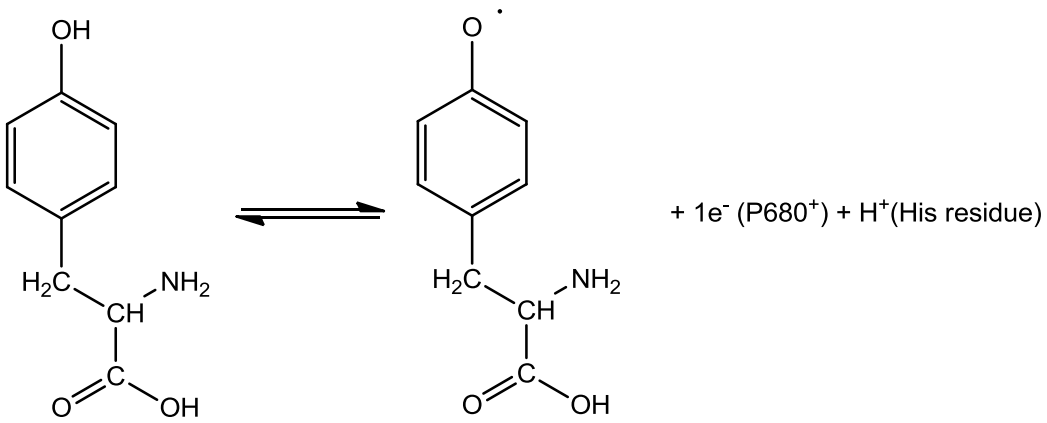

Tyrosine Tyrosil radical

Eq. 1.3

$$RSH \rightleftharpoons RS^{\cdot} + 1e^- + H^+$$

Eq. 1.4

Scheme 1.1B is commonly found in the literature as well but, unlike Scheme 1.1A, it depicts the case where proton and electron come from the same donor group on the substrate (XH) but are transferred to different acceptors (B and A^+).[7] Although Scheme 1.1B illustrates a more complicated scenario, it provides a closer description of the type of proton-coupled electron transfer processes this thesis and most current studies in this field are concerned with.

The study of PCET reactions over the years has involved theoretical as well as experimental approaches to unveil the mechanisms and influence of different variables on their kinetic and thermodynamic behavior. Within the last ten years, the groups lead by Hammes-Schiffer, Mayer, Thorp and Saveant have independently revised multiple cases of experimental PCETs from a theoretical point of view, thus equations for the rate constant of PCET (k_{PCET}) have been proposed based on properties of the systems such as reorganization energy (λ), driving force (ΔG°), electronic coupling, equilibrium proton-donor acceptor distance and frequency, temperature, pH, overpotential (in electrochemical processes) and solvent relaxation time in some cases.[5,7,12,19] However, in spite of all the work done analyzing different cases of PCET, it remains a challenge to agree on which is the best model to explain the variable kinetic dependence of these reactions on pH and on the nature and concentration of various proton acceptors (bases).

1.3 The oxidation of tyrosine: a case of PCET

The oxidation of tyrosine to produce tyrosine radical (Eq. 1.3) is one of the most studied reactions that involves the transfer of one electron coupled to the transfer of a proton.[3,7-9,12,20] The motivation for investigating tyrosine's PCET is that a tyrosine moiety in Photosystem II participates in a chain of proton-coupled electron transfer reactions in which this aminoacid is

oxidized by the $P680^+$ cofactor and the resulting tyrosil radical is reduced afterwards by a manganese cluster.[3,7-9,12]

(A)

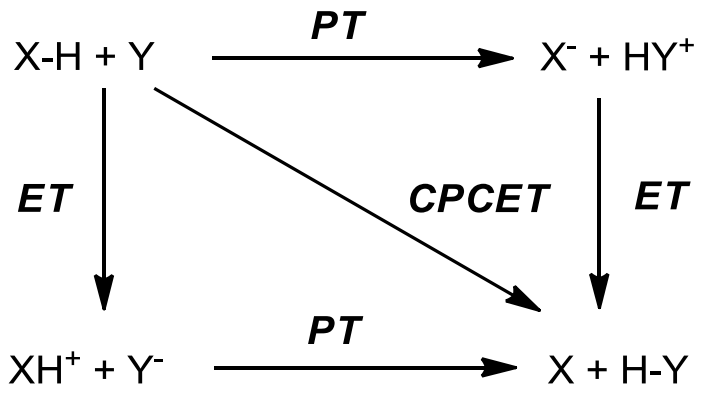

(B)

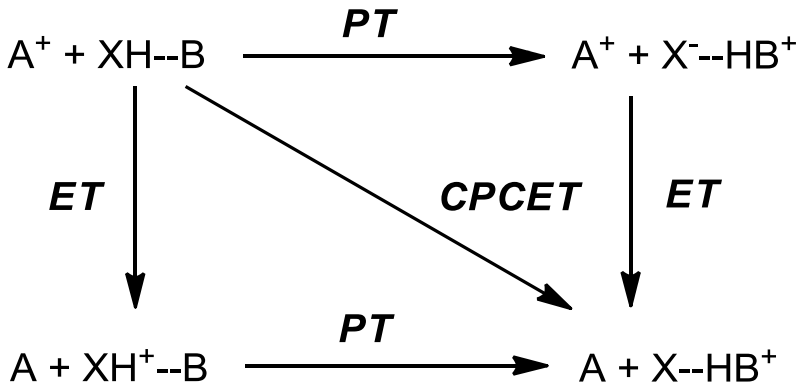

Scheme 1.1 Square schemes for proton-coupled electron transfer (PCET). (Adapted from reference 7 by permission of the Annual Reviews Inc. and the Copyright Clearance Center).

In such studies, the oxidation of tyrosine in model systems is achieved electrochemically, by using metal complexes like tris-bipyridil osmium III $[Os(bpy)_3]^{3+}$ that act as mediators [3,4] (see Scheme 1.2A); or photochemically where tyrosine is oxidized by a photo-excited metal

center [8,9,20] or by a radical species [6] (see Scheme 1.2B). The rate of oxidation of tyrosine has been investigated at different pH's, in buffered and unbuffered aqueous solutions, using different types and concentrations of buffers, and different oxidizing agents of variable redox potentials (usually metal complexes with different $E_{1/2}$). [3-6,8,9]

Most studies have shown that the rate of oxidation of tyrosine increases with the oxidizing power of the mediator, with the buffer's pH and concentration (normally histidine and $H_2PO_4^-$ /HPO_4^{2-} buffers were used) and, in particular cases, with the apparent pH of unbuffered solutions. [3-5,8] Other studies propose that the oxidation of tyrosine is a concerted PCET process when mild oxidizing agents are involved, and that the released proton is accepted by water molecules or by the basic form of the buffer present in solution (e.g. histidine or HPO_4^{2-}). [20] In contrast, in the presence of stronger oxidizing agents, the mechanism would be mostly stepwise, ETPT, or a mix of PCET and ETPT; and under highly basic (high concentration of OH-) and mildly oxidizing conditions, a stepwise PTET mechanism would operate instead. [20]

However, disagreement ensues when the oxidation of tyrosine in the complex Re(P-Y) (where P-Y represents a reduced triphenylphosphine-tyrosine ligand) is investigated in pure water and in the presence of variable concentrations of phosphate buffer. [20] The oxidation of tyrosine to tyrosil radical occurs directly from the metal-to-ligand charge transfer (MCLT) photo-excited state without an external electron quencher.[20] Hammarstrom and coworkers proposed that for this metal complex the oxidation of tyrosine in aqueous solution is primarily an ETPT with a pH-independent observed rate constant (k_{obs}) at low concentration of phosphate buffer ($< 10^{-3}$ M), and a pH and buffer-dependent k_{obs} at higher concentration of buffer ($> 10^{-3}$). [20] This study suggests that at low concentration of buffer water acts as a proton acceptor

(A)

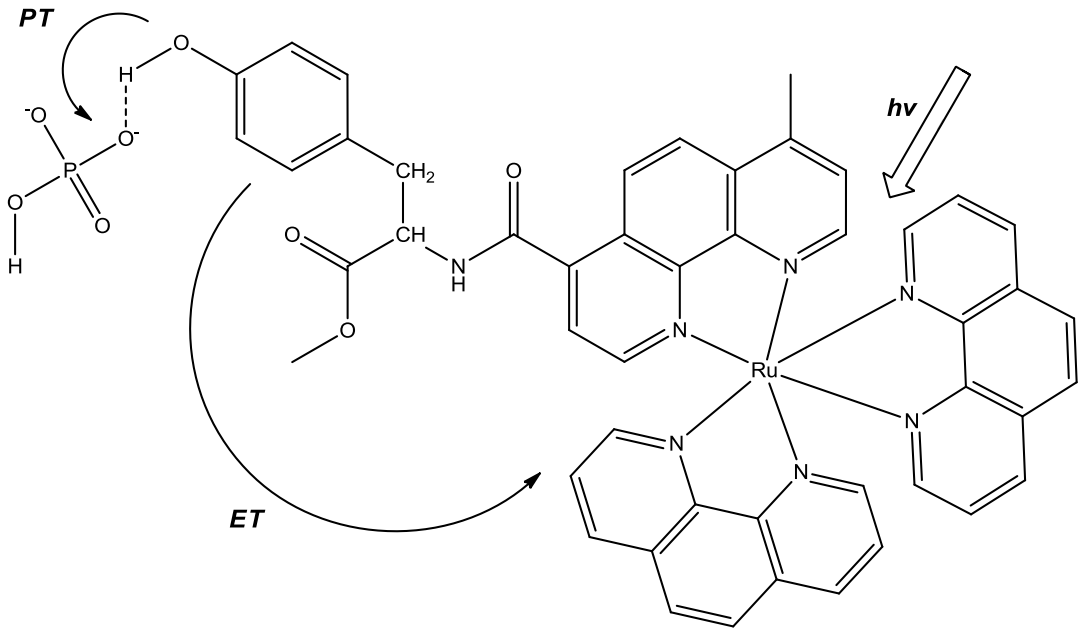

(B)

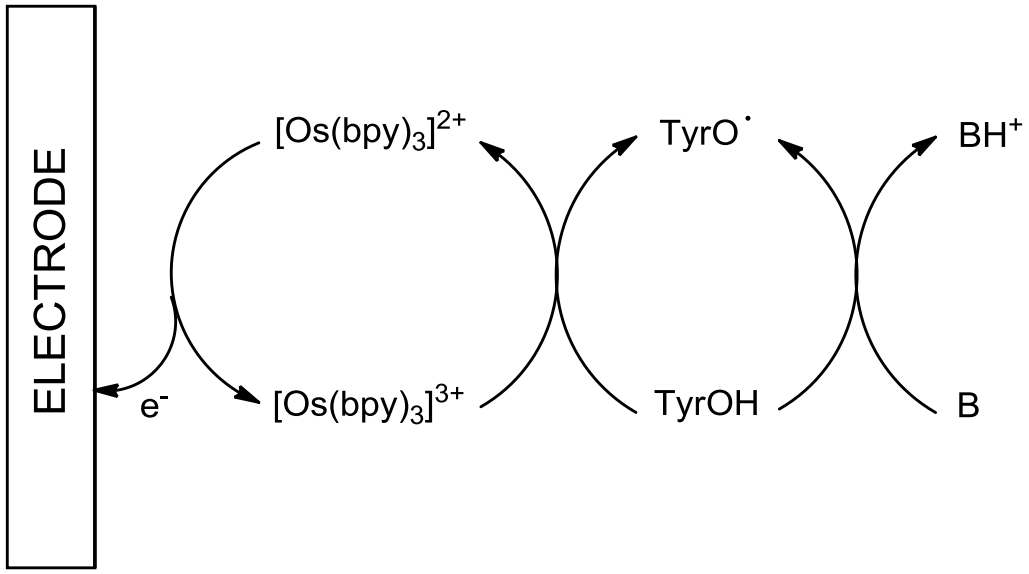

Scheme 1.2 (A) Oxidation of tyrosine by a photo-excited ruthenium center in a model compound (adapted from reference 20 by permission of The American Chemical Society); (B) Oxidation of tyrosine by electro-generated $[Os(bpy)_3]^{3+}$, in the presence of a buffer B/BH^+, as studied in references 3 and 4.

from tyrosine in Re(P-Y) while at higher concentration of buffer, HPO_4^{2-} becomes a more efficient proton acceptor. The proposition that water can be a good proton acceptor for tyrosine's oxidation in Re(P-Y) at low concentrations of buffer has been questioned by Hammes-Schiffer and coworkers in a theoretical study which indicates that the HPO_4^{2-} acceptor model (where HPO_4^{2-} is the actual proton acceptor for tyrosine) successfully reproduces the pH dependence of the overall rate whereas the water acceptor model is not physically reasonable for the Re(P-Y) system. [5,21]

This controversy serves as an example of the complexity that entails the research of proton-coupled electron transfer reactions. Furthermore, the impact of changing proton acceptors on the rate of proton-electron transfer reactions has not been explored as much as the influence of varying the electron transfer driving force alone, which in most cases can be predicted with the Marcus theory of electron transfer.[7,22,23] The Marcus theory predicts a positive linear relationship between the observed rate constant (RT ln k_{obs}) and the free energy of electron transfer ($-\Delta G°$) for redox reactions where the charge transfer process is rate determining.[7,22,23] Unfortunately, only a handful of electrochemical papers deal with the role of proton donors/acceptors in the kinetics of proton-coupled electron transfer reactions even though it is known that these reactions become faster as the proton transfer becomes more favorable by raising the pH or by increasing the concentration of proton donor/acceptor. [3-5,9,20,21]

Several studies done by Smith [14] and Alligrant and coworkers [1,13,24] show that the voltammetry of hydroquinones is in fact very susceptible to the type of proton acceptors available in solution, and that entirely different electrochemical mechanisms explain the voltammetry of this in aqueous solution or in a non-aqueous solvent like acetonitrile.[1,13,14,24] Those studies highlight the importance of hydrogen bonding interactions between hydroquinone/quinone and the solvent

molecules (in the case of water) or basic species present in solution: intermolecular hydrogen bonding determines the electrochemical mechanism and in some instances is responsible for facilitating the oxidation of hydroquinones by reducing their anodic overpotential. Smith's work in particular demonstrates the importance of studying hydroquinone's voltammetry in buffered and unbuffered conditions, a very unfamiliar practice to most electrochemists accustomed to working with well-buffered systems to avoid the complications of a variable pH, in order to gain a comprehensive view of the electrochemical mechanism of this extensively studied redox probe. [14]

Predictably, most of the work on the oxidation of biological thiols like cysteine and glutathione has been done under buffered conditions but little or no attention has been paid to the possible effects of buffer type and concentration, although pH-dependent rates are commonly reported. Following are some examples of research done on the oxidation of thiols using different metal complexes and radical species as mediators which looked to understand the dependence of the rate and mechanism of reaction on pH, strength of the oxidizing agents and concentrations of all reactants. Some of these studies investigate the oxidation of thiols because this type of compounds are present in a great number of proteins and knowing their redox chemistry is relevant to elucidating the functioning and reactivity of such proteins. [12] In contrast, other studies focus mainly on the electrochemical oxidation of thiols at functionalized electrode surfaces as this could be applied in the development of sensors to detect these species. Overall, none of the studies that will be described below explored in detail the proton-coupled electron character of the redox chemistry of thiols.

1.4 The oxidation of thiols: another case of PCET

Thiols like cysteine, glutathione and homocysteine are constant target of research due to their biological role as antioxidants in cells and because their concentration in biological systems is commonly related to various pathologies such as cancer, diabetes and HIV. [12,17,25,26] These compounds are also known for being electro-active; the sulfhydryl group –SH oxidizes to form a radical -S$^{\bullet}$ species upon abstraction of one electron (e^-) and one proton (H^+).[12,17,25] Upon oxidation, the thiol radical or thiyl species later dimerize through formation of a disulfide bond –S-S- (Eq. 1.5)[12,17,25] which usually happens in most biological systems. Nonetheless, the chemistry of thiyl radicals has proven very rich and they can also participate in reactions with other neutral, charged or radical species leading to byproducts different from the expected disulfides. [17]

Biological thiols are usually found in cells in milimolar concentrations (mM), and although their half-cell (redox) potential varies depending on their location within the cell, it usually has a negative value that ranges from -0.17 V to -0.27 V vs. NHE for glutathione and cysteine. [27,28]

In the last two decades, much work has been done trying to develop sensing techniques for detection of thiols; in fact electrochemical methods are one of the most common approaches adopted by scientists in this field.

$$2RSH \longrightarrow RS\text{-}SR + 2e^- + 2H^+ \qquad \textbf{Eq. 1.5}$$

In practice, most thiols do not produce a reproducible voltammetric signal at any of the most used electrode substrates such as glassy carbon, platinum or boron doped diamond, and the use of gold is precluded due to its strong chemical interaction with thiols which leads to blocking of the electrode surface. [15,29] The direct oxidation of thiols at electrode surfaces is usually irreversible and electrode fouling effects are usually encountered in such studies. [15,29] Therefore,

alternative approaches have been investigated, including the development of modified electrodes with electrocatalytic and anti-fouling properties for direct oxidation of thiols and the indirect or mediated oxidation of these species by metal complexes in solution.

Stanbury and coworkers studied the oxidation of thiols like cysteine and thioglycolic acid (TGA) by oxidant metal ions. [16,30] The metal complexes used were $[Fe(bpy)_2(CN)_2]^+$ and $[Fe(bpy)(CN)_4]^-$ to oxidize cysteine, and $[IrCl_6]^{2-}$ to oxidize TGA.[16,30] All these metal complexes react with the thiols by abstracting one electron from the sulfhydryl group and the products are the reduced metal complex and the corresponding thiyl radical. The electron transfer between thiol and metal complex is an outer sphere process with all of these metal oxidants.

Scheme 1.3 shows the reaction mechanism proposed for the reaction of TGA with $[IrCl_6]^{2-}$, as well as some of the derived rate constants. [30] Although the kinetics of these reactions were studied at different pH's, Stanbury's work focuses mostly on minimizing the catalytic effect of copper traces on the oxidation of the thiols (which is achieved by adding chelating agents that trap copper ions in solution) and proposing reasonable mechanistic pathways to explain the experimental results. The effect of the rate of proton transfer that accompanies the oxidation of these thiols on the observed rate of reaction is not explicitly discussed in Stanbury's articles, and it seems as though the rate constants determined for the reactions between cysteine and the two iron complexes are pretty much independent on pH. In contrast, a pH dependent observed rate constant was observed in the study of the oxidation of TGA by $[IrCl_6]^{2-}$.[30] In addition, all experiments were done in buffered solutions containing the thiol, metal complex and chelating agent that traps the copper ions but the effect of buffer type and concentration on the kinetics of the reactions was not fully investigated.

Similarly, Compton and coworkers studied the oxidation of cysteine by electrogenerated octacyanomolibdate V ($[Mo(CN)_8]^{3-}$) and by ferricyanide ($[Fe(CN)_6]^{3-}$) in aqueous solutions, seeking to apply this chemistry in the development of sensing techniques for the detection of thiols. [15,29] The electrochemical oxidation of cysteine by octacyanomolibdate (V) was studied through cyclic voltammetry at a boron doped diamond electrode, at pH's between 9 and 11.[15] The proposed electrochemical mechanism is an ECC' type, where E represents the reversible one-electron transfer of the redox couple $[Mo(CN)_8]^{3-}/[Mo(CN)_8]^{4-}$; C is for the homogeneous chemical reaction between $[Mo(CN)_8]^{3-}$ and cysteine (and this applies to homocysteine or glutathione as well) that generates $[Mo(CN)_8]^{4-}$ and the cysteinyl radical (Cys-S$^{\bullet}$); and C' is for the also homogeneous reaction of $[Mo(CN)_8]^{3-}$ with water which yields CN^- and $[Mo(CN)_7H_2O]^{2-}$ (see Scheme 1.4).[15]

The voltammetric responses obtained at different conditions of pH (pH 9-11) and reactants were reproduced through digital simulation by using DigiSim^{TM}, and a forward rate constant of $9.0 \pm 1.0 \times 10^4$ mol^{-1} cm^3 s^{-1} for the catalytic reduction of $[Mo(CN)_8]^{3-}$ by cysteine produced an excellent fit between experimental and simulated voltammograms. [15] According to the Compton and coworkers, octacyanomolibdate (V) can oxidize both protonated (Cys-SH) and de-protonated (Cys-S$^-$) thiol species, since the pK_{SH} of cysteine is 10.37, and the pH of all solutions used was between 9 and 11. [15] One problem with this analysis is that the reported pK_{SH} of cysteine is around 8.6 according to most literature sources [31-34] and not 10.37 like the authors suggest. Hence, at pH 9 or higher cysteine's sulhydryl group would be mostly deprotonated (% Cys-S$^-$ ≈ 71.5 % at pH 9 and ~99.6 % at pH 11) thus it is not surprising that a single rate constant value (although with a considerable standard deviation) could reproduce successfully all the voltammetry at pH's between 9-11.

$$HSCH_2COO^- + [IrCl_6]^{2-} \rightarrow^{\bullet} SCH_2COO^- + [IrCl_6]^{3-} + H^+, k_b$$

$$^-SCH_2COOH + [IrCl_6]^{2-} \rightarrow^{\bullet} SCH_2COOH + [IrCl_6]^{3-}, k_c$$

$$^-SCH_2COO^- + [IrCl_6]^{2-} \rightarrow^{\bullet} SCH_2COO^- + [IrCl_6]^{3-}, k_d$$

$$RS^{\bullet} + RSH \leftrightarrow RSSR^{\bullet-} + H^+, K_{as}$$

$$RSSR^{\bullet-} + [IrCl_6]^{2-} \rightarrow RSSR + [IrCl_6]^{3-}, k_2$$

$$RS^{\bullet} + [IrCl_6]^{2-} + H_2O \rightarrow RSOH + [IrCl_6]^{3-} + H^+, k_3$$

$$3RSOH[+Ir(IV)] \rightarrow RSO_3^- + 2RSH + H^+ (fast)$$

Scheme 1.3 Mechanism of oxidation of thioglycolic acid by $[IrCl_6]^{2-}$ as proposed by Stanbury and Sun (reference 29-reproduced by permission of The Royal Society of Chemistry).

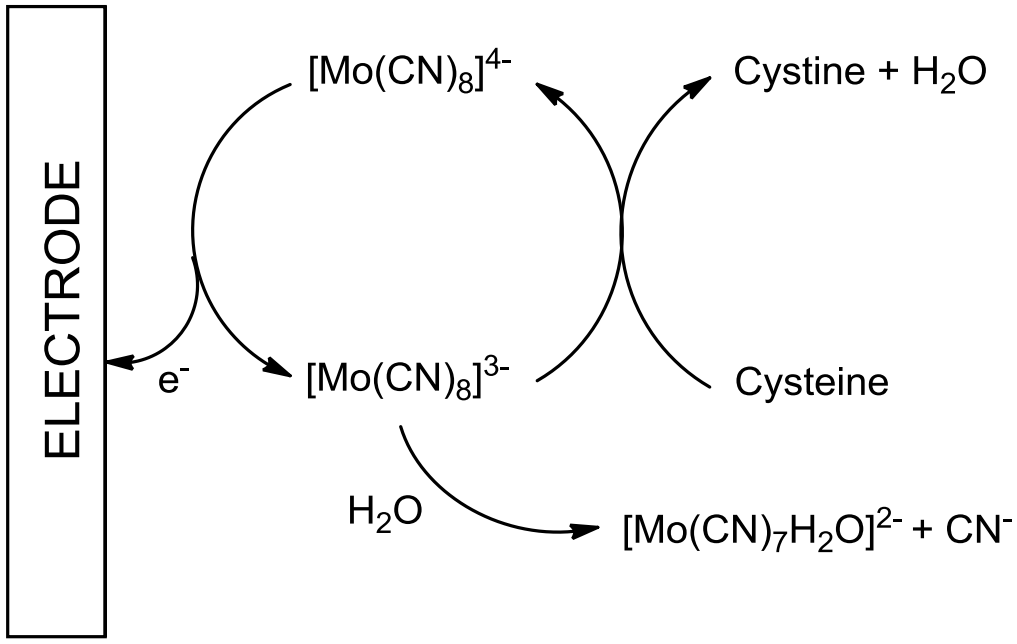

Scheme 1.4 Oxidation of cysteine in aqueous solution by electro-generated $[Mo(CN)_8]^{4-}$, as studied by Compton and coworkers (from reference 15- reproduced by permission of The Royal Society of Chemistry).

In addition, all the experiments were carried out under buffered conditions using 0.1 M borax pH > 9 as the buffer, therefore the effect of buffer concentration and pH on the rate of catalytic oxidation of cysteine by $[Mo(CN)_8]^{3-}$ cannot be appreciated from this study.

In the study of the oxidation of cysteine by electrogenerated $[Fe(CN)_6]^{3-}$, also by Compton and coworkers, an EC mechanism is suggested where E represents the reversible $1e^-$ transfer of the redox couple $[Fe(CN)_6]^{3-}$/ $[Fe(CN)_6]^{4-}$ and C the homogeneous reaction between cysteine and $[Fe(CN)_6]^{3-}$ to produce the cysteinyl radical and $[Fe(CN)_6]^{4-}$. [29] Through digital simulation of the voltammetric responses a pH-dependence of the rate constant for the homogeneous reaction was determined. [29] At pH's 9, 10 and 11 the values of the rate constant of reaction between $[Fe(CN)_6]^{3-}$ and cysteine were 3.0×10^3, 8.0×10^3 and 20×10^3 M^{-1} s^{-1}, respectively. [29] Furthermore, based on the assumption that the pK_{SH} of cysteine was 10.5, the rate constants of oxidation of protonated and deprotonated cysteine by $[Fe(CN)_6]^{3-}$ were estimated to be 2.3×10^3 M^{-1} s^{-1} and 2.5×10^4 M^{-1} s^{-1}, respectively. [29] Here a pH-dependent rate is observed, but once again the entire study was conducted using well-buffered solutions (0.1 M borate buffer pH 9, 10 or 11) and the assumed pK_{SH} for cysteine is about 2 pK_a units higher than the actual value.

As mentioned above, a different approach to study the redox properties and develop sensing platforms for detecting thiols is designing electrode surfaces with electrocatalytic properties toward the oxidation of this type of compounds. Examples of such approach were presented by Raoof and coworkers whom developed two voltammetric sensors for glutathione based on modified carbon paste electrodes. [35]

One of these voltammetric sensors is a ferrocene-modified carbon paste electrode where the oxidation of glutathione is enhanced by ferrocene groups on the surface of the electrode that mediate in the oxidation of glutathione. [35] The ferrocene groups at the electrode surface are

electrochemically oxidized (cyclic voltammetry and differential pulse voltammetry are applied) and further reduced upon reaction with reduced glutathione present in solution. [35,36] This reaction between oxidized ferrocene and glutathione produces an enhancement of the anodic current due to oxidation of ferrocene at the electrode and this enhancement is directly proportional to the concentration of glutathione in solution. [35] In this study Raoof and coworkers found that the detection of glutathione was optimal at pH 7.0 and a detection limit of 2.1×10^{-6} M was achieved when the sensor was operated through differential pulse voltammetry (DPV). [35]

The second sensor was a carbon paste electrode modified with 2,7-bis (ferrocenyl ethyl) fluoren-9-one groups. [36] With this sensor the detection of glutathione was optimal at pH 7.0 as well, and a detection limit of 5.1×10^{-7} M was observed using the DPV method. [36] These sensors could be used to measure glutathione in real samples like human plasma. [36]

Similar sensors have been developed by others, all based on the attachment of metal oxidants to the electrode surface which behave as mediators in the oxidation of the thiols, and the chemistry taking place at the electrode-solution interface has been more or less discussed. However, the fact that the oxidation of thiols is a process that involves the transfer of an electron and a proton, and that the rate is likely dependent on the pH and the type and concentration of all acids and bases present is not taken into account in any of these studies when proposing a mechanism of reaction or when the optimal conditions for detection are established.

This thesis presents the results and discussion of three different projects that explored the role of Brönsted bases and pH on the rate and the thermodynamics of redox reactions accompanied by proton transfer, the oxidation of glutathione and hydroquinone. This research proves that pH and buffer effects can be distinguished from each other when studying the electrochemical oxidation of glutathione and that these effects have the potential to determine the type of

mechanism and observed rate of reaction. Likewise, this work shows that the presence of Brönsted bases changes the pathways and the overpotential of electrochemical oxidation of hydroquinone and the overpotential for reduction of the corresponding products when phthalate bases are freely dissolved in solution as well as when phthalate groups are chemically attached to the surface of the glassy carbon working electrode. [13] Although catalysis of many organic and enzymatic reactions by weak acids and bases is a very well-known and fundamental subject in organic and biochemistry, [2,37-39] the study of this type of catalysis within the context of electrochemical reactions involving the transfer of protons is still underdeveloped.

Below, some examples of research done on proton coupled electron transfer reactions show that, even though it has been observed that pH and/or the presence of a buffer have definite effects on the rate of these processes, oftentimes the nature of such effects is unknown or simply neglected.

1.5 Acid-base catalysis in PCET reactions.

Acid-base catalysis is a subject researched and understood primarily by physical-organic and biochemists. [2,37-41] Numerous reactions including hydrolysis of organic molecules, enzymatic transformations and even some proton-coupled electron transfers that are kinetically enhanced by weak acid or basic species are defined as acid/base catalyzed processes.[2,37-42]

In the study of acid-base catalysis two different kinetic regimes have been identified, *specific* and *general acid-base catalysis*, based on whether the observed rate of reaction depends only on pH or on the concentration of all the acid and basic species present, respectively. *Specific acid-base catalysis* is thus characterized by a dependence of the observed rate constant k_{obs} on the concentration of either H^+ (specific acid catalysis) or OH^- (specific base catalysis) also known as

the *specific acid and base*, respectively. [2,38,39,42] Scheme 1.5 shows typical kinetic plots for specific acid and base catalysis and Eq. 1.6 describes the general mechanism of a specific acid catalyzed process. [42] From Scheme 1.5, the logarithm of the observed rate constant (log k_{obs}) is linearly dependent on pH but independent on the concentration of an added acid (HA) or base (B), and the reason for this is that neither the acid nor the base are involved in the rate determining step (RDS) of the reaction. [42] On the contrary, the acid or base are involved in an equilibrium prior to the rate determining step of the reaction, as indicated in Eq. 1.6 by the equilibrium between R and RH^+ species, which precedes the conversion of RH^+ into PH^+. [42]

According to Scheme 1.6, *general acid-base catalyzed* reactions will exhibit a linear dependence of k_{obs} on the concentration of acid (HA) or base (B) added, and a more complicated dependence on pH compared to specific acid-base catalysis reactions. [42] In general acid-base catalyzed processes the acid or base catalysts are involved in the rate determining step of the reaction, hence the dependence of k_{obs} on either [HA] or [B]. [42] Regarding the pH dependence of k_{obs}, log k_{obs} is independent on pH at those pH's where the concentration of HA or B is almost invariable, namely at $pH<pK_{HA}$ or at $pH>pK_{BH+}$, whereas at pH's where the concentration of either HA (general acid catalysis) or B (general base catalysis) are variable, log k_{obs} exhibits a linear dependence on pH with a slope of -1 for general acid catalysis or +1 for general base catalysis processes. [42] Scheme 1.7 shows examples of possible mechanisms for a general acid (A) and a general base (B) catalyzed hydration of acetone where the acid HA and the base B are involved in the slow, rate determining step of the reactions. [42] Kinetic plots like those shown in Schemes 1.5 and 1.6 are used as a diagnostic for specific and general acid-base catalyzed reactions.

For the mediated oxidation of glutathione by $[IrCl_6]^{2-}$, $[Mo(CN)_8]^{3-}$ and $[Fe(phen)_3]^{3+}$, similar experiments as those shown in Scheme 1.6 were done by running cyclic voltammetry in the presence of variable concentration of buffer, at a constant pH (i.e. in the presence of phosphate or histidine buffers) and also at variable pH, maintaining the concentration of buffer constant. Digital simulation of the respective voltammograms was carried out to estimate the observed rate constants of oxidation of GSH by the different mediators at all conditions of pH, buffer composition and concentration. The results of these experiments, which strikingly resemble the trends in Scheme 1.6 corresponding to general base catalysis, are discussed in Chapters 2 and 3.

As mentioned before, some proton coupled electron transfer reactions like the electrochemical oxidation of tyrosine or guanine have shown kinetic dependences on pH and on the concentration and type of basic species present in solution [3,4,10,11,20,21]; however none of these studies have discussed the possibility that such effects could be related to the acid-base catalysis phenomena. The reason acid-base catalysis is not considered in most studies of electrochemical reactions might be that buffers are usually employed to maintain a constant pH throughout the experiment, and the influence of the buffer components on the type of electrochemical response observed is often unknown or neglected. Furthermore, as Smith and coworkers pointed out in their article about the voltammetry of quinones in unbuffered aqueous solution, electrochemists are reluctant to work with unbuffered systems since Muller, Kolthoff and Lingane exhorted them about 75 years ago to perform polarographic studies in well buffered solutions due to irreproducibility of the voltammetry of quinhydrone and other organic compounds as the buffer was diluted. [14] Although acid-base catalysis was not specifically discussed in any of the studies that will described below, it is possible that such effects were still operating despite being ignored.

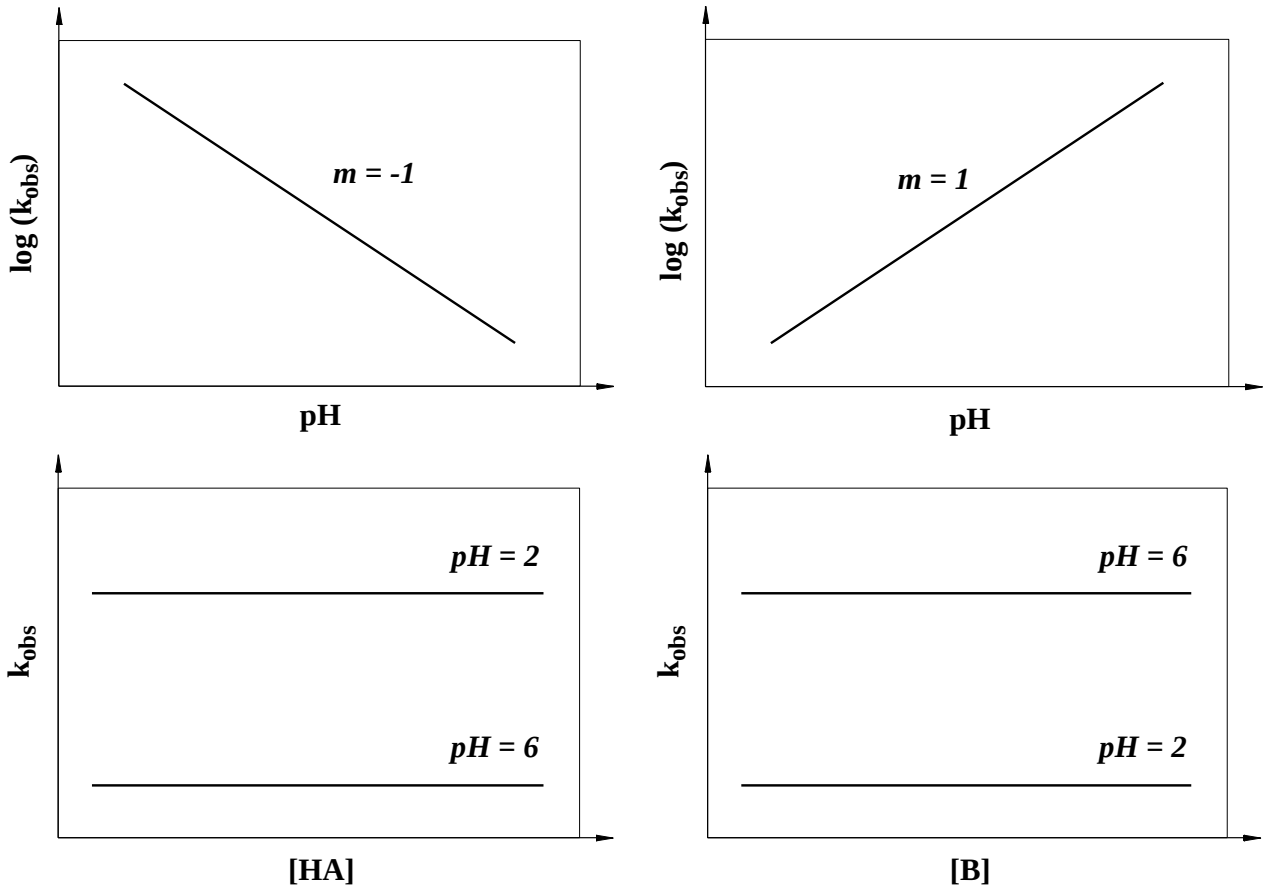

Scheme 1.5 Typical kinetic plots for specific acid (top and bottom left) and specific base catalysis (top and bottom right). Both log k_{obs} and k_{obs} are pH dependent, but independent on the concentration of HA (specific acid catalysis) or B (specific base catalysis). Reproduced from reference 42, with permission from University Science Books, Mill Valley, CA. All rights reserved.

$$R + H_3O^+ \leftrightarrow RH^+ \xrightarrow{slow} PH^+ \xrightarrow{fast} P + H_3O^+ \qquad \textbf{Eq. 1.6}$$

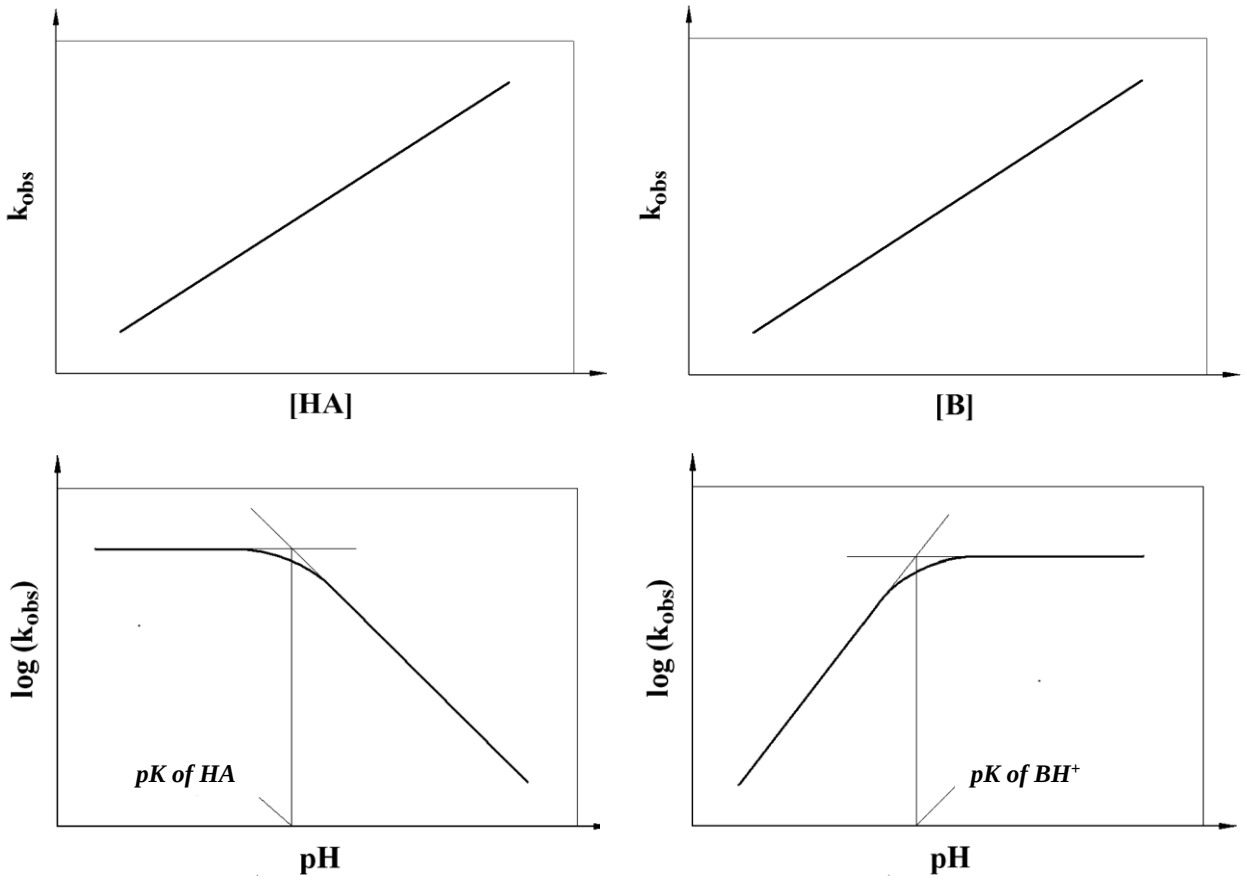

Scheme 1.6 Typical kinetic plots for general acid (top and bottom left) and general base catalysis (top and bottom right). k_{obs} is dependent on the concentration of HA in general acid catalysis or B in general base catalysis. log k_{obs} has a more complex dependence on pH, as explained in the text. Reproduced from reference 42, with permission from University Science Books, Mill Valley, CA. All rights reserved.

Oftentimes in acid-base catalyzed reactions, a linear relationship is observed between the logarithm of the observed rate constant of the reaction, log k_{obs}, and the pK_a of the general acid or bases that catalyze the reaction. [38,39,42] Linear Brönsted relationships appear when the proton transfer between the substrate and the general acid or base is involved in the rate determining transition state of the reaction, and its slope is a measure of the sensitivity of the rate of reaction to the structure of general acids or bases present. [38,39,42] For general base catalyzed reactions, the Brönsted slope is represented by the symbol β, and its value varies between 0 and 1. [38,39,42]

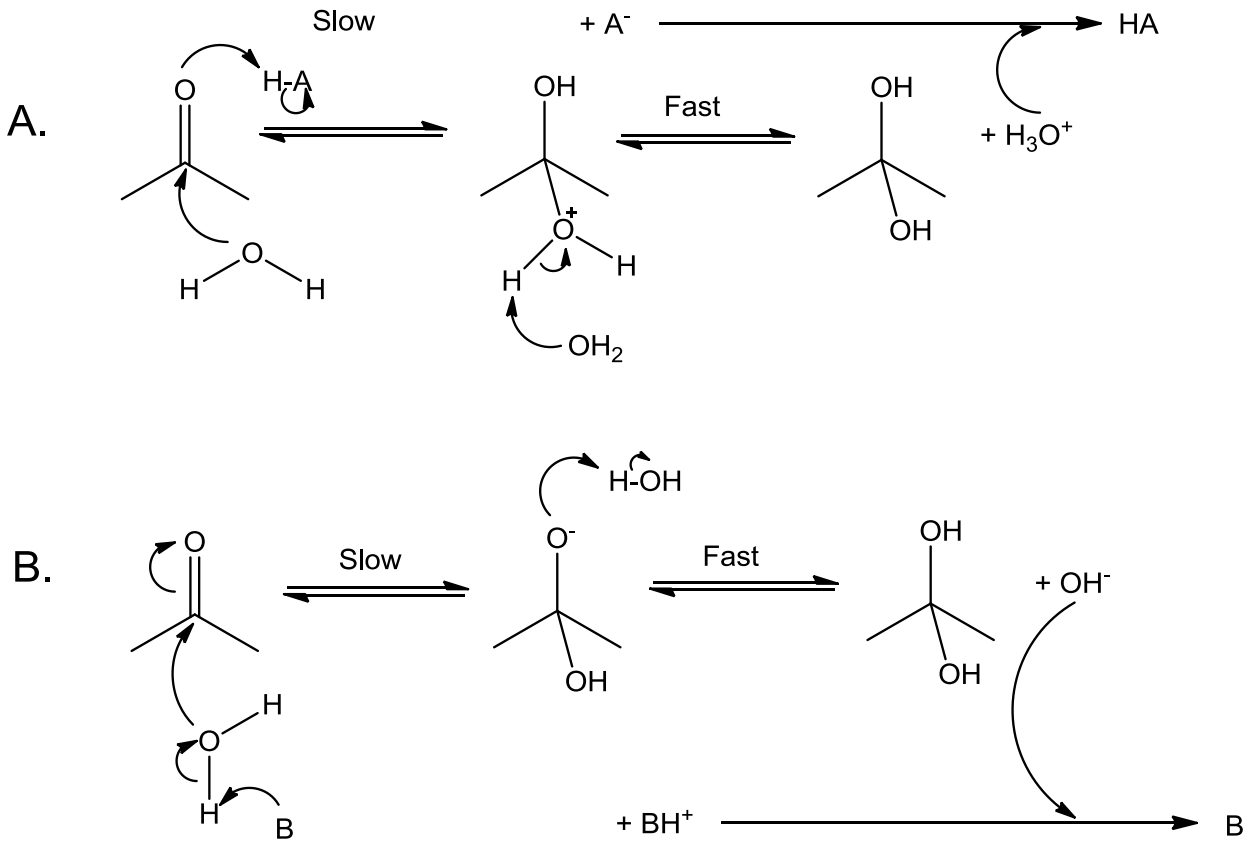

Scheme 1.7 Examples of possible mechanisms for a general acid (A) and a general base (B) catalyzed hydration of acetone where the acid HA and the base B are involved in the slow, rate determining step of the reactions. Reproduced from reference 42, with permission from University Science Books, Mill Valley, CA. All rights reserved.

A common interpretation of the value of β is that a β equal to 0 is observed when the proton transfer is completed before the transition state is achieved, whereas a β value of 1 indicates that the proton transfer takes place only after the transition state of the reaction is surpassed. [38,39,42]

Intermediate values of β define the degree of completion of the proton transfer step at the transition state; for example, a β coefficient of 0.5 would mean that 50% of the proton transfer would have been achieved once the reaction reaches the transition state. [38,39,42]

Stanbury and coworkers investigated the kinetics and mechanism of oxidation of thioglycolic acid (TGA) by hexachloroiridate (IV) and plotted $\log(k_{obs}/[TGA]_{total})$ vs pH (Fig. 8 in that paper) where k_{obs} is the observed rate constant for the reaction between TGA and $[IrCl_6]^{2-}$ and [TGA]total is the sum of the concentrations of the four protonation states of the thiol. [30] The plot of $\log(k_{obs}/[TGA]_{total})$ vs. pH was fitted through a non-linear squares analysis. [30] However, if this plot is simply approximated through a linear regression its slope would be ca. 0.74, which could be assumed to be the Brönsted slope for this reaction, since all experiments were done in buffered aqueous solutions with pH's values close to the pK_a of the respective buffer base. Assuming the validity of this approximation, the β coefficient for the reaction between TGA and $[IrCl_6]^{2-}$ would be very close to that determined for the reaction of GSH and $[IrCl_6]^{2-}$, which was estimated to be ca. 0.69 (see chapter 2). Thus, in the oxidation of both TGA and glutathione by $[IrCl_6]^{2-}$ around 70% of the proton transfer is completed at the transition state of the reaction.

Another example of the use of Brönsted relationships to elucidate the mechanism of a proton-coupled electron transfer reaction is the study of the electrochemical oxidation of tyrosine by $[Os(bpy)_3]^{3+}$ in the presence of various Brönsted bases of different pK_a done by Fecenko and coworkers. [3,4] The kinetics of this reaction was monitored through cyclic voltammetry and the observed rate constants k_{obs} were estimated through digital simulation of the voltammograms with DigiSim™ in a similar fashion as it was done in the present study. [3,4] The authors plotted log k_{obs} as a function of the change in free energy of proton transfer $-\Delta G°$, and through a linear regression a slope of 0.6 was obtained. [4] Although this was not stated by Fecenko and coworkers, this slope would be the same β coefficient or Brönsted slope, and its value indicates that 60% of proton transfer from tyrosine is achieved at the transition state of the oxidation of this aminoacid by $[Os(bpy)_3]^{3+}$, in the presence of the Brönsted bases used.

1.6 Relationship between the thermodynamics and kinetics of PCET reactions: the Marcus theory.

According to Mayer's review on proton coupled electron transfer reactions, the first linear free energy relationship (LFER) that shows the influence of thermodynamics on the kinetics of a reaction was the Brönsted catalysis law for proton transfer formulated in the 1920's. [7] The Brönsted law of catalysis applied to the electrochemical oxidation of glutathione and tyrosine was described above. Likewise, LFERs have been observed for many reactions other than proton transfers, and they usually appear when similar reagents are compared. [7] For example, rates of hydrogen atom transfer (HAT) reactions have been studied following the linear relationship proposed by Evans and Polanyi, which relates the activation energy E_a (energy barrier) and the change in enthalpy of the reaction $\Delta H°$(driving force)[7] :

$$E_a = \beta + \alpha \Delta H° \qquad \text{Eq. 1.7}$$

In general, LFERs can be represented as in Eq. 1.8

$$\Delta G^{\neq} = \alpha \Delta G° + \beta \qquad \text{Eq. 1.8}$$

where $\Delta G^{\neq}$ represents the free energy of activation, $\Delta G°$ is the free energy of reaction and α and β are constants for a particular reaction. [7] In Brönsted plots, $\Delta G^{\neq}$ and $\Delta G°$ are equivalent to *log k* (or *log* k_{obs}) and log K_{eq} (which can be related to the pK_a or the acid or base catalyst) respectively. [7,38,42] In the original Marcus equation for ET, the dependence of $\Delta G^{\neq}$ on $\Delta G°$ is quadratic as shown in Eq. 1.9

$$\Delta G^{\neq} = \frac{\lambda}{4}\left(1+\frac{\Delta G^{\circ}}{\lambda}\right)^{2} \qquad \text{Eq. 1.9}$$

where λ is the reorganization energy and is the sum of outer-sphere (solvent) and inner-sphere (vibrational) reorganization energies. [7,22,23] According to Marcus, when λ is much larger than ΔG°, $\Delta G^{\neq}$ depends linearly on ΔG° with a slope of ½. [22,23] Several electrochemical studies have confirmed this linear relationship with plots of RT ln k ($\approx \Delta G^{\neq}$) vs. ΔG° (= nFE°), where k is the reaction's rate constant, T is temperature, R is the gases constant, n is the number of electrons transferred, F is the Faraday's constant and E° is the reaction's redox potential. [7,22,23]

In this thesis, Marcus-like plots for the electrochemical oxidation of glutathione by different metal complexes are presented, where RT ln k_{obs} values are plotted against the half-way redox potential of the metal complex involved, $E_{1/2}$ (here the approximation $E^{\circ} \approx E_{1/2}$ was made). As Fecenko and coworkers did in their studies of tyrosine's oxidation, this work compared the Marcus and Brönsted slopes and, furthermore, it explored the influence of buffer type and concentration on the Marcus plots. [4]

Dependence of the Marcus slope value on the proton acceptor present in solution was observed when the electrochemical oxidation of guanine and related purines was studied in aqueous and in acetonitrile solutions. [10,11] The Marcus slope for the oxidation of guanine and related purines in aqueous solution was ca. 0.80 whereas a slope of ca. 0.50 was observed in acetonitrile where proton transfer to the solvent was not available. [10,11] Since the expected slope according to the Marcus equation for ET is 0.5, as explained above, Weatherly and coworkers attributed the higher Marcus slope value to the coupling of electron and proton transfer controlling the rate of oxidation of guanine by $[Os(bpy)_3]^{3+}$ in water. [10,11]

In the case of the electrochemical oxidation of glutathione, the importance of finding a Marcus relationship is two-fold: first of all, it provides another example that validates the Marcus electron transfer theory in spite of the disparate group of metal complexes used as oxidants; secondly, together with the Brönsted relationship, the dependence of the observed rate of oxidation k_{obs} on the concentration of phosphate buffer pH 7.0 (Figure 2.3B, chapter 2) and the results of the kinetic isotope effect experiments (Table 2.3, chapter 2), it supports the proposal of a concerted proton-coupled electron transfer as the principal mechanism for the mediated oxidation of glutathione.

The value of the Marcus plots for the oxidation of glutathione by various mediators ($[Mo(CN)_8]^4$, $[IrCl_6]^{2-}$, $[Fe(bpy)_3]^{3+}$, $[Fe(phen)_3]^{3+}$) increases with the concentration and pK_a of the buffer present in solution (from 0.46 to 0.7 with 5.0 mM and 35.0 mM histidine buffer pH 6.5, and from 0.57 to 0.71 with 10 mM and 50 mM phosphate buffer pH 7.0, respectively; see chapter 3). Likewise, the value of the Brönsted slope increases with the oxidizing strength of the mediator, being 0.42 with $[Mo(CN)_8]^{4-}$, 0.69 with $[IrCl_6]^{2-}$ and 0.92 with $[Fe(phen)_3]^{3+}$ (see Fig. 3.4 in chapter 3). These trends observed for the Marcus and Brönsted plots indicate that the rate of electron transfer is influenced by the magnitude of the proton transfer driving force, which explains the variable Marcus slope as the concentration and type of buffer are changed; and, vice versa, the different rate of proton transfer between GSH and the various Brönsted bases used is affected by the magnitude of the electron transfer driving force achieved with each mediator. In other words, both Marcus and Brönsted relationships suggest that the oxidation of GSH by the different mediators, in the presence of the Brönsted bases used, is a case of concerted proton-coupled electron transfer, where both electron and proton are being transferred in a single rate determining step because the overall rate can be controlled by changing the redox mediator or

the proton acceptor species. Again, the KIE values between 5.4 and 2.1 (see chapters 2 and 3) obtained for the oxidation of GSH by $[IrCl_6]^{2-}$, $[Mo(CN)_8]^{4-}$ and $[Fe(phen)_3]^{3+}$ in phosphate buffer solutions support this proposal of a concerted proton-coupled electron transfer mechanism.

The acid-base catalysis theory, and especially the extensive work of Jencks on this subject provides insight into why the mediated oxidation of glutathione in the presence of weak bases and mild oxidizing agents favors a concerted PCET mechanism over the two possible stepwise pathways, ETPT or PTET (see scheme 1.1). In the concerted PCET pathway, the formation of the highly unstable species $GSH^{\bullet+}$ through ETPT, or the unfavorable deprotonation of GSH to give GS^- at pH ≤ 7, via PTET mechanism, are avoided. According to the libido rule postulated by Jencks, which states that *"concerted general acid-base catalysis of complex reactions in aqueous solution can occur only (a) at sites that undergo a large change in pK in the course of the reaction and (b) when this change in pK converts an unfavorable to a favorable proton transfer with respect to the catalyst, i.e., the pK of the catalyst is intermediate between the initial and final pK values of the substrate site";* the oxidation of GSH be a concerted reaction primarily at intermediate pH's ranging from ~ 0 to 8.7 because the change of pK_a in the course of the reaction would be large enough (i.e. the pK_{SH} of GSH changes from 8.7 in its reduced form, to <0 in its oxidized from, $GSH^{\bullet+}$) to converting an initially unfavorable proton transfer (e.g. $GSH + HPO_4^{2-} = GS^- + H_2PO_4^-$, K_{eq} = 0.032) into a favorable one (e.g. $GSH^{\bullet+} + HPO_4^{2-} \rightarrow GS^{\bullet} + H_2PO_4^-$, very fast).

A large change in pK value of the substrate in the course of a PCET reaction would produce a very negative ΔG of proton transfer, and this highly favorable ΔG_{PT} would compensate for the positive change in entropy (ΔS) required for the 'alignment' of substrate (i.e. GSH), redox mediator and base catalyst in a concerted reaction.

The applicability of the libido rule to understanding the mechanism of mediated oxidation of glutathione, which is discussed in chapters 2 and 3, constitutes one of the most remarkable findings of this work because it proves the usefulness of studying acid-base catalysis effects in proton-coupled electron transfer reactions. We strongly believe that bringing together acid-base catalysis and PCET would be highly beneficial in the research of redox processes of scientific and technological relevance such as the oxygen reduction reaction (ORR), hydrogen evolution reaction (HER) and in the development of new catalysts for PCET reactions in general.

1.7 How was this investigation carried out.

The investigation of the electrochemical oxidation of glutathione presented here involved experiments at variable pH, under buffered and unbuffered conditions, and in the presence of variable concentration of different Brönsted bases. These experiments were design after realizing that Brönsted bases like hydrogenophosphate (HPO_4^{2-}) produced the enhancement of the electrochemical oxidation of glutathione by $[IrCl_6]^{2-}$, and that such kinetic effects were not observed with unbuffered solutions.

Likewise, based on previous work done by Alligrant and coworkers [1,24], the oxidation of hydroquinone was studied in the presence of variable concentration of phthalate bases and compared to that in pure acetronitrile. Alligrant and coworkers found that hydrogen bonding between hydroquinone and bases like acetate, benzoate and trifluoroacetate caused the decrease of the oxidation overpotential for hydroquinone in acetonitrile, and these findings inspired the project of studying the redox chemistry of hydroquinone in the presence of phathalates (HP^- and P^{2-}) which, unlike other bases used before, can have to two proton accepting functionalities (i.e. two carboxylate groups) depending on their protonation state. [1,24] Different concentrations of

mono and dibasic phthalate were added to solutions of hydroquinone in acetonitrile and cyclic voltammetry of the solutions was run at a bare glassy carbon surface. [13] The second part of this project involved the use of glassy carbon electrodes modified with phthalate groups to observe the voltammetric behavior of hydroquinone and compare to what was seen having phthalate freely dissolved in solution. [13] The phthalate groups were electrochemically attached to the glassy carbon surface through electrochemical reduction of the diazonium salt of phthalic acid. [13]

Cyclic voltammetry was the electrochemical method applied in all the studies discussed herein and digital simulation of the experimental voltammograms was used to test the validity of the reaction mechanisms proposed. Diffusion coefficients of glutathione and hydroquinone were experimentally determined through Pulse Gradient Echo ^{1}H-NMR and X-Ray photoelectron spectroscopy was used to characterize the surface of phthalate-modified glassy carbon electrodes used in the voltammetry of hydroquinone. [13] The next section of this introduction describes the fundamentals of cyclic voltammetry and Digital Simulation of cyclic voltammograms.

1.7.1 Cyclic Voltammetry

Cyclic voltammetry is an electrochemical techniques commonly used in the investigation of the redox behavior of electro-active species, including purely inorganic and organometallic complexes, organic compounds (e.g. quinones, thiols), biomolecules (e.g. proteins, aminoacids), macromolecules, ionic, zwitterionic and neutral species, metals, non-metals and semiconductor materials. Cyclic voltammetry experiments typically provide information such as the redox potential of analytes of interest (i.e. E° or $E_{1/2}$), the degree of reversibility of charge transfer reaction(s), the number of electrons involved in a specific electrochemical process and,

ultimately, the rate of electron transfer between an analyte and an electrode surface (working electrode).

A standard cyclic voltammetry experiment requires a three-electrode cell containing the analyte solution as that shown in Scheme 1.8, and an instrument called potentiostat used to control the potential applied to the working electrode. It is at the surface of the working electrode where the charge transfer reaction(s) of interest takes place. In a voltammetric scan, the potential of the working electrode is increased (i.e. in the positive or anodic direction) or decreased (i.e. in the negative or cathodic direction) at a uniform rate (i.e. scan rate) while it is measured with respect to the reference electrode. The potential scan function used in cyclic voltammetry is depicted in Scheme 1.9, which shows the potential difference between working and reference electrode increasing from E_i to E_f at a rate of 1 V/s, followed by a decreasing potential difference from E_f to E_i changing at the same scan rate of 1 V/s.

The third electrode in the voltammetric cell, known as the auxiliary or counter electrode, completes a circuit with the working electrode that holds the flow of electrons (current) generated by the potential applied to the working electrode. In the past, only a working and a reference electrode were used in voltammetric studies; however, the use of a counter electrode soon became imperative in order to expand the lifespan of reference electrodes that would readily degrade due to the flow of current produced by the redox reactions occurring in the electrochemical system.

In the studies presented herein, glassy carbon disks were used as working electrodes. Glassy carbon is a highly conductive, smooth and relatively inert material well suited for the voltammetric experiments carried out. A silver/ silver chloride (Ag/ AgCl/ 1.0 M NaCl; 1.0 M NaCl is the solution filling the inside of the reference electrode) electrode was used as the

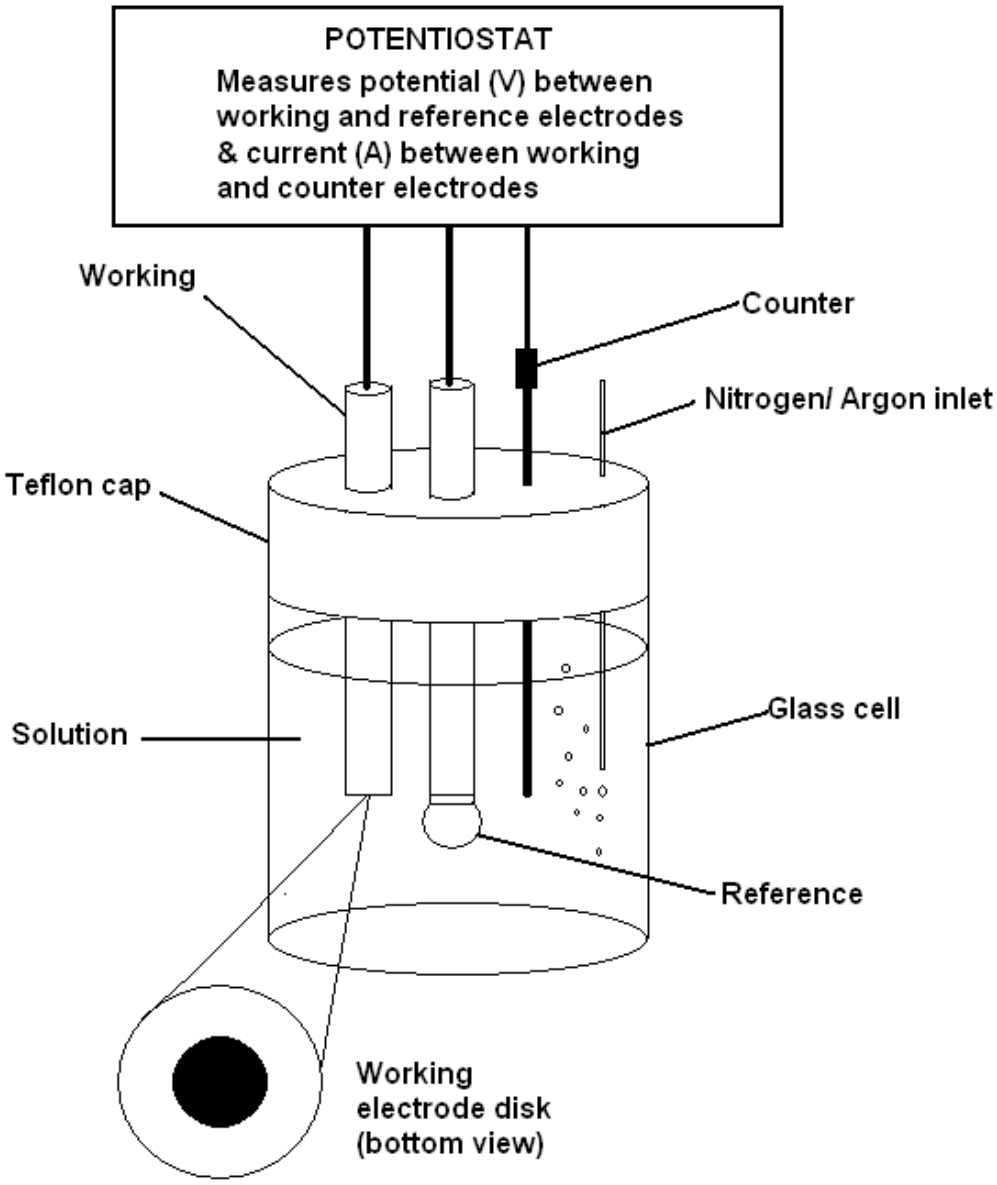

Scheme 1.8 Standard three-electrode cell used for cyclic voltammetry experiments, containing the analyte solution. The three electrodes are connected to an instrument called potentiostat used to control the potential applied to the working electrode with respect to a reference electrode.

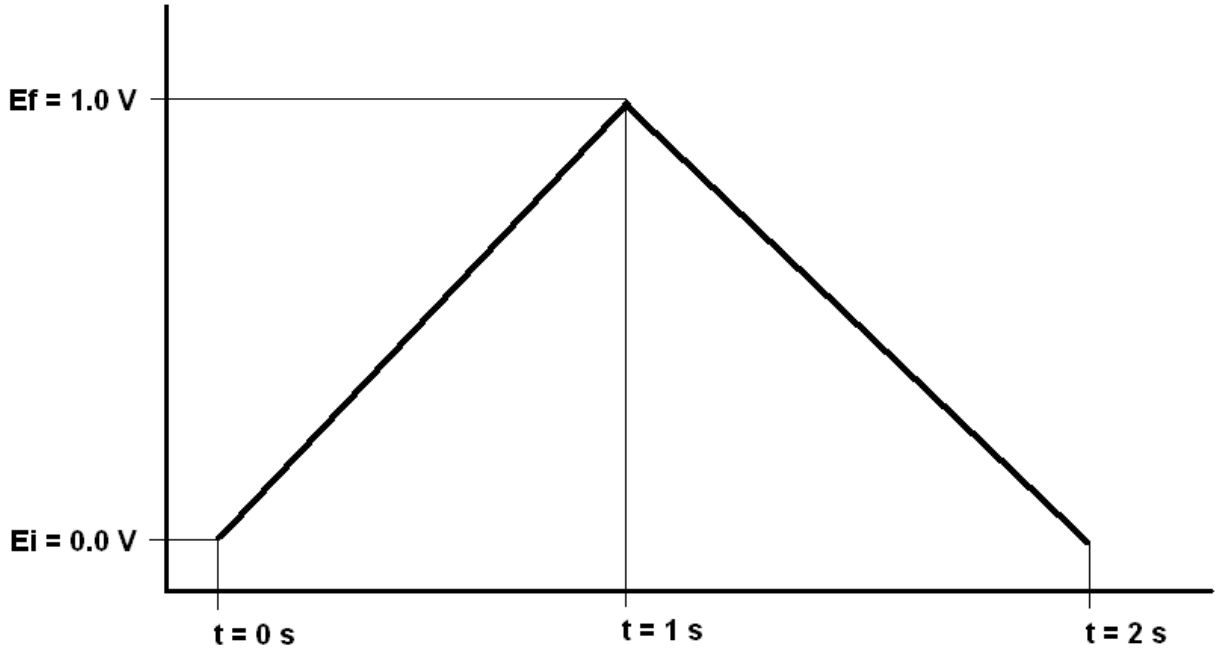

Scheme 1.9 Potential scan function used in cyclic voltammetry showing the potential difference between working and reference electrode increasing from E_i to E_f at a rate of 1 V/s, followed by a decreasing potential difference from E_f to E_i changing at the same scan rate of 1 V/s.

reference electrode in all aqueous experiments, while a silver/ silver ion reference electrode (Ag/ $AgNO_3$/ 200 mM $TBAPF_6$ in MeCN; 200 mM $TBAPF_6$ in MeCN is the filling solution to this electrode) was used for electrochemical experiments performed in acetonitrile. A platinum wire served as the counter electrode. The electrochemical cell was assembled as depicted in Scheme 1.8, using a 10 mL glass vessel to contain the solutions. A CH Instruments potentiostat equipped with a Faraday cage (the latter is used to enclose the electrochemical cell and minimize any electromagnetic interference from the surroundings) was used to run all the voltammetry.

Figure 1.1 shows a voltammogram of a solution of 1.0 mM K_3IrCl_6 in 1.0 M NaCl, which illustrates the outcome of a typical cyclic voltammetry experiment. This cyclic voltammogram of K_3IrCl_6 was recorded between +0.30 V (initial potential or E_i) and +1.00 V (high potential or E_f) vs. Ag/ AgCl/ 1.0 M NaCl, with an initial scan from +0.30 V to +1.00 V (forward scan)

followed by a return scan from +1.00 V to +0.30 V (backward scan). The potential of the glassy carbon working electrode was changed at a rate of 0.1 V/s in the forward and backward scans. The choice of potential limits for this cyclic voltammograms was made based on preliminary information that the oxidation and reduction peaks of the electro-active species involved $[IrCl_6]^{3-}$ and $[IrCl_6]^{2-}$ would appear within this potential window. In the forward scan (+0.30 V→+1.00 V) a wave of negative current appears as the potential increases past +0.65 V and a maximum appears around +0.75 V followed by a decrease in the negative current that levels-off at higher potentials. This 'negative current wave' is due to the $1e^-$ oxidation of $[IrCl_6]^{3-}$ to $[IrCl_6]^{2-}$, and it is called the anodic wave or peak of the voltammogram. The decrease of the anodic current past +0.75 V occurs because the concentration of $[IrCl_6]^{3-}$ in the vicinity of the working electrode decreases dramatically and the oxidation process becomes limited by diffusion of this species from the bulk of the solution. On the other hand, when the potential is reversed at +1.00 V toward less positive potentials, below +0.80 V a wave of positive current originates, which reaches a maximum at +0.70 V and then levels off as lower potentials are scanned. This 'wave of positive current' or cathodic wave is due to the $1e^-$ reduction of $[IrCl_6]^{2-}$, formed nearby the electrode surface in the forward scan, to $[IrCl_6]^{3-}$. The cathodic current decays because the concentration of $[IrCl_6]^{2-}$ near the electrode is depleted and the reduction reaction becomes limited by diffusion of $[IrCl_6]^{2-}$ towards the electrode surface.

In summary, from a voltammogram as that in Figure 1.1 several remarks about the redox couple $[IrCl_6]^{3-}/[IrCl_6]^{2-}$ can be made: (1) the oxidation and reduction peaks for this redox couple appear within +0.55 V and +0.85 V vs. Ag/ AgCl; (2) $E_{1/2}$ = 0.725 V; and (3) the separation between the anodic and cathodic peak potentials, E_{pa} and E_{pc}, or ΔE_p is ~60 mV, which indicates

that the $1e^-$ transfer between the couple $[IrCl_6]^{3-}/[IrCl_6]^{2-}$ and the glassy carbon working electrode is fast and electrochemically reversible.

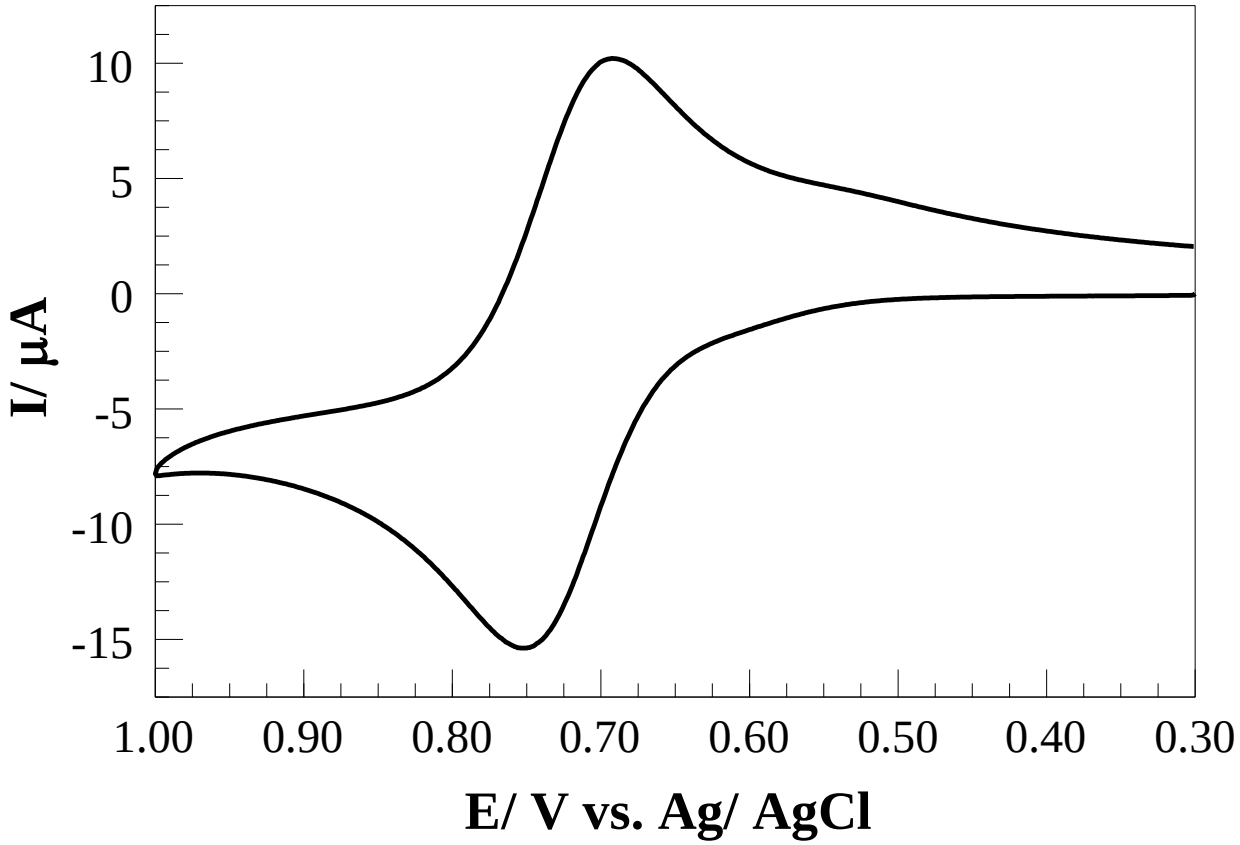

Figure 1.1 Cyclic voltammogram of a solution of 1.0 mM K_3IrCl_6 in 1.0 M NaCl, which illustrates the outcome of a typical cyclic voltammetry experiment. Glassy carbon was used as the working electrode, Ag/ AgCl/ 1.0 M NaCl was the reference electrode and a platinum wire was used as the counter electrode.

Oftentimes, the voltammetry of some electro-active molecules can be more challenging to interpret than that of the redox couple $[IrCl_6]^{3-}/[IrCl_6]^{2-}$. As an example, the cyclic voltammograms of $[IrCl_6]^{3-}$ in the presence of glutathione (GSH) that are discussed in chapters 2 and 3, which show a completely different behavior for the couple $[IrCl_6]^{3-}/[IrCl_6]^{2-}$ upon addition of the thiol, have to be simulated using DigiSim™ in order to test the validity of an electrochemical mechanism proposed and to extract kinetic and thermodynamic information

associated with that mechanism. In the next section, the process of simulating a cyclic voltammogram using DigiSim™ is described for the case of the voltammetric response of the redox pair $[IrCl_6]^{3-}$/ $[IrCl_6]^{2-}$ alone. The details of the simulations of voltammograms showing the oxidation of GSH by the different metal complexes used are given in chapters 2 and 3.

1.7.2 Digital simulations of voltammograms using DigiSim™

DigiSim™ is a software used for simulating experimentally obtained voltammograms and testing hypothetical reaction mechanisms by fitting their kinetic and thermodynamic parameters until a match between experimental and simulated voltammograms is achieved. This program is fairly simple to use and can be run in computers with Microsoft Windows as their operating system. Obtaining decent fits for experimental voltammograms is a more or less difficult task depending on the complexity of the mechanism proposed and the number or unknown simulation parameters. In addition, a fundamental knowledge of kinetics and thermodynamics of chemical and electrochemical reactions is imperative to be able to evaluate the outcomes of simulations, especially when good fits are observed.

The process of simulating voltammetric responses begins by entering an electrochemical mechanism into DigiSim™. The mechanism entered to simulate the voltammogram of the redox couple $[IrCl_6]^{3-}$/ $[IrCl_6]^{2-}$ is shown in Scheme 1.10. DigiSim™ requires a simplified notation for chemical species, usually single letters or combinations of them are acceptable. For the simulation of the CV in Figure 1.1, O was used to represent the oxidized form of the iridium complex, $[IrCl_6]^{2-}$, R was used for its reduced form $[IrCl_6]^{3-}$ and 'e' corresponded to one electron (DigiSim™ uses 'e' always to represent an electron). The sign '=' is used to represent an arrow in a chemical equation as well as a double arrow if the reaction is an equilibrium.

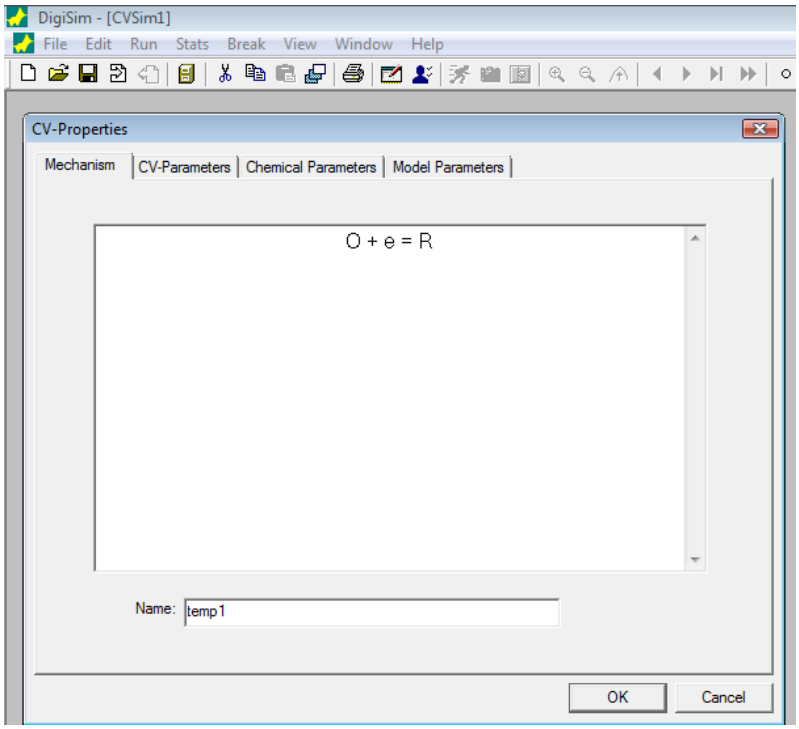

Scheme 1.10 Mechanism entered into DigiSim™ used to simulate the CV in Figure 1.1. Reproduction authorized by BASi.

After the mechanism is entered, in the next window the CV parameters are set (see scheme 1.11): initial potential (Estart in V), high potential (Erev in V), lower potential (Eend in V), scan rate (in V/s), number of cycles (1 for a single CV), uncompensated solution resistance (Ru in Ohms; usually zero), double layer capacitance (Cdl in F; normally zero for background-subtracted CV's), temperature (Temp. in K), electrode geometry (planar disk), electrode area (0.07 cm^2 for the glassy carbon electrodes used), concentration of O and R species (Canal in mol/L or m/l), diffusion mode (semi-infinite) and concentrations pre-equilibration (enabled selected).

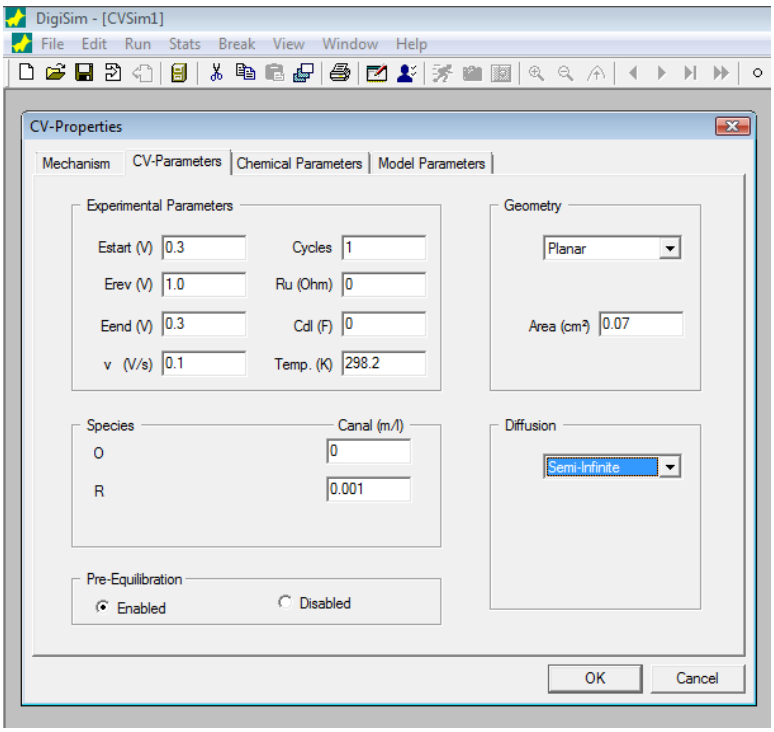

Scheme 1.11 DigiSim™ CV-Parameters window. These parameters were used to simulate the CV shown in Figure 1.1. Reproduction authorized by BASi.

The following window (scheme 1.12) contains the chemical parameters associated with the mechanism proposed. The heterogenous redox reaction O + e = R was simulated according to the Butler-Volmer model. The redox potential Eo (V) was initially estimated from the experimental CV as the half-way potential [$E_{1/2} = (E_{pa} + E_{pc})/2$]; a typical value for the α factor (0.5), a heterogeneous rate constant k_s of $1x10^4$ cm/s and diffusion coefficients for O and R of $1x10^{-5}$ cm^2/s are set by DigiSim™ as default values to start the simulation. The last window (scheme 1.13) is used to set the mode parameters inherent to the simulation program where default parameters are applied to all simulations done for this work.

Once all the parameters required by DigiSim™ were entered, the experimental CV was loaded and the fitting process started by gently adjusting the redox potential value Eo (V). When this was done, the simulated (black circles) and experimental (red line) CV's appeared overlaid as

seen in scheme 1.14A. Further adjustment of the diffusion coefficients of O and R species to $6.5x10^{-5}$ cm^2/s, Eo to 0.732 V and k_s to 0.1 cm/s drastically improved the fitting of experimental and simulated voltammetric responses (see scheme 1.14B).

The 'rate' of fitting or maximum change per iteration can be set manually for each chemical parameter or for several parameters changing at the same time. Usually, small changes per iteration are applied to previously known or estimated parameters (e.g. Eo, k_s or diffusion coefficients, which can be consulted in the literature or estimated from other experiments) and larger change rates are applied to unknown parameters such as rate of reactions or equilibrium constants. As the simulation approaches a decent fit, the maximum change per iteration of a parameter(s) is lowered in order to do a fine tuning of the respective parameter value.

Simulations of experimental CV's need to hold at different voltammetric scan rates in order to consider a proposed mechanism as valid. Furthermore, kinetic and thermodynamic parameters estimated through simulation of CV's have to make sense with the mechanism proposed, with other experimental observations and with the established chemical and electrochemical theories. For example, rate constants for bimolecular reactions exceeding the diffusion controlled limit value of $1x10^{10}$ M^{-1} s^{-1} cannot be accepted even if a successful match of experimental and simulated voltammetry is obtained.

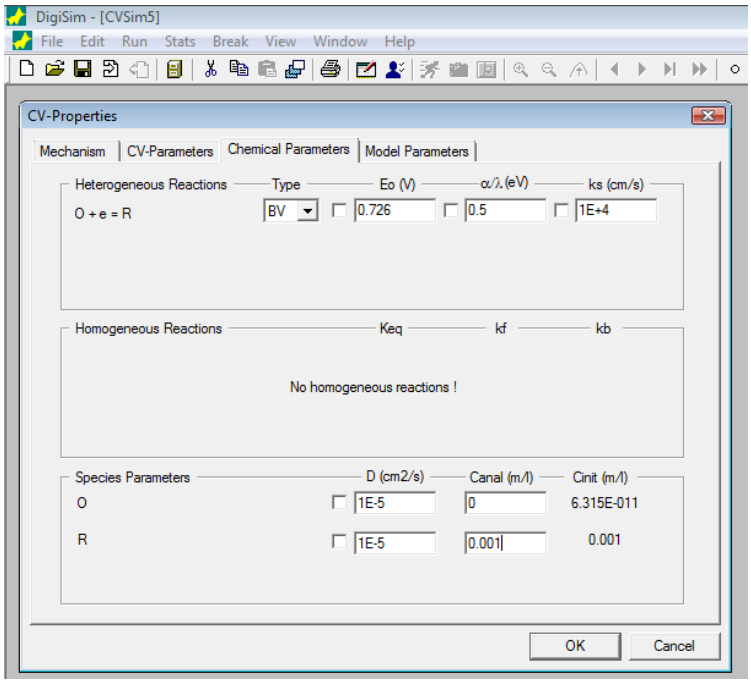

Scheme 1.12 DigiSim™ Chemical Parameters window. These parameters were used to simulate the CV shown in Figure 1.1. Reproduction authorized by BASi.

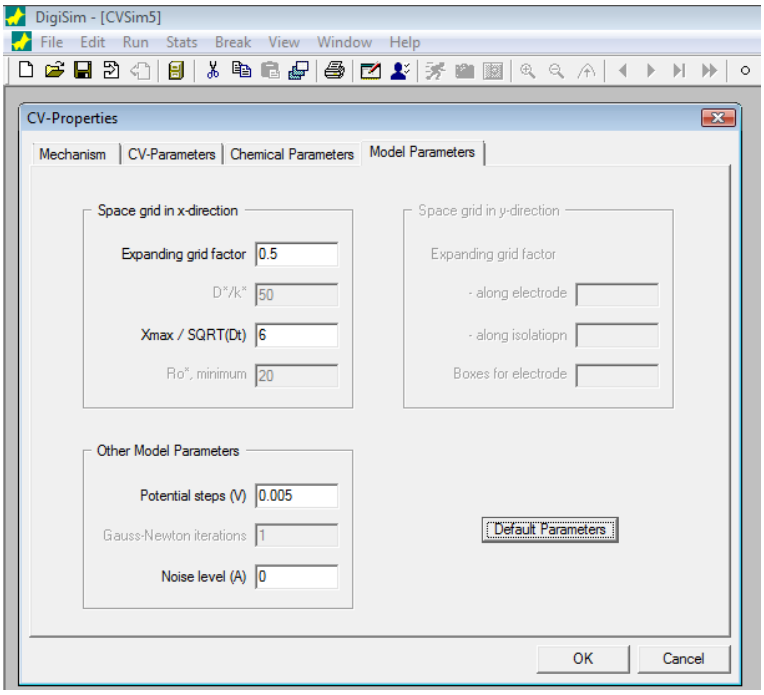

Scheme 1.13 DigiSim™ Model Parameters window. These parameters were used to simulate the CV shown in Figure 1.1. Reproduction authorized by BASi.

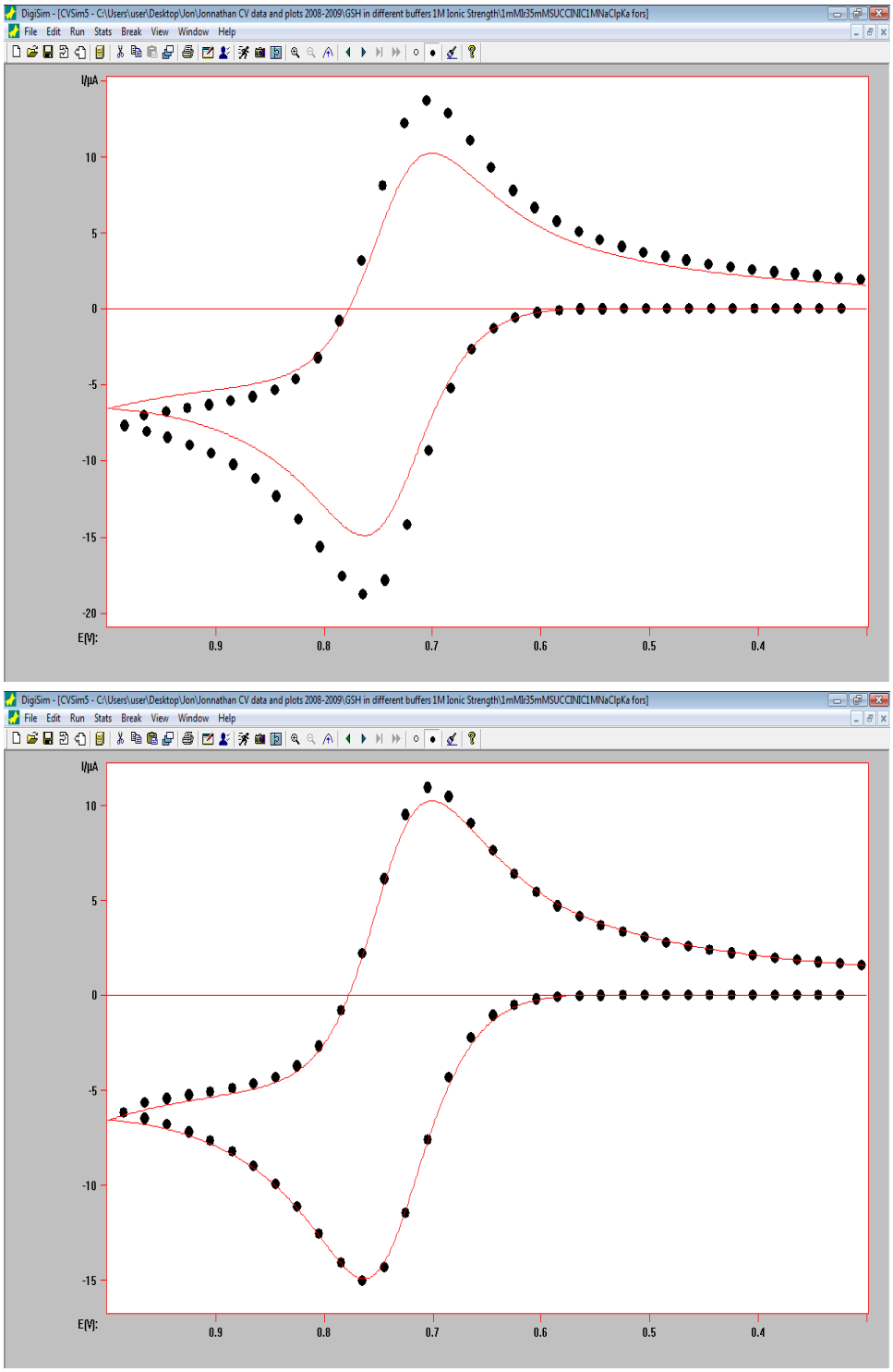

Scheme 1.14 DigiSim™ Simulation window. The top view shows the simulated (black circles) and experimental (red line) CV's before the adjusting of chemical parameters started (A). The bottom view corresponds to the final fit of the experimental and simulated CV's after adjusting Eo, k_s and diffusion coefficients of O and R (B). Reproduction authorized by BASi.

1.8 References

1. Alligrant, T. M.; Hackett, J. C.; Alvarez, J. C. *Electrochim. Acta* **2010**, *55*, 6506-6516.
2. Eigen, M. *Angew. Chem. Int. Ed. Engl.* **1964**, *3*, 1-72.
3. Fecenko, C. J.; Meyer, T. J.; Thorp, H. H. *J. Am. Chem. Soc.* **2006**, *128*, 11020-11021.
4. Fecenko, C. J.; Thorp, H. H.; Meyer, T. J. *J. Am. Chem. Soc.* **2007**, *129*, 15098-15099.
5. Hammes-Schiffer, S. *Acc. Chem. Res.* **2009**, *42*, 1881-1889.
6. Kaila, V. R. I.; Hummer, G. *J. Am. Chem. Soc.* **2011**, *133*, 19040-19043.
7. Mayer, J. M. *Annu. Rev. Phys. Chem.* **2004**, *55*, 363-390.
8. Sjodin, M.; Ghanem, R.; Polivka, T.; Pan, J.; Styring, S.; Sun, L.; Sundstrom, V.; Hammarstrom, L. *Phys. Chem. Chem. Phys.* **2004**, *6*, 4851-4858.
9. Sjodin, M.; Styring, S.; Akermark, B.; Sun, L.; Hammarstrom, L. *J. Am. Chem. Soc.* **2000**, *122*, 3932-3936.
10. Weatherly, S. C.; Yang, I. V.; Armistead, P. A.; Thorp, H. H. *J. Phys. Chem. B* **2003**, *107*, 372-378.
11. Weatherly, S. C.; Yang, I. V.; Thorp, H. H. *J. Am. Chem. Soc.* **2001**, *123*, 1236-1237.
12. Warren, J. J.; Tronic, T. A.; Mayer, J. M. *Chem. Rev.* **2010**, *110*, 6961-7001.
13. Medina-Ramos, J.; Alligrant, T. M.; Clingenpeel, A.; Alvarez, J. C. *J. Phys. Chem. C* **2012**.
14. Quan, M.; Sanchez, D.; Wasylkiw, M. F.; Smith, D. K. *J. Am. Chem. Soc.* **2007**, *129*, 12847-12856.
15. Nekrassova, O.; Kershaw, J.; Wadhawan, J. D.; Lawrence, N. S.; Compton, R. G. *Phys. Chem. Chem. Phys.* **2004**, *6*, 1316-1320.
16. Wang, X.; Stanbury, D. M. *Inorg. Chem.* **2008**, *47*, 1224-1236.
17. Madej, E.; Wardman, P. *Arch. Biochem. Biophys.* **2007**, *462*, 94-102.
18. Miyashita, T.; Matsuda, M. *Bull. Chem. Soc. Jpn.* **1985**, *58*, 3031-3032.
19. Costentin, C.; Robert, M.; Saveant, J.-M. *Acc. Chem. Res.* **2010**, *43*, 1019-1029.
20. Irebo, T.; Reece, S. Y.; Sjodin, M.; Nocera, D. G.; Hammarstrom, L. *J. Am. Chem. Soc.* **2007**, *129*, 15462-15464.
21. Ishikita, H.; Soudackov, A. V.; Hammes-Schiffer, S. *J. Am. Chem. Soc.* **2007**, *129*, 11146-11152.
22. Marcus, R. A. *Rev. Mod. Phys.* **1993**, *65*, 599-610.
23. Marcus, R. A.; Sutin, N. *Biochim. Biophys. Acta* **1985**, *811*, 265-322.
24. Alligrant, T. M.; Alvarez, J. C. *J. Phys. Chem. C* **2011**, *115*, 10797-10805.
25. *Biological Inorganic Chemistry: Structure and Reactivity*; I ed.; Bertini, I., Ed.; University Science Books, 2007.
26. Meyer, A. J.; Hell, R. *Photosynth. Res.* **2005**, *86*, 435-457.
27. Jocelyn, P. C. *Eur. J. Biochem.* **1967**, *2*, 327-331.
28. Millis, K. K.; Weaver, K. H.; Rabenstein, D. L. *J. Org. Chem.* **1993**, *58*, 4144-4146.
29. Nekrassova, O.; Allen, G. D.; Lawrence, N. S.; Jiang, L.; Jones, T. G. J.; Compton, R. G. *Electroanal.* **2002**, *14*, 1464-1469.
30. Sun, J.; Stanbury, D. M. *Dalton Trans.* **2002**, 785-791.
31. In *CRC Handbook of Chemistry and Physics (Internet Version 2011)*; 91st ed.; Haynes, W. M., Ed.; CRC Press/Taylor and Francis: Boca Raton, FL, 2011.
32. Edsall, J. T. *Biochemistry* **1965**, *4*, 28-31.
33. Danehy, J. P.; Parameswaran, K. N. *J. Chem. Eng. Data* **1968**, *13*, 386-389.

34. Benesch, R. E.; Benesch, R. *J. Am. Chem. Soc.* **1955**, *77*, 5877-5881.
35. Raoof, J. B.; Ojani, R.; Kolbadinezhad, M. *J. Solid State Electr.* **2009**, *13*, 1411-1416.
36. Raoof, J. B.; Ojani, R.; Karimi-Maleh, H. *J. Appl. Electrochem.* **2009**, *39*, 1169-1175.
37. Ahren, M. L.; Maass, G. *Angew. Chem. Int. Ed. Engl.* **1968**, *7*, 818-819.
38. Kirby, A. J. In *Encyclopedia of Life Sciences*; John Wiley & Sons: 2001.
39. Jencks, W. P. *Catalysis in Chemistry and Enzymology*; Courier Dover Publications, 1987.
40. Fox, J. P.; Page, M. I.; Satterhwait, A.; Jencks, W. P. *J. Am. Chem. Soc.* **1972**, *94*, 4731-4732.
41. Jencks, W. P. *Chem. Rev.* **1972**, *72*, 705-718.
42. Anslyn, E. V.; Dougherty, D. A. *Modern Physical Organic Chemistry*; University Science Books, 2006.

Chapter 2:

'Buffer effects in the kinetics of concerted proton-coupled electron transfer (PCET): the electrochemical oxidation of glutathione (GSH) mediated by $[IrCl_6]^{2-}$ *at variable buffer* pK_a *and concentration'*

2.1 Introduction

This paper describes a series of buffer effects in the kinetics of a proton-coupled electron transfer (PCET) that seem to decide the *concerted* character of the reaction. The oxidation of the naturally occurring thiol glutathione (GSH), by the electrogenerated mediator $[IrCl_6]^{2-}$ in the presence of a base, (B = HPO_4^{2-}), was studied in buffered and un-buffered solution using cyclic voltammetry (Scheme 2.1). The evidence indicates that the reaction is slightly accelerated by proton acceptors such as HPO_4^{2-} or $H_2PO_4^-$ present in the buffer, when they accept the H^+ released during the GSH oxidation (Scheme 2.1). This favorable effect is manifested when the phosphate buffer concentration is raised at constant pH (5.0 or 7.0). The evidence also shows that the rate acceleration happens in a pH range when GS^- can barely exist (*i.e.* only2 % of GSH is deprotonated at pH 7.0) and despite of the phosphate species being bases weaker than GSH (*i.e.* $pK_{aH3PO4-} = 2.1 < pK_{aH2PO4-} = 7.2 < pK_{aSH} = 8.7$). Thus, the PT from GSH to B is thermodynamically unfavorable for either phosphate base. To explain these results, along with the observation that $[IrCl_6]^{2-}$ hardly oxidizes GSH in un-buffered neutral solution, we propose that B accepts the H^+ at the PCET *transition state* (Scheme 2.1) rather than directly from the reactant GSH. This hypothesis, which in essence expresses the *libido* rule of *general acid-base catalysis*,[1] seems plausible when realizing that the acidity of the S-H bond should increase as GSH gets oxidized by $[IrCl_6]^{2-}$. Such expectation is not unreasonable, given that the orbitals involved in the oxidation and deprotonation of SH, are in the same atomic center and therefore can affect each other greatly.

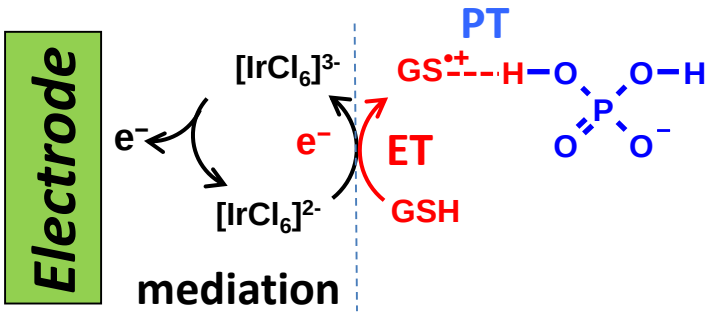

Scheme 2.1 Base catalysis of PCET in phosphate buffer at pH = 7.0 or lower.

The *libido* rule initially introduced by Jencks,[1b, c] establishes the mechanistic hallmarks that determines the *concerted* character of reactions coupled to PT. As such, this rule states that: "*concerted general acid-base catalysis* of reactions coupled to PT in aqueous solution can occur only at sites that undergo a large change in pK in the course of the reaction and when this change in pK converts an unfavorable to a favorable PT with respect to the catalyst, *i.e.* the pK of the catalyst is intermediate between the initial and final pK values of the substrate site."[1b, c] The study of many of the reactions that follow this rule, have provided a few mechanistic insights.[1b, c] For instance, the *concerted* pathways occur simply in order to avoid the high-energy intermediates usually encountered in the corresponding *stepwise* reactions.[1b, c] Hence, the concerted paths can only be important if the free energy requirements for their *transition state* are balanced by the extreme instability in the *transition state* of the corresponding *stepwise* reactions.[1b, c] Furthermore, because the *concerted* reaction requires an additional loss of entropy to include a properly positioned catalyst molecule in the *transition state*, (in this case B), the free energy gained from the favorable ΔpK with the transition state, has to be more than enough to compensate the negative entropy.[1b, c] For the past fifty years, the *libido* rule and its ramifications have been amply confirmed in many reactions that are coupled to PT and by virtue of it,

susceptible of being catalyzed by acids or bases.[1a] Most of them however involve the breaking or formation of bonds at carbon centers like in the case of condensations, substitutions and isomerizations.[1a] Interestingly, these principles seem to also be applicable to ET reactions that do not involve breaking or formation of bonds, and are just merely coupled to PT, namely PCET.[2] In the last seven years, considerations similar to what the *libido* rule states have been proposed independently by different groups who have studied chemical and electrochemical PCET systems including buffer effects.[3] In particular, Saveant, Meyer and Thorp,[3d-g] who have recognized the ΔpK parameter (see above) as key marker that determines the *concerted* or *stepwise* nature of these reactions and in accord with the principles originally proposed by Jencks.[1b, c]

The present work is an attempt to help the understanding of the complex effects that buffers can induce in PCET reactions, which in certain instances have led to some debate.[3b, c, 4] We are aware that in terms of magnitude, the kinetic effects described here (a mere six-fold increase in the reaction rate) do not represent an exemplary case of catalysis. However, it turns out that the GSH oxidation displays all the experimental and mechanistic characteristics of a predominantly *concerted* PCET obeying the *libido* rule of *general base catalysis*. As a matter of fact, the experiments in this work were designed following the criteria typically used to determine *acid-base catalysis* by changing the buffer concentration and buffer pK_a.[1, 5] We believe this approach may benefit the ongoing research in PCET, because the essence of the *acid-base catalysis* approach is to account for the role of acids and bases (buffers) in the kinetics of reactions coupled to PT, of which PCET is just one type. This approach as outlined by Jencks, offers a comprehensive view of the possible mechanistic scenarios and conditions that control them. There are two types of rates, whenever a reaction is coupled to a PT regardless of the sequence

or the reaction that is coupled to.[1a, 5] These two cases arise from the PT being the rate determining step (RDS) or not.[1a, 5] Thus, if the PT occurs in a fast equilibrium and is not the RDS, the overall rate will depend on the pH but not on the concentration of acids or bases comprising the buffer, because they will not appear in the rate law.[1a, 5] On the other hand, if the PT is involved in the RDS, then besides being pH-dependent, the rate will also depend on the buffer concentration because now its components will show up explicitly in the rate law.[1a, 5] Like so, a *concerted* PCET will most likely occur in the latter scenario because in such a case the PT will take place at the *transition state* of the RDS. As a consequence, there will be a range of buffer concentration in which the reaction will be kinetically controlled when limited supply of acid or base to the *transition state* becomes prevalent. Conversely, the reaction will reach diffusion control when the buffer provides enough acid or base to the *transition state* so that the observed rate does not increase any longer as a function of the buffer concentration. This diffusion limited rate may not be as fast as it is for bimolecular reactions because the *concerted transition state* will have three reactants.

We believe that the catalytic effects shown by the GSH oxidation are not huge because the PT involves sulfur which is a fairly electronegative atom. It is well documented that PT involving elements like O, S and N tend be pretty fast, sometimes even diffusion limited.[5-6] Therefore, reactions coupled to PT involving these elements should have a narrow window of concentration before they reach their diffusion controlled rate. On the other hand, the principles of *acid-base catalysis* were established mostly with non-ET reactions comprising the breaking and formation of bonds on carbon centers, which may increase the entropic toll for any *concerted* pathway.[1a, 1c, 5] In that way, the range of concentration available for an acid or a base to accelerate these reactions before their diffusion limit would be wider, in addition to the fact that PT on carbon

atoms can be quite slow.[1a, 1c, 5] This work is an extension of our previous efforts to facilitate PCET reactions by *in-situ* electrogeneration of acid or by hydrogen bonding with Brönsted bases.[7]

Scheme 2.2 shows the reduced form of GSH, which is a tri-peptide that contains four pH-active functional groups including two carboxylic acids (pK_{a1} = 2.1, pK_{a2} = 3.5) a thiol (pK_{a3} = 8.7) and an amine (pK_{a4} = 9.7).[8] The thiol group undergoes a one electron oxidation to form a thiyl radical that can dimerize into a disulfide species. In this work, we monitor the oxidation of GSH at different conditions of pH, buffer pK_a, and buffer concentration by cyclic voltammetry.

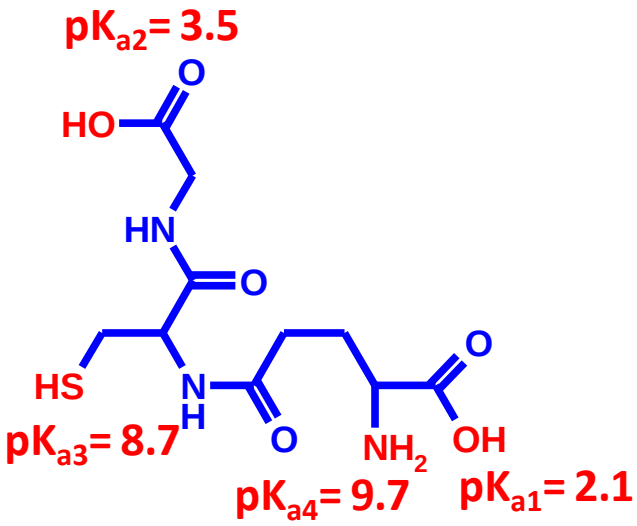

Scheme 2.2 Glutathione (GSH)

Digital simulations (DigiSim™) fitted to the experimental voltammograms were used to evaluate the proposed and discarded mechanisms. We employed similar simulation strategies as Thorp and Meyer have used in other analogous mediation systems.[9] The diffusion coefficient for GSH, used in the digital simulations was determined by NMR.

2.2 Experimental Section

2.2.1 Reagents and Materials

Reduced L-glutathione (Aldrich, 99%), potassium hexachloroiridate III (K_3IrCl_6, Aldrich), sodium hydroxide (NaOH, Aldrich, 99.9%), sodium chloride (NaCl, Aldrich, 99.9%), sodium deuteroxide (NaOD, Aldrich, 40 % wt. in D_2O, 99 + % atom D), deuterium oxide (D_2O, Acros Organics, 100.0 % atom D), sodium hydrogenphosphate (Na_2HPO_4, EM Science, 99%), sodium di-hydrogen phosphate (NaH_2PO_4, EM Science, 98%), potassium dideuterium phosphate (D_2PO_4, Sigma Aldrich, atom 98% D), hydrochloric acid (HCl, Fisher Scientific, 37.3%), maleic acid (Fluka, $\geq$99.0%), citric acid monohydrate (Fluka, >99.5%), malic acid (Fluka, >99.5%) and succcinic acid (Fluka, >99.5%) were used without further purification. The pH of all solutions was measured with an Oakton pH meter (pH 1100 series), calibrated with pH 4.00, 7.00, and 10.00 buffers (Microesential Laboratory, Brooklyn, NY). Diluted NaOH and HCl (~0.1 M) were used to adjust the pH when required. All solutions were prepared using deionized (DI) water with a resistivity of 18.2 MΩ cm; water was purified with a MilliQ purification system (Billerica, MA). Deuterated phosphate buffer solutions were prepared by mixing D_2PO_4 and NaOD in D_2O to attain the desired pD of 7.0. The measured pH (Oakton pH meter 1100 series) was converted to pD by using formula pD = pH + 0.4.[10] All experiments were carried out in a solution volume of 10.00 mL at room temperature (22 ± 1 °C) with deoxygenation using nitrogen or argon. A nitrogen/argon atmosphere was maintained inside the electrochemical cell during experiments.

Reduced L-glutathione (Aldrich, 99%), potassium hexachloroiridate III (K_3IrCl_6, Aldrich), sodium hydroxide (NaOH, Aldrich, 99.9%), sodium chloride (NaCl, Aldrich, 99.9%), deuterium oxide (D_2O, Aldrich, 99.9%), sodium hydrogenphosphate (Na_2HPO_4, EM Science, 99%), sodium

di-hydrogen phosphate (NaH_2PO_4, EM Science, 98%), hydrochloric acid (HCl, Fisher Scientific, 37.3%), maleic acid (Fluka, ≥99.0%), citric acid monohydrate (Fluka, >99.5%), malic acid (Fluka, >99.5%) and succcinic acid (Fluka, >99.5%) were used without further purification. The pH of all solutions was measured with an Oakton pH meter (pH 1100 series), calibrated with pH 4.00, 7.00, and 10.00 buffers (Microesential Laboratory, Brooklyn, NY). Diluted NaOH and HCl (~0.1 M) were used to adjust the pH when required. All solutions were prepared using deionized (DI) water with a resistivity of 18.2 MΩ cm; water was purified with a MilliQ purification system (Billerica, MA). All experiments were carried out in a solution volume of 10.00 mL at room temperature (22 ± 1 °C) deoxygenated with nitrogen. A nitrogen atmosphere was maintained inside the electrochemical cell during experiments.

2.2.2 Cyclic Voltammetry

Cyclic voltammograms (CV's) were collected using a potentiostat (CH Instruments, Austin, TX) with a regular glass cell equipped with a glassy carbon (GC) working electrode (area = 0.07 cm^2), a Pt-wire counter electrode, and Ag/AgCl reference electrode (1.0 M KCl). The glassy carbon electrode was polished with 0.05 µm alumina mixed with deionized water on a Buehler cleaning pad (Lake Bluff, Illinois) and rinsed with DI water between experiments. Working solutions contained 1.00 mM K_3IrCl_6 and 3.00 mM of reduced L-glutathione dissolved in 10.00 mL of variable mM concentration of buffer with NaCl added to maintain an ionic strength of 1.0 M. The potential was scanned from 0.30 V to 1.00 V vs. Ag/ AgCl/ 1.0 M KCl. The CV's were background subtracted and obtained at room temperature. The half-wave potential $E_{1/2}$ which is directly measurable from a CV, was regarded as approximately equal to the redox potential

reduction E°, thus assuming that the diffusion coefficients for both species in the redox couple were very similar.[11]

2.2.3 Digital Simulations and Fitting

Experimental CV obtained at different conditions of pH, buffer pK_a/concentration and scan rate were simulated with DigiSim™ version 3.03 (Bioanalytical Systems, Inc., West Lafayette, IN). For a particular buffer concentration and pH, the CV's were recorded at five scan rates: 0.1, 0.2, 0.3, 0.4 and 0.7 V/s and the concentrations of all species that were entered in DigiSim were the actual values used in the experiments. The buffers and pK_a's used were: malic (5.11), maleic (6.20), succinic (5.64), citrate (6.40), and phosphate (7.21). The variable concentration range for pH 7.0 of phosphate buffer was 0.0, 5.0, 10.0, 20.0, 35.0, 50.0, 100 and 200 mM. At 35.0 mM of phosphate buffer the different pH values were: 4.0, 5.0, 6.0, 7.2, 8.0, 9.0 and 10.0. The Brönsted plots were constructed at 35.0 and 5.0 mM of each buffer adjusting the pH to the pK_a of the corresponding buffer. Every parameter that was obtained through DigiSim was iteratively fitted and its corresponding standard deviation was determined from fitted values obtained at the scan rates listed above. Some electrochemical parameters like the half-wave redox potential ($E_{1/2} \approx E°$), the transfer coefficient (α) and the electrochemical rate constant (k_s), were established by fitting CV's at the conditions needed in independent experiments. For instance, the electrochemical parameters obtained after fitting for pure $[IrCl_6]^{3-}$ in 35.0 mM of phosphate buffer pH 7.0 were: E° = 0.72 V vs. Ag/AgCl/1M KCl, $\alpha = 0.5$ and $k_{s1} = 0.1$ cm/s.

Scheme 2.3 shows the mechanism comprising the reactions that were considered for the simulation. The GSH oxidation by $[IrCl_6]^{2-}$ was written in Digisim as: $G + [IrCl_6]^{2-} = G^{\bullet} + [IrCl_6]^{3-}$ (Eq. 2.2), where G symbolizes the reactant species GSH and $G^{\bullet}$ represents the products

$GS^{\bullet} + H^{+}$. By introducing reaction 2 as a compound process without the explicit appearance of the B and H^{+}, the match between simulated and experimental CV's improved greatly because of the reduced number of parameters to fit. Thus, the forward rate constant, k_{f2}, was regarded as k_{obs} representing all possible pathways in the mechanism, that is, PT-ET, ET-PT and the *concerted* PCET. Given that at 25 °C $K = 10^{nE°/0.059}$, the equilibrium constant K_2 was automatically set by DigiSim once the values of E° for each redox couple involved was introduced, namely, $[IrCl_6]^{2-}/[IrCl_6]^{3-}$ and $G^{\bullet}/G$ (or $GS^{\bullet},H^{+}/GSH$). The E° value for $[IrCl_6]^{2-}/[IrCl_6]^{3-}$ was estimated from fitted simulations of experimental CV's recorded for the pure mediator at the required conditions.

$[IrCl_6]^{2-} + e^{-} = [IrCl_6]^{3-}$ (2.1) E° and k_{s1} obtained from fitted experimental CV's.

$G + [IrCl_6]^{2-} = [IrCl_6]^{3-} + G^{\bullet}$ (2.2) k_{obs} estimated from fitted CV's; K_2 is automatically set by the E° values for reactions (2.1) and (2.3).

$G = G^{\bullet} + e^{-}$ (2.3) $E°_{app}$ was estimated by Eq. 2.7; k_{s3} was fitted by DigiSim.

$G^{\bullet} + G^{\bullet} = GG$ (2.4) K_4 and kf_4 were fitted by DigiSim.

$G^{\bullet} + [IrCl_6]^{2-} = [IrCl_6]^{3-} + G'$ (2.5) K_5 and k_{f5} were fitted by Digisim (overoxidation)

$[IrCl_6]^{2-} = P$ (2.6) K_6 and kf_6 obtained from fitted experimental CV's

Scheme 2.3. Reaction mechanism entered into DigiSim™ to simulate experimental CV results.

Madej has shown that in buffered solution, the apparent redox reduction potential ($E°_{app}$) for $GS^{\bullet},H^{+}$/GSH, follows a pH Nernstian behavior with an approximate slope of ~0.06 V/pH-unit in the pH range 3.0 to 8.0.[12] This slope becomes 0 V/pH-unit above pH ~10.0 when all functional groups in GSH are deprotonated and the $E°_{app} = E°(GS^{\bullet}/ GS^{-})$.[12] We employed the Nernst expression reported by Madej (Eq. 2.7) to calculate the $E°_{app}$ values entered in Digisim for reaction 3. We used $K_{aSH} = 8.7$ and $E°(GS^{\bullet}/GS^{-}) = 0.8$ V vs NHE (0.58 V vs. Ag/ AgCl), which were the values assumed Madej as well.[12]

$$E°_{app} = E°(GS^{\bullet}/GS^{-}) + 0.059 \log\left(1 + \frac{[H^{+}]}{K_{aSH}}\right) \quad (2.7)$$

Once GSH (G) is oxidized by $[IrCl_6]^{2-}$, the thiyl radical $GS^{\bullet}$ ($G^{\bullet}$) is dimerized to the disulfide GSSG represented as GG in Eq. 2.4. Sulfur radical annihilations are known to be very fast with rate constant values of up to ~10^9 M^{-1} s^{-1}.[13] The best simulation fittings were obtained when the equilibrium constant K_4 was in the range 10^9-10^{10} and the forward rate constant k_{f4} was between 10^8 and 10^9 M^{-1} s^{-1}. A K_4 of ~2.3 x 10^{27} ($E° = 1.10$ V for $GS^{\bullet}$/GSSG) can be estimated based on the E° (vs. NHE) values at pH 7.0 for the redox couples $GS^{\bullet},H^{+}$/GSH (0.90 V from Eq. 2.7) and $GSSG,H^{+}$/GSH (+0.093 V).[14] The parameters for reaction 4 that worked well in the simulations (*i.e.* $K_4 = 1$ x 10^9 and $k_{f4} = 5$ x 10^8) show a fairly irreversible dimerization of $GS^{\bullet}$ with a forward rate complying with the literature value and faster than reaction 2, which has to be the case if the PCET is the rate determining. Reaction 5 was proposed to account for other chemical reactions different than the dimerization of the thiyl radical to generate higher sulfur oxidation states from $GS^{\bullet}$ and yield products represented as G'. This type of reaction is commonly known as a *thiol overoxidation* and occurs when thiyl radicals are oxidized by metal complexes.[15] The

equilibrium and forward rate constants for reaction 5 were labeled as K_5 and k_{f5} respectively. Although the influence of reaction 5 was especially evident in simulations at higher concentration of buffer, it is reaction 2 that determines the peak potential and 90 % of the observed peak current in all CV's. Thorp and coworkers, have also proposed an analogous overoxidation reaction in the electrochemical oxidation of guanine and DNA by the mediator $Ru(bpy)_3^{3+}$.[9b, 16] Reaction 6 was included to account for some decomposition of $[IrCl_6]^{2-}$ in which P represents an unidentified degradation product.[17]

2.2.4 Diffusion Coefficients

The value of $D_{[IrCl6]3-/[IrCl6]2-}$, (7 ± 1) x 10^{-6} cm^2/s, was obtained the from fitted simulations of CV's for $[IrCl_6]^{3-}$ alone and it is comparable to the reported value of $D_{[IrCl6]3-}$ = 8.20 x 10^{-6} cm^2/s.[18] The diffusion coefficient for GSH was determined in D_2O through Pulsed Gradient Echo (PGE-) ^{1}H-NMR on a Varian Inova 400MHz NMR at 25 °C. The NMR samples were prepared in an argon atmosphere and placed in clean NMR tubes (400 MHz, 5 mm, 7 in. length, Norell, Inc. Landisville, NJ). The applied gradients in the PGE-^{1}H NMR experiments were calibrated by measuring the diffusion coefficient of HDO[19] (2.23×10^{-5} cm^2 s^{-1}, at 25 °C, 0.03%) in a D_2O sample and the diffusion coefficient of 1,6-diaminohexane[20] (6.98×10^{-6} cm^2 s^{-1}, at 25 °C, 6.8%). To correct for viscosity differences between deuterated water without electrolytes (NaCl and buffer) and isotopically nonenriched water with electrolytes, the relation $Dc = (\eta_{D2O}/\eta)\, D_{NMR}$ was applied. Here, Dc is the corrected diffusion coefficient, η_{D2O} is the viscosity of deuterium oxide at 25 °C (1.09622 mPa·s)[21] η is the viscosity of nonenriched water with electrolytes in mPa·s at 25 °C and D_{NMR} is the value determined from NMR measurements.[19c] The average diffusion coefficient of glutathione after correction for viscosity differences was

$(5.13 \pm 0.05) \times 10^{-6}$ cm^2 s^{-1}. This diffusion coefficient value was used in all simulations. The diffusion coefficients for the buffers components were obtained from the CRC Handbook of Chemistry and Physics (see Appendix 2).[22]

2.3 Results and Discussion

2.3.1 Mechanistic pathways and rate laws

Scheme 2.4 shows the different steps in the oxidation of GSH, which takes place in two major stages, the first, is the PCET that generates the thiyl radical $GS^{\bullet}$ and the second is the dimerization reaction that leads to the final product GSSG. The evidence shows that in some conditions of pH and buffer concentration the PCET is rate determining and in others is not. For that reason the experiments in this work, always start in conditions in which the PCET is rate limiting but gradually change into a scenario where that is no longer the case. At this point, we believe the overall reaction proceeds as fast as it is allowed by the dimerization of the thiyl radical. Scheme 2.4 also illustrates the three possible pathways (Eq. 2.8–2.12) by which the PCET part of the reaction can occur. The homogeneous oxidation of GSH by the electrogenerated mediator $[IrCl_6]^{2-}$ produces $GS^{\bullet}$, $[IrCl_6]^{3-}$ and BH^+. The species B represents the main proton acceptor for the PCET and it can come from the buffer system B/BH^+ or the solvent. Pathways 1 and 3 are the stepwise routes PT-ET and ET-PT, respectively, whereas pathway 2 is the *concerted* mechanism in which the PT and ET occur in one single kinetic step.

The species B corresponds to HPO_4^{2-} in Scheme 2.1 and its conjugate acid BH^+ represents $H_2PO_4^-$. Likewise, when the proton acceptor is $H_2PO_4^-$, H_3PO_4 is the corresponding conjugate acid BH^+. For simplicity, the direct reactions of $[IrCl_6]^{3-}$ and GSH at the electrode surface are not shown in Scheme 2.4. Equally, the secondary oxidation of $GS^{\bullet}$ (Eq. 2.5) that was introduced

in the simulations to account for the overoxidation of the thiyl radical, presumably leading to other sulfur oxidation states (*i.e*. sulfones, sulfoxides),[15] is also omitted. The kinetic analysis to derive the rate laws for pathways 1 to 3 (Eq. 2.14A-2.14C), assumes that the dimerization of the thiyl radical to produce the disulfide GSSG (Eq. 2.13) is faster than any of the PCET pathways generating $GS^{\bullet}$. This assumption is true when running experiments in condition in which the PCET is rate limiting and is also supported by reports indicating that sulfur radical annihilations are usually fast enough to produce rates in the range of $\sim 10^9$ M^{-1} s^{-1}.[13] Hence, for conditions in which the PCET is rate determining, the rate of the overall reaction can be expressed in terms of the $GS^{\bullet}$ production rate (Eq. 2.14A-2.14C). The species GS^- and $GSH^{\bullet+}$ are intermediates for the *stepwise* pathways 1 and 3, respectively. Their corresponding rate expressions were derived considering the steady state approximation for each intermediate (see Appendix 2).

The best matches for the simulations were attained with Scheme 2.3, which does not consider explicitly any of the pathways (see experimental section). When simulating routes 1 or 3 directly, we tried several combinations of rate and equilibrium constants, however the matches were never better than with Scheme 2.3 and in some cases the fitting only occurred at low buffer concentration or after unrealistic changes to the diffusion coefficient for GSH, which we measured very accurately by NMR. Furthermore, the kinetic parameters estimated from the fitted simulations using Scheme 2.3 show the PCET being slower than the dimerization of the thiyl radical. For all the conditions tried in this work, the estimated rate constants (see supporting information) for the dimerization of $GS^{\bullet}$, are in the same order of magnitude (10^8 - 10^9 M^{-1} s^{-1}) as the reported values.[13] The forward rate constant for the reaction between GSH and $[IrCl_6]^{2-}$ (Eq. 2.2) was regarded as k_{obs} and each simulated CV recorded at a specified condition provided one value of k_{obs} (see experimental section).

Stepwise 1

$$GSH + B \underset{k_{-PT1}}{\overset{k_{PT1}}{\rightleftharpoons}} GS^- + BH^+ \quad (2.8)$$

$$GS^- + IrCl_6^{2-} \xrightarrow{k_{ET1}} GS^\bullet + IrCl_6^{3-} \quad (2.9)$$

Concerted 2

$$GSH + B + IrCl_6^{2-} \xrightarrow{k_{B2}} GS^\bullet + BH^+ + IrCl_6^{3-} \quad (2.10)$$

Stepwise 3

$$GSH + IrCl_6^{2-} \underset{k_{-ET3}}{\overset{k_{ET3}}{\rightleftharpoons}} GSH^{\bullet+} + IrCl_6^{3-} \quad (2.11)$$

$$GSH^{\bullet+} + B \xrightarrow{k_{PT3}} GS^\bullet + BH^+ \quad (2.12)$$

$$GS^\bullet + GS^\bullet \xrightarrow{fast} GSSG \quad (2.13)$$

$$Rate_1 = \frac{k_{PT1}\,k_{ET1}\,[B]\,[GSH][IrCl_6^{2-}]}{k_{-PT1}\,[BH^+] + k_{ET1}\,[IrCl_6^{2-}]} = k_{obs1}\,[GSH][IrCl_6^{2-}] \quad (2.14A)$$

$$Rate_2 = k_{B2}\,[B]\,[GSH][IrCl_6^{2-}] = k_{obs2}\,[GSH][IrCl_6^{2-}] \quad (2.14B)$$

$$Rate_3 = \frac{k_{PT3}\,k_{ET3}\,[B]\,[GSH][IrCl_6^{2-}]}{k_{PT3}\,[B] + k_{-ET3}\,[IrCl_6^{3-}]} = k_{obs3}\,[GSH][IrCl_6^{2-}] \quad (2.14C)$$

Scheme 2.4. Pathways for the oxidation of GSH by $[IrCl_6]^{2-}$ in the presence of a buffer system B/BH^+. The rate expressions are derived assuming that any of the pathways 1 to 3 are rate limiting.

2.3.2 General base catalysis: effects of pH and phosphate buffer concentration

Figure 2.1 shows the background subtracted CV's for different solutions at 1.0 M ionic strength and using glassy carbon as the working electrode and Ag/AgCl as the reference electrode. Every CV in Figure 2.1 shows a forward oxidation scan from 0.30 to 1.0 V and a reverse reduction scan that returns to the initial potential value. Voltammogram A is the response for pure mediator showing an oxidation peak at 0.75 V for the conversion of $[IrCl_6]^{3-}$ to $[IrCl_6]^{2-}$ and a reduction peak at 0.69 V comprising the opposite reaction during the reverse scan. The fact that both peaks appear pretty symmetric in shape to one another and render almost the same values of current, indicates that, the conversion between the two oxidation states of the mediator, is reversible and is unperturbed by other chemical reactions.

The inset in Figure 2.1 shows the CV for a solution of pure GSH under the same conditions but the absence of voltammetric peaks reveals that the kinetics for the GSH oxidation directly at the electrode surface in this potential window is extremely slow on glassy carbon. Voltammogram B shows the response for a mixture of $[IrCl_6]^{3-}$ and GSH in an un-buffered solution with an apparent pH of 7.6. The CV shows the reversible conversion between $[IrCl_6]^{3-}$ and $[IrCl_6]^{2-}$ somewhat perturbed by GSH, with the oxidation and reduction peaks displaying slightly different values of current and potential than in the CV for pure $[IrCl_6]^{3-}$. The degree of GSH oxidation that appears to occur under un-buffered neutral conditions is very low because the enhancement of the CV oxidation peak is very small (see below).

Voltammograms C and D display the response for the same mixture of $[IrCl_6]^{3-}$ and GSH but in a solution with phosphate buffer at pH 5.0 and 7.0, respectively. At pH 5.0 the oxidation peak of the CV is larger whereas the reduction peak becomes smaller in comparison to the corresponding peaks in the CV for pure mediator. This implies that the reaction between GSH

and electrogenerated $[IrCl_6]^{2-}$ is starting to occur at pH 5.0 and this trend is amplified when the pH is raised to 7.0 as shown in voltammogram D. The circles superimposed on the CV line denote the fitted simulation obtained following the mechanism in Scheme 2.3 (see experimental section). In voltammogram D at pH 7.0, the reduction peak has disappeared completely and the current for the oxidation peak is enhanced significantly. This is typical "mediation" behavior in which the reduction of $[IrCl_6]^{2-}$ back to $[IrCl_6]^{3-}$ is no longer observed on the reverse scan because the $[IrCl_6]^{2-}$ electrogenerated is being depleted from the electrode surface as it oxidizes GSH to produce additional $[IrCl_6]^{3-}$. Consequently, the extra current observed in the oxidation peak of voltammogram D is directly related to the ET reaction between GSH and $[IrCl_6]^{2-}$.

The normalized current for GSH oxidation, I_{GSH}, is defined as $[(I_{M\text{-}GSH}/I_M) -1]$ where $I_{M\text{-}GSH}$ is the oxidation peak current for the mixture of mediator (M) and GSH, while I_M is the oxidation peak current for pure M. So when there is no GSH oxidation $I_{M\text{-}GSH} = I_M$ and I_{GSH} approaches 0. The parameter I_{GSH} has no units but is an experimental factor that expresses how high the current for the GSH oxidation is in respect to the current for the mediator alone. The closer the value of I_{GSH} is to 0, the less GSH oxidation is occurring. Thus, the I_{GSH} value of 0.1 estimated from the CV recorded in un-buffered neutral solution reflects a finite but very low level of GSH oxidation. Conversely, the I_{GSH} values of 0.8 (Fig. 1C) and 4.0 (Fig. 1D) are indicative of low and high levels of GSH oxidation, respectively. The presence of an abnormally high background current at potentials more positive than the oxidation peak in CV's B and C is attributed to the current produced by GSH directly at the electrode as observed for pure GSH in the inset of Figure 2.1. Two corollaries can be drawn from the CV's in Figure 2.1: first, there has to be a proton acceptor in solution for the GSH oxidation to occur, and second, the concentration of the proton acceptor and the pK_a of its conjugate acid, determine the peak current associated with the GSH oxidation.

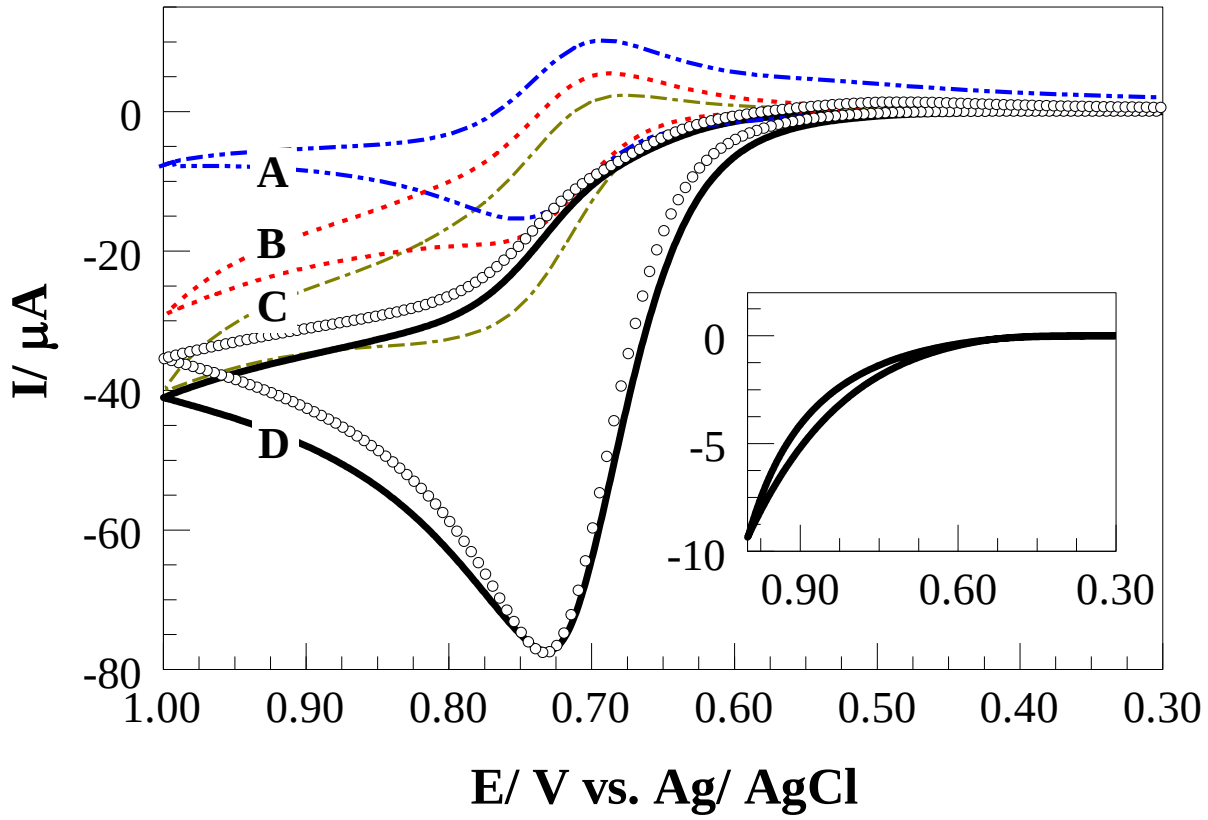

Figure 2.1 CV response of 1.00 mM K_3IrCl_6 in the presence of 35.0 mM phosphate buffer pH 7.2 **(A)**; 3.00 mM GSH + 1.00 mM K_3IrCl_6 un-buffered solution with apparent pH of 7.6 **(B)**; 3.00 mM GSH + 1.00 mM K_3IrCl_6 in the presence of 35.0 mM phosphate buffer pH 5.0 **(C)** and pH 7.0 **(D)**, respectively. The simulated CV response for **(D)** is also shown (open circles). Inset: CV of 3.00 mM GSH + 35.0 mM phosphate buffer pH 7.0. CV scan rate: 0.1 V/s

The trends in Figure 2.1 were further corroborated by doing experiments in a wider range of pH and phosphate buffer concentrations. Figure 2.2A shows the normalized current I_{GSH} at different pH values, both in buffered and un-buffered conditions. Buffered solutions were prepared with phosphate buffer at the indicated pH, whilst the pH of the un-buffered solutions was adjusted prior to each experiment by addition of either diluted HCl or NaOH as needed. Figure 2.2A confirms there is very low degree of GSH oxidation under un-buffered conditions as implied by the I_{GSH} value of 0.2, which remains constant throughout the range of apparent pH values 4.0 to 9.6. When the concentration of OH^- reaches a value close to ~10^{-3} M at the

apparent pH of 11.2, some GSH oxidation is observed as indicated by the I_{GSH} value of 0.83. In phosphate buffer 0.035 M, the degree of GSH oxidation displays a maximum at pH 7.0 followed by a slight decline that continues until pH 10.0. Despite the overall decrease above pH 7.0, the I_{GSH} value of 3.0 at pH 10.0 shows a substantial degree of GSH oxidation. The value of I_{GSH} increases by a factor of 4, when raising the pH from 4.0 to 7.0, which is attributed to the rise in the concentration of the proton acceptor HPO_4^{2-} as the pH of the buffer increases. The concentration of HPO_4^{2-} increases from 2.2 x 10^{-5} to 0.014 M in the pH range 4.0 to 7.0. The maximum of I_{GSH} at pH 7.0 occurs because above 0.014 M of HPO_4^{2-}, the GSH oxidation is switching from kinetic to diffusion control (see Figure 2.2B). We think other pH-dependent processes that kick in when the pH is raised above 7.0 produce the slight decline observed in I_{GSH}. Among them could be the variation in charge of GSH from -1 to -3 in the pH range 7-10 because of deprotonation of the SH and the amine groups, which likely produce different rates for each anion species.

Figure 2.2B displays values of I_{GSH} as a function of the phosphate buffer concentration while maintaining the pH constant at 7.0 and 5.0. Both conditions provide different concentration and basicity strength for the proton acceptors available. For instance, at pH 5.0, 99.4 % of the total buffer is $H_2PO_4^-$, whereas at pH 7.0, there is 61.3 % of $H_2PO_4^-$ and only 38.7 % of HPO_4^{2-}. Because the pK_a of the conjugate acid for $H_2PO_4^-$, is 2.1 and for HPO_4^{2-} is 7.2, the deprotonation rate expected for $H_2PO_4^-$ is much slower than for HPO_4^{2-} (see below). Consequently, the rate of GSH oxidation rendered by each phosphate species must be different and the concentration range in which the kinetic and diffusion control behavior appear for each proton acceptor must be also different. Accordingly, the profile at pH 7.0 shows a steep rise of I_{GSH} to a plateau value of 4.4 at 0.050 M of buffer which corresponds to 0.0193 M of HPO_4^{2-}.

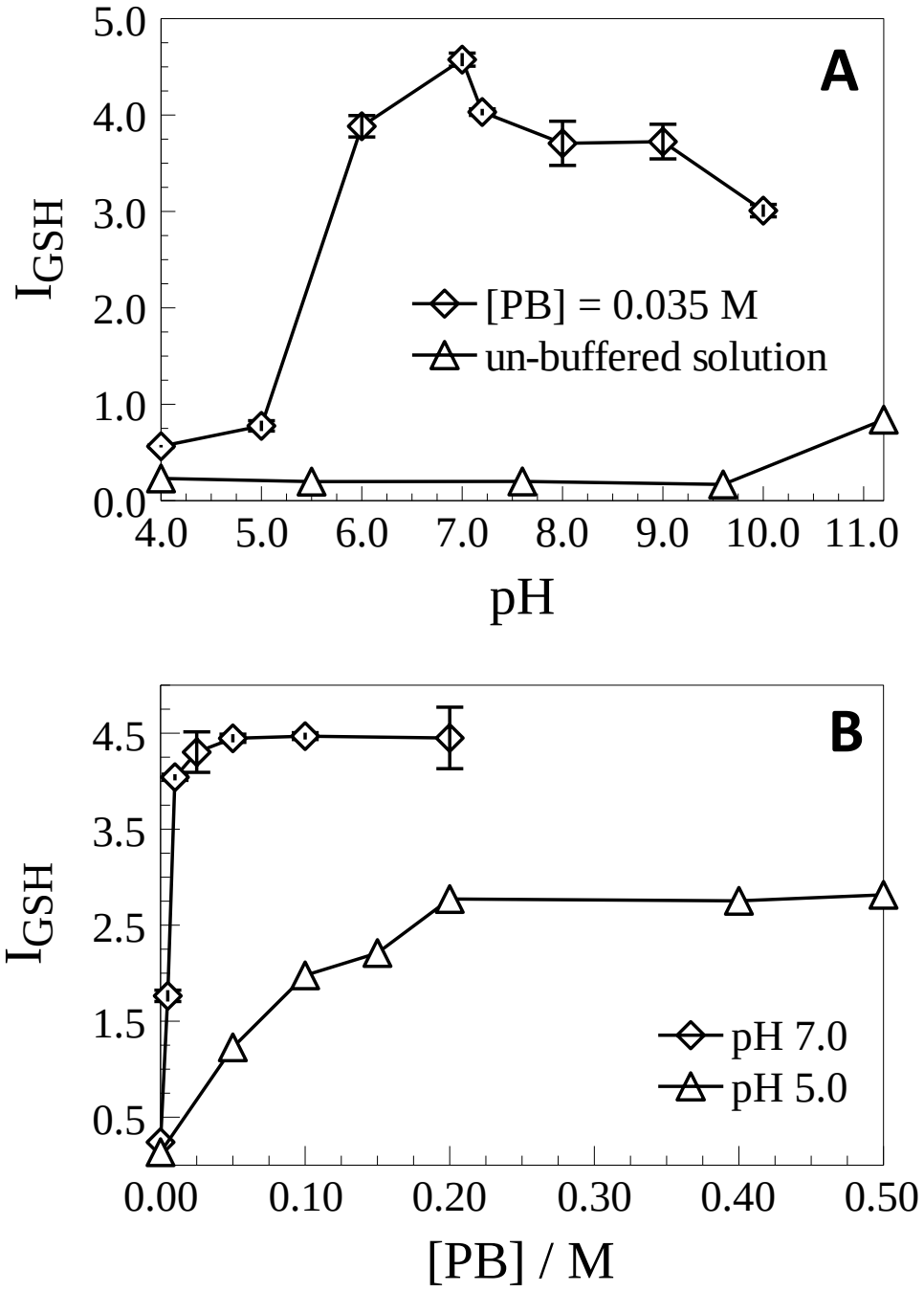

Figure 2.2 Normalized current (I_{GSH}) for 3.00 mM GSH and 1.00 mM K_3IrCl_6 (0.1 V s^{-1}) at: different pH of phosphate buffer (PB) 0.035 M and at different apparent pH of un-buffered solution **(A)**; at variable concentration of PB pH 5.0 and 7.0 **(B)**.

Because further increments in concentration do not produce higher current values, the reaction is said to be under diffusion control.[11, 23] At pH 5.0 when $H_2PO_4^-$ is the dominant proton acceptor, the plateau value for I_{GSH} is 2.7 and it takes up to ~0.200 M of $H_2PO_4^-$ to reach it. Therefore, the proton acceptor HPO_4^{2-} reaches the diffusion control limit in a much shorter range of concentration and with a higher value of I_{GSH} than HPO_4^{2-} because this latter is a stronger base that $H_2PO_4^-$ (see below).

Figure 2.3A illustrates the change in the logarithm of k_{obs} as a function of the pH from 4.0 to 9.0, using phosphate buffer 0.035 M. The rise in log k_{obs} as the pH increases is attributed to the concomitant increase of the component HPO_4^{2-} with the pH of the buffer. This trend starts leveling off at pH 7.2 indicating that at this concentration of HPO_4^{2-} (0.017 M) the reaction is entering the diffusion control region. Figure 2.3B shows the values of k_{obs} as a function of the buffer concentration at constant pH (7.0) and approximately, a six-fold increase in k_{obs} occurs when the concentration of phosphate buffer is raised from 0.005 to 0.200 M. Once again, the magnitude of k_{obs} increases when raising the concentration of the buffer, but a leveling effect starts occurring higher buffer concentration, when the reaction is switching from kinetic to diffusion control. As seen in Figure 2.2, this effect happens irrespective of the way the concentration of HPO_4^{2-} is raised, that is, by increasing the buffer pH or by raising the buffer concentration at constant pH. The equivalence of these two experimental approaches is easily appreciated in Table 2.1 where the values of k_{obs} are listed for different concentrations of HPO_4^{2-} obtained in both experiments. The correlation between k_{obs} and $[HPO_4^{2-}]$ is evident from all the data points in the table. Also, both experimental approaches show a transition of k_{obs} from kinetic to diffusion control in a similar way that was observed for the peak currents in Figure 2.2.

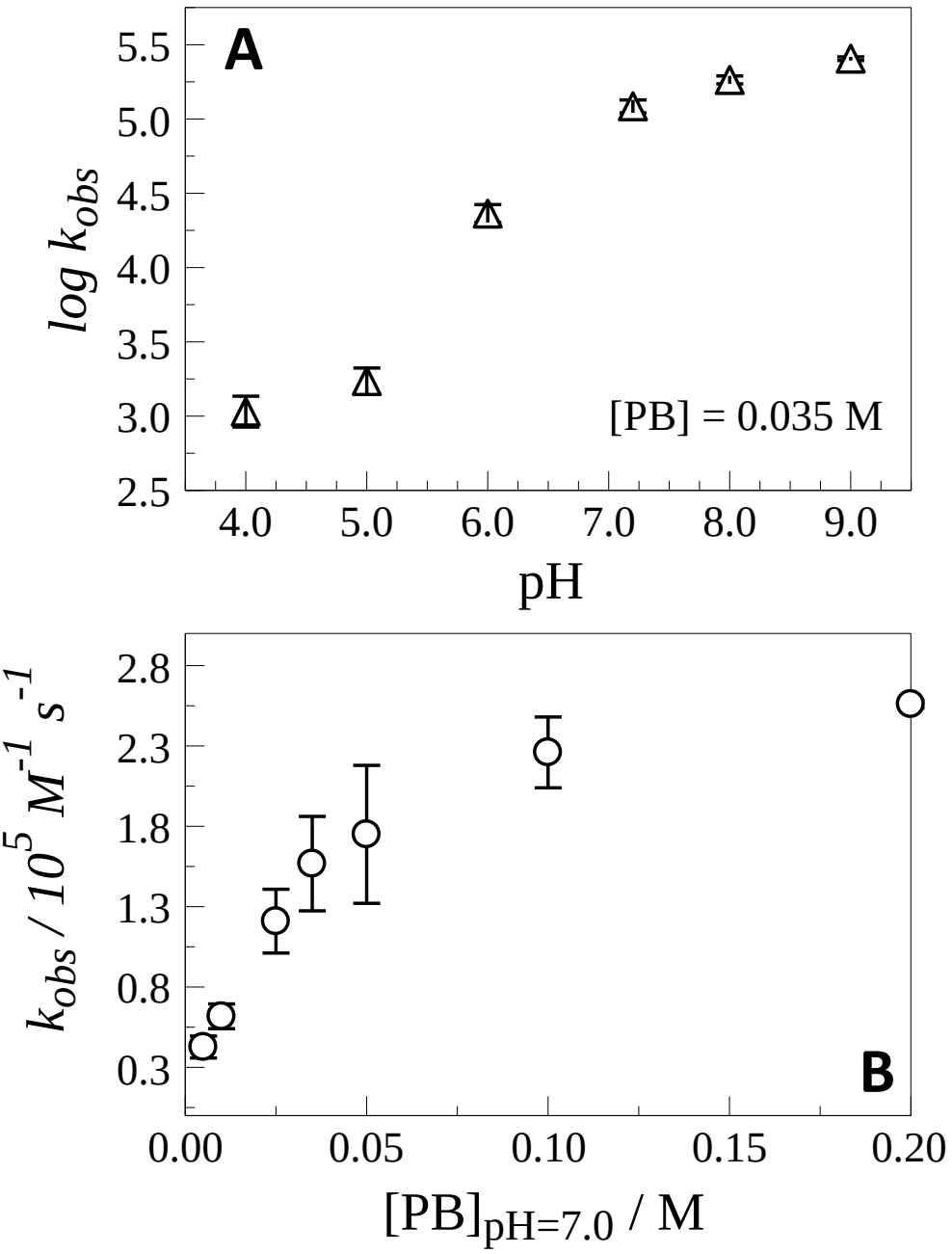

Figure 2.3 Plot of log k_{obs} vs. pH in phosphate buffer (PB) 0.035 M **(A)**; plot of k_{obs} vs. $[PB]_{pH=7.0}$ **(B)**.

According to Jencks, an expression for k_{obs} should contain terms for all possible proton acceptors in the system,[5] including the solvent (w), the hydroxide ion and buffer components (Eq. 2.15).[1a, 5]

$$k_{obs} = k_{obs,w} + k_{obs,OH^-} + k_{obs,BH^+} + k_{obs,B} \quad (2.15)$$

$$k_{obs2} = k_{w2}[H_2O] + k_{OH\text{-}2}[OH^-] + k_{BH+2}[H_2PO_4^-] + k_{B2}[HPO_4^{2-}] \quad (2.16)$$

$$k_{obs} = k_{obs1} + k_{obs2} + k_{obs3} \quad (2.17)$$

Table 2.1 Values of k_{obs} at different $[HPO_4^{2-}]$ obtained from two different experimental approaches

Phosphate Buffer [PB] 0.035 M			**Phosphate Buffer [PB] at pH 7.0**		
PH	**$[HPO_4^{2-}]$ / M**	**k_{obs} / M^{-1} s^{-1}**	**[PB]/ M**	**$[HPO_4^{2-}]$ / M**	**k_{obs} / M^{-1} s^{-1}**
4.0	2.2×10^{-5}	$1.1 \pm 0.3 \times 10^{3}$	**0.005**	0.0019	$4.3 \pm 0.7 \times 10^{4}$
5.0	2.2×10^{-4}	$1.7 \pm 0.3 \times 10^{3}$	**0.010**	0.0039	$6.2 \pm 0.8 \times 10^{4}$
6.0	0.0021	$2.3 \pm 0.3 \times 10^{4}$	**0.025**	0.0097	$1.2 \pm 0.2 \times 10^{5}$
7.0	0.0135	$1.6 \pm 0.3 \times 10^{5}$	**0.035**	0.0135	$1.6 \pm 0.3 \times 10^{5}$
7.2	0.0175	$1.2 \pm 0.1 \times 10^{5}$	**0.050**	0.0193	$1.8 \pm 0.4 \times 10^{5}$
8.0	0.0302	$1.8 \pm 0.1 \times 10^{5}$	**0.100**	0.0387	$2.3 \pm 0.2 \times 10^{5}$
9.0	0.0345	$2.55 \pm 0.07 \times 10^{5}$	**0.200**	0.0774	$2.56 \pm 0.02 \times 10^{5}$

Each proton acceptor could in principle proceed by any of the three PCET pathways listed in Scheme 2.4, therefore it is possible to write an expression of k_{obs} for each route. For example, Eq. 2.16 is written as if each proton acceptor considered in Eq. 2.15 is following the *concerted* pathway 2 (Eq. 2.14B) and the expression $k_{obs2} = k_{B2}$ [B] is applied to each term in the

polynomial. The overall k_{obs} (Eq. 2.17), which is the main parameter estimated from each experimental CV, is what is plotted in Figure 2.3 and contains the contributions of all routes for all proton acceptors in the system. According to Anslyn, for a reaction in which only the base component of the buffer serves as proton acceptor, the plot of *log* k_{obs} vs. pH is should have a curvature that levels off about two pH units above the pK_a of BH^+.[1a] For that same case, the plot of k_{obs} vs [B] at constant pH is expected to be a straight line with intercept at k_B.[1a] In Figure 2.3A, the plot of *log* k_{obs} vs. pH does not show a perfect plateau beyond pH 7.2, which is the pK_a for the conjugate acid of HPO_4^{2-}. This is attributed to changes in the contribution of proton acceptors like OH^- and PO_4^{3-} (not shown in Eq. 2.16), which increase in concentration as the pH rises above 7.0. Both of these species may have the whole set of parallel PCET routes contributing. However, the *stepwise* PT-ET is the most likely pathway to the dominant at pH > 7.0, because both OH^- and PO_4^{3-}, are bases stronger than GSH and therefore can deprotonate the thiol to produce the intermediate GS^- (see below). The non-linearity of the plot of k_{obs} vs $[PB]_{pH=7.0}$ in Figure 2.3B is attributed to the parallel contributions to k_{obs} by $H_2PO_4^-$ and H_2O compounded with the transition from kinetic to diffusion control.

We believe that the *concerted* pathway 2 and the *stepwise* 3 (ET-PT) occur mostly in the presence of bases that are weaker than GSH (H_2O, $H_2PO_4^-$, HPO_4^{2-}) because direct deprotonation of the thiol by them is thermodynamically uphill. Therefore, the deprotonation happens at the *transition state* of the *concerted* pathway or from the intermediate $GSH^{\bullet+}$ of the ET-PT pathway. Given that only 2 % of thiol is deprotonated at pH 7.0, we can safely say that at this pH at least 2 % of the GSH is following the *stepwise* pathway 1 (PT-ET), which requires conditions for the intermediate GS^- to exist.

2.3.3 Effect of the base pK_a on the PCET rate

Given that in dilute conditions, the PCET is kinetically controlled by the concentration of the proton acceptor B (Figures 2.2 and 2.3), the rate should also depend on the pK_a of the conjugate acid BH^+.[1a, 5] Figure 2.4 displays a plot of log k_{obs} as a function of the buffer pK_a with the pH set equal to the pK_a so that the same 50% of relative concentration of B is present in each case. The plot was prepared at 0.005 and 0.035 M for all buffers (Figure 2.4). The linear correlations found for both concentrations, suggest that the GSH oxidation follows a linear Brönsted relationship. Such Brönsted plots have been reported before by Meyer and Thorp to explain the role of the driving force in PCET.[2, 9a] The slope at 0.035 M was found to be 0.69 ± 0.05 (R^2 = 0.98) whereas at 0.005 M was 0.6 ± 0.1 (R^2 = 0.87).

The Brönsted catalysis law is an empirical relationship that relates the rate of a *general-base-catalyzed* reaction with the pK_a of the conjugate acid of the base, or vice versa for *general acid catalysis*. The relationship is linear between the log of *k* and the pK_a of the conjugate acid for the catalytic base (Eq. 2.18), where β is the slope and the intercept C is a constant with no physical meaning.[1a, 1c, 5-6, 24] For *base catalysis*, the value of β which can go from 0 to 1 denotes the extent of rate acceleration attainable for a given increase in driving force of pK_a and also reveals the extent of deprotonation of the reactant at the transition state.[1a, 1c, 5-6, 24] The actual correlation obtained at 0.035 M of buffer is written as Eq. 2.19.

$$\log k = \beta\ pK_a + \log C \tag{2.18}$$

$$\log k_{obs} = 0.69\ pK_a + 0.24 \tag{2.19}$$

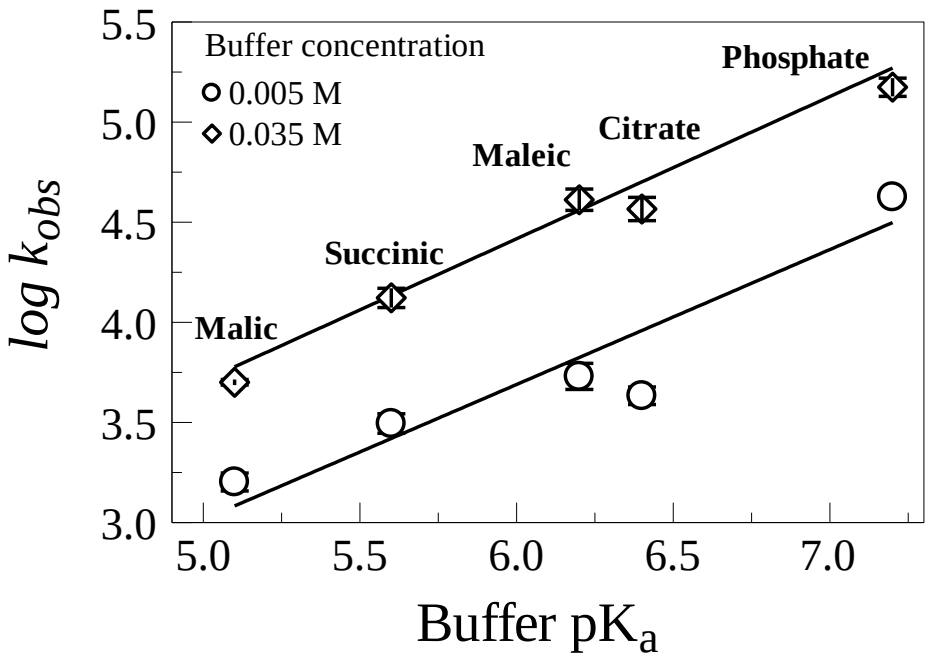

Figure 2.4 Plot of log k_{obs} vs. pK_a of the buffer with pH = pK_a ; GSH 3.0 mM +1.0 mM K_3IrCl_6.

To put this in perspective, given that the pK_a for the conjugate acid of $H_2PO_4^-$ is 2.1 and for the conjugate acid of HPO_4^{2-} is 7.2, HPO_4^{2-} is expected to have a value of k_{obs} about 3.3 x 10^3 times faster than $H_2PO_4^-$.[1a] This result explains why the kinetically controlled behavior appears at different range of concentration when the PCET involves a different proton acceptor (Figure 2.2B). Likewise, the fact that the GSH oxidation follows a Brönsted relationship is definite evidence that the proton acceptor is present in the transition state and because of that, the PCET can control the kinetics through the concentration and the pK_a of the proton acceptor. Consequently, there must be a range of concentration for each proton acceptor B in which the PCET will be rate determining. According to Jencks, almost every reaction that is coupled to PT and shows a Brönsted slope between 0.2 and 0.8 has a great chance of proceeding by a concerted mechanism.[1b, c]

2.3.4 Base participation in the RDS: scan rate and deuterated experiments

Figure 2.5 shows a series of CV's obtained at variable scan rate and two different concentrations of succinic buffer (pK_a = 5.64) to determine if the limited supply of the proton acceptor (B) in the buffer, could affect the oxidation rate of GSH by $[IrCl_6]^{2-}$. The same set of CV's were recorded with phosphate buffer (pK_a = 7.2) to see if the pK_a had an effect on the scan rate results (Figure 2.6). The CV's were run at a pH equal to the pK_a of the corresponding buffer so that both species B and BH^+ were present as 50 % of the total buffer concentration. The superimposed circles on the CV's denote the fitted simulations following the mechanism in Scheme 2.3. In a normal CV, if neither of the two oxidation states of the redox couple are involved in a chemical reaction, an increase of the scan rate would cause both the oxidation and reduction peaks to increase symmetrically.[11] This increase in current occurs because at faster scans, greater fluxes of reagents are drawn to the electrode, which generate larger currents when higher potentials are reached quicker.[11] When the reaction between GSH and $[IrCl_6]^{2-}$ is taking place, the reduction peak in the backward scan disappears because the electrochemical reduction of $[IrCl_6]^{2-}$ at the electrode surface is no longer possible as this latter is depleted by the homogeneous reaction with GSH (Scheme 2.1). The extra $[IrCl_6]^{3-}$ produced by the GSH reaction with $[IrCl_6]^{2-}$, manifests itself as an enhanced peak in the forward scan, which is a measure of the GSH oxidation (I_{GSH}). Thus, an increase in scan rate can reveal kinetic information for the reaction of GSH with $[IrCl_6]^{2-}$, because faster voltammetric scans accelerate the time scale of the electrochemical reduction of $[IrCl_6]^{2-}$. So if the reaction of GSH with $[IrCl_6]^{2-}$ is slower than the reaction of $[IrCl_6]^{2-}$ at the electrode, a reduction peak produced by the $[IrCl_6]^{2-}$ that does not react with GSH will appear in the backward scan only at higher scan rates. Moreover, the ratio of reduction and oxidation currents furnished by the iridium complex is

related to the sluggishness of the reaction of GSH with $[IrCl_6]^{2-}$, because this ratio falls to zero, when all $[IrCl_6]^{2-}$ reacts with GSH, or becomes one, when all $[IrCl_6]^{2-}$ is reduced at the electrode surface instead of reacting with GSH.

At 0.005 M of buffer (succinic or phosphate) the reduction peak (backward scan) of the mediator gradually reappears when increasing the scan rate from 0.2 to 0.7 V s^{-1}. No such reappearance is observed when doing the same scan rate increase at 0.035 M of either buffer. In addition to that, there is a significant loss of oxidation current in all CV's just because of decreasing the buffer concentration from 0.035 to 0.005 M. For instance, at the fastest scan rate tried (0.7 Vs^{-1}), the relative decrease in the oxidation peak current observed when diluting the buffer was 43.9 % for succinic and 45.7 % for phosphate (Figure 2.6). This result unambiguously indicates that the proton acceptor(s) present in the buffer, can limit the rate of GSH oxidation at low concentration. Table 2.2 shows the voltammetric peak currents for the fastest scan at different concentration of buffer and pK_a. The ratio of reduction to oxidation current calculated for the CV's at 0.005 M of buffer, shows an increase from 0.40 to 0.59 when the pK_a of the buffer decreases from 7.2 to 5.64. In other words, succinate, which is a base weaker than HPO_4^{2-}, renders a slower reaction of GSH with $[IrCl_6]^{2-}$, producing less oxidation and more electrochemical reduction of $[IrCl_6]^{2-}$. This observation which is in agreement with the Brönsted relationship, translates into a ratio of reduction/oxidation current higher for succinate than for HPO_4^{2-}.

Table 2.2 Voltammetric peak current values obtained at 0.7 V s^{-1} and different conditions of buffer concentration and pK_a. The pH was set equal to the pK_a of the buffer.

Buffer (pK_a)	[Buffer] / M	*[B] / M	Oxidation Peak Current / μA	Reduction Peak Current / μA	Reduction/ Oxidation Ratio
Succinic (5.6)	0.005	0.0025	60.33	35.80	0.59
	0.035	0.0175	107.5	~0	~0
Phosphate (7.2)	0.005	0.0025	91.40	36.19	0.40
	0.035	0.0175	168.3	~0	~0

*B = base component of the buffer system B/BH^+, with pK_a for BH^+.

The conclusion that the concentration of the proton acceptor in the buffer, limits the reaction rate in dilute conditions, and therefore, is part of the RDS, is a direct observation of the experimental CV's (Figures 2.5 and 2.6). This conclusion is reached without introducing any model or simulation and it strongly supports the major contention of this paper, that is, for the conditions studied, the deprotonation barely occurs from the GSH itself. Instead, it happens in the *transition state* of the PCET, which at low proton acceptor concentration cannot be formed fast enough to keep up with the scan rate of the experiment. So, the experiment shows that in conditions of limited supply of B or of lower pK_a for BH^+, the reaction GSH + B + $[IrCl_6]^{2-}$ to produce $GS^{\bullet}$ + BH^+ + $[IrCl_6]^{3-}$, becomes slower. Additionally, the observation of the rate limitation at 0.005 M of buffer, which disappears at 0.035 M, is another confirmation of the transition between kinetic and diffusion control behavior stated earlier. At low buffer concentration there is not sufficient supply of proton acceptors to allow enough successful encounters for the *transition state* to be formed and the PCET is limited by kinetics. Once the

concentration of proton acceptor reaches certain value, the reaction is no longer kinetically controlled and the rate depends on how fast the encounters are formed by diffusion.

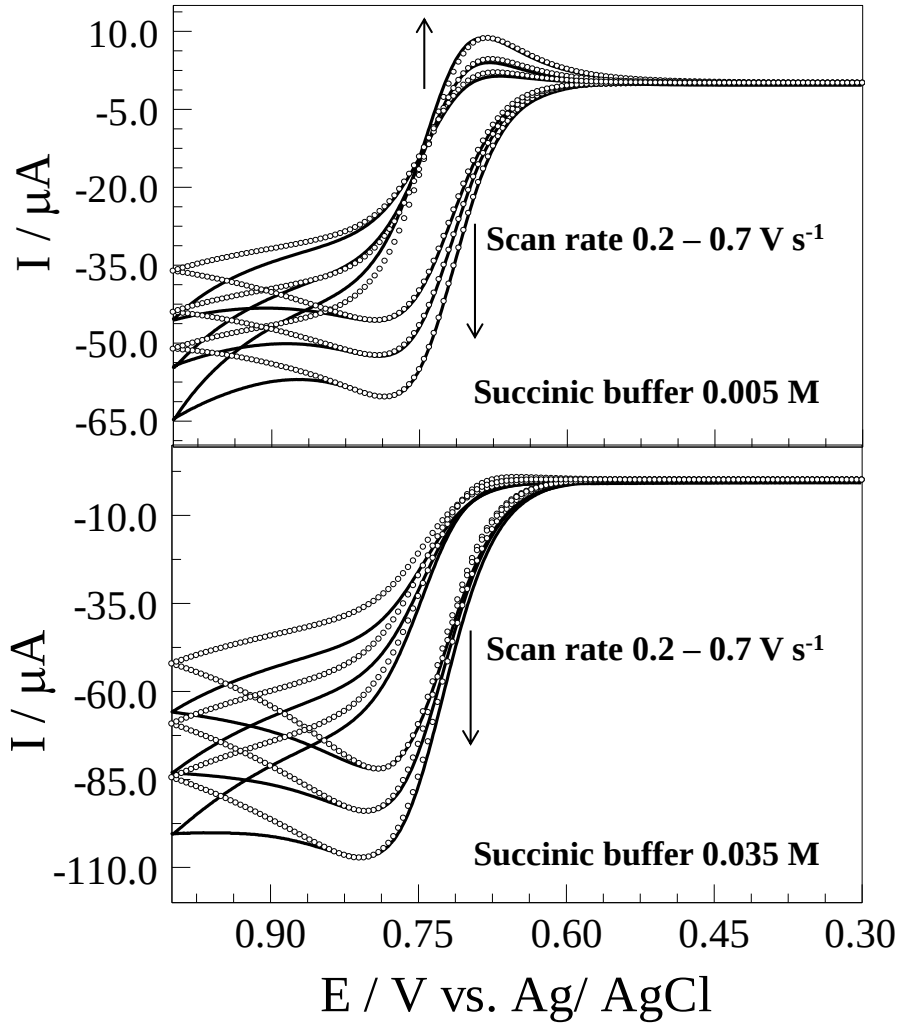

Figure 2.5 Experimental (solid line) and simulated (open circles) CV response for 3.0 mM GSH + 1.0 mM K_3IrCl_6, in succinic buffer pH = pK_a = 5.6.

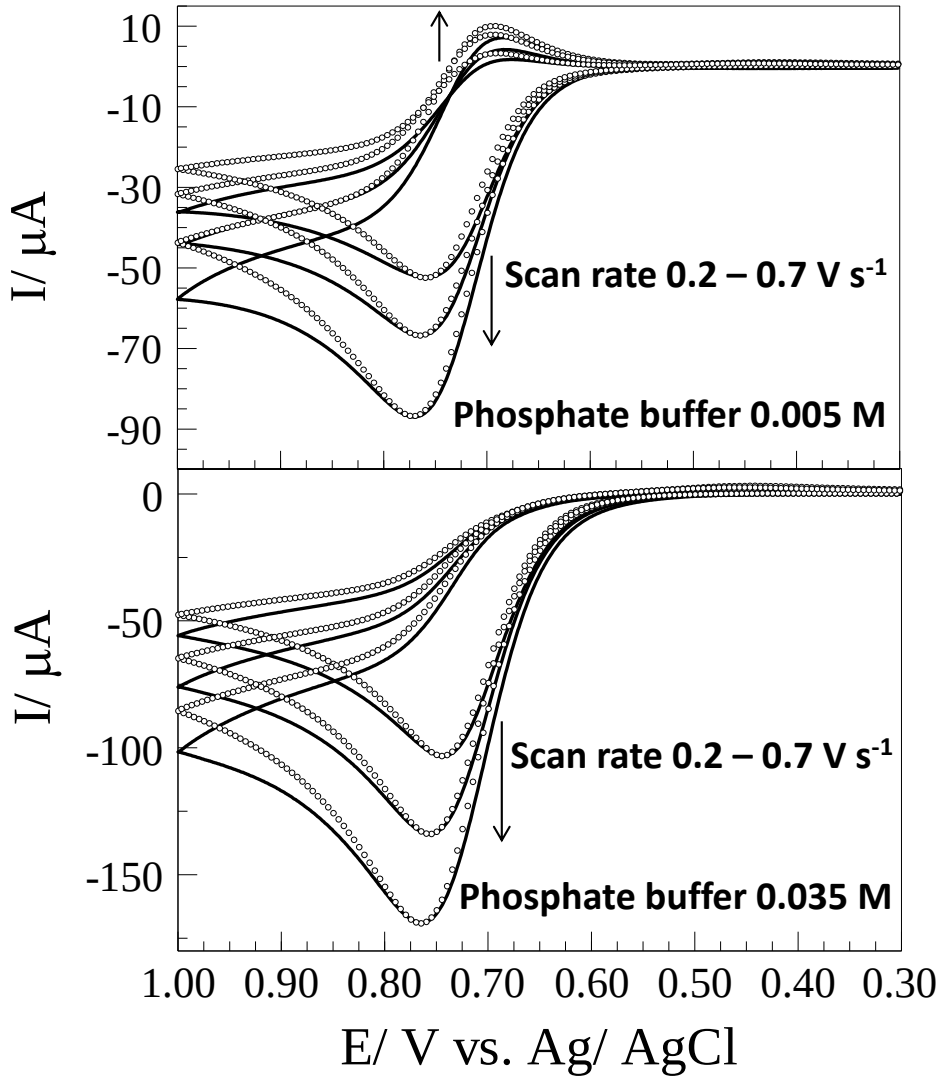

Figure 2.6 Experimental (solid line) and simulated (open circles) CV response of 3.0 mM GSH + 1.0 mM K_3IrCl_6, in phosphate buffer pH = pK_a = 7.2.

We performed CV's in deuterated conditions at pD 7.0 and variable concentration of deuterated phosphate buffer in the range 0.005 - 0.200 M (Table 2.3, Figure 2.7). The values of kinetic isotope effect (KIE) were calculated using the expression k_{obsH} / k_{obsD} and they confirm that at low buffer concentration the SH bond is being broken in the RDS, further corroborating that the PCET is rate determining in dilute buffer conditions. Nevertheless, because at pH 7.0, phosphate buffer contains 38.7 % of HPO_4^{2-} and 61.3 % of $H_2PO_4^-$, and because HPO_4^{2-} is

expected to deprotonate 3.3 x 10^3 times faster than $H_2PO_4^-$, PCETs involving $H_2PO_4^-$ and HPO_4^{2-} will show kinetic control behavior in different concentration range. Consequently, at 0.005 M of buffer when both PCETs are rate limiting, the estimated KIE is 4.9 ± 0.8. Once the PCET with HPO_4^{2-} reaches diffusion control at 0.035 M of buffer, the value of KIE decreases to 2.0 ± 0.5 because the PCET with $H_2PO_4^-$ still remains rate determining. This scenario continues at 0.200 M of buffer when the KIE is 2.20 ± 0.05, indicating that the PCET with $H_2PO_4^-$ is still under kinetic control as confirmed by the I_{GSH} plot in Figure 2.2B. Therefore, it is expected that once diffusion control ensues for the PCET with $H_2PO_4^-$ (~0.33 M PB pH 7.0) the remaining KIE will also disappear signaling a change in mechanism. This change implies that the PCET with either HPO_4^{2-} or $H_2PO_4^-$ is no longer rate determining and the formation of the disulfide GSSG proceeds as fast as it is allowed by the dimerization reaction. We interpret the disappearance of KIE as merely indicating that the S-H bond is no longer being broken during the RDS, which by general consensus is the widely accepted interpretation of any KIE,[1a, 25] and this occurs simply because the PCET has ceased to be the RDS. So, the proposed predominance of the *concerted* pathway for both phosphate species still remains viable as this system displays all the mechanistic hallmarks of a *concerted* PCET in the conditions investigated. These include: the adherence to the *libido* rule of *general acid-base catalysis*, the discovery of two different values of KIE for two different proton acceptors, the presence of kinetic controlled behavior elicited by dilute conditions and measured in different manners (peak currents and k_{obs} in Figure 2.2 and 2.3, time scale change in Figures 2.5 and 2.6, and, isotopic substitution shown in Table 2.3 and Figure 2.7), the appearance of a Brönsted linear relationship and finally, the finding that the *stepwise* routes though coexisting in the conditions studied, cannot be prevalent.

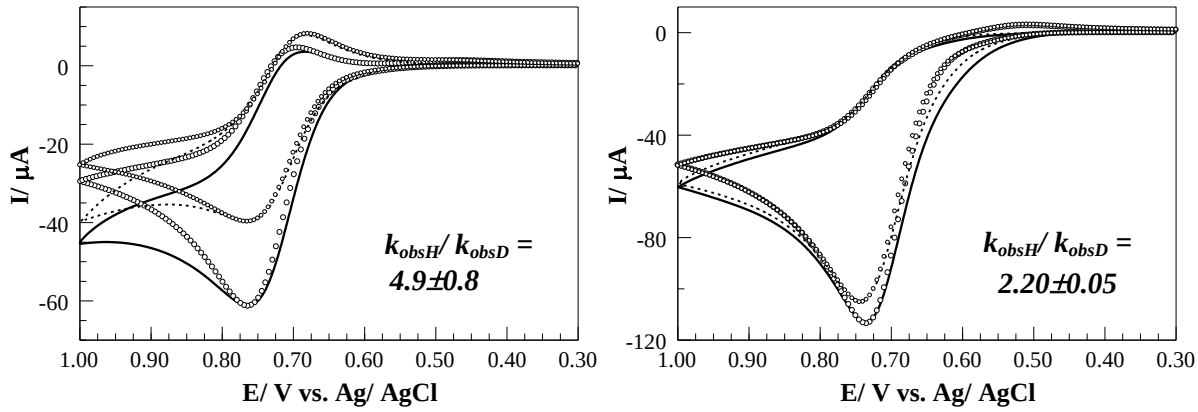

Figure 2.7 CVs in 1.0 mM K_3IrCl_6 + 3.0 mM GSH in 5.0 mM (A) and 200 mM (B) deuterated phosphate buffer pD 7.0 (dashed line); and in 5.0mM and 200 mM aqueous phosphate buffer pH 7.0 (solid line). k_H and k_D are the observed rate constants for the reaction between GSH and $[IrCl_6]^{2-}$ in aqueous and deuterated solution, respectively. Simulation results are overlaid (open circles). (A) k_{obsH} =(4.3±0.7)x10^4 M^{-1} s^{-1} and k_{obsD} = (8.7±0.5) x10^3 M^{-1} s^{-1}; (B) k_{obsH} = (2.56 ±0.03)x10^5 M^{-1} s^{-1} and k_{obsD} = (1.16 ±0.03)x10^5 M^{-1} s^{-1}. Scan rate of CVs shown: 300 mV/s**.**

Table 2.3 Kinetic isotope effect (KIE) at different concentration of phosphate buffer (PB) pD 7.0.

$[PB]_{pD=7.0}$ / M	$[DPO_4^{2-}]$ / M	KIE = k_{obsH} / k_{obsD}
0.005	0.0019	4.9 ± 0.8
0.035	0.0135	2.0 ± 0.5
0.100	0.0387	2.4 ± 0.4
0.200	0.0774	2.20 ± 0.05

For instance, the *stepwise* PT-ET (route 1 in Scheme 2.4) is unlikely to be dominant because at pH 7.0 (1.7 units below pK_{aSH}) the intermediate GS^- is not stable, as a matter of fact only 2% of GSH is deprotonated at this pH. Another reason to support this claim is the fact that for the PT-ET to be successful, the re-protonation rate constant k_{-PT1} from BH^+ to GS^- must be slower

than the ET so that the oxidation can happen before GS^- is re-protonated. This seems not to be the case for GSH or thiols in general, for example, the k_{-PTI} for thioglycolic acid with an amine of similar pK_a as $H_2PO_4^-$ has been reported to be 4.03 x 10^7 M^{-1} s^{-1},[26] which is one order of magnitude faster than the rate reported when the same deprotonated thioglycolic acid is oxidized by $[IrCl_6]^{2-}$ (3.5 x 10^6 M^{-1} s^{-1}).[15a] So, even though a PT-ET pathway with a PT as the RDS could show the observed KIEs, the occurrence of this PCET route in the conditions investigated does not seem to be able to dominate.

For s*tepwise* pathway 3, the PT happens from the protonated radical species $GHS^{\bullet+}$ after GSH is oxidized, however this route cannot contribute with any KIE because it is very unlikely that the PT from $GHS^{\bullet+}$ could ever be a RDS given the high acidity this radical is expected to have. In addition to that, based on experiments with other mediators conducted in our lab, which will be published elsewhere, we know that $[IrCl_6]^{2-}$ is a mediator with a rather mild oxidizing power. So the extent of intermediate $GHS^{\bullet+}$ produced is not thought to be as high as needed to make this pathway prevalent. In actuality, Jencks has pointed out that many *concerted* reactions come about when an intermediate with high Brönsted acidity or basicity (*i.e.* $GHS^{\bullet+}$) undergoes a subsequent PT.[1c] Such PT is usually very fast because of the high driving force, especially if the transfer involves atoms such O, N and S, that the intermediate has no finite existence and the reaction in the end proceeds in *concerted* fashion.[1c]

Therefore, in the light of this analysis, we are left with the option most favorably supported by the results, which indicates that despite parallel occurrence of *stepwise* PT-ET and ET-PT at pH 7.0 in phosphate buffer, the *concerted* route appears to be dominant. Because such a concerted mechanism would require for GSH, $[IrCl_6]^{2-}$ and B, to be in the *transition state*, this result could help rationalize the lower values of diffusion controlled constants implied by the

values of k_{obs} measured, as opposed to the typical diffusion limit values observed in bimolecular reactions. More studies in this type of reactions are needed to clarify this observation.

2.4 Conclusion

The oxidation of GSH by the electrogenerated mediator $[IrCl_6]^{2-}$ in the presence of bases (B) to produce the radical species $GS^{\bullet}$, $[IrCl_6]^{3-}$ and BH^{+}, was studied by cyclic voltammetry in buffered and un-buffered solution. This PCET reaction is the first step in the formation of the disulfide GSSG during the oxidation of GSH. The reaction exhibits a slight acceleration of the rate when the phosphate buffer concentration is raised at pH 7.0, from dilute levels of 0.005 M to regular working conditions of 0.2 M. This result is interpreted as indicative that in dilute conditions of buffer the PCET is rate determining but as the buffer concentration increases, that is no longer the case and the GSH oxidation proceeds as fast as it is allowed but the dimerization of the thiyl radical. The acceleration of the PCET occurs because the proton acceptors present in the buffer take the H^{+} released during the GSH oxidation and they do so despite being bases weaker than GSH (*i.e.* H_2O, $H_2PO_4^{-}$ and HPO_4^{2-}). Nevertheless, stronger bases produce higher rate accelerations. Despite being small, the kinetic effects produced by these proton acceptors obey the *libido* rule of *general base catalysis*. So, instead of occurring directly from the reactant GSH, the PT happens at the *transition state*, as the SH group increases its acidity due to its concurrent oxidation by $[IrCl_6]^{2-}$. As a consequence, the PCET becomes *concerted* because now both the oxidant mediator and the proton acceptor have to be present at the *transition state* with GSH. The free energy gained by doing a more favorable PT in the *transition state* is thought to offset the negative entropy needed for the *concerted transition state*. The KIE disappears when increasing the buffer concentration not because the reaction is losing *concerted* character but

because the PCET ceases to be rate determining. The *concerted* pathway is postulated to be prevalent because the investigated conditions would not allow the other pathways to dominate and explain the observed results. For example, the pathway that goes through the intermediate $GSH^{\bullet+}$ could never render a rate determining PT (to $H_2PO_4^{2-}$ or HPO_4^{-}) and allow the KIEs observed. Likewise, the pathway that goes through the intermediate GS^- is greatly hindered at pH 7.0 or lower, because this species can barely exist in such conditions (only 2 % of deprotonated GSH can exist at pH) and as Jencks has pointed out, if an intermediate cannot have finite existence in a *stepwise* pathway the *concerted* route becomes preferred. Therefore, we are forced to conclude that despite parallel occurrence of these *stepwise* pathways in the conditions studied they are unable to be dominant.

This investigation reveals that the principles of *general acid-base catalysis* are useful in the investigation of the complex and subtle kinetic effects produced by buffers in PCET reactions. We think these principles are completely applicable to PCET and can serve as a guideline for interpretation and experimental design to determine the occurrence of *concerted* pathways in these reactions. Nevertheless, more studies are needed to test this method of enquiry.

2.5 References

1. (a) Anslyn, E. V.; Dougherty, D. A., *Modern Physical Organic Chemistry*. University Science Books: Sausalito, CA, 2006; p 1079; (b) Jencks, W. P., *J. Am. Chem. Soc.* **1972,** *94*, 4731-4732; (c) Jencks, W. P., *Chem. Rev.* **1972,** *72*, 705-718.
2. Sinha, A.; Bruice, T. C., *J. Am. Chem. Soc.* **1984,** *106*, 7291-7292.
3. (a) Mayer, J. M., *Annu. Rev. Phys. Chem.* **2007,** *55*, 363-390; (b) Fecenko, C. J.; Meyer, T. J.; Thorp, H. H., *J. Am. Chem. Soc.* **2006,** *128*, 11020-11021; (c) Irebo, T.; Reece, S. Y.; Sjodin, M.; Nocera, D. G.; Hammarstrom, L., *J. Am. Chem. Soc.* **2007,** *129*, 15462-15464; (d) Costentin, C.; Robert, M.; Saveant, J. M.; Teillout, A. L., *Proc. Natl. Acad. Sci. U.S.A.* **2009,** *106*, 11829-11836; (e) Costentin, C.; Louault, C.; Robert, M.; Saveant, J. M., *Proc. Natl. Acad. Sci. U.S.A.* **2009,** *106*, 18143-18148; (f) Weinberg, D. R.; Gagliardi, C. J.; Hull, J. F.; Fecenko, C. J.; Kent, C. A.; Westlake, B. C.; Paul, A.; Ess, D. H.; Granville, D. M.; Meyer, T. J., *Chem. Rev.* **2012,** *112*, 4016-4093; (g) Gagliardi, C. J.; Binstead, R. A.; Thorp, H. H.; Meyer, T. J., *J. Am. Chem. Soc.* **2011,** *133*, 19594-19597; (h) Ishikita, H.; Soudackov, A. V.; Hammes-Schiffer, S., *J. Am. Chem. Soc.* **2007,** *129*, 11146-11152; (i) Sjodin, M.; Styring, S.; Wolpher, H.; Xu, W.; Sun, L.; Hammarstrom, L., *J. Am. Chem. Soc.* **2005,** *127*, 3855-3863; (j) Anxolabehere-Mallart, E.; Costentin, C.; Policar, C.; Robert, M.; Saveant, J. M.; Teillout, A. L., *Faraday Discuss* **2011,** *148*, 83-95.
4. Costentin, C.; Robert, M.; Saveant, J. M., *J. Am. Chem. Soc.* **2007,** *129*, 5870-5879.
5. Jencks, W. P., *Catalysis in Chemistry and Enzymology*. McGraw-Hill: New York, 1969; p 644.
6. Kirby, A. J., General Acid-Base Catalysis in Model Systems. In *Hydrogen Transfer Reactions*, 2007; Vol. 3, pp 975-1012.
7. (a) Khalid, I. M.; Pu, Q.; Alvarez, J. C., *Angew. Chem. Int. Ed. Engl.* **2006,** *45*, 5829-5832; (b) Khalid, I. M.; Alvarez, J. C., *J. Electroanal. Chem.* **2009,** *631*, 76-79; (c) Alligrant, T. M.; Alvarez, J. C., *J. Phys. Chem. C.* **2011,** *115*, 10197-10805; (d) Alligrant, T. M.; Hackett, J.; Alvarez, J. C., *Electrochim. Acta* **2010,** *55*, 6507-6516; (e) Medina-Ramos, J.; Alligrant, T. M.; Clingenpeel, A.; Alvarez, J. C., *J. Phys. Chem. C* **2012,** *116*, 20447-20457.
8. (a) Ison, A.; Odeh, I. N.; Margerum, D. W., *Inorg. Chem.* **2006,** *45*, 8768-8775; (b) Kruusma, J.; Benham, A. M.; Williams, J. A.; Kataky, R., *Analyst* **2006,** *131*, 459-473.
9. (a) Fecenko, C. J.; Thorp, H. H.; Meyer, T. J., *J. Am. Chem. Soc.* **2007,** *129*, 15098-15099; (b) Weatherly, S. C.; Yang, I. V.; Armistead, P. A.; Thorp, H. H., *J. Phys. Chem. B* **2003,** *107*, 372-378.
10. Covington, A. K.; Paabo, M.; Robinson, R. A.; Bates, R. G., *Anal. Chem.* **1968,** *40*, 700-706.
11. Bard, A. J.; Faulkner, L. R., *Electrochemical Methods: Fundamentals and Applications*. 2nd ed.; John Wiley & Sons Inc.: New York, 2001; p 833.
12. Madej, E.; Wardman, P., *Arch. Biochem. Biophys.* **2007,** *462*, 94-102.
13. (a) Hoffman, M. Z.; Hayon, E., *J. Am. Chem. Soc.* **1972,** *94*, 7950-7957; (b) Hoffman, M. Z.; Hayon, E., *J. Phys. Chem.* **1973,** *77*, 990-996.
14. Kolthoff, I. M.; Stricks, W.; Kapoor, R. C., *J. Am. Chem. Soc.* **1955,** *77*, 4733-4739.
15. (a) Sun, J.; Stanbury, D. M., *Dalton Trans.* **2002**, 785-791; (b) Wang, X.; Stanbury, D. M., *Inorg. Chem.* **2008,** *47*, 1224-1236.

16. (a) Campbell, J. F.; Napier, M. E.; Feldberg, S. W.; Thorp, H. H., *J. Phys. Chem. B* **2010,** *114*, 8861-8870; (b) Weatherly, S. C.; Yang, I. V.; Thorp, H. H., *J. Am. Chem. Soc.* **2001,** *123*, 1236-1237.
17. Poulsen, I. A.; Garner, C. S. J., *J. Am. Chem. Soc.* **1962,** *84*, 2032-2037.
18. Petrovic, S., *Chem. Educator* **2000,** *5*, 231-235.
19. (a) Stejskal, E. O.; Tanner, J. E., *J. Chem. Phys.* **1965,** *42*, 288-292; (b) Berger, S.; Braun, S., *200 and More NMR Experiment A Practical Course*. Wiley-VCH: 2004; p 467; (c) Sun, H.; Chen, W.; Kaifer, A., *Organometallics* **2006,** *25*, 1828-1830.
20. Cohen, Y.; Avram, L.; Frish, L., *Angew. Chem. Int. Ed. Engl.* **2005,** *44*, 520-554.
21. Millero, F. J.; Dexter, R.; Hoff, E., *J. Chem. Eng. Data* **1971,** *16*, 85-87.
22. "Ionic Conductivity and Diffusion at Infinite Dilution". In *CRC Handbook of Chemistry and Physics (Internet Version 2011)*, 91st ed.; Haynes, W. M., Ed. CRC Press/ Taylor and Francis: Boca Raton, FL, 2011.
23. White, R. J.; White, H. S., *Anal. Chem.* **2005,** *77*, 214A-220A.
24. (a) Bell, R. P., *Acid-Base Catalysis*. Oxford University: London, 1941; p 91; (b) Kirby, A. J., Acid-Base Catalysis by Enzymes. In *Encyclopedia of Life Sciences*, John Wiley & Sons: 2001.
25. Wolsberg, M.; Van Hook, W. A.; Paneth, P., *Isotope effects in the chemical, geological and bio sciences*. Springer: New York, 2010; p 466.
26. Hibbert, F.; Thomas, G. A. L., *J. Chem. Soc., Perkin Trans. 2* **1986,** *512*, 1761-1763.

Chapter 3:

'Effect of Varying the Free Energy of Electron Transfer on the Rate of Proton-Coupled Electron Transfer (PCET): the Electrochemical Oxidation of Glutathione by Different Mediators at Variable Buffer Concentrations'

3.1 Introduction

This chapter presents new evidence of Marcusian behavior and kinetic effects by Brönsted bases on the mediated oxidation of glutathione. Previously, we showed that the oxidation of glutathione by the mediator $[IrCl_6]^{2-}$ is an example of proton-coupled electron transfer (PCET), where an electron is transferred from glutathione's sulfhydryl group to the iridium metal complex and a proton coming from the same thiol group is abstracted by a Brönsted base in solution. Similar PCET reactions occur in biologically relevant processes like the photosynthesis of plants and the oxidation of purines and proteins. [1-11] However, most of the research on PCETs focuses on elucidating reaction mechanisms and usually neglects the potential role of Brönsted acids or bases, often present as functional groups on the molecules studied or as buffers in solution. [1-10] On the contrary, from the study of numerous organic chemistry and enzymes reactions, it is well known that Brönsted acid and bases may have a profound influence on the type of mechanism and rate of reactions that involve the transfer of protons. In fact, two types of catalysis by acids and bases have been identified: one where the rate of the reaction depends on the pH but not on the concentration of acid or base species (i.e. *specific acid-base catalysis*) and the other one observed when the rate of reaction depends on the concentration of all acid or base species involved (i.e. *general base catalysis*). Despite all the knowledge accumulated on acid-base catalysis of chemical reactions, such effects on are still debated in studies of electron transfer reactions that are accompanied by the exchange of protons.

The relationship between kinetic and thermodynamics of redox reactions is commonly described in terms of the famous Marcus theory of electron transfer. However, this model does not predict the effect of acids or bases when electron and proton transfers occur together. Therefore, in order to draw a more detailed picture of the kinetic and thermodynamic landscape of the mediated oxidation of glutathione, we performed voltammetric experiments varying the

oxidizing species (mediator) the buffer type and concentration, and their analysis was done in terms of both the acid-base catalysis and Marcus theories.

Chapter 2 showed that the observed rate constant k_{obs} for the reaction of glutathione (GSH) and the mediator $[IrCl_6]^{2-}$, estimated through digital simulation of cyclic voltammograms, exhibits a linear dependence on the concentration of buffer present in solution (i.e. concentration of phosphate buffer pH 7.0).[4] Likewise, log k_{obs} depends linearly on the pK_a's of a series of Brönsted bases. [4] The dependence of log k_{obs} on the pK_a's of base catalysts is known as the Brönsted relationship, and its linearity is characteristic of general base catalyzed reactions. [12-15] The slope of a Brönsted relationship plot (β for general base catalysis) can be viewed as the extent of proton transfer achieved at the transition state of the reaction. [14,15] For the GSH-$[IrCl_6]^{2-}$ system β ~0.7, hence close to 70% of the proton transfer from GSH to the Brönsted base involved has taken place when the reaction reaches the transition state. The linearity of a plot of k_{obs} vs. buffer concentration is also considered as evidence of general base catalysis. [14,15]

Based on the experimental and simulations findings described above, and the observation of kinetic isotope effects (see chapter 2; kinetic isotope effect 'KIE' values of 4.9 and 2.2 were determined in the presence of 5.0 mM and 200 mM phosphate buffer pH 7.0, respectively) we proposed a *primarily concerted* proton-coupled electron transfer mechanism to depict the mediated oxidation of GSH. [4] The strong dependence of the reaction activation energy (ΔG~log k_{obs}) on the proton transfer driving force proves that the rate of reaction can be controlled by changing the concentration of buffer (at constant pH) or by substituting the proton acceptor (i.e. by changing the Brönsted base). Thus, in the concerted PCET pathway the transfer of the proton from glutathione to the base in solution occurs most likely at the transition state of the reaction, coupled to the transfer on one electron to the mediator $[IrCl_6]^{2-}$. The deprotonation of GSH

occurring at the transition state of the concerted PCET is therefore what causes the dependence of the observed rate of reaction on the nature and concentration of the base present in solution.

In order to gain further insight into glutathione's proton-coupled electron transfer, it was imperative to explore the effect of varying the free energy of electron transfer on the rate of oxidation of this thiol by using a series of metal complexes as mediators, all with a different redox potential [i.e. $Mo(CN)_8^{3-}$, $IrCl_6^{2-}$, $Fe(bpy)_3^{3+}$ and $Fe(phen)_3^{3+}$]. The electrochemical measurements were done in the presence of different concentrations of histidine buffer pH 6.5 and phosphate buffer pH 7.0. Marcusian linear relationships resulted from the analysis of the observed rate of reaction, k_{obs}, as a function of the mediator's redox potential (i.e. plots of RT ln k_{obs} vs. $E_{1/2}$ of the mediators were obtained). Thus, it was confirmed that the Marcus theory of electron transfer applies to the oxidation of GSH by these metal complexes. In addition, it was also observed that the slope of the Marcus plots drifted from the expected 0.5 as the concentration of buffer was raised above ~10 mM for either histidine or phosphate buffer. This phenomenon is discussed here in terms of a buffer concentration effect on the rate of oxidation of glutathione.

Secondly, this chapter presents the results of investigating the effect of changing the mediator (i.e. changing the free energy of electron transfer) on the magnitude of the Brönsted plot slope, β. Brönsted plots for the oxidation of GSH by $[Fe(phen)_3]^{3+}$ and $[Mo(CN)_8]^{3-}$ were obtained in the presence of five bases: $malate^{2-}$ (pK_a = 5.1), $maleate^{2-}$ (pK_a = 6.2), $succinate^{2-}$ (pK_a = 5.6), histidine (pK_a = 6.5) and HPO_4^{2-} (pK_a = 7.2). The observed rate constants were estimated for all different combinations of buffer and mediator through digital simulation of the respective cyclic voltammograms. The bases' pK_a's were extracted from the literature. The Brönsted plot for each one of the mediators had a different β value, being β ~ 0.4 with $[Mo(CN)_8]^{3-}$ ($E_{1/2}$ ~ 0.59 V vs.

Ag/AgCl) and β ~ 0.9 with $[Fe(phen)_3]^{3+}$ ($E_{1/2}$ ~ 0.83 V vs. Ag/AgCl) as the mediator. This relationship between β and the redox potential of the metal complex confirmed that the degree of deprotonation of GSH at the transition state of the reaction is also a function of the free energy of electron transfer.

In similar studies, Weatherly [5,6], Fecenko and coworkers [3] determined a linear dependence of RT Lnk_{obs} on the free energy of electron transfer (-ΔG) for the mediated oxidation of guanine and tyrosine, in aqueous media. The slope of their Marcus plots was ca. 0.5 and 0.8, respectively. The free energy of oxidation of tyrosine was varied by using different mediators or by having different buffer components in solution; the free energy of oxidation of guanine was varied by using different mediators only. Unfortunately, neither of these studies explicitly discusses the effect of the buffer base on the rate of PCET, or on the slope of the Brönsted or Marcus plots.

The role of the buffer on PCET reactions was however studied in a few systems where the proton and electron donor species is covalently attached to the electron acceptor. [8] Species containing a tyrosine group attached to a ruthenium or rhenium metal center via a ligand i.e. a bipyridine bridge ligand, are examples of molecules synthesized for these studies. Various competing PCET pathways were detected with these species, one of them being a buffer-assisted concerted proton-coupled electron transfer (CEP) path. Remarkably, the CEP mechanism appeared as a generalized phenomenon at higher buffer concentrations. [8]

In this study, we propose that the oxidizing strength of the mediator as well as the pK_a and concentration of the buffer base can exert control over the rate of oxidation of glutathione. Therefore, to explain the observed kinetic dependence of glutathione oxidation on the strength and concentration of a Brönsted base this research adopts concepts from the theory of acid-base catalysis, originally developed as a model for hydrolysis and other nucleophilic reactions of

organic compounds and enzymes. [14,15] All the findings presented herein suggest that, although buffers are usually present in electrochemical experiments as a means to maintain a desired pH, the choice of buffer composition and concentration can under some circumstances influence the kinetics of PCETs and must not be underestimated. In addition, this chapter shows that predicting the effect of changing the free energy of electron transfer on the rate of oxidation of a substrate is a relatively easy through the Marcus theory. Nonetheless, when it comes to establishing an accurate mechanism of reaction, it is crucial to contemplate possible kinetic effects promoted by Brönsted acids and bases in redox reactions that involve the transfer of protons like the oxidation of glutathione or tyrosine.

Finally, this chapter ends with a discussion of the concerted vs. stepwise character of the mediated oxidation of GSH by different metal complexes, based on the KIE values obtained for the oxidation of GSH by $[Mo(CN)_8]^{3-}$, $[IrCl_6]^{2-}$ and $[Fe(phen)_3]^{3+}$. The KIE values obtained for the oxidation of GSH with each mediator show that, even though a kinetic isotopic effect is observed with all three metal complexes, as the concentration of phosphate buffer pH 7.0 is increased above 10 mM, the KIE values decrease below 2.0 with $[Mo(CN)_8]^{3-}$ and $[Fe(phen)_3]^{3+}$, which are the weakest and the strongest oxidizing agents used in this study. This is interpreted as indicative of different contributions of the concerted and stepwise PCET pathways at variable buffer concentration for each mediator.

3.2 Experimental Section

3.2.1 Reagents and Materials

L-glutathione reduced (Aldrich, 99%), K_3IrCl_6 (Aldrich), $K_4Mo(CN)_8$ (Aldrich, 99.99%), NaOH (Aldrich, 99.9%), NaCl (Aldrich, 99.9%), $Na_2HPO_4{\cdot}2H_2O$ (Sigma, >99.0%), HCl (Fisher Scientific, 37.3%), sodium deuteroxide (NaOD, Aldrich, 40% wt. in D_2O, 99+% atom D),

deuterium oxide (D_2O, Acros Organics, 100.0 atom % D), potassium dideuterium phosphate (D_2PO_4, Sigma Aldrich, atom 98% D), L-histidine (Acros Organics, 98%), malic acid (Fluka, > 99.5%), maleic acid (Fluka, > 99.0%) and succinic acid (Fluka, >99.5 %) were used without further purification. $Fe(bpy)_3SO_4$ and $Fe(phen)_3SO_4$ were prepared following the procedure reported by Drago and DeSimone. [16] Stoichiometric amounts of $FeSO_4.7H_2O$ (Aldrich, 99%) and 2,2'-dipyridil (Sigma, 99%) or 1,10-phenanthroline (Aldrich, 99%) were mixed in warm deionized water, and 3 mL of 1 M H_2SO_4 were added. A red solid was obtained in both cases upon evaporation of the solvent. Further purification of the solids was achieved through re-crystallization from a 20 mL ethanol + 10 mL ether mixture.

The pH of all solutions was measured with an Oakton pH meter (pH 1100 series), calibrated with pH 4.00, 7.00, and 10.00 buffers (Microesential Laboratory, Brooklyn, NY). Diluted NaOH and HCl (~ 1 M) were used to adjust the pH when required. All aqueous solutions were prepared using deionized (DI) water with a resistivity of 18.2 MΩ cm; water was purified with a MilliQ purification system (Billerica, MA). Deuterated phosphate buffer solutions used for KIE determination experiments were prepared with deuterium oxide (D_2O 100.0 % atom D) and potassium dideuterium phosphate (D_2PO_4 98% atom D). The pD of deuterated phosphate buffers was adjusted to pD 7.0 by adding microliter amounts of NaOD, and the pH measured by the pH meter (Oakton pH meter 1100 series) was converted to pD by using the formula $pD = pH + 0.4$. [17]

All experiments were carried out in a solution volume of 10.00 mL at room temperature (22 ± 1 °C) deoxygenated with nitrogen, in the case of aqueous solutions, and argon for deuterated solutions. A nitrogen/ argon atmosphere was maintained inside the electrochemical cell during experiments.

3.2.2 Cyclic Voltammetry

Cyclic voltammograms (CVs) were collected using a potentiostat (CH Instruments, Austin, TX), and an electrochemical cell equipped with a glassy carbon (GC) working electrode (area = 0.07 cm^2), a Pt-wire counter electrode, and Ag/AgCl reference electrode (1.0 M NaCl). The glassy carbon electrode was polished with 0.05 μm alumina mixed in DI water over a Buehler cleaning pad (Lake Bluff, Illinois), and rinsed with DI water after polishing and between experiments. Working solutions contained 1.00 mM of metal complex and 1.00 mM L-glutathione (reduced) dissolved in 10.00 mL of *x* mM aqueous buffer, added with NaCl to maintain an ionic strength of 1.0 M. The potential was scanned from 0.20 V to 1.00 V vs. Ag/ AgCl/ 1.0 M NaCl, except for voltammograms of solutions containing $K_4Mo(CN)_8$, in which case it was scanned from 0.20 V to 0.85 V vs. Ag/ AgCl/ 1.0 M NaCl. The cyclic voltammograms were background subtracted and obtained at room temperature (~22 ± 1 °C).

3.2.3 Digital Simulations and Fitting

Digital simulations were performed using the software package DigiSim™ version 3.03 (Bioanalytical Systems, Inc., West Lafayette, IN). The electrochemical mechanism depicted in Scheme 3.1 was entered into Digisim™ to fit experimental CVs obtained in the presence of the different metal complexes and buffers. All the thermodynamic and kinetic parameters used for simulation of all CVs are listed in the Appendix 3.

The concentrations of all species were the actual values used in the experiments. Initially k_{obs}, k_{obs}', k_{s3}, K_4, k_5 and K_5 and were allowed to vary iteratively while keeping one of them constant at a time, until a close match to the experimental CV was obtained. The rest of the kinetic parameters were estimated from literature values or fitted by Digisim and then kept constant throughout simulations (see appendix 3). The kinetic and thermodynamic parameters $E_{1/2}$, k_{s1}, K_6

$M^{(n+1)+} + e^- = M^+$	(3.1) $E_{1/2}$ and k_{s1} obtained from fitted experimental CVs.
$G + M^{(n+1)+} = M^+ + G^\bullet$	(3.2) K_2 and k_{obs} were fitted by Digisim.
$G = G^\bullet + e^-$	(3.3) $E_{1/2}$ was estimated through Eq. 7; k_{s3} was fitted by DigiSim. This reaction was included only in simulations of CVs in phosphate buffer.
$G^\bullet + G^\bullet = GG$	(3.4) K_4 and k_4 were fitted by DigiSim
$G^\bullet + M^{(n+1)+} = M^+ + G'$	(3.5) K_5 and k_{obs}' were fitted by Digisim.
$M^{(n+1)+} = P$	(3.6) K_6 and k_6 estimated from fitted experimental CVs.

Scheme 3.1. Reaction mechanism entered into DigiSim™ to simulate experimental CV results. $M^{(n+1)+}$ and M^+ represent the oxidized and reduced forms of the mediator, respectively; P is the product of the decomposition of the oxidized mediator; G, $G^\bullet$ and GG represent the reduced, radical, and disulfide forms of glutathione, respectively; and G' is the product of the further oxidation of the glutathione radical $G^\bullet$ by the mediator.

and k_6 for the redox couples $M^{(n+1)+}$/ M^+ listed in the Appendix 3 were determined by fitted simulation of CVs recorded for each metal complex alone. For a particular buffer and mediator, the CVs were recorded at five scan rates 0.1, 0.3, 0.5, 0.7 and 1.0 V/s. The fitted equilibrium and rate constant values obtained from simulations of CVs at the various scan rates were averaged and their corresponding standard deviation determined.

In the simulation of CV's run in phosphate buffer solutions, the equilibrium constant K_2 was automatically fixed by DigiSim from the $E_{1/2}$ value of the redox couples $M^{(n+1)+}$/ M^+, estimated from fittings of CV's of the mediator alone, and the reduction potential of GSH (E_{GSH}) which

was estimated through Eq. 3.7. Equation 3.7 is the Nernst expression for the reduction potential of GSH and it relates E_{GSH} with the standard redox potential E° of the couple $GS^{\bullet}/ GS^{-}$, the concentration of H^{+} and the acidity constant of glutathione's thiol group K_{SH}. In this work, we used E° ($GS^{\bullet}/ GS^{-}$) = 0.80 V vs. NHE (0.58 V vs. Ag/ AgCl) proposed as a plausible approximation by Wardman and Madej [18] the respective $[H^{+}]$ ($\sim 10^{-pH}$) and $K_{SH} = 10^{-8.7}$ to estimate the reduction potential of GSH at different pH's (see Appendix 3).

$$E_{GSH} = E^{\circ}(GS^{\bullet}/GS^{-}) - \frac{RT}{F}\ln\left(1+\frac{[H^{+}]}{K_{SH}}\right) \qquad \text{Eq. 3.7}$$

The values of E_{GSH} thus determined were entered into DigiSim as the $E_{1/2}(G^{\bullet}/G)$ of reaction (3.3). Then, DigiSim fixed the value of the equilibrium constant of reaction (3.2) because K_2 is related to E_2 [= $E_{1/2}$ ($M^{(n+1)+}/ M^{+}$) - $E_{1/2}(G^{\bullet}/G)$] by the following form of the Nernst equation at 25 ° C (Eq. 3.8):

$$K_2 = e^{\left(\frac{nFE_2}{RT}\right)} = 10^{nE_2/0.059} \qquad \text{Eq. 3.8}$$

In Eq. 3.8 the approximation that $E_{1/2} \approx E°$ is made if the diffusion coefficients for both species of the redox couple are very similar.

However, reaction (3.3) is part of the mechanism to simulate CVs run in the presence of phosphate buffer but not for those run in histidine, maleic, succinic or malic buffer, because the direct oxidation of glutathione at the electrode surface is greatly reduced in these buffers. Hence, to simulate CVs of all other solutions different from those prepared with phosphate buffer, the value of $E_{1/2}$ for reaction (3.3) calculated using Eq. 3.7, and the $E_{1/2}$ of reaction (3.1) were combined to determine K_2 by applying the Nernst equation 3.8.

Reaction (3.5) was proposed to account for mediation currents due to the production of further oxidation states of the sulfur in GSH (represented as G') or chemical routes different than the dimerization of the thiyl radical (Eq. 3.4). Although the influence of reaction (3.5) is especially evident in simulations of CVs at higher concentrations of buffer, it is reaction (3.2) the one determining the peak potentials and ~90% of the current. The need of secondary electron transfer steps like reaction (3.5) also applies to the simulation of the mediated oxidation of guanine, other purines and even DNA-wrapped carbon nanotubes. [5,6,19] Furthermore, the oxidation of thiyl radicals by metal complexes (also known as thiol overoxidation) was already reported by Sun, Wang and coworkers. [20,21] CV simulations showed that the formation of glutathione disulfide from the combination of two radical species (Eq. 3.4) has equilibrium and rate constants of K_4~10^9-10^{10} $M^{-1}$and k_4~10^8-10^9 $M^{-1}s^{-1}$, respectively. A report shows values for k_6 between $1.5x10^9$ $M^{-1}s^{-1}$ and $3.4x10^9$ $M^{-1}s^{-1}$, which are comparable to those used in our simulations. [18]

Reaction (3.6) accounts for any instability of the oxidized metal complexes. The decomposition of $[Mo(CN)_8]^{3-}$ into $[Mo(CN)_7H_2O]^{2-}$ + CN^- was reported by Nekrassova et al[22] in the oxidation of cysteine by electro-generated octacyanomolibdate (V). The instability of the iron-based mediators $Fe(phen)_3SO_4$ and $Fe(bpy)_3SO_4$ was taken into account by Campbell et al[19] in their paper about the mediated oxidation of DNA-wrapped carbon nanotubes, and similar kinetic parameters for their decomposition were used in our simulations. In regards to the instability of $[IrCl_6]^{2-}$, it was accounted for in the simulation of CVs of phosphate buffer pH 7.0 solutions, but those run in histidine buffer fitted well without including reaction (3.6).

Figure 3.3(E-F) shows some CVs of the mediators alone and after addition of glutathione and their respective digital simulations. The diffusion constants of the mediators ($D_{M+/M}$) in Table 3.S1 in Appendix 3 were obtained from fitted simulations of CVs of the mediators alone,

and they are comparable with those found in the literature. [19,22-24] The diffusion coefficient of glutathione in D_2O was measured through Pulsed Gradient Echo (PGE-) ^{1}H-NMR on a Varian Inova 400MHz NMR at 25 °C as described in a previous work.[1,4] The average diffusion coefficient of glutathione after correction for viscosity differences was $(5.13 \pm 0.05) \times 10^{-6}$ cm^2 s^{-1}.

3.3 Results and Discussion

3.3.1 The Marcus Theory and the oxidation of glutathione

Chapter 2 dealt with the catalytic effect of various Brönsted bases on the mediated oxidation of glutathione (GSH) by $[IrCl_6]^{2-}$. [4] For this reaction, the observed rate constant k_{obs} revealed a linear dependence on the concentration of phosphate buffer at a constant pH of 7.0, within the range of 0-50.0 mM, which leveled off at concentrations above 100 mM phosphate buffer. Likewise, with a series of buffers (malic, succinic, maleic, citrate and phosphate buffers) at a pH =. pK_a of the buffer's conjugate acid, the relationship RT lnk_{obs} vs. pK_a was fitted through linear regressions, and slope values of 0.62 and 0.69 were obtained using 5.0 mM and 35.0 mM of buffer, respectively. [4] Given the dependence of k_{obs} on the concentration and strength (pK_a) of the bases used, and based on the theory of acid-base catalysis, [4,12,14,15,25] it was proposed that the oxidation of GSH by $[IrCl_6]^{2-}$ involved the transfer of glutathione's sulfhydryl proton to the buffer base in the rate determining transition state of this PCET. As an extension of that previous work, this study compares the oxidation of glutathione by the mediators $[Mo(CN)_8]^{3-}$, $[Fe(bpy)_3]^{3+}$, $[Fe(phen)_3]^{3+}$ and $[IrCl_6]^{2-}$ in the presence of different concentrations of phosphate buffer pH 7.0 and histidine buffer pH 6.5. The objective of this work was to investigate if the oxidation of GSH by different mediators could be described by the Marcus theory of electron transfer, which is the most well-known theoretical approach to describe the relationship between

kinetics and thermodynamics of electron transfer processes. [26,27] Also, this investigation aimed to determine whether the concentration and/or pK_a of the Brönsted base in solution would influence the slope of linear free energy plots of RTF^{-1} lnk_{obs} vs. redox potential of the mediator ($E_{1/2}$ in this work), as Thorp and coworkers observed in the study of the oxidation of guanine and other purines by $Os(bpy)_3^{3+}$ in aqueous. [5,6] This appeared to be a valid question, given that the drifting of the Marcus slope for oxidation of guanine in aqueous solutions from the expected value of 0.5 was attributed to the coupling of PT and ET, and the same is suspected to be taking place during the oxidation of GSH in the presence of Brönsted bases such as HPO_4^{2-} or histidine.

Weatherly et al showed that the Marcus plot for the oxidation of guanine by ruthenium-based metal complexes in water had a slope of 0.8 ± 0.1, instead of the expected 0.5 observed for reactions where the electron transfer is rate-limiting. [6,26] Similar and even higher slope values were obtained by replacing guanine with other 7-deazapurines. [5] The high slope of the Marcus plot was ascribed to the involvement of the proton transfer from guanine to the solvent (water) in the transition state of the reaction, which resulted in a concerted proton-coupled electron transfer (CPCET) process. [5,6] Although the authors made reference to Ram and Hupp's paper on Linear Free Energy Relations for Multielectron Transfer Kinetics [28] to support this assignment, we believe that it is not safe to conclude from that work that the high value of the Marcus slope for the oxidation of guanine is due to the coupling of proton and electron transfers. Hence, this work focuses in the analysis of the oxidation of GSH from the frameworks of both the Marcus and the acid-base catalysis theories in order to explore to what extent the oxidation of GSH by different mediators is (1) a base catalyzed reaction with PT and ET coupled in the rate determining TS; and (2) find out if the slope of the Marcus relationship is sensitive to the coupling of PT and ET.

Cyclic voltammetry was used to monitor the oxidation of GSH by the different mediators. The observed rate constant (k_{obs}) for the reaction between glutathione and the metal complexes was

estimated through simulation of the respective voltammograms at different concentration and type of buffer according to the mechanism described in Scheme 3.1. Marcus plots of RTF^{-1} lnk_{obs} vs. $E_{1/2}$ for the oxidation of glutathione in the presence of various concentrations of phosphate buffer pH 7.0 and histidine buffer pH 6.5 appear in Figure 3.1. The linearity of these plots demonstrates that the oxidation of the thiol by the four metal complexes used follows a Marcusian behavior, at least within the range of redox potentials studied. [26,27] Also, it is remarkable that the slopes in Figs. 3.1A and 3.1B become steeper as the concentration of buffer increases, at a constant pH (Table 3.1). At low concentrations of buffer (10 mM phosphate buffer or 5-10 mM histidine buffer pH 6.5) the slope is around the expected value of 0.5. However, higher concentrations of histidine and phosphate buffer produced Marcus slopes above the typical 0.50 (Table 3.1). In the presence of phosphate buffer, for example, the oxidation of glutathione achieved the highest slope measured, 0.75 ± 0.04 at 50.0 mM phosphate buffer pH 7.0. This value is about 0.05 units larger than the highest slope obtained with histidine buffer ($0.69_8 \pm 0.09_1$). This difference could be tentatively attributed to the stronger basic character of HPO_4^{2-} ($pK_a = 7.2$) compared to histidine ($pK_a = 6.5$) based on the fact that stronger bases cause a larger enhancement of the oxidation of GSH by the different mediators. The evidence to support the statement above are the larger values of k_{obs} obtained with phosphate buffer compared to those obtained with histidine and other buffers of even lower pK_a's which can be seen when comparing the RTF^{-1} lnk_{obs} values of Figs. 3.1A and 3.1B (see Appendix 3 for k_{obs} values obtained with other buffers). The observation of a higher Marcus slope for the oxidation of GSH as the concentration of buffer increases is therefore indicative of a higher sensitivity of the observed rate constant to the amount of base present, a landmark of general base catalyzed processes. Likewise, it is well known that the rate of general base catalyzed reactions will show a dependence on the pK_a of the bases involved, hence it is

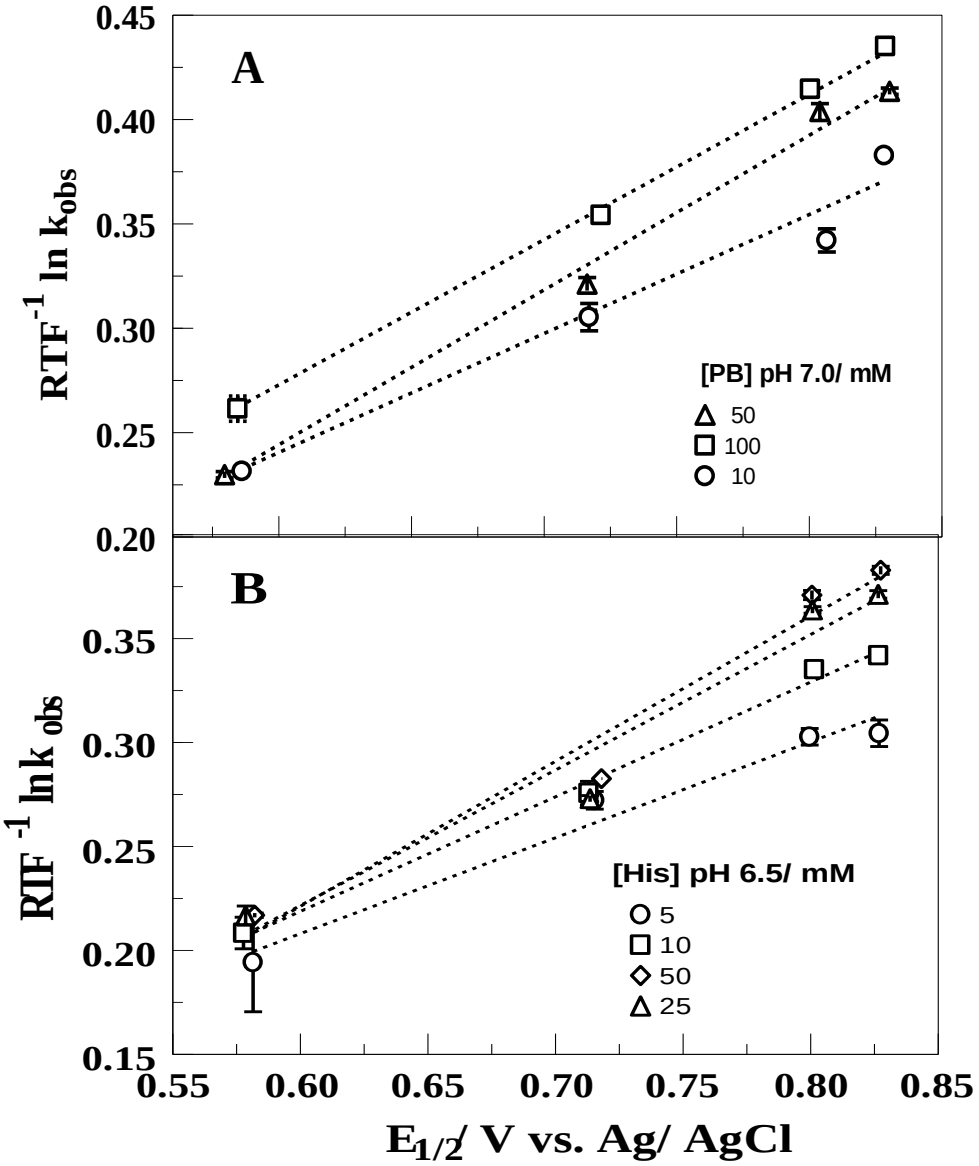

Figure 3.1. $RTF^{-1} \ln k_{obs}$ vs. $E_{1/2}$ of the mediator, at varying concentrations of phosphate buffer pH 7.0 (A) and histidine buffer pH 6.5 (B); k_{obs} is the observed rate constant for the oxidation of GSH (1.0 mM) by each mediator (1.0 mM mediator in the reduced form) estimated through digital simulation of CVs run at various scan rates. The mediators, in increasing order of $E_{1/2}$, were $[Mo(CN)_8]^{4-/3-}$, $[IrCl_6]^{2-/3-}$, $[Fe(bpy)_3]^{3+/2+}$ and $[Fe(phen)_3]^{3+/2+}$.

Table 3.1. Slope and R^2 of the Marcus plots (RTF^{-1} lnk_{obs} vs. $E_{1/2}$) for the electron transfer from GSH to metal complexes.

Buffer	**Buffer Concentration/**	**Slope**	**R^2**
Phosphate pH 7.0	10	0.57 ± 0.08	0.9671
	50	0.75 ± 0.04	0.9931
	100	0.71 ± 0.01	0.9991
Histidine pH 6.5	5	0.46 ± 0.05	0.9721
	10	0.55 ± 0.03	0.9945
	25	$0.65_1 \pm 0.09_8$	0.9562
	35	0.7 ± 0.1	0.9499
	50	$0.69_8 \pm 0.09_1$	0.9669

reasonable to expect that in the presence of HPO_4^{2-} the changes in the Marcus slope for the mediated oxidation of GSH would be larger than in the presence of a weaker base like histidine.

Plots of RTF^{-1} lnk_{obs2} vs. $E_{1/2}$ for the overoxidation of glutathione radicals by the mediators (Eq. 3.4 in Scheme 3.1) appear in the Appendix 3 (Figs. 3.S1 and 3.S2). In the presence of phosphate buffer, RTF^{-1} ln k_{obs2} exhibits a linear dependence on $E_{1/2}$ (Fig. 3.S1), with a slope of 0.31 ± 0.03 and 0.31 ± 0.05 when using 50.0 mM and 100 mM phosphate buffer pH 7.0, respectively, although marked deviations from linearity were observed in 10.0 mM phosphate buffer pH 7.0. In the presence of histidine buffer, plots of RTF^{-1} lnk_{obs2} vs. $E_{1/2}$ (Fig. 3.S2) deviate from linearity even more, especially at higher driving forces, i.e. with mediators $[Fe(bpy)_3]^{3+}$ and $[Fe(phen)_3]^{3+}$. The overoxidation of GSH is included to account for ~10% of the anodic current measured in cyclic voltammograms of the mediators in the presence of GSH. This reaction would represent a route to higher oxidation derivatives of GSH such as GSOH and possibly GSO_3^- and was proposed in previous mechanistic studies of the oxidation of cysteine and thioglycolic acid by $[IrCl_6]^{2-}$ and Fe^{3+} metal complexes. [20,21] However, a thorough analysis of the kinetics of overoxidation of glutathione is beyond the scope of this work, which focuses on the first oxidation of glutathione as the primary PCET of the mechanism.

According to the electron transfer theory developed by Marcus [26,27] the equation for the rate constant of electron transfer *k* is

$$k = A\exp[-k_B^{-1}T^{-1}\Delta G^*] \qquad \text{Eq. 3.9}$$

where the reaction activation energy ΔG* is described by

$$\Delta G^* = \frac{\lambda[1+\Delta G^\circ/\lambda]^2}{4} \qquad \text{Eq. 3.10}$$

In equation 3.9, A is a term that depends on the nature of the electron transfer; ΔG° is the standard free energy of reaction; and λ is the reorganization energy of the species involved in the electron transfer, which is a combination of solvational and vibrational components. [26,27] When $|\Delta G^\circ/\lambda|$ is small, ΔG* (= k_BT lnk) depends linearly on -ΔG° with a slope of 0.5. [26,27] As ΔG° becomes larger, the slope value decreases, becoming zero at ΔG°= -λ. For the reactions between GSH and the mediators used, ΔG° is more negative as $E_{1/2}$ of the mediator increases, however the region at which the slope of RT $\ln k_{obs}$ vs. ΔG° approaches zero is not observed in this study.

Nonetheless, the Marcus theory does not offer an explanation for slope values above 0.5 as those observed at higher concentrations of buffer (Table 3.1). [26,27] Based on the experimental evidence discussed in chapter 2, which shows that higher electrochemical currents are achieved through oxidation of GSH by $[IrCl_6]^{2-}$ as the concentration of buffer increases, or by using stronger Bronsted bases (see Fig. 2.5); and because larger k_{obs} values are obtained by increasing the concentration of phosphate or histidine buffers (see Fig. 3.1) we propose that the abnormally high values of the Marcus plots are caused by the coupling of proton and electron transfer during oxidation of GSH by the mediators. On the other hand, although it may be possible that specificities of the mediators used (i.e. chemical structure, charge, reorganization energy, etc.) affect the slope value as well, those specific effects would be minimized by working with

solutions of high ionic strength and using metal complexes that exhibit fast, reversible outer-sphere one-electron transfer.

3.3.2 Voltammetry of the oxidation of GSH by different mediators

Figure 3.2 shows experimental and simulated CVs of the mediators $[Mo(CN)_8]^{3-}$ (A-D) and $[Fe(phen)_3]^{3+}$ (E-H) in the presence of 1.0 mM GSH and either phosphate buffer pH 7.0 or histidine buffer pH 6.5, at increasing CV scan rate. The mediators $[Mo(CN)_8]^{3-}$ and $[Fe(phen)_3]^{3+}$ have the lowest and the highest redox potential used in this study, ~0.59 V and ~ 0.82 V vs. Ag/AgCl respectively. As it was explained it chapter 2, all the voltammetry shown in Fig. 3.2 is showing the electrochemical oxidation of the mediator M^{n+} into $M^{(n+1)+}$ in the forward potential scan (negative current wave) and the reduction of $M^{(n+1)+}$ into M^{n+} in the reverse potential scan (positive current wave). When the reaction between GSH and $M^{(n+1)+}$ ($M^{(n+1)+}$ is electro-generated in the forward voltammetric scan) takes place in solution, the radical $GS^{\bullet}$ and the reduced mediator M^{n+} are produced and the electrochemical reduction of $M^{(n+1)+}$ is diminished to a degree that depends on the rate of the homogenous oxidation of GSH by $M^{(n+1)+}$. In that case, a decreased cathodic current is observed in the reverse potential scan and an enhanced anodic current is seen in the forward scan. Thus, the magnitude of the cathodic current is lower when the velocity of reaction between $M^{(n+1)+}$ and GSH in solution is faster compared to the rate of reduction of M(n+1)+ at the electrode surface. Also, as the rate at which the potential is scanned increases, the electrochemical reduction might compete more effectively with the homogeneous reaction and a larger cathodic current could be detected in the reverse scan, as shown in Fig. 3.2A. Here, where applicable, we will use the ratio of cathodic-to-anodic peak current I_{pc}/I_{pa} to measure the effect of the homogenenous reaction between $M^{(n+1)+}$ and GSH on the CVs. Therefore, the closest this I_{pc}/I_{pa} ratio is to 1, the less the electrochemical reduction and oxidation

of the mediator are perturbed by the homogeneous reaction; on the contrary, the closest this I_{pc}/I_{pa} ratio is to 0, the faster the homogeneous reaction has become and able to compete with the electrochemical reduction of $M^{(n+1)+}$. The I_{pc}/I_{pa} ratio will be calculated for those CVs run at 1.0 V/s only.

Figures 3.2(A-D) correspond to CVs at variable scan rates of 1.0 mM $[Mo(CN)_8]^{3-}$ + 1.0 mM GSH in (A) 5.0 mM histidine buffer pH 6.5, (B) 35 mM histidine buffer pH 6.5, (C) 10 mM phosphate buffer pH 7.0 and (D) 50 mM phosphate buffer pH 7, respectively. Overlaid circles represent the results of digital simulations according to Scheme 3.1. Increasing the concentration of histidine buffer pH 6.5 from 5.0 mM to 35 mM appears to have a small effect on the anodic and cathodic currents of CVs 3.2A and 3.2B, which show I_{pc}/I_{pa} ratios of 0.74 and 0.69 respectively. Something similar is observed when comparing CVs 3.2C and 3.2D where the concentration of phosphate buffer pH 7.0 was raised from 10 mM to 50 mM with I_{pc}/I_{pa} ratios of 0.55 and 0.58, respectively. However, when comparing CVs 3.2A (I_{pc}/I_{pa} = 0.74) with 3.2C (I_{pc}/I_{pa} = 0.55) and 3.2B (I_{pc}/I_{pa} = 0.69) with 3.2D (I_{pc}/I_{pa} = 0.58) it is clear that overall the anodic current increases and the cathodic current decreases by changing histidine buffer pH 6.5 for phosphate buffer 7.0. The increase in anodic current is due to a faster oxidation of GSH by mediator $[Mo(CN)_8]^{3-}$ in the presence of phosphate buffer pH 7.0 than in histidine buffer pH 6.5. This highlights once again the larger kinetic effect of HPO_4^{2-} (pK_a = 7.2) over histidine (pK_a = 6.5) on the oxidation of GSH. Likewise, the decrease in the cathodic current when histidine is replaced by phosphate buffer is due to the same effect: in the presence of HPO_4^{2-} a higher extent of GSH oxidation by $[Mo(CN)_8]^{3-}$ is achieved, causing more of the oxidized mediator to be reduced by GSH in solution than at the electrode surface.

In Figure 3.2, CVs E-H were run at the same conditions of GSH and buffer type and concentration as CVs A-D except that the mediator was $[Fe(phen)_3]^{3+}$. Unlike $[Mo(CN)_8]^{3-}$, the

mediator $[Fe(phen)_3]^{3+}$ (which is a stronger oxidizing agent than the former) produces markedly different CV responses in the presence of GSH depending on the type and concentration of buffer used. Increasing the concentration of histidine buffer from 5.0 mM (E) to 35 mM (F) causes the increase of the anodic current due to mediated oxidation of GSH by $[Fe(phen)_3]^{3+,}$ and the decrease of the cathodic current for electrochemical reduction of the mediator around 0.8 V. Furthermore, in Figure 3.2F the anodic peak seen at ~0.82 V at a scan rate of 1 V/s becomes less sharp as the scan rate is decreased almost as if it was splitting into two peaks. The splitting of this anodic peak actually occurs in the presence of phosphate buffer pH 7.0 as can be seen in Figures 3.2G-H. Both CVs 3.2G and 3.2H show two overlapped anodic peaks, one around 0.82 V and a 'new' one at ~0.78 V, with the latter peak being especially defined when the scan rate is lowered and in the presence of 50 mM PB. Although the anodic peak currents at 1.0 V/s are smaller in CVs 3.2G and 3.2H (~ 62 μA in both) than in 3.2E (~ 70 μA) and 3.2F (~90 μA) and the cathodic peak around 0.83 V is more evident in 3.2G and 3.2H than in CVs 3.2E and 3.2F, this does not mean that in the presence of histidine buffer pH 6.5 the rate of oxidation of GSH by $[Fe(phen)_3]^{3+}$ is larger than in phosphate buffer pH 7.0: k_{obs}still increases from $1.8x10^5$ to $2.7x10^6$ $M^{-1}s^{-1}$ when replacing 5.0 mM histidine pH 6.5 by 10 mM phosphate buffer pH 7.0; and from $2.4x10^6$ to $9.7x10^6$ $M^{-1}s^{-1}$ when changing 35 mM histidine pH 6.5 by 50 mM phosphate buffer pH 7.0 (see Appendix 3).

The splitting of the anodic peak due to oxidation of $[Fe(phen)_3]^{2+}$ in the presence of GSH and PB pH 7.0 can be explained in terms of the theory developed by Saveant [29] to describe the voltametric responses of electrochemical reactions involving homogeneous catalysis, specifically those where the homogeneous electron transfer is the RDS.

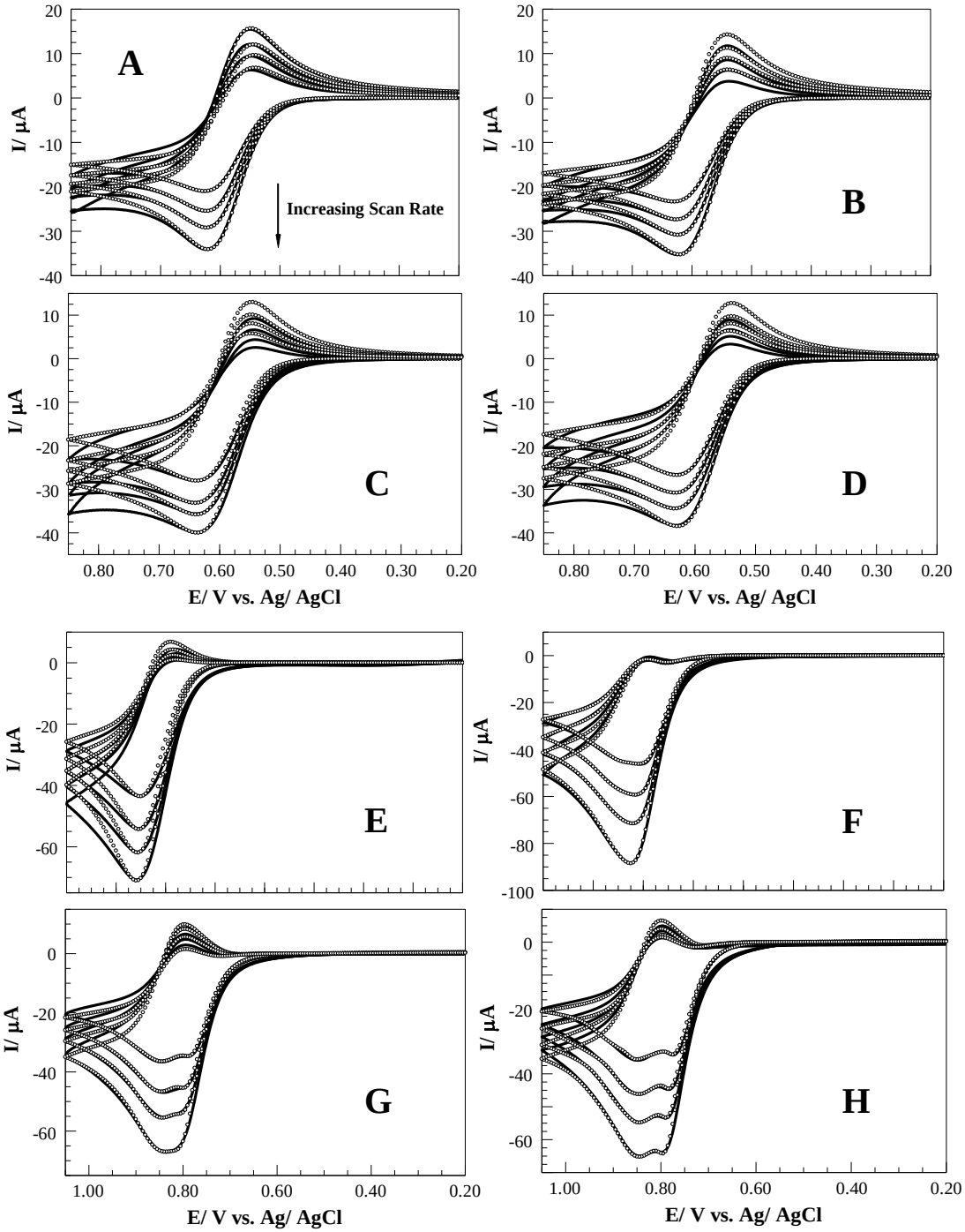

Figure 3.2. CVs A-D: experimental (solid line) and simulated (open circles) CV responses of 1.0 mM GSH + 1.0 mM $K_4Mo(CN)_8$, in the presence of (A) 5.0 mM and (B) 35 mM histidine buffer pH 6.5; and (C) 10 mM and (D) 50 mM phosphate buffer pH 7.0. CVs run at 0.3, 0.5,0.7 and 1.0 V/s. CVs E-H: experimental (solid line) and simulated (open circles) CV responses of 1.0 mM GSH + 1.0 mM $Fe(phen)_3SO_4$, in the presence of (E) 5.0 mM and (F) 35 mM histidine buffer pH 6.5; and (G) 10 mM and (H) 50 mM phosphate buffer pH 7.0. CVs run at 0.3, 0.5, 0.7 and 1.0 V/s.

Given that in all the experiments done in this study the concentration of both GSH and the reduced mediators in solution are the same ($1x10^{-3}$ M) the excess factor γ that Saveant defines as the ratio of the substrate to mediator bulk concentrations is equal to 1 for all voltammograms shown here; this value of γ would place all the voltammetric responses in the 'substrate diffusion' regime, which means that the reaction between GSH and the mediators would be limited by the diffusion of GSH from the bulk. [29] As a result of this, when the rate of the homogeneous electron transfer from GSH to the mediator is forced to increase by using mediators of higher redox potential ($E_{1/2}$) the voltammetric responses will vary as well: from a voltammogram showing an enhanced anodic peak and a diminished cathodic wave due to the catalytic oxidation of GSH by the metal complex (like those in Figs. 3.2C-D) to CVs that have two overlapped anodic peaks, one due to the catalytic oxidation of GSH and the other due to oxidation of the mediator alone (as those shown in Figs. 3.2G-H).

Based on the same theory, the transition from CVs having a single anodic peak to those with doubled anodic waves (maintaining γ constant) provides experimental evidence that the rate of catalytic oxidation of the substrate by the mediator is increasing. In the case of GSH oxidation, the rate of reaction increases when $[Mo(CN)_8]^{3-}$ is replaced by $[Fe(phen)_3]^{3+}$ (Figs. 3.2A-H) because the redox potential of the latter (~0.82 V) is larger than that of the former metal complex (~ 0.59 V). Furthermore, by inspecting the CVs in Figs. 3.2E-H, it becomes evident that changing the buffer type (histidine or phosphate) and/or concentration while using the same mediator can produce a similar outcome since a single anodic peak, like that observed in Fig. 3.2E for the oxidation of GSH by $[Fe(phen)_3]^{3+}$ in 5.0 mM histidine buffer pH 6.5, splits into a double anodic wave in Figs. 3.2G-H when the same experiment is done in phosphate buffer pH 7.0 instead. In Figs. 3.2E-H the rate of homogeneous electron transfer between GSH and $[Fe(phen)_3]^{3+}$ is

increasing as the concentration and/or the pK_a of the buffer base are increased, a consequence of this being a base catalyzed process that depends on the amount and strength of the Brönsted bases involved. In the CVs showing two overlapped anodic peaks (Figs. 3.2G-H) the peak at the lower potential (~0.75- 0.78 V) is attributed to the mediated oxidation of GSH, while the peak at higher potential (~ 0.82 V) marks the oxidation of metal complex that does not participate in the catalytic cycle. According to Saveant, when the reaction between mediator and substrate is so fast that only a small amount of the mediator is required to complete the reaction, the concentration of substrate nearby the electrode surface is quickly depleted and the process becomes limited by diffusion. [29] As the rate constant of homogeneous electron transfer *k* increases, the rate of reaction goes from being controlled by 'substrate diffusion', with a CV showing a single catalytic peak, to a 'total catalysis' regime with a CV having two anodic waves. [29] However, it would not be accurate to assume that the CV responses shown in Figs. 3.2G-H correspond to the achievement of a 'total catalysis' regime because the current of the catalytic peak (~0.78 V) is not larger than that of the peak due to pure oxidation of $[Fe(phen)_3]^{2+}$ (~0.82 V) as it is predicted to occur at such regime.

What is unambiguous from the experiments shown in Figure 3.2 is that definite CV responses, which are dependent the rate of homogeneous electron transfer between GSH and the mediators (i.e. k_{obs} in this work) constitute empirical evidence of the differences in catalytic activity of the mediators and the Brönsted bases used to study this PCET. Both Figures 3.1 and 3.2 show that the rate of oxidation of GSH increases by raising the oxidizing power of the mediator i.e. by using metal complexes of higher redox potential. However, the analysis of these figures demonstrates that the effect of Brönsted bases on the rate of reaction is always in the background and that it appears to influence the value of the slope in the Marcus plots as well. In other words,

the analysis of the Marcus plots reiterates that one way to catalyze the oxidation of GSH by a certain mediator is by changing the concentration and type of Brönsted base.

3.3.3 Origin of the kinetic effects if Brönsted bases on the oxidation of GSH

Although higher concentration and stronger bases tend to afford higher kinetic effects, from our previous study we learned that a suitable base is that which pK_a makes the proton transfer from GSH (pK_{SH} = 8.7) downhill in the TS of the PCET reaction, even if the proton transfer step is initially uphill in the ground-state. GSH would exhibit an uphill PT in the ground-state to histidine and HPO_4^{2-}, according to the calculated equilibrium constants K_{PT} ($=10^{pKBH+ - pKSH}$) of $6.31x10^{-3}$ and 0.0316, respectively; however, in the TS of this PCET the unfavorable ground state PT may become feasible due to a drop in pK_a of the forming glutathione radical cation $GSH^{\bullet+}$ which is predicted to have a $pK_a < 0$. [30] This difference in pK_a for $GSH^{\bullet+}$ compared to GSH (pK_{SH} = 8.7) would be responsible for the effect that bases like histidine and HPO_4^{2-} have on the rate oxidation of GSH, and the corresponding enhancement of the mediators oxidation current observed in CVs run in the presence of this thiol.

According to the libido rule postulated by Jencks, a pioneer of the acid-base catalysis theory, a *concerted* general base catalysis process is favored by a drastic change in pK_a of the substrate in the course of the reaction with a nucleophile. [31,32] A dramatic change in pK_a of the reaction site would afford a sufficiently negative free energy to compensate for the loss of entropy in the concerted pathway that requires the encounter of three species in solution, the base catalyst, the substrate and the nucleophile, without formation of an stable intermediate. [31,32] In the mediated oxidation of GSH, a concerted pathway seems reasonable to explain why bases of pK_a lower than that of the thiol can effect on the observed rate: the coupling of PT and ET at the transition state of a concerted oxidation of GSH would be favored by the decrease in pK_a of the thiol as the

electron transfer takes place and, at the same time, a concerted route would avoid the formation of the highly unstable protonated radical $GSH^{\bullet+}$.

Although a concerted pathway was proposed as the primary mechanism of GSH oxidation of GSH by $[IrCl_6]^{2-}$, especially at neutral pH conditions, stepwise routes like PTET and ETPT could not be discarded. A PTET route may still play a role in the oxidation of GSH because even though the initial deprotonation of GSH to GS^- is not thermodynamically favorable at pH< 7 (only ~2% of GSH exists as GS^- at pH 7) the oxidation of available GS^- would be significantly fast with an expected rate constant in the order of 10^6 M^{-1} s^{-1}. [20] Likewise, an ETPT pathway (oxidation of GSH followed by proton transfer from $GSH^{\bullet+}$) is not unreasonable especially for stronger mediators like $[Fe(bpy)_3]^{3+}$, $[Fe(phen)_3]^{3+}$ and even $[IrCl_6]^{2-}$, which may be able to abstract an electron from the protonated GSH, or from GS^- if the reaction takes place at pH > 8 where deprotonation of GSH becomes significant. However, an ETPT from GSH would be disfavored by the generation of the unstable intermediate $GSH^{\bullet+}$, something that could become less relevant in the presence of high concentrations of good proton acceptors like HPO_4^{2-}.

3.3.4 Effects of other Brönsted bases and mediators

Figure 3.3 compares the effect of (1) changing the mediator only and varying the buffer type and (2) increasing the buffer concentration, while using the same mediator, on CVs showing the mediated oxidation of GSH. These experiments are of a similar type as those in presented in Fig. 3.2; however, in Figure 3.3 the spectrum is extended to include two more mediators and three additional buffers in the investigation of this PCET. The CVs 3.3E-H correspond to 1.0 mM of reduced mediator in the presence of 1.0 mM GSH and 100 mM PB pH 7.0: the mediators, in their oxidized form, were (E) $[Mo(CN)_8]^{3-}$, (F) $[IrCl_6]^{2-}$, (G) $[Fe(bpy)_3]^{3+}$ and (H) $[Fe(phen)_3]^{3+}$

and their redox potentials are ~ 0.59 V, ~0.72 V, ~0.80 V and ~0.82 V vs. Ag/ AgCl, respectively. The CV responses of the mediators before and after addition of GSH are shown as well as the CVs obtained through digital simulation according to the reaction mechanism depicted in Scheme 3.1 (see Experimental Section). All the CVs in Fig. 3.3(E-H) show the enhancement of the mediator's anodic current due to reaction of the oxidized metal complexes with GSH, which takes care of the reduction of the former species that otherwise would occur at the electrode surface. The increasing values of k_{obs} obtained from simulations of CVs 3.3E-H show that the rate of reaction between each mediator and GSH increases with the redox potential of the metal complex (see Appendix 3).

Although it is hard to determine that the rate of oxidation of GSH is actually increasing with the redox potential of the mediator just by looking at CVs 3.3E-H, a remarkable phenomenon appears because of the kinetic differences for each mediator mentioned above: while $[Mo(CN)_8]^{4-}$ and $[IrCl_6]^{3-}$ give rise to a single anodic peak in the presence of GSH (k_{obs}'s are $(2.6\pm0.6) \times 10^4$ M^{-1} s^{-1} and $(9.7\pm0.7) \times 10^5$ $M^{-1}s^{-1}$, respectively) mediators $[Fe(bpy)_3]^{2+}$ and $[Fe(phen)_3]^{2+}$ produced two overlapped anodic peaks under the same conditions of GSH and buffer type and concentration (k_{obs}'s are $(1.02\pm0.05) \times 10^7$ $M^{-1}s^{-1}$ and $(2.3\pm0.1) \times 10^7$ $M^{-1}s^{-1}$, respectively). This phenomenon is undoubtedly an outcome of differences in the rate of reaction of each mediator with GSH (as indicated by the differences in k_{obs} values as well) being the enhancement of the rate of PCET as the mediator's redox potential increases from $[Mo(CN)_8]^{4-}$ to $[IrCl_6]^{2-}$ (single anodic peaks) and from $[Fe(bpy)_3]^{2+}$ to $[Fe(phen)_3]^{2+}$ (two overlapped anodic peaks) what causes the splitting of the anodic peak as explained above.

A similar phenomenon occurs when using the same mediator, $[Fe(phen)_3]^{3+}$, while varying the type and concentration of buffer in solution, as can be seen in Figures 3.3(A-D).

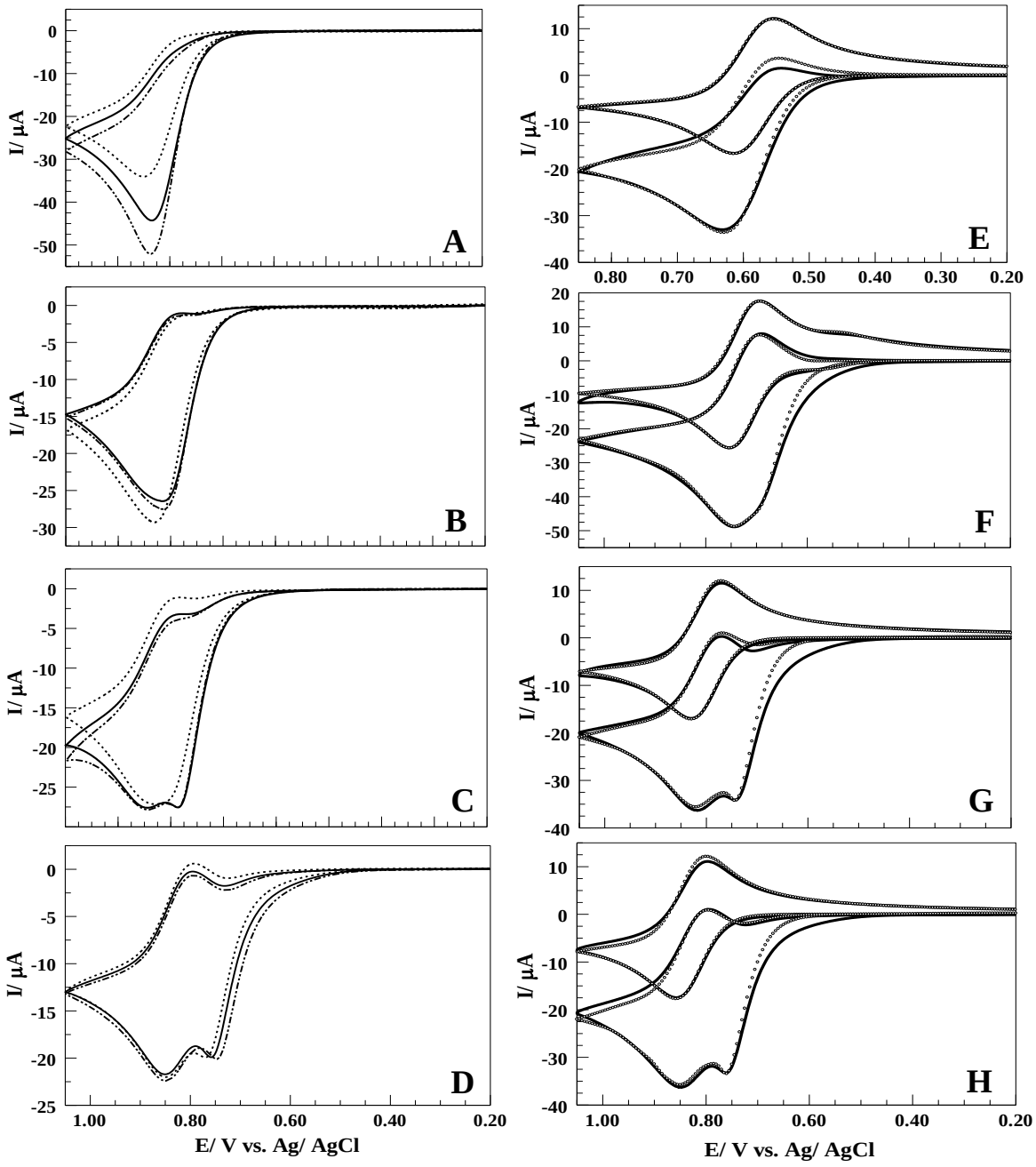

Figure 3.3 CVs A-D: CV response of 1.00 mM $Fe(phen)_3SO_4$ + 1.00 mM GSH in 10 mM (dashed line), 50 mM (solid line) and 100 mM (dashed-solid line) of different buffers. The buffers used were: malic buffer pH 5.1 (A), succinic buffer pH 5.6 (B), histidine buffer pH 6.5 (C) and phosphate buffer pH 7.0 (D); CV scan rate: 0.1 V/s. CVs E-H: experimental (solid line) and simulated (circles) CV response of 1.00 mM metal complex before and after addition of 1.00 mM GSH, in 100 mM phosphate buffer pH 7.0. The metal complexes used were $[Mo(CN)_8]^{4-/3-}$ (E), $[IrCl_6]^{2-/3-}$ (F), $[Fe(bpy)_3]^{3+/2+}$ (G) and $[Fe(phen)_3]^{3+/2+}$ (H); CV scan rate: 0.3 V/s.

These CVs are the response of 1.0 mM $[Fe(phen)_3]^{2+}$ in the presence of 1.0 mM GSH and either 10 mM, 50 mM or 100 mM of the following buffers: malic pH 5.1 (A), succinic pH 5.6 (B), histidine pH 6.5 (C) and phosphate pH 7.0 (D). In Figs. 3A-D the splitting of the anodic peak is again attributed to the increasing rate of reaction between $[Fe(phen)_3]^{3+}$ and GSH as the base in the buffer solution becomes stronger. Figure 3.3A exhibits a single anodic peak at ~0.83 V and which peak current increases from 34 μA to 52 μA by increasing the concentration of malic buffer pH 5.1 from 10 mM to 100 mM, respectively. The cathodic peak is gone in all CVs of Fig. 3.3A, which indicates an efficient oxidation of GSH that consumes all of the electrogenerated $[Fe(phen)_3]^{3+}$. In Figure 3.3B, at the highest concentration of succinic buffer pH 5.6 buffer (100 mM) the splitting of the anodic peak insinuates already. The splitting is unambiguous in histidine and phosphate buffer (Figs. 3.3C-D) and the transition from a single two a double anodic wave is definitive in histidine buffer as the concentration increases from 10 mM to 50 mM. The initial anodic peak at ~ 0.83V remains located around the same potential while the 'new' peak appears below 0.80 V, between 0.75V and 0.78 V, shifting more negative with PB than in histidine and as the concentration of either buffer increases (Figs. 3.3C-D). Phosphate buffer is responsible for the maximum splitting observed, with a separation of up to ~0.10 V between the initial and the 'new' anodic peaks (Fig. 3.3D) compared to histidine with a maximum splitting of ~0.06 (Fig. 3.3C). This greater effect of phosphate buffer ($H_2PO_4^-$ has a $pK_a = 7.2$) compared to malic ($pK_a = 5.1$), succinic ($pK_a = 5.6$) and histidine buffers ($pK_a = 6.5$) on the shape of the CVs and on the k_{obs} values obtained for the oxidation of GSH by $[Fe(phen)_3]^{3+}$ (see Fig. 3.4 and Appendix 3 for k_{obs} values) point toward base catalysis once again, since it is characteristic of this phenomenon to show a dependence of the observed rate constant on the pK_a of the bases involved when the PT step is in the rate determining TS of the reaction.

To corroborate the existence of a relationship between k_{obs} and pK_a of the Brönsted bases when $[Fe(phen)_3]^{3+}$ and $[Mo(CN)_8]^{3-}$ are the mediators in the oxidation of GSH, CVs of solutions containing 1.0 mM of the reduced metal complex, 1.0 mM GSH and 50 mM of malic, succinic, maleic, histidine or phosphate were fitted through digital simulation to the reaction mechanism shown in Scheme 3.1, and the respective k_{obs} values were thus estimated. The pH of the different buffers used was adjusted to be the same as the pK_a of the respective conjugate base present in order to have 50% of both the acid and base components of the buffers in solution.

Figure 3.4 shows the plots of log k_{obs} vs. pK_a of the buffer base, also known as Brönsted relationship, for the mediators $[Fe(phen)_3]^{3+}$, $[IrCl_6]^{2-}$, and $[Mo(CN)_8]^{3-}$. The Brönsted plot corresponding to $[IrCl_6]^{2-}$ was reported in chapter 2 (Fig. 2.5) and each solution analyzed by CV contained 35 mM of the same buffers mentioned above, except that citrate buffer (pK_a = 6.4) was used instead of histidine. All three plots in Figure 3.4 were fitted through linear regressions and the corresponding slope and correlation coefficients are included in the graph. Linear Brönsted relationships are characteristic of general base catalyzed reactions, as they prove a dependence of the observed rate of reaction on the structural specificities of a series of general bases.

In essence, the slope of a Brönsted plot β is a measure of the sensitivity of the observed rate of reaction to the strength of the base involved or its pK_a. Figure 3.4 shows that even though all three mediators exhibit linear relationships between log k_{obs} and pK_a, each plot has a different β value, which also happens to increase as the redox potential of the mediator becomes higher: β is 0.42 ± 0.02 for $[Mo(CN)_8]^{3-}$ ($E_{1/2}$ ~0.59V), 0.69 ± 0.05 for $[IrCl_6]^{2-}$ ($E_{1/2\sim}$ 0.72 V) and 0.92 ± 0.05 for $[Fe(phen)_3]^{3+}$ ($E_{1/2}$~ 0.82 V). This variation of the β coefficient with the redox potential of the mediator calls for an analysis of the meaning of β in terms of its value. According to the acid-base catalysis theory, when β is equal to zero, the PT step is not involved in the rate determining transition state of the reaction; a β value of 0.5 would indicate that 50% of the PT is

achieved in the rate determining transition state while a β of 1.0 means that the PT is complete at the transition state of the reaction. Since all the β values obtained with the mediators above range between 0.42 and 0.92, in all three cases the PT that accompanies the oxidation of GSH is completed to different extents in the transition state of this PCET, with the degree of PT completion increasing as the redox potential of the mediator increases.

From Figure 3.4, an increase in $E_{1/2}$ of about 0.24 V achieved by replacing $[Mo(CN)_8]^{3-}$ with $[Fe(phen)_3]^{3+}$ {$E_{1/2}$ is ~ 0.59 V for the redox couple $[Mo(CN)_8]^{3-}/[Mo(CN)_8]^{4-}$, ~0.72 V for $[IrCl_6]^{2-}/ [IrCl_6]^{3-}$ and ~ 0.82 V for $[Fe(phen)_3]^{3+}/ [Fe(phen)_3]^{2+}$} affords an increase of ~0.50 in β, which is equivalent to 50% more PT transfer in the transition state of the reaction; likewise, an increase in $E_{1/2}$ of about 0.13 V by replacing $[Mo(CN)_8]^{3-}$ with $[IrCl_6]^{2-}$ results in an increase of ~0.23 in β, or 23% more PT in the TS. This dependence of β on $E_{1/2}$ of the mediator can be rationalized by considering that the higher the oxidizing power of the metal complex involved, the more favorable the oxidation of GSH will be; consequently, a higher degree of thiol oxidation increases the extent of PT to the base in solution at the TS likely to avoid the formation of the highly unstable radical $GSH^{\bullet+}$. Thus, bypassing the formation of an unstable intermediate is probably the ultimate driving force for the coupling of PT and ET.

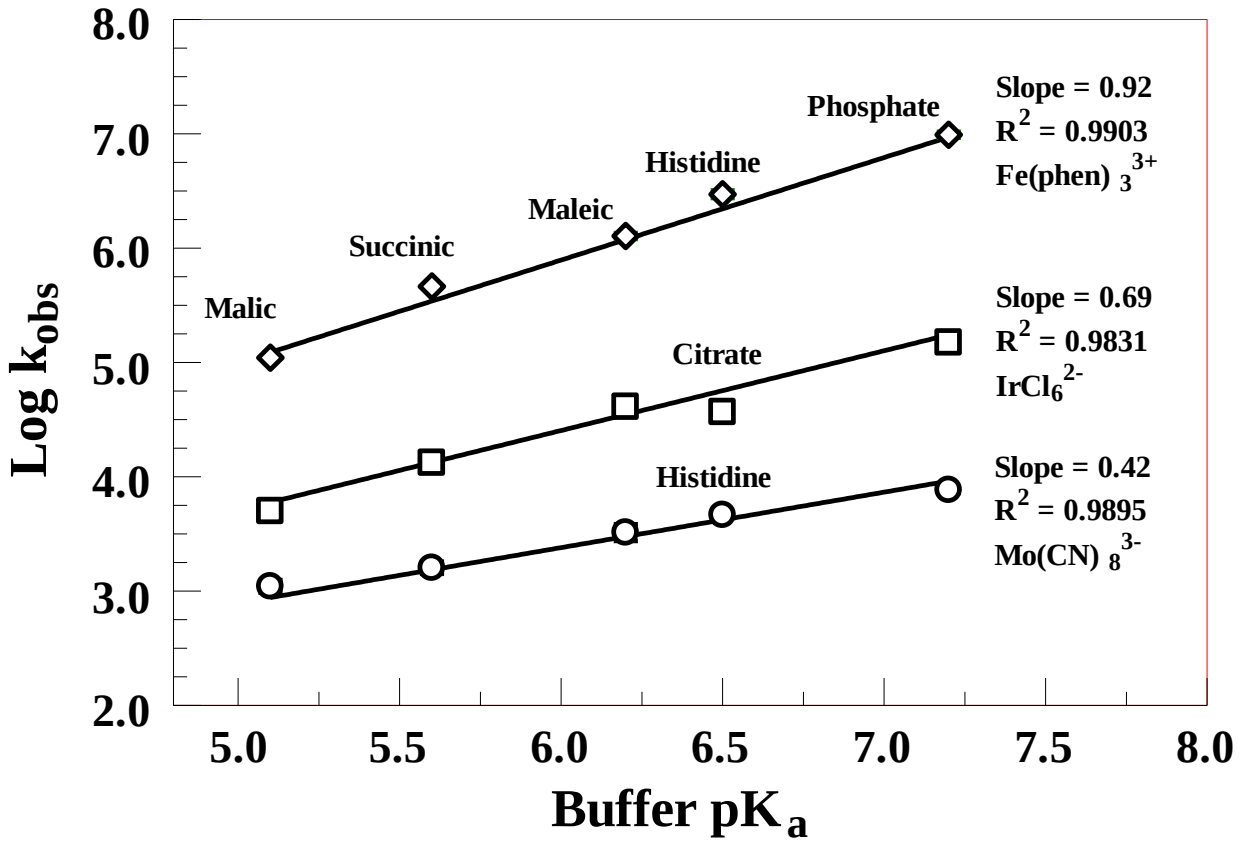

Figure 3.4 Log k_{obs} vs. pK_a of the buffer's base component; k_{obs} is the observed rate constant for the oxidation of GSH (1.0 mM) by the respective metal complex (1.0 mM in the reduced form) estimated through digital simulation of CVs run at various scan rates. The metal complexes used were $[Mo(CN)_8]^{4-/3-}$ (circles), $[IrCl_6]^{2-/3-}$ (squares) and $[Fe(phen)_3]^{3+/2+}$ (rhombus); The concentration of each buffer was 35 mM for experiments with $[IrCl_6]^{2-/3-}$ and 50 mM for experiments with $[Mo(CN)_8]^{4-/3-}$ and $[Fe(phen)_3]^{3+/2+}$. Buffer types and pH indicated on the top curve apply for all plots, except for citrate buffer which was used in experiments with $[IrCl_6]^{2-/3-}$ only.

3.3.5 KIE experiments

As it was done in chapter 2, experiments in deuterated water were carried out in order to determine the existence of kinetic isotopic effects in the oxidation of GSH by other mediators. The experiments were done in solutions of deuterated phosphate buffer pD 7.0, at two different concentrations of buffer (10 mM and 50 mM) and using the mediators with the lowest and the highest redox potentials considered in this work, $[Mo(CN)_8]^{3-}$ and $[Fe(phen)_3]^{3+}$. The KIE values obtained at these conditions are reported in Table 3.2.

Table 3.2. KIE values for the oxidation of GSH by $[Mo(CN)_8]^{3-}$ and $[Fe(phen)_3]^{3+}$ in 10 mM and 50 mM phosphate buffer pH 7.0.

Phosphate Buffer pH 7.0/ mM	**KIE with $[Mo(CN)_8]^{3-}$**	**KIE with $[Fe(phen)_3]^{3+}$**
10	2.53 ± 0.30	2.08 ± 0.14
50	1.17 ± 0.10	1.72 ± 0.13

The values of KIE ≥ 2 measured in the lower concentration of phosphate buffer indicate that the PT between GSH and the base in solution is involved in the RDS of the reaction with both mediators (Table 3.2). As the concentration of buffer was increased to 50 mM, the KIE obtained with $[Mo(CN)_8]^{3-}$ dropped from 2.53 to 1.17, whilst the KIE with $[Fe(phen)_3]^{3+}$ as the mediator decreased much less from 2.08 to 1.72. In the case of the oxidation of GSH by $[IrCl_6]^{2-}$ the KIE values decreased upon increasing the phosphate buffer concentration as well. However, with $[IrCl_6]^{2-}$ the KIE value remained at 2.2 with concentrations of buffer as high as 200 mM (see Appendix 2). The KIE with $[Fe(phen)_3]^{3+}$ is still significant even at 50 mM phosphate buffer (KIE =1.72) which indicates that PT from GSH to HPO_4^{2-} is still rate determinant at such conditions of buffer concentration, but this is not the case with $[Mo(CN)_8]^{3-}$. These KIE results

may suggest that, like with $[IrCl_6]^{2-}$, the oxidation of GSH by $[Fe(phen)_3]^{3+}$ maintains a concerted character even at relatively high concentrations of buffer. The concerted pathway being the reaction's RDS would be the cause of having KIE values above 1. However, a concerted pathway with the mediator $[Fe(phen)_3]^{3+}$ may as well be accompanied by PTET and ETPT as explained above, and possibly a rate determining PT in the PTET route could contribute to the observed KIE values. A PT from GSH to any of the buffer bases used in this work can be considered rate determining in a PTET pathway because the acidity of glutathione (pK_{SH} = 8.7) is much lower than that of the bases considered i.e. the pK_a of $malate^{2-}$ in malic buffer is only 5.11 and the pK_a of HPO_4^{2-} in phosphate buffer is 7.2; therefore, the deprotonation of GSH by any of these bases is unfavorable and the backward PT from BH^+ to GS^- would be faster with a rate constant $k_{-PT} \geq 10^7\ M^{-1}\ s^{-1}$. [33]

On the other hand, the case of the oxidation of GSH by $[Mo(CN)_8]^{3-}$ appears to be different than that of the other mediators because the KIE drops to ~ 1 in 50 mM phosphate buffer, which means that at this concentration of buffer the PT would no longer be involved in the reaction's RDS. The comparatively smaller k_{obs}'s obtained for the reaction of GSH and $[Mo(CN)_8]^{3-}$, which range between $\sim 10^3$ and 2×10^4 $M^{-1}\ s^{-1}$ for pH conditions between 5 and 7 and buffer concentrations varying between a 5 mM and 100 mM (see Appendix 3 and Figs. 3.1 and 3.4), and the value of its Brönsted slope ($\beta = 0.42 \pm 0.02$ from Fig. 3.4) show that the oxidation of GSH by this mediator is slow compared to other mediators, with its transition state closer to the reactants coordinates. An stepwise ETPT route could account for a KIE of ~1 but not for a KIE of ~2, yet is seems unlikely that $[Mo(CN)_8]^{3-}$ being the less oxidizing of the mediators studied would be able to oxidize fully protonated GSH, which is in agreement with the small K_2 values for this reaction (the equilibrium constant of reaction between GSH and $[Mo(CN)_8]^{3-}$) which range from $\sim 6 \times 10^{-3}$ at pH 6.5 to $\sim 3 \times 10^{-2}$ at pH 7.0. On the other hand, proposing a pure PTET

pathway would be in conflict with the fact that deprotonation of GSH is unfavorable at pH's below 8.0 and all the experiments with $[Mo(CN)_8]^{3-}$ were carried out at pH's between 5.0 and 7.0.

Lastly, there is the possibility that concerted and stepwise PTET are both operative in the oxidation of GSH by $[Mo(CN)_8]^{3-}$ but additional experiments will have to be conducted to better understand the trend of the KIE values with the concentration of buffer, and the contribution of every PCET route to the rate of reaction with each mediator.

3.4 Conclusions

This study of the mediated oxidation of glutathione provides new experimental evidence to validate the Marcus theory of electron transfer. Although this theory allows one to predict the relationship between thermodynamics and kinetics of most electrochemical reactions, we believe that in order to investigate and deeply understand redox processes that involve the transfer of protons it is appropriate to consider the theory of acid-base catalysis as well. The case of glutathione is an example of how the Marcus electron transfer theory cannot explain the influence of pH, buffer composition and concentration, on the rate of proton coupled electron transfer reactions. To understand such effects, it was necessary to look into the acid-base catalysis theory to discover that the rate of electron transfer reactions accompanied by proton(s) transfer(s) can be affected by the presence of Brönsted species. Furthermore, such kinetic effects and their dependence on pH, and the pK_a and concentration of Brönsted species appear to be of the same kind than those observed in non-electrochemical systems like some proteases enzymes and even in the hydrolysis of a variety of organic compounds.

The mediated oxidation of glutathione can be now recognized as a general base catalyzed reaction, characterized by a linear relationship between the observed rate of oxidation, k_{obs}, and

the concentration of buffer, at a constant pH. Also, this redox process follows a Brönsted behavior, which implies that a proton transfer between glutathione and a Brönsted base in solution takes place in the rate-determining transition state of the reaction. These findings lead to think of the oxidation of glutathione, in the presence of Brönsted bases, as a proton-coupled electron transfer process, something that could not be concluded solely from the Marcus relationships obtained.

The motivation for studying both the Marcus and the acid-base behavior of an electrochemical process that involves proton transfer(s) should be the possibility of drawing a clear map of the relationships between the different thermodynamic and kinetic factors in play. We strongly believe that this kind of approach would facilitate the search for optimal conditions to observe redox catalysis of other proton coupled electron transfer processes, which is often a rather complicated trial an error process.

3.5 References

1. Alligrant, T. M.; Hackett, J. C.; Alvarez, J. C. *Electrochim. Acta* **2010**, *55*, 6506-6516.
2. Fecenko, C. J.; Meyer, T. J.; Thorp, H. H. *J. Am. Chem. Soc.* **2006**, *128*, 11020-11021.
3. Fecenko, C. J.; Thorp, H. H.; Meyer, T. J. *J. Am. Chem. Soc.* **2007**, *129*, 15098-15099.
4. Medina-Ramos, J.; Oyesanya, O.; Alvarez, J. C. **2010**.
5. Weatherly, S. C.; Yang, I. V.; Armistead, P. A.; Thorp, H. H. *J. Phys. Chem. B* **2003**, *107*, 372-378.
6. Weatherly, S. C.; Yang, I. V.; Thorp, H. H. *J. Am. Chem. Soc.* **2001**, *123*, 1236-1237.
7. Mayer, J. M. *Annual Review of Physical Chemistry* **2004**, *55*, 363-390.
8. Irebo, T.; Reece, S. Y.; Sjodin, M.; Nocera, D. G.; Hammarstrom, L. *Journal of the American Chemical Society* **2007**, *129*, 15462-15464.
9. Sjodin, M.; Ghanem, R.; Polivka, T.; Pan, J.; Styring, S.; Sun, L.; Sundstrom, V.; Hammarstrom, L. *Phys. Chem. Chem. Phys.* **2004**, *6*, 4851-4858.
10. Sjodin, M.; Styring, S.; Akermark, B.; Sun, L.; Hammarstrom, L. *J. Am. Chem. Soc.* **2000**, *122*, 3932-3936.
11. Mayer, J. M. *Annu. Rev. Phys. Chem.* **2004**, *55*, 363-390.
12. Kirby, A. J. In *Encyclopedia of Life Sciences*; John Wiley & Sons: 2001.
13. Eigen, M. *Angew. Chem. Int. Ed.* **1964**, *3*, 1-72.
14. Jencks, W. P. *Catalysis in Chemistry and Enzymology*; Courier Dover Publications, 1987.
15. Anslyn, E. V.; Dougherty, D. A. *Modern Physical Organic Chemistry*; University Science

Books, 2006.
16. DeSimone, R. E.; Drago, R. S. *J. Am. Chem. Soc.* **1970**, *92*, 2343-2352.
17. Covington, A. K.; Paabo, M.; Robinson, R. A.; Bates, R. G. *Anal. Chem.* **1968**, *40*, 700-706.
18. Madej, E.; Wardman, P. *Arch. Biochem. Biophys.* **2007**, *462*, 94-102.
19. Campbell, J. F.; Napier, M. E.; Feldberg, S. W.; Thorp, H. H. *J. Phys. Chem. B* **2010**, *114*, 8861-8870.
20. Sun, J.; Stanbury, D. M. *Dalton Trans.* **2002**, 785-791.
21. Wang, X.; Stanbury, D. M. *Inorg. Chem.* **2008**, *47*, 1224-1236.
22. Nekrassova, O.; Kershaw, J.; Wadhawan, J. D.; Lawrence, N. S.; Compton, R. G. *Phys. Chem. Chem. Phys.* **2004**, *6*, 1316-1320.
23. Petrovic, S. *Chem. Educator* **2000**, *5*, 231-235.
24. Carter, M. T.; Rodriguez, M.; Bard, A. J. *J. Am. Chem. Soc.* **1989**, *111*, 8901-8911.
25. Ahren, M. L.; Maass, G. *Angew. Chem. Int. Ed.* **1968**, *7*, 818-819.
26. Marcus, R. A. *Rev. Mod. Phys.* **1993**, *65*, 599-610.
27. Marcus, R. A.; Sutin, N. *Biochim. Biophys. Acta* **1985**, *811*, 265-322.
28. Ram, M. S.; Hupp, J. T. *J. Phys. Chem.* **1990**, *94*, 2378-2380.
29. Saveant, J.-M. *Elements of Molecular and Biomolecular Electrochemistry: An Electrochemical Approach to Electron Transfer Chemistry*; John Wiley & Sons Inc.: Hoboken, 2006.
30. Warren, J. J.; Tronic, T. A.; Mayer, J. M. *Chemical Reviews* **2010**, *110*, 6961-7001.
31. Fox, J. P.; Page, M. I.; Satterhwait, A.; Jencks, W. P. *Journal of the American Chemical Society* **1972**, *94*, 4731-4732.
32. Jencks, W. P. *Chemical Reviews* **1972**, *72*, 705-718.
33. Hibbert, F.; Thomas, G. A. I. *Journal of the Chemical Society Perkin Transactions II* **1986**, 1761-1763.

Chapter 4:

'Comparing the Hydrogen Bonding Effect of Brönsted Bases in Solution and When They are Covalently Bound to the Surface of Glassy Carbon Electrodes in the Electrochemical Behavior of Hydroquinone'

4.1 Introduction

This chapter describes the favoring effects of monobasic and dibasic phthalate on the electrochemistry of hydroquinone when these Brönsted bases are free in solution, and when they are attached to the surface of glassy carbon electrodes. The unique aspect of this work relies on correlating the favorable effects observed in solution with the surface effects induced by the same species on the oxidation of hydroquinone. This approach to electrocatalysis is very particular because the mechanism of events occurring in solution is well supported by evidence presented in this and previous work by our group.[1] The catalysis of electrochemical reactions is a subject of intense research, due to the great number of scientific and technological applications that rely on redox processes such as amperometric sensors, fuel cells, and electrosynthetic methods.[2] However, the development of electrocatalysts is challenging and rarely follows a mechanistic rationale, mostly because the structure-function factors that lead to catalysis of redox reactions confined at electrode surfaces are not well understood.[3] Previous work by this group has shown that acid-base effects and hydrogen bonding associations with certain Brönsted bases can decrease the overpotential of the two-proton/two-electron oxidation of hydroquinone and catechol.[1, 4] Although proton-coupled electron transfer (PCET) reactions like these are widespread in chemistry, not much research has been done about the hydrogen bonding influence of Brönsted acids and bases on their thermodynamics and kinetics. Studies by several groups are amongst the few that offer substantial insight on the importance of hydrogen bonding and proton transfer (PT) on the electrochemistry of quinones or phenols.[5] Hence, our interest in exploring the coupling of acid-base chemistry with the electrochemistry of probes like hydroquinone, in solution as well as at the electrode interface, aiming for a better understanding of such interactions and their potential role in electrocatalysis.[1b, 6] Previously, we showed that some Brönsted bases make the oxidation of 1,4 hydroquinone (1,4-H_2Q) easier in acetonitrile, via

hydrogen bonding and PT.[1b] Acetate, benzoate and trifluoroacetate are three of the carboxylate bases used in prior studies that undergo hydrogen bond association with 1,4-H_2Q, leading to the formation of molecular complexes that oxidize at easier (less positive) potentials than 1,4-H_2Q alone.[1] The simulation of voltammetric responses allowed for testing the validity of the mechanisms proposed to describe the electrochemistry of these 1,4-H_2Q-carboxylate systems. Pulse Gradient Echo (PGE) and ^{1}H-NMR experiments confirmed the formation of complexes between 1,4-H_2Q and the carboxylates, by measuring changes in the diffusion coefficient of 1,4-H_2Q upon titration with these carboxylate bases.[1b, 7]

The first part of the current work examines the electrochemistry of 1,4-H_2Q in the presence of two new carboxylates in acetonitrile (MeCN), tetrabutylammonium phthalate (HP^-) and bis-(tetrabutylammonium)phthalate (P^{2-}). Phthalate has two carboxylate groups that could participate in hydrogen bonding and PT with 1,4-H_2Q. Therefore, the monobasic and dibasic phthalate seemed appropriate for evaluating whether or not increasing the number of carboxylate groups in the base had a greater thermodynamic effect on the redox behavior of 1,4-H_2Q. The second part of this work describes the effects of the phthalate bases on the oxidation of 1,4-H_2Q when they were chemically attached to the surface of a glassy carbon electrode. The notion behind this approach is that the effects that take place in solution will also occur when the bases are immobilized on the electrode surface. The work by McCreery *et al*. on the electrochemistry of 1,4-H_2Q and catechols at modified glassy carbon electrodes highlights the importance of the electrode surface composition on the type of redox response observed for these compounds.[8] The purpose of our work was to demonstrate that, in addition to physical phenomena like adsorption and electrostatic interactions, the chemistry between electro-active species and functionalities on the electrode surface may also bring about changes in the electrochemical response of 1,4-H_2Q.

The electrochemistry of 1,4-H_2Q alone in MeCN and in the presence of phthalate was monitored through cyclic voltammetry. Adding the HP^- and P^{2-} bases caused the shifting of anodic and cathodic peaks in the voltammetry of hydroquinone to more negative potentials, with the P^{2-} causing a greater shift. Thus, two different reaction mechanisms were needed to model the different responses obtained with each phthalate. The agreement between simulated and experimental CV's, and the drastic changes in the diffusion coefficient of 1,4-H_2Q when it complexes with phthalate species in solution (measured by the PGE-^{1}H-NMR technique)[1, 7, 9] validates the electrochemical mechanisms proposed herein.

The modification of glassy carbon electrodes was achieved through electrochemical reduction of in-situ generated 4-aminophthalic acid diazonium salt. The electrodes were analyzed by X-ray photoelectron spectroscopy (XPS) [8a, 10] and the presence of a peak at 288eV in the XPS spectrum, corresponding to a carboxylic carbon, confirmed the existence of phthalate groups covalently bound to the electrode surface.[10b] Furthermore, comparing the cyclic voltammetry of two common redox probes, hexaammineruthenium (II/III) ($Ru(NH_3)_6^{3+}$/ $Ru(NH_3)_6^{2+}$) and ferro/ferricyanide ($[Fe(CN)_6]^{4-}$/$[Fe(CN)_6]^{3-}$), before and after modification of the glassy carbon electrodes, helped in the characterization of the chemisorbed phthalate layers.

The voltammograms of 1,4-H_2Q at the surface of modified glassy carbon electrodes showed a new anodic peak at less positive potentials than the main oxidation peak (Ea ~ 0.7 V vs. Fc/Fc^+). The appearance of this peak is likely a consequence of acid-base interactions between superficial phthalate groups and 1,4-H_2Q, which reduces the overpotential of oxidation for a population of 1,4-H_2Q molecules. This feature of the voltammetry of 1,4-H_2Q on phthalate-functionalized glassy carbon electrodes illustrates how the composition of the electrode surface can modify the electrochemical response of the redox probe, something that goes in the way of understanding the desired characteristics of an electrocatalytic surface.

4.2 Experimental Section

4.2.1 Reagents and Materials

Acetonitrile (MeCN, 99.9%, Acros Organics) was used to prepare solutions used for electrode modification, and for cleaning of electrodes and electrochemical cells. Anhydrous acetonitrile, (99.8 % with < 10 ppm H_2O, Aldrich) for cyclic voltammetry of 1,4-H_2Q in the presence of phthalate salts was used as received and transferred via microsyringe under argon. Tetrabutylammonium hexafluorophosphate ($TBAPF_6$, ≥99.0%, Fluka Electrochemical Grade) was heated to ~100 ^oC in a vacuum oven for at least 24 hours prior to use as the supporting electrolyte. Acetonitrile-d_3 (MeCN-d_3, 99 % atom D, Aldrich,), 4-aminophthalic acid (H_2P, 97%, Aldrich), benzene (Aldrich, 99 + %), D_2O (Aldrich, 99 % atom D), ethanol (200 proof, anhydrous, Pharmco-AAPER), ferrocene (Fc, Fluka), hydrochloric acid (37.3%, Fisher Scientific ACS plus), 1,4-hydroquinone (1,4-H_2Q, 99.5%, Riedel-de Haën), hydrogen peroxide (35 wt.% solution in water, Acros Organics), hexaammineruthenium (III) chloride ($Ru(NH_3)_6^{3+}$, 98%, Aldrich), potassium chloride (Fisher Scientific), potassium hexacyanoferrate (II) trihydrate ($[Fe(CN)]_6^{4-}$, 98.5-102.0%, Sigma-Aldrich), ≥ 99 %), silver nitrate (Aldrich, ≥ 99.0 %), sodium nitrite (Sigma Reagent Plus), sulfuric acid (98%, Fisher Scientific), tetrabutylammonium hydroxide-30 hydrate (TBAOH, ≥98%, Sigma-Aldrich), were all used as received.

The mono- and bis(tetrabutylammonium)-salts of o-phthalate were prepared in a similar manner to that discussed by Brown et al.[11] First, approximately 1.28 g of phthalic acid (H_2P) was placed in a 500 mL round-bottom flask containing 100 mL ethanol and 150 mL benzene. Then, either one or two equivalents of hydrated TBAOH solid were added to the mix above in order to prepare tetrabutylammonium phthalate (HP^-) or bis(tetrabutylammonium) phthalate (P^{2-}), respectively. The round bottom flask was connected to a Dean-Stark adapter, a condenser and a drying tube. Afterwards, it was lowered into an oil bath and heated to reflux for approximately 6

hours, with continuous magnetic stirring. The azeotrope was distilled at 64.9 ^{o}C and water was removed overnight. After stopping the reflux, the flask was cooled to room temperature and the solvent was removed via rotary evaporation, producing the precipitation of a dry white crystalline solid, which was stored in a dessicator and used only under an inert argon atmosphere. ^{1}H-NMR of 10.0 mM HP^{-} (CD_3CN, 400 MHz): δ 0.96 (t, 12H), 1.30 – 1.65 (mm, 16H), 3.08 (t, 8H), 7.490 (m, 2H) and 8.259 (m, 2H). ^{1}H-NMR of 10.0 mM P^{2-} (CD_3CN, 400 MHz): δ 0.96 (t, 12H), 1.30 – 1.65 (mm, 16H), 3.08 (t, 8H), 6.948 (m, 2H) and 7.184 (m, 2H).

4.2.2 Manufacturing of glassy carbon electrodes

Disk electrodes were made with glassy carbon rods of 4 mm diameter (V25 glassy carbon rod, SPI supplies) sealed into a piranha cleaned glass tube (3:1, 98 % sulfuric acid and 35 % wt. hydrogen peroxide. Warning: piranha solution is a strong oxidant and reacts violently with organic material, it should be handled with care and all work should be performed in a fume hood and utilizing the proper personal protection) by using a 14 wt. % mix of methaphenylendiamine and EPON^{TM} 828 Resin as the sealant. The glass tube used had an external and internal diameter of 6 mm and 4 mm, respectively, hence a tight fit with a thin layer of resin was achieved when the carbon electrodes were sealed. The resin was allowed to harden by placing the electrodes in the oven at ~60 °C for about a week. Electrical contact was ensured by attaching the inner end of the glassy carbon to a piece of copper wire using Epoxy resin (H20E Kit, parts A and B, Epoxy Technology).

To remove excess epoxy covering the glassy carbon electrode faces, the electrodes were first sanded down using 220-grit Al_2O_3 sandpaper, followed by wet sanding on 600-grit sandpaper. Following this rough removal of excess epoxy, the electrode faces were polished with diamond paste (METADI II, Buehler), starting with 6 µm, then 1 µm and finally 0.25 µm. Ultimately and

between experiments the electrodes were polished with a 0.05 µm alumina slurry (micropolish II, Buehler). After polishing, the electrodes were rinsed and sonicated in deionized water for five minutes.

4.2.3 Electrochemical modification of glassy carbon electrodes

The modification of glassy carbon disk electrodes involved cycling the potential applied to the working electrode between 0.80 V and -0.20 V vs. Ag/AgCl/1M KCl, in order to reduce the 4-aminophthalic acid diazonium salt formed in situ.[10] A glassy carbon electrode was immersed in a solution containing 5.0 mM 4-aminophthalic acid, 10 mM sodium nitrite, 400 µL of 1.0 M HCl and 9.60 mL of MeCN, previously deareated with argon for about 10 min. The reaction between the aminobenzene compound and sodium nitrite, in acidic media, yielded the corresponding diazonium salt that was further reduced at the electrode surface at a potential around 0.20 V vs. Ag/ AgCl/ 1M KCl.[10a] An average of five cycles at 0.1V s^{-1} was required to achieve complete passivation of the electrode within this potential region. Scheme 4.1 depicts the modification procedure.

The modification of glassy carbon surfaces was examined through X-ray photoelectron spectroscopy (XPS). A Thermofisher ESCALab 250 X-Ray Photoelectron Spectrometer was utilized to determine carbon, nitrogen and oxygen on the surface of bare and modified glassy carbon plates (Glas-T25 glassy carbon plate, 2 mm thickness, SPI supplies). Survey and point spectra were obtained along a linear path drawn across the plates, in order to sample modified and unmodified spots on the surface.

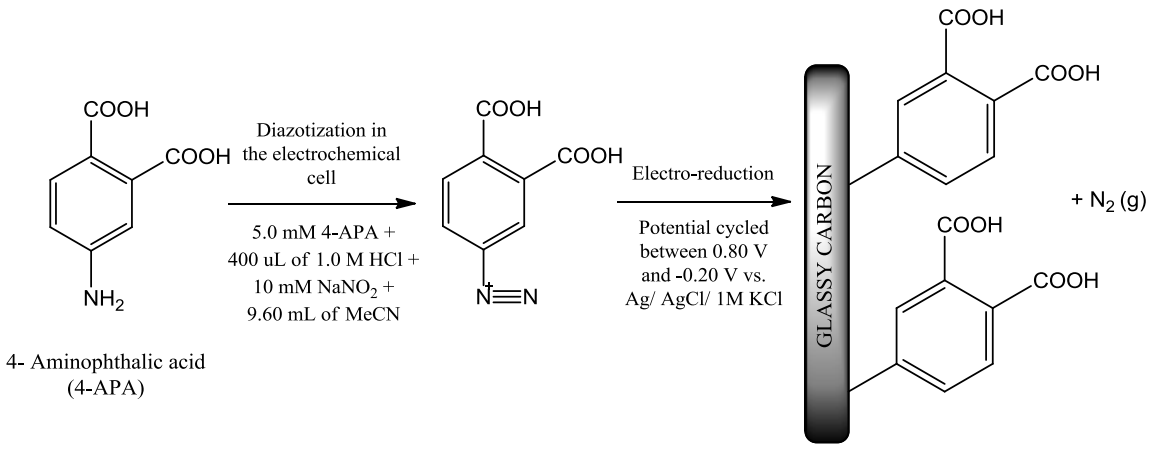

Scheme 4.1 Modification of glassy carbon electrodes by reduction of the diazonium salt of 4-aminophthalic acid, generated in situ.

The functionalization of glassy carbon plates followed the same procedure described in Scheme 4.1, except the potential was cycled between 0.80 V and -1.00 V vs. Ag/AgCl/1M KCl, because the reduction peak of the arydiazonium salt was observed around -0.40 V. Five voltammetric cycles were sufficient to observe the passivation of the electrode surface during reduction of the aryldiazonium salt. The shifting of the diazonium salt reduction to more negative potentials is likely due to a higher uncompensated resistance resulting from the electrochemical setup used, where the carbon plate served as the bottom of a hollow glass cell clamped between two Teflon panels. In that setup, a sheet of brass provided electrical contact between the glassy carbon plate and the potentiostat.

After modification, disk and plate electrodes were rinsed and sonicated in deionized water for five minutes, and then for an additional five minutes in MeCN.

4.2.4 Electrochemistry of 1,4-H_2Q on modified glassy carbon electrodes

Cyclic voltammetry (CV) was used to investigate the electrochemical behavior of 1,4-H_2Q in MeCN, before and after modification of the glassy carbon electrodes. Solutions containing 1.00 mM and 0.50 mM 1,4-H_2Q were used. The effect of treating the electrodes (bare and modified) with a dilute solution of TBAOH on the CV response of 1,4-H_2Q was also studied. The modified electrodes were rinsed and sonicated in MeCN for 3 min and then soaked in a 10 mM TBAOH solution. Afterwards, they were quickly rinsed with acetonitrile, immersed in the electrochemical cell containing the 1,4-H_2Q solution and CVs were measured.

4.2.5 Electrochemistry of 1,4-H_2Q in the presence of free phthalate bases

All electrochemical experiments were performed with a 1,4-H_2Q concentration of 5.0 mM in 10.0 mL of dry MeCN + 0.2 M tetrabutylammonium hexafluorophosphate ($TBAPF_6$) on a glassy carbon electrode. Tetrabutylammonium phthalate (HP^-) and bis(tetrabutylammonium) phthalate (P^{2-}) were added separately to 1,4-H_2Q solutions in order to study their effect on the electrochemistry of this compound. The electrochemical experiments were performed using a three electrode cell (10.0 mL) in an inert argon atmosphere. Several 0.3 cm diameter glassy carbon electrodes (CH Instruments, areas were consistent, between 0.07 to 0.073 cm^2) were used, and their electro-active areas determined by applying the Randles-Sevcik equation to CVs run in aqueous 1.0 mM $[Ru(NH_3)_6]^{3+}$ + 0.1 M KCl ($D_{Ru(NH3)6}$ = 6.3 x 10^{-6} was used in our calculations).[12] Before use, glassy carbon electrodes were polished using 0.05 μm alumina paste (Buhler, Lake Bluff, Il) washed with deionized water, carefully wiped, and then sonicated in MeCN for three minutes. In each experiment the solution resistance (R_u) was fully compensated via positive feedback. Voltammograms were fitted using DigiSim version 3.03b (Bioanalytical Systems, Inc., West Lafayette, IN). The voltammetry of 1,4-H_2Q in the presence of 20, 30 and

40 mM HP^-, as well as in the presence of 20 mM P^{2-} was simulated at different scan rates, including 0.5, 1.0 and 5.0 V s^{-1} (see Appendix 4). The diffusion coefficients of 1,4-H_2Q, HP^- and P^{2-} determined through PGE-^{1}H NMR experiments were used in the digital simulations of experimental voltammograms (see Tables 4.1 and 4.S1). All the kinetic and thermodynamic parameters that best fitted the voltammetry of 1,4-H_2Q in the presence of different concentrations of HP^- and P^{2-} are presented in the Appendix 4.

4.2.6 Electrochemical instrumentation

All electrochemical experiments were carried out using a CH Instruments potentiostat (CH Instruments, Austin, TX) equipped with a Faraday cage. A Ag/AgCl/1M KCl reference electrode was used for experiments in aqueous media and during the modification of the glassy carbon electrodes. A Ag/3mM $AgNO_3$/200 mM $TBAPF_6$ (in MeCN) reference electrode was used for experiments in MeCN, and it was separated from the rest of the solution by a glass tube capped with a porous vycor frit (CH Instruments). The potential of the silver reference electrode was periodically measured versus the formal potential (measured as the average of the peak potentials) of the ferrocene/ferrocenium (Fc/Fc^+) couple, thus all voltammetric potentials are reported versus ferrocene as Fc/Fc^+, as it is recommended by the IUPAC.[13]

4.2.7 NMR spectroscopic measurements

All NMR samples were prepared in a nominally dry argon environment and placed in screw-cap NMR sample tubes (600-MHz, 5 mm, 7" length, Norell, Inc., Landisville, NJ) in order to prevent contact of the solutions with atmospheric humidity and/or oxygen. Variable temperature ^{1}H-NMR was performed with a Bruker AVANCE III 600 MHz NMR. Standard ^{1}H-NMR and

Pulsed Gradient Echo ^{1}H-NMR were performed on a Varian Inova 400 MHz NMR at 25.0 ^{o}C. The applied gradients in the ^{1}H-NMR experiments were calibrated by measuring the diffusion coefficient of HDO (2.23×10^{-5} cm^2 s^{-1}, at 25.0 °C, 0.03%) in a D_2O sample [7b, c, 14], and the diffusion coefficient of 1,6-diaminohexane (6.98×10^{-6} cm^2 s^{-1}, at 25.0 °C, 0.04%) (see Appendix 4).[7b] To correct for viscosity differences between deuterated acetonitrile (MeCN-d_3) without electrolyte and isotopically unenriched MeCN with electrolyte, the relation $D_o = (1.04)\, D_{NMR}$ was employed. Here, D_o is the corrected diffusion coefficient and D_{NMR} is the value determined from NMR measurements.[15]

4.3 Results and Discussion

4.3.1 ^{1}H-NMR of 1,4-H_2Q in the presence of free phthalate bases

Proton NMR spectra of 1,4-H_2Q in the presence of monobasic phthalate (HP^-) and dibasic phthalate (P^{2-}) were obtained in order to assess the acid-base and hydrogen bonding interactions between these species in solution. Knowing the extent of these interactions has proven useful in the analysis of the voltammograms obtained and further establishment of the reaction mechanism(s).[1] The ^{1}H-NMR spectra of 5.0 mM 1,4-H_2Q exhibits the loss of the phenolic proton peak (δ = 6.630 ppm) upon addition of HP^- or P^{2-}, at 25 ^{o}C. On the contrary, the aromatic proton of 1,4-H_2Q (δ = 6.680 ppm) remains intact in the presence of either one of the phthalate species. The addition of P^{2-} to 1,4-H_2Q produces a total of four sets of 'phthalate peaks' centered at 6.959, 7.224, 7.471 and 8.260 ppm. The two sets of peaks up-field, located at 6.959 and 7.224 ppm, correspond to those of P^{2-} alone, while those noted down-field, centered at 7.471 and 8.260 ppm, match with the peaks found in ^{1}H-NMR spectra of HP^- or phthalic acid (H_2P) alone. The appearance of peaks for HP^- and H_2P suggests that proton transfer from 1,4-H_2Q to P^{2-} takes place. The ^{1}H-NMR spectra of 5.0 mM 1,4-H_2Q + 20.0 mM HP^- at temperatures between 5.0 and

15.0 °C exhibits a broad peak down field (δ ≈ 7.11 ppm, at 5 °C) from the original phenolic peak frequency (δ = 6.496 ppm at 5.0 °C). The broadening of the phenolic peak is indicative of an intermediate proton exchange occurring within the NMR timescale. This relatively fast proton exchange impedes the accurate determination of the association constants of 1,4-H_2Q with HP^- or P^{2-}.[7b, 9, 16]

Since interpretation of ^{1}H-NMR spectra alone did not yield values for the association constants of 1,4-H_2Q and the phthalate bases, molecular diffusion analysis via ^{1}H-NMR was chosen as an alternative method to investigate these associations. Diffusion coefficients (D) are sensitive to the size, shape, orientation and interactions of species in solution.[7b] For example, the diffusion coefficient (D) of 1,4-H_2Q changes after mixing with HP^- or P^{2-} in acetonitrile. Table 4.1 shows values of D for 1,4-H_2Q ($D_{1,4\text{-}H2Q}$) in the presence of HP^- and P^{2-} from Pulse Gradient Echo (PGE) experiments using two different concentrations of phthalate base ([1,4-H_2Q] = 5.0 mM for all experiments).

Table 4.1 presents the diffusion coefficient of 1,4-H_2Q with 20 and 40 mM of both bases HP^- and P^2, and the pK_a's of HP^- and P^{2-} in MeCN.[17] As the concentration of phthalate increases, $D_{1,4\text{-}H2Q}$ becomes smaller, and there is a marked difference in $D_{1,4\text{-}H2Q}$ in the presence of HP^- versus P^{2-}. With 20 mM HP^-, $D_{1,4\text{-}H2Q}$ decreases by 16.9 %, from 2.79 x 10^{-5} to 2.32 x 10^{-5} cm^2 s^{-1}.[1b] On the other hand, with 20 mM P^{2-}, $D_{1,4\text{-}H2Q}$ decreases by 53.4%, from 2.79 x 10^{-5} to 1.30 x 10^{-5} cm^2 s^{-1}.[1b]

Table 4.1 pK_a's and diffusion coefficients of 1,4-H_2Q by ^{1}H-NMR at 25 °C.

	pK_a[a]	$D_{1,4\text{-}H2Q}$ (x 10^{-5} cm^2 s^{-1}) [b]2.79 ± 0.04	$D_{1,4\text{-}H2Q}$ (x 10^{-5} cm^2 s^{-1}) [b]2.79 ± 0.04
		20 mM of base	**40 mM of base**
HP^-	14.3	2.32 ± 0.01	2.16 ± 0.009
P^{2-}	29.8	1.30 ± 0.03	1.15 ± 0.03

[a.] For COOH.[17]
[b.] $D_{1,4\text{-}H2Q}$ in the absence of HP^- or P^{2-}.

The $D_{1,4\text{-}H2Q}$ diminishes even more as the phthalate base concentrations increase so that $D_{1,4\text{-}H2Q}$ is 2.16 x 10^{-5} cm^2 s^{-1} in the presence of 40 mM HP^-, and 1.15 x 10^{-5} cm^2 s^{-1} with 40 mM P^{2-}. Likewise, the $D_{1,4\text{-}H2Q}$ values with HP^- are comparable to those from a previous study of trifluoroacetate with 1,4-H_2Q.[1a] Furthermore, the pK_a values of both trifluoroacetate (pK_a = 12.65) and HP^- (pK_{a1} =14.3) in MeCN are close, therefore the association constants with 1,4-H_2Q should be of similar magnitude for both species, assuming that the correlation between pK_a and the association constants between acetates and 1,4-H_2Q applies to this system as well.[1a] Titrating 1,4-H_2Q with P^{2-} causes larger changes in the diffusion coefficient of 1,4-H_2Q than previously measured *i.e.* the addition of acetate and benzoate produced changes in $D_{1,4\text{-}H2Q}$ no greater than 46.2 %.[1a] The advent of new phthalate peaks down field from the original P^{2-} peaks and the higher basicity of P^{2-} (pK_{a2} = 29.8) dictates that 1,4-H_2Q loses at least one proton upon titration with P^{2-}.[1b, 17] However, 1,4-HQ^- ($pK_{a,\ MeCN}$ = 40.96) has a significantly greater pK_a than P^{2-} (pK_1=29.8) therefore a deprotonation of both phenolic protons of 1,4-H_2Q to form the dianion 1,4-Q^{2-} is unlikely.[1b, 17] Measurements of the diffusion coefficient of 1,4-Q^{2-}, which forms upon mixing 5.0 mM 1,4-H_2Q and 10 mM of the strong base tetrabutylammonium hydroxide (TBAOH) did not show a change in $D_{1,4\text{-}Q2\text{-}}$ as large as that of 1,4-H_2Q with P^{2-}. The diffusion

coefficient of 1,4-Q^{2-} is (2.86 ± 0.4) x 10^{-5} cm^2 s^{-1}, which differs only by +2.5 % of the $D_{1,4\text{-}H2Q}$ measured in a 5.0 mM 1,4-H_2Q solution in MeCN.[1b] Therefore, an intermolecular association between 1,4-HQ^- and P^{2-} or one of the phthalate conjugates in MeCN is a plausible explanation for the changes in the diffusion coefficient and ^{1}H-NMR spectra of 1,4-H_2Q in the presence of HP^- or P^{2-}. The stoichiometry of complexation between 1,4-H_2Q and HP^- is 1:2 (1,4-H_2Q: HP^-) while that of 1,4-H_2Q with P^{2-} is 1:1, according to a plot of the $D_{1,4\text{-}H2Q}$ versus concentration of HP^- and P^{2-} (see Appendix 4). Voltammetric measurements of these solutions assisted in elucidating the nature and electrochemical behavior of the complexes formed, using the well-studied electrochemistry of 1,4-H_2Q in MeCN as a baseline for comparison.

4.3.2 Electrochemistry of 1,4-H_2Q in the presence of free phthalate bases

Cyclic voltammetry of 1,4-H_2Q undergoing titration with HP^- and P^{2-} expands our previous work on proton coupled electron transfer (PCET) processes thermodynamically influenced by Brönsted bases. The electrochemical oxidation of 1,4-H_2Q involves the loss of two protons and two electrons, converting the phenolic 1,4-H_2Q into the quinoid 1,4-Q (Figure 4.1). Nonetheless, this is an oversimplification of a complex process amply studied in aqueous as well as non-aqueous conditions.[1, 5a, 5c, 5e, 18] Figure 4.1 presents the voltammetry of 5.0 mM 1,4-H_2Q in MeCN with HP^- (Figure 4.1A) and P^{2-} (Figure 4.1B) at a scan rate of 0.1 V s^{-1}. The CV's at more positive potentials in show the response for 5.0 mM 1,4-H_2Q alone, which consists of a anodic peak current (I_a) at a peak potential (E_{pa}) of 0.722 V, and a cathodic peak current (I_c) at E_{pc} = 0.050 V. The peaks at negative potentials in Figure 4.1 show the response for 20 mM HP^- (Figure 4.1A) and 20 mM P^{2-} added (Figure 4.1B). The open circles that overlap the CV's of 1,4-H_2Q with the bases represent voltammetric simulations. A previous report contains the simulations for 1,4-

H_2Q alone in MeCN. [1b] Mixing HP^- or P^{2-} and 1,4-H_2Q causes the shifting of both I_a and I_c peaks to

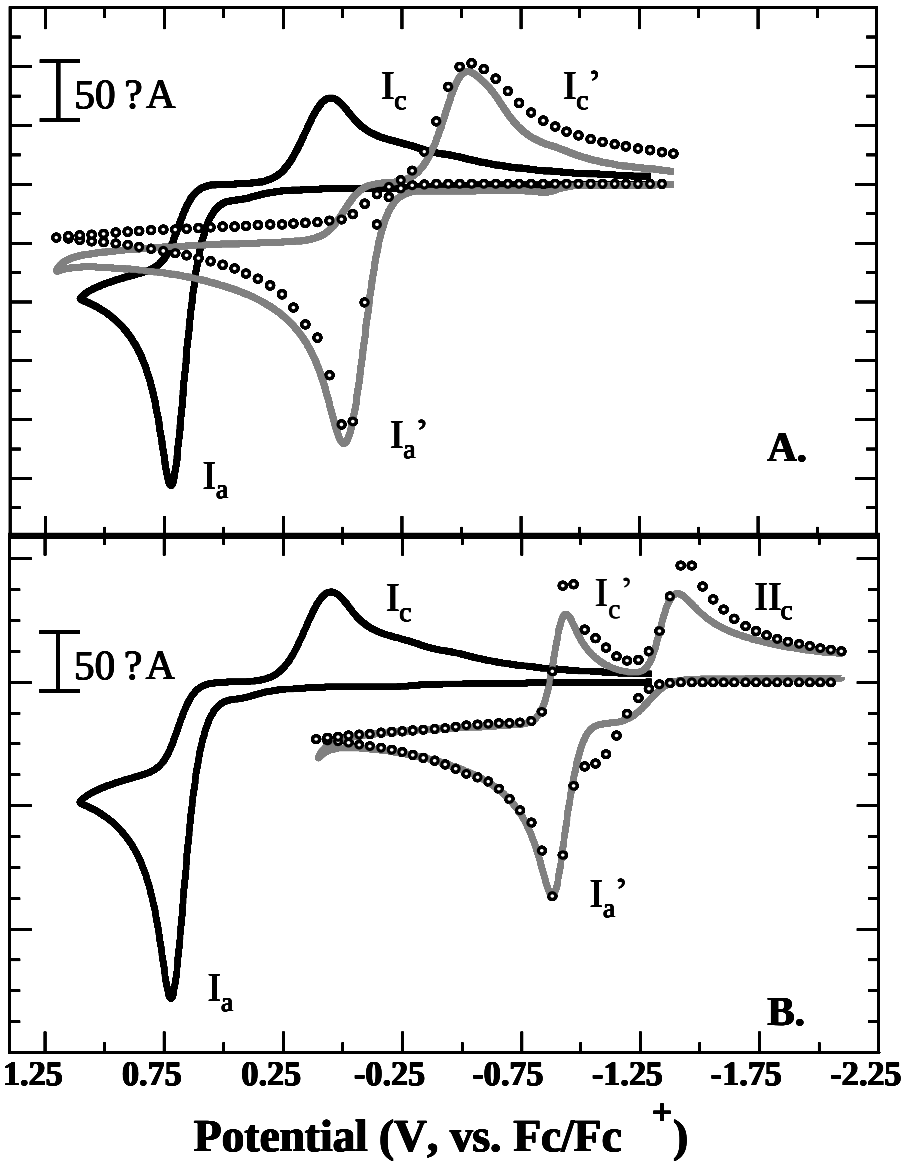

Figure 4.1 CV responses at 0.1 V s^{-1} for 5.0 mM 1,4-H_2Q alone (black line) in MeCN with 0.2 M $TBAPF_6$ and 5.0 mM 1,4-H_2Q with 20 mM of A.) HP^- (grey line) and B.) P^{2-} (grey line). Fitted simulations (circles).

easier (more negative) potentials, analogous to the addition of acetate to 1,4-H_2Q.[1] The CV of 5.0 mM 1,4-H_2Q with 20 mM HP^- shows a set of peaks similar to those of 1,4-H_2Q alone, with an oxidation peak (I_a') at -0.006 V and a reduction peak (I_c') at -0.526 V. On the other hand, mixing P^{2-} and 1,4-H_2Q produces a single oxidation peak (I_a') at -0.879 V, a reduction peak (I_c') at -0.059 V from peak I_a' ($E_{pc'}$ = -0.938 V) and a second reduction peak (II_c) at -1.405 V. The anodic peak I_a' is more negative than the second oxidation peak of 1,4-Q (II_a; 1,4-Q is the completely oxidized form of 1,4-H_2Q) alone in MeCN by -0.030 V (see Figure 4.2; further details about this figure can be found in Appendix 4). An anodic peak at such a negative potential could be indicative of a mixed oxidation process involving the 1,4-H_2Q radical anion (1,4-$Q^{\cdot-}$) and a negatively charged complex formed between the anion 1,4-HQ^- (formed upon deprotonation of 1,4-H_2Q) and one of the phthalate species in solution, either P^{2-} or HP^-. Furthermore, the anodic peak (I_a') generated upon addition of 20 mM P^{2-} is significantly smaller (-134.7 μA versus -244.2 μA) than that of 1,4-H_2Q alone. Less oxidation current might arise from the formation of a complex, as oxidation of 1,4-H_2Q-acetate aggregates often yields smaller currents than that of 1,4-H_2Q alone, due to slower diffusion of the aggregates.[1]

Running cyclic voltammetry of 1,4-H_2Q with HP^- and P^{2-} at several scan rates from 0.1 to 25 V s^{-1} and 10 mM of base did not result in new peaks. However, at higher concentrations of P^{2-} (> 10 mM) and scan rates above 1V s^{-1}, a new anodic peak evolves at a more positive potential relative the main anodic peak (I_a') (see Appendix 4). Overall, the presence of phthalate bases decreases the oxidation overpotential for 1,4-H_2Q and delays the reduction of the respective products. ^{1}H-NMR and cyclic voltammetry results point towards hydrogen bonding and deprotonation processes as responsible for these effects.

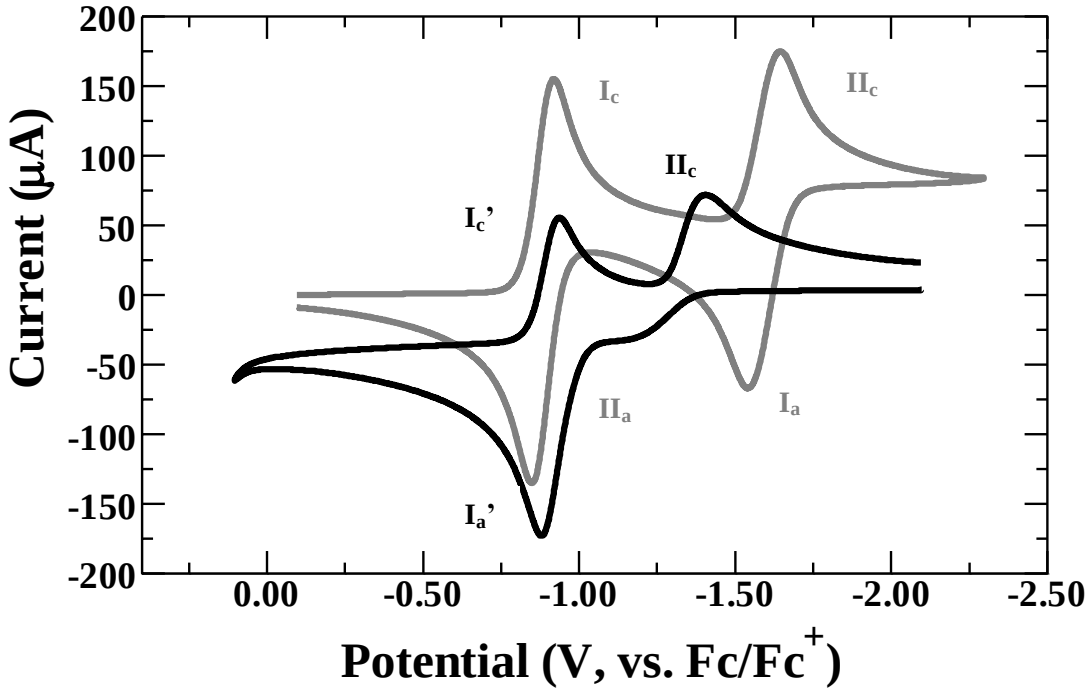

Figure 4.2 CV response of 5.0 mM 1,4-H_2Q with 20 mM P^{2-} (black line) and 5.0 mM 1,4-Q alone in MeCN with 0.2 M $TBAPF_6$ as supporting electrolyte.

4.3.3 Simulation of the voltammetric responses

The mechanism proposed to model the cyclic voltammetry of 1,4-H_2Q/acetate systems also fits the behavior of 1,4-H_2Q in the presence of HP^-, while the mechanism for the system 1,4-H_2Q/P^{2-} is completely original to the present study.[1a] The oxidation of 1,4-H_2Q alone in MeCN corresponds to an ECEC process coupled to a disproportionation reaction.[1b] The notation ECEC and its equivalent ET-PT-ET-PT represent the sequence of Electrochemical (E or ET = electron transfer) and Chemical (C or PT = proton transfer) steps responsible for 1,4-H_2Q's voltammetric response. The inclusion of a disproportionation reaction is common to redox sequences that involve the transfer of multiple electrons.[1b, 2d, 18c, 18f, g, 19] We suggest a similar ECEC mechanism with a coupled disproportionation reaction to replicate the voltammetry of 1,4-H_2Q with 20, 30

and 40 mM HP^-. This mechanism is based on ^{1}H-NMR and CV data (Appendix 4) as well as on prior knowledge of the electrochemistry of 1,4-H_2Q in the presence of various acetates[1].

In this mechanism, HP^- hydrogen bonds with 1,4-H_2Q in a 2:1 stoichiometric ratio, equations 4.1 and 4.2, forming a complex of 1,4-H_2Q with two bound HP^- molecules, 1,4-$H_2Q(HP)_2^-$. The association constants for equations 4.1 and 4.2 were estimated through fitting of CVs to this mechanism, since the determination by ^{1}H-NMR analysis was unsuccessful. The complex 1,4-$H_2Q(HP)_2^-$ oxidizes to the 1,4-H_2Q radical cation with two bound HP^- molecules, (1,4-$H_2Q^{\cdot}(HP)_2$, Eq. 4.3), which then undergoes PT to generate the 1,4-H_2Q radical with a single bound HP^- molecule (1,4-$HQ^{\cdot}(HP)^-$) and phthalic acid (H_2P) Eq. 4.4. Next, 1,4-$HQ^{\cdot}(HP)^-$ either oxidizes and forms the protonated quinone with a single bound HP^- molecule (1,4-HQ(HP), Eq. 4.5), or disproportionates to quinone (1,4-Q) and 1,4-$H_2Q(HP)_2^-$, Eq. 4.7. In the neutral complex 1,4-HQ(HP), the hydroquinone moiety loses its proton producing 1,4-Q and H_2P, Eq. 4.6. In the reduction cycle, 1,4-Q is reduced to the quinone radical anion (1,4-Q.-, Eq. 4.8), which is subsequently protonated by H_2P, giving 1,4-HQ.$(HP)^-$, Eq. 4.9. H_2P and HP^- produce the phthalic acid homoconjugate, H_3P^{2-}, Eq. 4.10.[17] Homoconjugation is common for charged organic acids and bases in some aprotic solvents, however K_{Homo} is significantly smaller for phthalate species than for trifluoroacetate (TFAC), benzoate (BZ) and acetate (AC), ($K_{Homo,H2P}$ = 89 M^{-1}, versus K_{Homo} for TFAC, BZ and AC which ranges from 4 x 10^4 to 7.6 x 10^4 M^{-1}) therefore only a single oxidation peak is noted over the HP^- concentration range studied, 10 to 40 mM.[1, 17] Neglecting the homoconjugation reaction had little influence on the simulated voltammetry, yet it allows for a comprehensive overview of this mechanism.

Scheme 4.2 Fitted Mechanism of 1,4-H_2Q with HP^-

$$1,4\text{-}H_2Q + HP^- \rightleftharpoons 1,4\text{-}H_2Q(HP)^- \quad (4.1)$$

$$1,4\text{-}H_2Q(HP)^- + HP^- \rightleftharpoons 1,4\text{-}H_2Q(HP)_2^{2-} \quad (4.2)$$

$$1,4\text{-}H_2Q(HP)_2^{2-} \rightleftharpoons 1,4\text{-}H_2Q^{\bullet}(HP)_2^- + e^- \quad (4.3)$$

$$1,4\text{-}H_2Q^{\bullet}(HP)_2^- \rightleftharpoons 1,4\text{-}HQ^{\bullet}(HP)^- + H_2P \quad (4.4)$$

$$1,4\text{-}HQ^{\bullet}(HP)^- \rightleftharpoons 1,4\text{-}HQ(HP) + e^- \quad (4.5)$$

$$1,4\text{-}HQ(HP) \rightleftharpoons 1,4\text{-}Q + H_2P \quad (4.6)$$

$$1,4\text{-}HQ^{\bullet}(HP)^- + 1,4\text{-}HQ^{\bullet}(HP)^- \rightleftharpoons 1,4\text{-}Q + 1,4\text{-}H_2Q(HP)_2^- \quad (4.7)$$

$$1,4\text{-}Q + e^- \rightleftharpoons 1,4\text{-}Q^{\bullet -} \quad (4.8)$$

$$1,4\text{-}Q^{\bullet -} + H_2P \rightleftharpoons 1,4\text{-}HQ^{\bullet}(HP)^- \quad (4.9)$$

$$H_2P + HP^- \rightleftharpoons H_3P_2^- \quad (4.10)$$

Scheme 4.3 describes the mechanism that best fitted the major features of the voltammetry of 1,4-H_2Q with P^{2-} at different scan rates. This mechanism is more intricate than the others proposed by our group because, unlike P^{2-}, all of the previous carboxylates studied have a pK_a lower than that of 1,4-H_2Q ($pK_{a,\ MeCN}$ = 26.2).[1b] Since P^{2-} is a moderately strong base in MeCN ($pK_{a,\ MeCN}$ = 29.8) proton transfer (PT) initially occurs forming 1,4-HQ^- and HP^-, Eq. 4.11.[1b] However, because the pK_a of 1,4-HQ^- (40.96) and HP^- (29.8) are so far apart, P^{2-} is unable to remove both protons from 1,4-H_2Q.[1b, 17] Through hydrogen bonding, P^{2-} coordinates the lone phenolic proton on 1,4-HQ^- to form the complex 1,4-$HQ(P)^{3-}$ (Eq. 4.12), and a drastic decrease

in $D_{1,4\text{-}H2Q}$ occurs with 20 and 40 mM P^{2-} (Table 4.1). This association helps delocalize the negative charge on P^{2-}, as charged species are not adequately solvated in aprotic solvents. Subsequent oxidation of 1,4-HQ(P)$^{3-}$ generates the 1,4-H_2Q radical bound to P^{2-} (1,4-HQ$^{\cdot}$(P)$^{2-}$, Eq. 4.13), which can undergo PT and dissociation to form 1,4-Q$^{\cdot-}$ and HP^- (Eq. 4.14) followed by ET to generate the protonated quinone with a single bound P^{2-} molecule (1,4-HQ(P)$^-$, Eq. 4.15) The radical species (1,4-HQ$^{\cdot}$(P)$^{2-}$) may also disproportionate with 1,4-Q$^{\cdot-}$ into 1,4-Q and 1,4-HQ(P)$^{3-}$ (Eq. 4.20). Next, 1,4-HQ(P)$^-$ dissociates into 1,4-Q and HP^-, as shown in Eq. 4.16. The radical 1,4-Q$^{\cdot-}$ in Eq. 4.14 and 1,4-Q, product of a disproportionation (Eq. 4.20) are electrochemically interconvertible according to Eq. 4.17. At all scan rates, oxidation of 1,4-Q$^{\cdot-}$ to 1,4-Q is the principle reaction occurring at peak I_a', while reduction of 1,4-Q to 1,4-Q$^{\cdot-}$ occurs at peak I_c'. Any 1,4-Q$^{\cdot-}$ that does not associate with the generated HP^- (Eq. 4.14), becomes 1,4-Q^{2-} (Eq. 4.18), which gains a proton and complexes with HP^- to form 1,4-HQ(P)$^{3-}$ (Eq. 4.19). Reduction of 1,4-Q$^{\cdot-}$ occurs at peak II_c. Our assignment of the reactions occurring at each peak is based on comparisons with the CV's of 5.0 mM 1,4-Q alone in MeCN (Appendix 4). At higher scan rates, 1 to 25 V s^{-1}, oxidation of 1,4-HQ(P)$^{3-}$ and 1,4-HQ$^{\cdot}$(P)$^{2-}$ occurs at peak II_a (Appendix 4). Scheme 4.3 does not involve a phthalate homoconjugation, (see Scheme 4.2, Eq. 4.10) because H_2P is not a product in this mechanism and, for diprotic acids, homoconjugation only occurs between H_2P and HP^-.[17]

Scheme 4.3 Fitted Mechanism of 1,4-H_2Q with P^{2-}

$$1,4\text{-}H_2Q + P^{2-} \rightleftharpoons 1,4\text{-}HQ^{-} + HP^{-} \quad (4.11)$$

$$1,4\text{-}HQ^{-} + P^{2-} \rightleftharpoons 1,4\text{-}HQ(P)^{3-} \quad (4.12)$$

$$1,4\text{-}HQ(P)^{3-} \rightleftharpoons 1,4\text{-}HQ^{\bullet}(P)^{2-} + e^{-} \quad (4.13)$$

$$1,4\text{-}HQ^{\bullet}(P)^{2-} \rightleftharpoons 1,4\text{-}Q^{\bullet-} + HP^{-} \quad (4.14)$$

$$1,4\text{-}HQ^{\bullet}(P)^{2-} \rightleftharpoons 1,4\text{-}HQ(P)^{-} + e^{-} \quad (4.15)$$

$$1,4\text{-}HQ(P)^{-} \rightleftharpoons 1,4\text{-}Q + HP^{-} \quad (4.16)$$

$$1,4\text{-}Q + e^{-} \rightleftharpoons 1,4\text{-}Q^{\bullet-} \quad (4.17)$$

$$1,4\text{-}Q^{\bullet-} + e^{-} \rightleftharpoons 1,4\text{-}Q^{2-} \quad (4.18)$$

$$1,4\text{-}Q^{2-} + HP^{-} \rightleftharpoons 1,4\text{-}HQ(P)^{3-} \quad (4.19)$$

$$1,4\text{-}HQ^{\bullet}(P)^{2-} + 1,4\text{-}Q^{\bullet-} \rightleftharpoons 1,4\text{-}Q + 1,4\text{-}HQ(P)^{3-} \quad (4.20)$$

4.3.4 Electrochemistry of 1,4-H_2Q on phthalate-modified GCE

The thermodynamic enhancement of the oxidation of 1,4-H_2Q by HP^- and P^{2-} inspired the electrochemical functionalization of glassy carbon electrodes with phthalate groups. Our hypothesis was that having the phthalate bases attached to the electrode surface would favor the oxidation of 1,4-H_2Q by similar effects of hydrogen bonding and PT as found for the bases in solution, even though the surface coverage may reduce the actual electrode area and in turn the observed current. The modification of glassy carbon electrodes, outlined in Scheme 4.1, involves

the electrochemical reduction of the in-situ generated 4-aminophthalic acid diazonium salt, following a very similar procedure developed by Cougnon and coworkers.[10a, 20] It is generally accepted that the reduction of phenyldiazonium salts produces a phenyl radical which can bind covalently to glassy carbon (Eq. 4.21 and Eq. 4.22).[10, 20-21] Figure 4.3 presents the cyclic voltammetry of the diazonium salt, with the peak around 0.24 V vs. Ag/ AgCl attributed to the reduction of the salt. Upon repetitive CV's, the reduction peak vanishes due to passivation of the electrode by covalently attached phthalate groups.

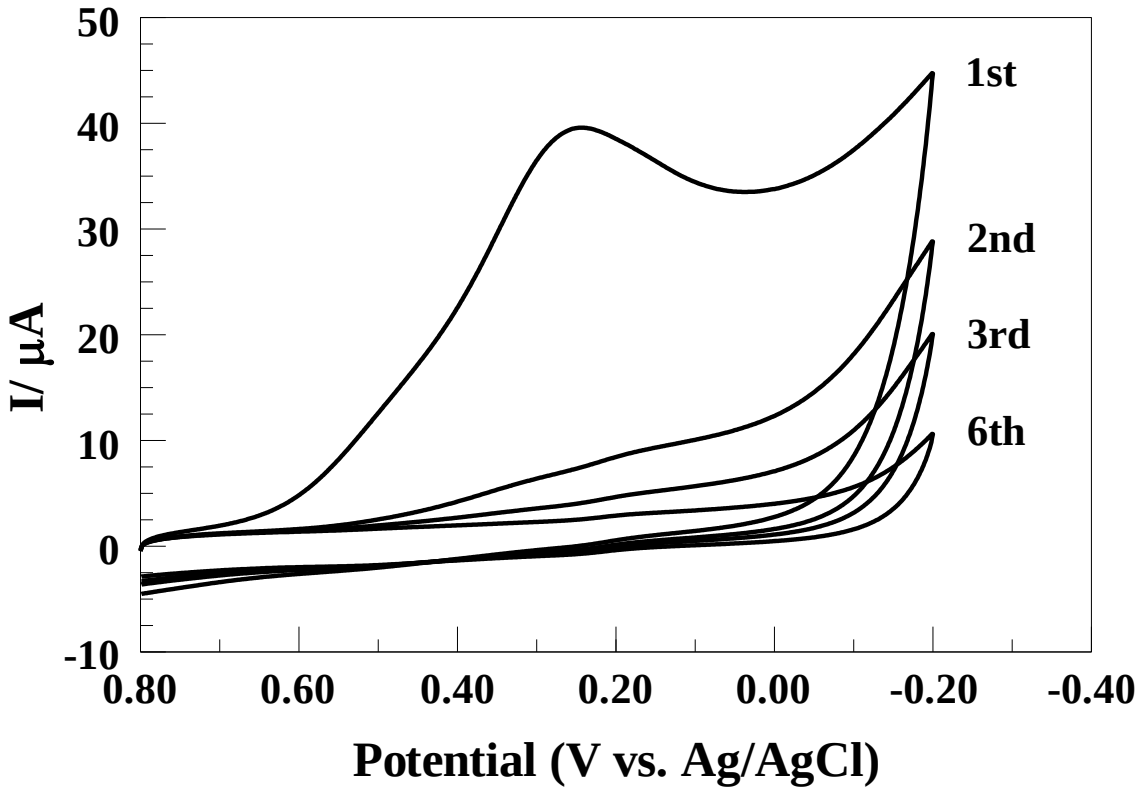

Figure 4.3 CV showing the reduction of the 4-aminophthalic acid diazonium salt on glassy carbon. The diazonium salt was formed in situ upon mixing 5.0 mM 4-aminophthalic acid +10 mM $NaNO_2$ + 400 µL HCl + 200 mM $TBAPF_6$ in 9.60 mL of MeCN. Scan rate: 0.1 V s^{-1}. The peak at 0.24 V corresponds to the reduction of the phenyldiazonium ion, and it vanishes as more cycles are run repeatedly: 1st, 2nd, 3rd and 6th cycle are shown here.

$$R\text{-}C_6H_4N_2^+ + e^- \rightarrow N_2 + R\text{-}C_6H_4^{\cdot} \quad (4.21)$$

$$\text{Glassy Carbon (GC)} + R\text{-}C_6H_4 \rightarrow GC\text{-}C_6H_4\text{-}R \quad (4.22)$$

The following sections describe the electrochemical and spectroscopic characterization of the modified glassy carbon electrodes.

4.3.5 Characterization of modified electrodes by XPS

Bare and modified glassy carbon plate electrodes were analyzed by X-ray photoelectron spectroscopy (XPS). Since carbon and oxygen are native constituents to glassy carbon, the appearance of a peak around 288 eV, corresponding to the binding energy of carboxylic carbon (C_{1s}, CO_2H) was used to detect the phthalate modification layer.[10b] Figure 4.4 contains the carbon C_{1s} spectra collected along an XPS line scan on the surface of a modified plate. The peak around 290 eV is attributed to carboxylic carbons from the phthalate groups, since it only appears in the spectra of modified spots of the glassy carbon surface. Like bare glassy carbon, unmodified spots exhibit a single carbon peak at a binding energy of *ca.* 283 eV (Figs. 4.4 and 4.6).

The ratio of atomic percentages of oxygen and carbon At% O/ At% C (or the O/C ratio) was also determined from XPS survey spectra measured along a linear path swept by the instrument across the electrode surface. The atomic percentages were determined by calculating the area under the oxygen and carbon peaks from the XPS spectra and then dividing it by the corresponding atomic sensitivity factor or ASF of each element (the ASF for oxygen O_{1s} is 0.66 and 0.25 for carbon C_{1s}).[22] Linear scans were manually set up to sample bare and modified areas of the glassy carbon plates, and consisted of several point spectra equally spaced. Figure 4.5 shows a plot of At% O/ At% C versus distance along the linear scan on a bare glassy carbon

plate, a modified glassy carbon plate, and on a glassy carbon plate soaked in the phenyldiazonium solution.

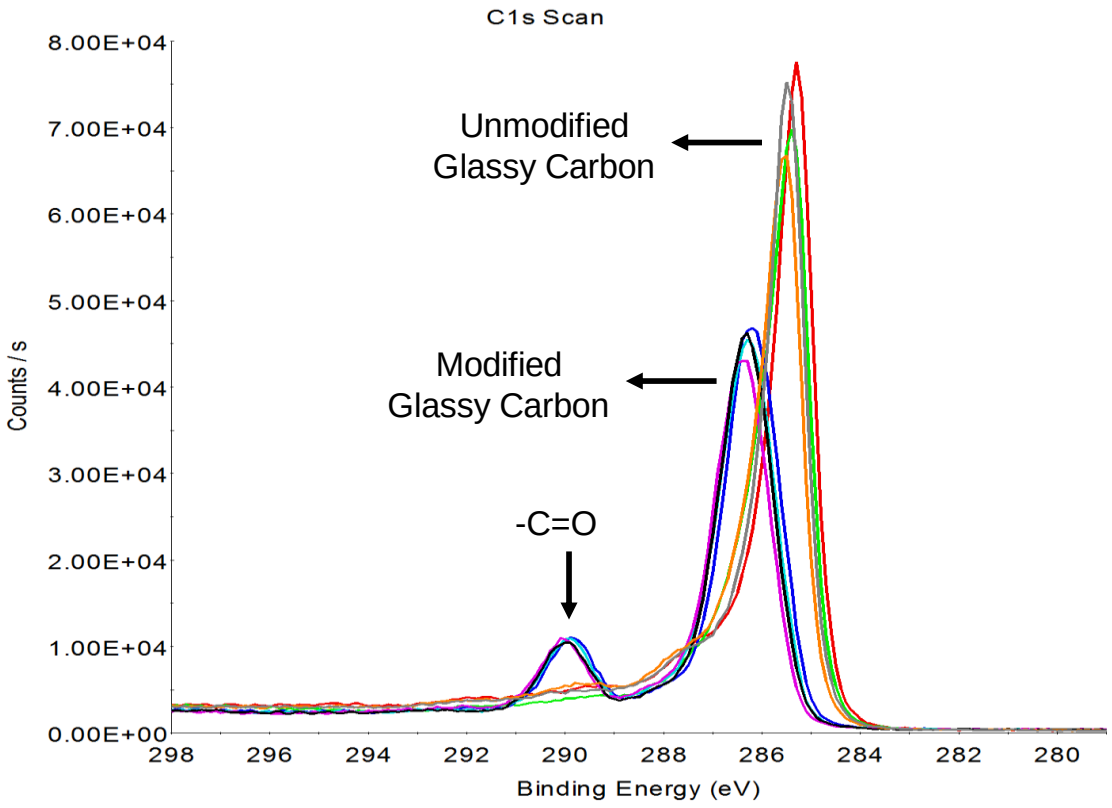

Figure 4.4 Linear scan carbon C_{1s} XPS spectra of a glassy carbon plate modified with 4-aminophthalic acid diazonium salt. Each spectrum along the linear scan appears in a different color.

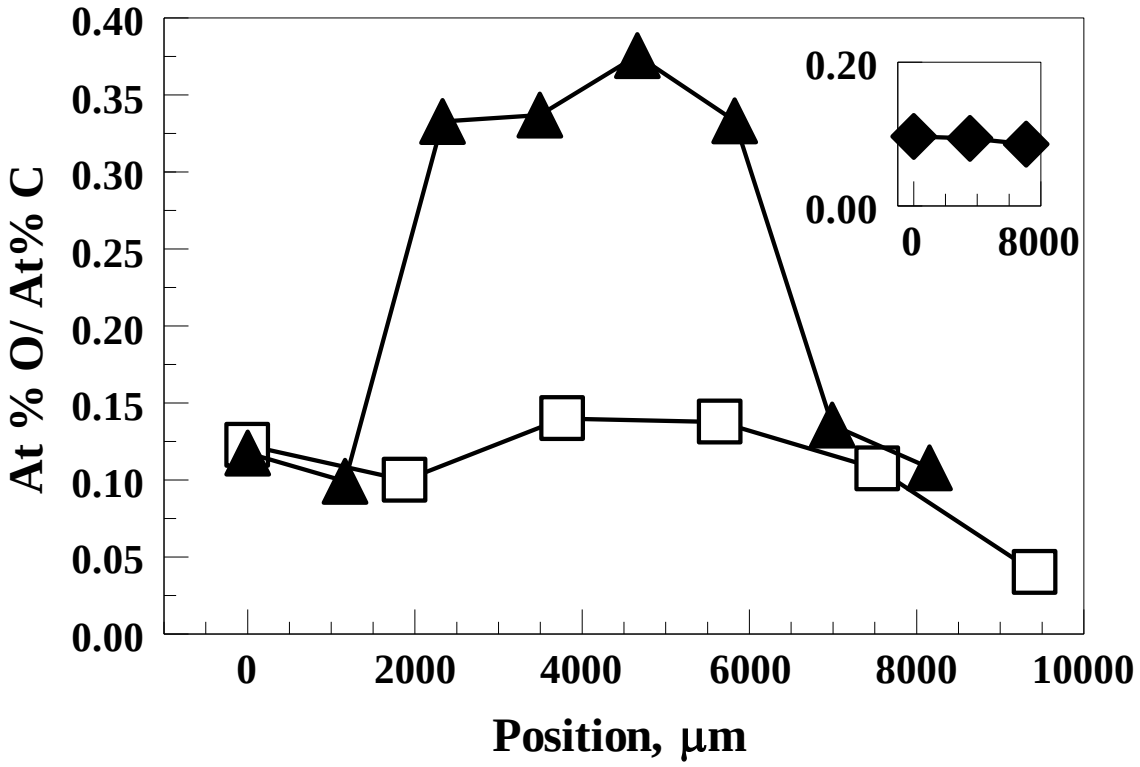

Figure 4.5 Ratio of the atomic percentages of oxygen (At% O) and carbon (At% C) measured by XPS at specific spots on the surface of a glassy carbon plate modified with phthalate groups (filled triangles) and a glassy carbon plate soaked in the diazonium salt of 4-aminophthalic acid for 20 min (open squares). Ratio %At O/ %At C at the surface of a bare glassy carbon plate (inset).The position of the spots where spectra were collected formed a line across the plate surface.

The inset in Figure 4.5 shows that bare glassy carbon exhibits a consistent O/C ratio of ~0.10, while glassy carbon electrodes modified with phthalate groups have an O/C ratio of ~0.34, within the modification layer area. This increase of the O/C ratio at the surface of the glassy carbon plates is attributed to the presence of covalently attached phthalate groups. Control glassy carbon surfaces were prepared by immersion of the plates in a solution containing all the species required for the modification of the electrodes for 20 minutes without applying any potential to reduce the diazonium salt. These controls were analyzed by XPS and the profile of O/C atomic percentage ratio with respect to surface position is also shown in Figure 4.5. The O/C ratios are

very similar to those of a bare surface (O/C≈0.1; Fig. 4.5, inset), therefore adsorption or chemical interaction of the phenyldiazonium salts with glassy carbon could not account for the larger O/C ratios measured for the plates that underwent electrochemical modification. None of the XPS spectra of a control plate exhibit the peak at 290 eV, which confirms the absence of superficial phthalate groups (Fig. 4.6).

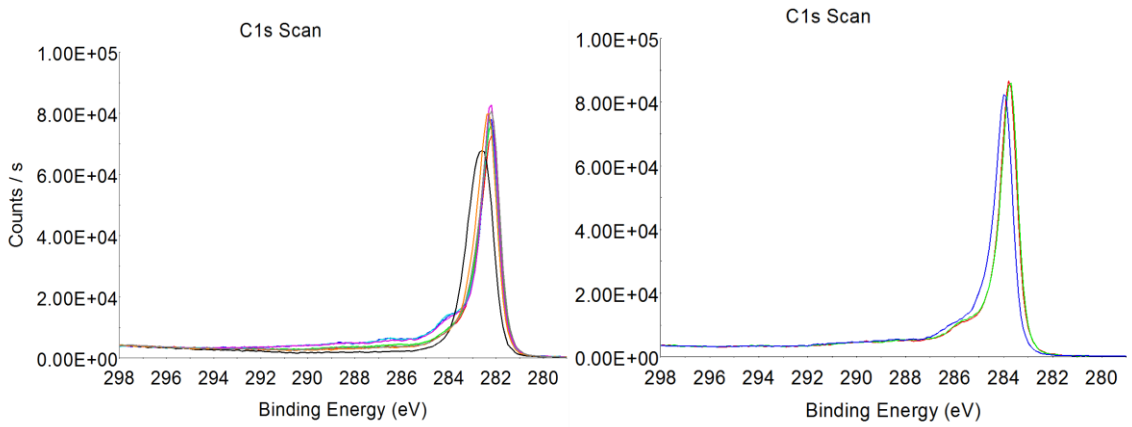

Figure 4.6 Carbon C_{1s} XPS spectra of a glassy carbon soaked in the 4-aminophthalic acid diazonium salt solution for 20 min (LEFT) and a bare glassy carbon plate (RIGHT). These spectra were recorded along a linear scan of points equally spaced across the plate surface and each spectrum along the linear scan appears in a different color.

The O/C ratio may also be used to estimate the chemical formula of the species at the analyzed surface. Assuming that phthalate groups with the formula $–C_6H_3(CO_2H)_2$ end up attached to glassy carbon, an O/C ratio close to 0.5 should be expected for the modified surface. The average O/C ratio for a modified plate is only 0.34, therefore it is possible that only a monolayer of phthalate groups forms on the surface, as in the case of glassy carbon modified with 4-nitrophenyl and 4-carboxyphenyl groups discussed by Saby *et al.*[21a] If only a monolayer of phthalate groups is present, the XPS instrument may still be able to detect native carbon from the

glassy carbon plate, given that the mean free path for C_{1s} photoelectrons is ~32 Å and the sampling depth is typically 100 Å. In contrast, the length of a phthalate molecule would be only in the order of 10 Å.[21a] Furthermore, considering the molecular structure of phthalate groups, the bulkiness of two adjacent carboxyl groups could be considered a factor that would favor the deposition of a monolayer. Nevertheless, the formation of multilayers on glassy carbon via the reduction of phenyldiazonium salts has been detected using scan force microscopy (SFM) to map the surface of electrodes modified with diethylaniline (DEA).[21b, 23] McDermott and coworkers proposed that the reduction of DEA diazonium yields DEA radicals that bind to glassy carbon and continue reacting with groups already on the surface, generating a multilayer arrangement. The formation of multilayers depends on the modification time, means of electrochemical modification (CV or chronoamperometry), the concentration of diazonium salt used and the electrode material.[21b, 23] Therefore, it would be unjustified to rule out the formation of multilayers of phthalate groups on glassy carbon under the experimental conditions used, without knowing the thickness of the layers obtained.

4.3.6 Electrochemical performance of modified glassy carbon electrodes

The electrochemical characterization of modified glassy carbon electrodes involved cyclic voltammetry (CV) of $Ru(NH_3)_6^{3+}$/ $Ru(NH_3)_6^{2+}$ and $[Fe(CN)_6]^{4-}$/$[Fe(CN)_6]^{3-}$ in 1.0 M KCl. It is appropriate to test modified electrodes with these redox probes because (1) their electrochemical behavior is well known and predictable and (2) their particular response to physical and chemical changes of the electrode surface may assist in the characterization of the modification layer(s).[8b, 24]

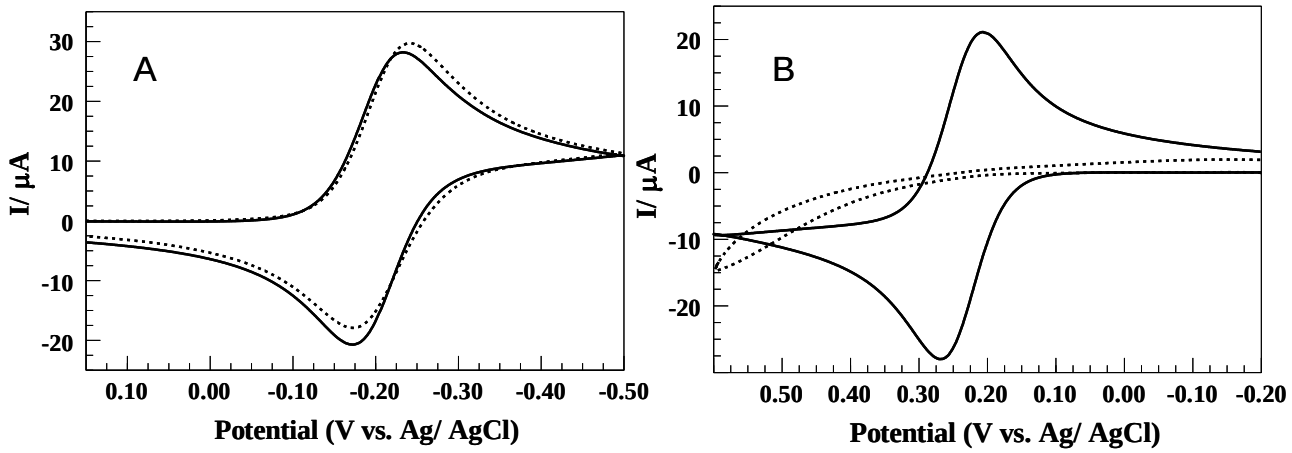

Figure 4.7 CV responses at 0.1 V s^{-1} for 1.0 mM $Ru(NH_3)_6Cl_3$ + 1.0 M KCl (A) and 1.0 mM $K_4Fe(CN)_6$ + 1.0 M KCl (B) on a bare (solid line) and a glassy carbon electrode modified with phthalate groups (dashed line).

Figure 4.7 compares the voltammetric response of these metal complexes on bare and modified electrodes. While the modification layer does not have major effect on the voltammetry of $Ru(NH_3)_6^{3+}$/ $Ru(NH_3)_6^{2+}$ (Fig. 4.7A), the CV's of $[Fe(CN)_6]^{4-}$/$[Fe(CN)_6]^{3-}$ are drastically affected by modification of the electrode surface (Fig. 4.7B). At a bare glassy carbon surface, the oxidation and reduction peaks of $[Fe(CN)_6]^{4-}$/$[Fe(CN)_6]^{3-}$ are present, with a peak-to-peak separation (ΔE_P) of ~ 60 mV typical of a reversible redox couple; however, using a modified electrode the anodic and cathodic peaks do not appear within the same potential window (Fig. 4.7B). Other studies about glassy carbon derivatization by reduction of phenyldiazonium salts, explain the almost unperturbed electrochemistry of $Ru(NH_3)_6^{3+}$/ $Ru(NH_3)_6^{2+}$ by claiming that oxidation and reduction of these species occur through electron tunneling *i.e.* the electron travels back and forth across the barrier imposed by the modification layer, between the electrode surface and the metal complex solution.[8b, 24a, 24c] On the other hand, the modification layer hinders the redox chemistry of $[Fe(CN)_6]^{4-}$/$[Fe(CN)_6]^{3-}$ because in this case a fast electron transfer requires a closer interaction between the metal complex and the electrode

surface.[8b, 24a, 24c] Raising the pH of the $[Fe(CN)_6]^{4-}/[Fe(CN)_6]^{3-}$ system enhances the passivation of the electrode towards the oxidation and reduction of the complex, while acidifying this solution improves its CV response (Figure 4.8). The phthalate groups at the electrode surface are negatively charged at high pH, due to deprotonation of their carboxylic groups, and under such conditions the electrostatic repulsion between the modification layer and the pair $[Fe(CN)_6]^{4-}/[Fe(CN)_6]^{3-}$ inhibits the electron transfer. An acidic pH neutralizes negative charges within the modification layer, due to protonation of the carboxylic groups, hence the electrostatic repulsion between layer and metal complexes decreases, and the rate of electron transfer improves.

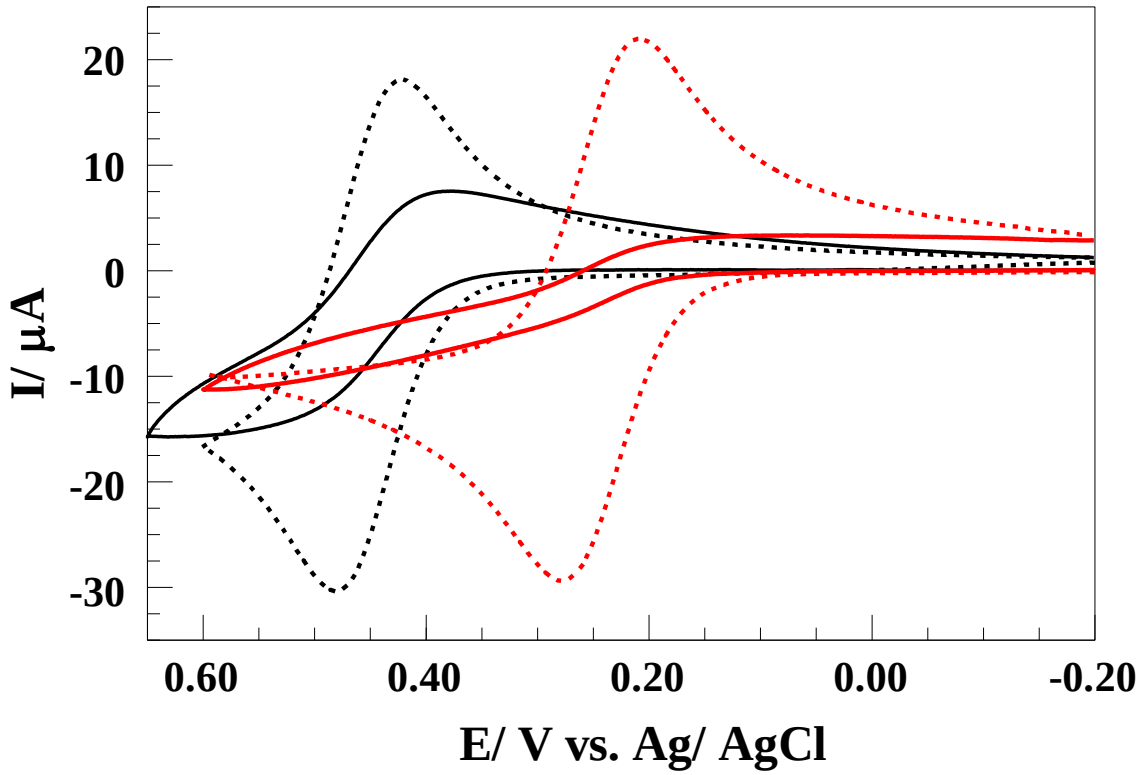

Figure 4.8 CV response of 1.0 mM $K_4Fe(CN)_6$ in 0.1 M HCl and in 0.1 M phosphate buffer pH 7.0, at a glassy carbon electrode before (black and red dashed, respectively) and after modification with phthalate groups (solid black and red, respectively). The CV scan rate was 0.1 V/s and 1.0 M KCl was used as supporting electrolyte.

Blocking of the electrode surface upon modification also affects the CV response of 1,4-H_2Q (Fig. 4.9) in MeCN. While 1,4-H_2Q's anodic peak shifts in the positive direction by approximately 100 mV, its cathodic peak appears at a more negative potential upon electrode modification (Fig. 4.9). McCreery and co-workers studied the effect of modifying glassy carbon electrodes with nitrophenyl (NP) and (trifluoromethyl)phenyl (TFMP) groups (also by reduction of the

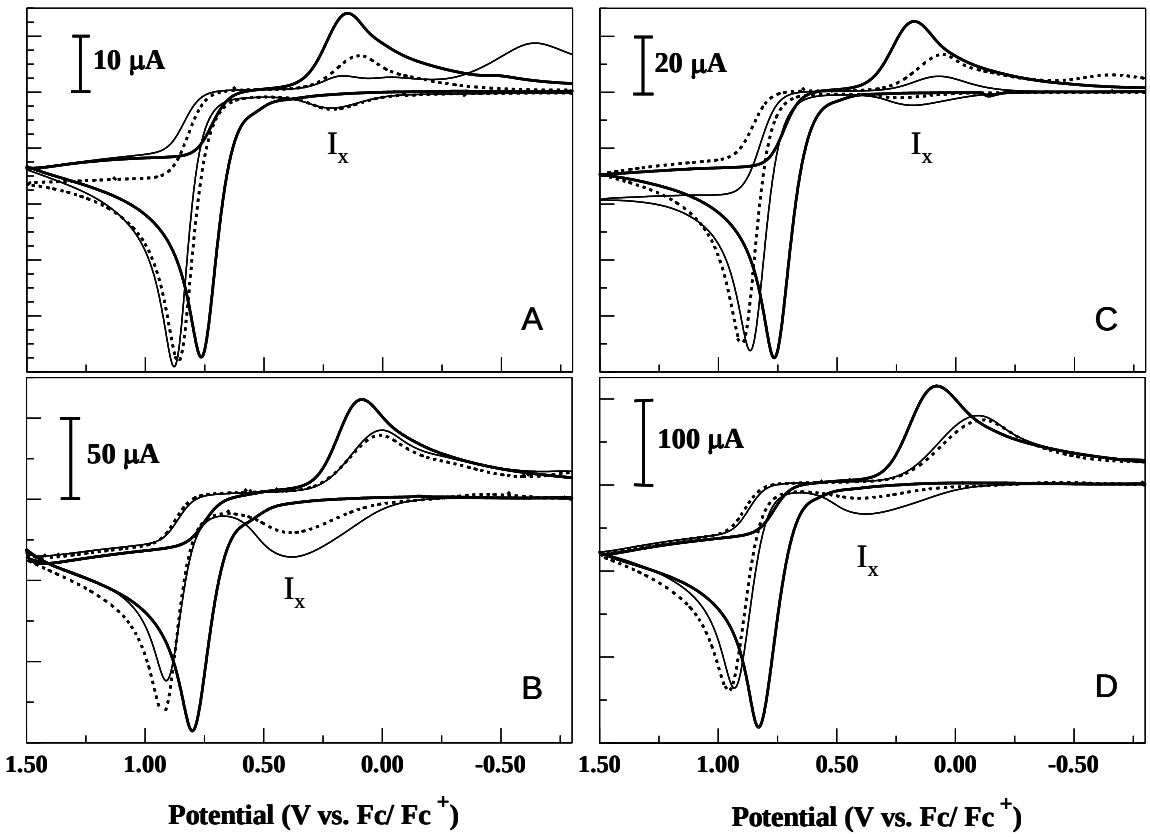

Figure 4.9 CV responses at 0.1 V s^{-1} (top) and 1 V s^{-1} (bottom) for 0.5 mM 1,4-H_2Q (A and B) and 1.0 mM 1,4-H_2Q (C and D) in MeCN, at a bare glassy carbon electrode (thick solid line) and at a glassy carbon electrode modified with phthalate groups, before (dashed line) and after immersion in 10 mM TBAOH for 120 sec (thin solid line).

corresponding diazonium salt in MeCN) on the electrochemistry of cathecol (1,2-H_2Q) and 1,4-H_2Q [8b], and found that NP and TFMP monolayers inhibit electron transfer for both phenolic

compounds. They attributed this to the blocking of the adsorption of 1,2-H_2Q and 1,4-H_2Q to the electrode surface by the NP and TFMP monolayers[8b] Adsorption of 1,2-H_2Q and 1,4-H_2Q seems to reduce the energy required for the structural reorganization that these molecules undergo during their oxidation and reduction.[8b, 25] It is likely that phthalate groups at the glassy carbon electrode surface obstruct to some degree the adsorption of 1,4-H_2Q, causing the shifting of anodic and cathodic peaks to more positive and negative potentials, respectively.

In contrast, a new interesting feature of the CVs of 1,4-H_2Q at modified glassy carbon is the small peak I_x that shows up during the anodic half-cycle (Fig. 4.9). I_x has a peak potential (E_x) that varies with the scan rate (~0.25 V vs. Fc/ Fc^+ at 0.1 V s^{-1} and ~0.37 V vs. Fc/ Fc^+ at 1 V s^{-1}). Also, I_x increases as the concentration of 1,4-H2Q and the CV scan rate are raised. (Fig. 4.9). A plot of peak current versus CV scan rate for I_x is linear (Fig. 4.10) which implies that adsorption of either 1,4-H_2Q or an intermediate governs this oxidation process. Control CV's in MeCN without 1,4-H_2Q show that this peak appeared using modified electrodes and 1,4-H_2Q-containing solutions only, discarding the oxidation of any impurities or the phthalate groups attached to the electrode surface as its original cause. Voltammograms of 1,4-H_2Q with HP^- free in solution as well as those of 1,4-H_2Q at glassy carbon modified with phthalate groups show a second anodic peak at a less positive potential than that of 1,4-H_2Q alone (I_a' in Fig 4.1A and I_x in Fig. 4.9). When HP^- is in solution the secondary anodic peak appears at a more negative potential ($E_{pa'}$ = 0.00 V vs. Fc/Fc'; Fig. 4.1) and has a larger current than that obtained with a modified electrode (E_{px} is between 0.25 V and 0.37 V vs. Fc/ Fc^+, Fig. 4.9). Nonetheless, the processes originating these new peaks must be of similar nature because in both cases the presence of phthalate bases, either in solution or at the electrode surface, is required for them to appear.

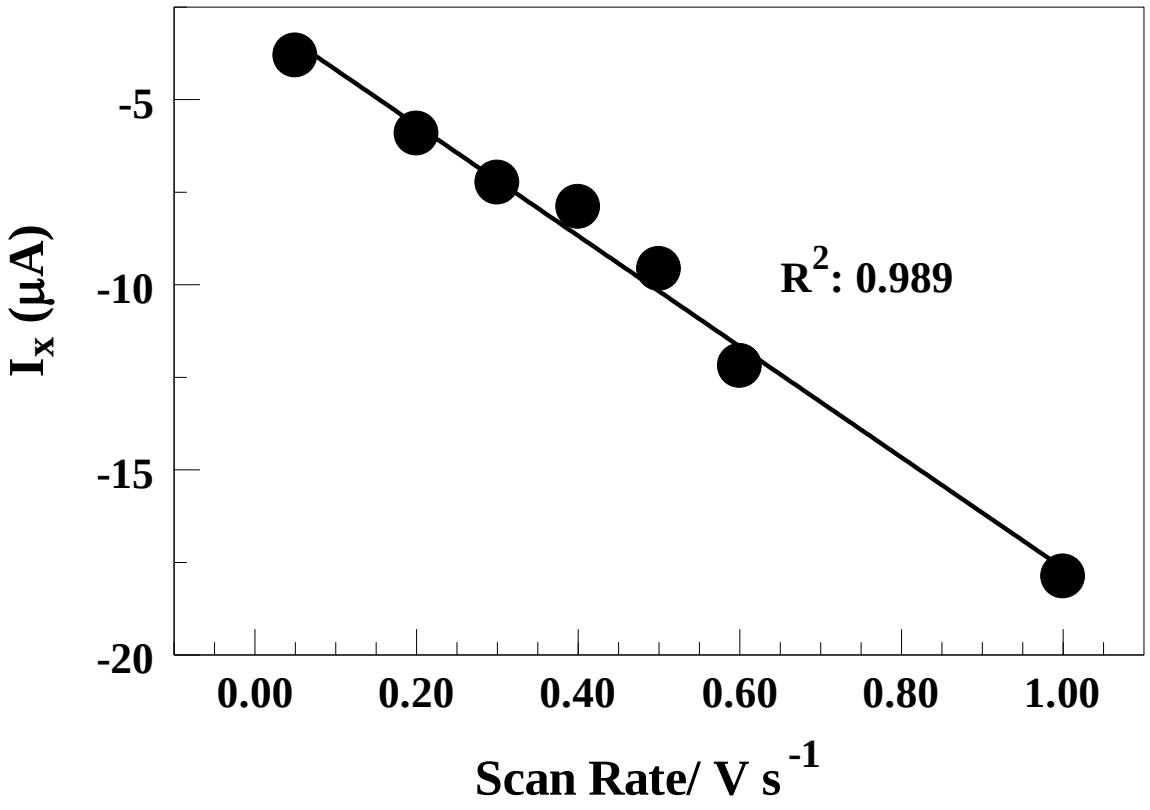

Figure 4.10 Peak current vs. scan rate for the anodic peak I_x in the voltammetry of 1.0 mM hydroquinone + 0.2 M $TBAPF_6$ in MeCN.

Although a very small amount of phthalate groups on the electrode surface would exist in the deprotonated form in MeCN (the pK_a of phthalic acid in acetonitrile at 25 °C are pK_{a1}=14.3 and pK_{a2}=29.8) the presence of microscopic amounts of water in the solvent could facilitate their deprotonation (the pK_a of phthalic acid in water at 25 °C are pK_{a1}= 2.943 and pK_{a2}= 5.432). Therefore, it is reasonable to postulate that those deprotonated phthalate groups would be able to abstract a proton from 1,4-H_2Q (the estimated pK_{a1} of 1,4-H_2Q in acetonitrile is 26.20) thus leading to its early oxidation. Also, in a similar fashion as seen in the studies with freely

dissolved phthalate, hydrogen bonding is another likely interaction between 1,4-H_2Q and the phthalate groups at the electrode interface that could contribute to this phenomenon.

In order to test this hypothesis, we investigated the effect of increasing the amount of deprotonated phthalate groups at the glassy carbon surface on the current and potential of this new anodic peak. The experiment entailed soaking the modified electrodes in a solution of the strong base tetrabutylammonium hydroxide (10 mM TBAOH in MeCN) for 60 seconds, prior to running CVs of 1,4-H_2Q at a scan rate of 0.1 V/s. The I_x peak current (i_{px}) increased from ~ 5 μA to ~ 7 μA upon treatment of the electrode with TBAOH, because the number of deprotonated phthalate groups increased, and with it the number of sites for hydrogen bonding and/or proton transfer with 1,4-H_2Q to take place (Fig. 4.11). By alternating the soaking of modified electrodes in the TBAOH solution with a treatment in a strongly acidic solution (10mM HCl), i_{px} decreased to almost its initial value of ~ 5 μA. These results demonstrate that the rate of the process originating the anodic pre-peak depends on the protonation state of the groups at the electrode surface, since the effects of treating the electrode with a strong base can be reversed by treatment with a strong acid and vice versa (Fig. 4.11). Then, it is proposed that peak I_x marks the early oxidation of 1,4-H_2Q, facilitated by a mix of proton transfer and hydrogen bonding between 1,4-H_2Q and the phthalate groups at the electrode surface. Regarding the mechanism that may apply to the voltammetry presented in Figure 4.9, it could be a combination of the typical ET-PT-ET-PT for 1,4-H_2Q alone in MeCN, dicussed in a previous report [1] and the one depicted in Scheme 4.2, where complexes formed between 1,4-H_2Q and HP^- are the active redox species. However, the stoichiometry of association among 1,4-H_2Q and phthalates on the electrode surface is probably not the same as in solution, due to steric interactions. Thus, the chemistry between 1,4-H_2Q and phthalate bases is localized at the surface of modified glassy carbon electrodes. In spite

of the smaller currents obtained for the base-enhanced oxidation of 1,4-H_2Q at these modified electrodes, which must be limited by the small number of molecules attached to their surface, this work highlights once again the influence of the electrode surface composition on the voltammetric response of electroactive compounds.

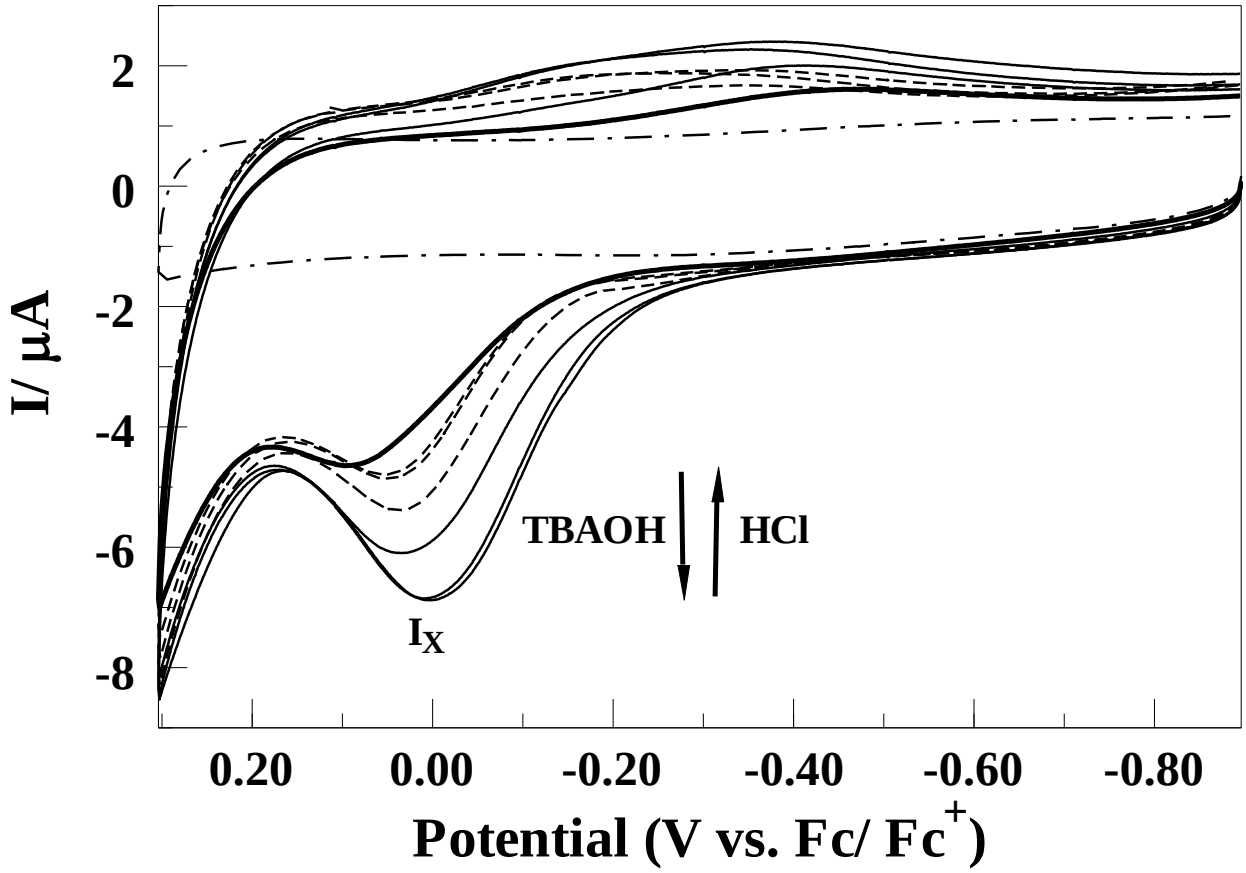

Figure 4.11 CVs of 1.0 mM 1,4-H_2Q + 0.2 M $TBAPF_6$ in MeCN at a glassy carbon electrode modified with phthalate groups, treated alternately in 10 mM TBAOH (thin solid line) and 10 mM HCl (dashed line) for 60 sec each time. A blank CV run in MeCN containing 0.2 M $TBAPF_6$ (dashed-solid line) as well as the CV of 1.0 mM 1,4-H_2Q + 0.2 M $TBAPF_6$ (thick solid line) run before treating the electrode in the basic and acidic solutions are also shown. Scan Rate = 0.1 V s^{-1}.

4.4 Conclusion

Phthalate bases (HP^- and P^{2-}) interact with 1,4-H_2Q in MeCN through hydrogen bonding and proton transfer (P^{2-}) to form molecular complexes that oxidize at easier (less positive) potentials than pure 1,4-H_2Q. The relatively large decrease in the oxidation overpotential for 1,4-H_2Q, observed upon introducing these Brönsted bases, is an example of thermodynamic control of a PCET achieved with weak bases. The participation of weak acid and basic groups in redox reactions involving proton transfer is rather common in biological systems, where harsh conditions of pH, and potentially denaturizing agents such as OH^- are thus avoided. In electrochemical applications, a decrease of the redox overpotential promoted by Brönsted species may be advantageous in the development of biosensors, for example, since most electroactive bioanalytes are sensitive to strongly acidic or basic environments, as well as to highly oxidative or reductive conditions. Comparable thermodynamic/kinetic effects on the redox behavior of 1,4-H_2Q seen upon attachment of phthalate bases to the surface glassy carbon electrodes demonstrate the importance of the electrode's composition on the electrochemistry of acidic redox species such as 1,4-H_2Q. Hydrogen bonding and proton transfer interactions between 1,4-H_2Q and phthalate observed in solution likely take place when the electrode is modified with such bases. Although the presence of phthalates in solution or at the electrode surface results in a thermodynamic shift of 1,4-H_2Q's oxidation to easier potentials, the rate of 1,4-H_2Q electron transfer does not appear to change much. Therefore, for future work, the design of electrocatalytic surfaces should aim for the functionalization of the electrode surface with chemical groups capable of stabilizing the transition state, rather than the products of the reaction. In this case, phthalate bases in solution or attached to glassy carbon surfaces are seemingly better at stabilizing the final products of the reaction than its transition state. This is

done by accepting the protons (supported by hydrogen bonding) released in the oxidation of 1,4-H_2Q.

4.5 References

1. (a) Alligrant, T. M.; Alvarez, J. C., *J. Phys. Chem. C* **2011,** *115*, 10797-10805; (b) Alligrant, T. M.; Hackett, J. C.; Alvarez, J. C., *Electrochim. Acta* **2010,** *55*, 6507-6516.
2. (a) Buratti, S.; Brunetti, B.; Mannino, S., *Talanta* **2008,** *76*, 454-457; (b) Raoof, J. B.; Ojani, R.; Kolbadinezhad, M., *J. Solid State Electrochem.* **2009,** *13*, 1411-1416; (c) Milani, M. R.; Stradiotto, N. R.; Cardoso, A. A., *Electroanalysis* **2003,** *15*, 827-830; (d) Bard, A. J.; Faulkner, L. R., *Electrochemical Methods: Fundamentals and Applications*. 2 ed.; John Wiley & Sons: New York, 2001; (e) Winter, M., *Chem. Rev.* **2004,** *104*, 4245-4270.
3. (a) Bard, A. J., *J. Am. Chem. Soc.* **2010,** *132*, 7559-7567; (b) Gong, K.; Zhu, X.; Zhao, R.; Xiong, S.; Mao, L.; Chen, C., *Anal. Chem.* **2005,** *77*, 8158-8165.
4. Khalid, I. M.; Pu, Q.; Alvarez, J. C., *Angew. Chem. Int. Ed.* **2006,** *45*, 5829-5832.
5. (a) Quan, M.; Sanchez, D.; Wasylkiw, M. F.; Smith, D. K., *J. Am. Chem. Soc.* **2007,** *129*, 12847-12856; (b) Lehmann, M. W.; Evans, D. H., *J. Phys. Chem. B* **2001,** *105*, 8877-8884; (c) Gupta, N.; Linschitz, H., *J. Am. Chem. Soc.* **1997,** *119*, 6384-6391; (d) Garza, J.; Vargas, R.; Gomez, M.; Gonzalez, I.; Gonzalez, F. J., *J. Phys. Chem. A* **2003,** *107*, 11161-11168; (e) Astudillo, P. D.; Tiburcio, J.; Gozalez, F. J., *J. Electroanal. Chem.* **2007,** *604*, 57-64; (f) Laviron, E., *J. Electroanal. Chem.* **1983,** *146*, 15-36; (g) Markle, T. F.; Mayer, J. M., *Angew. Chem. Int. Ed.* **2008,** *47*, 738-740.
6. (a) Fecenko, C. J.; Thorp, H. H.; Meyer, T. J., *J. Am. Chem. Soc.* **2007,** *129*, 15098-15099; (b) Fecenko, C. J.; Meyer, T. J.; Thorp, H. H., *J. Am. Chem. Soc.* **2006,** *128*, 11020-11021; (c) Kirby, A. J., Acid-Base Catalysis by Enzymes. In *Encyclopedia of Life Sciences*, John Wiley & Sons: 2001; (d) Eigen, M., *Angew. Chem. Int. Ed.* **1964,** *3*, 1-72.
7. (a) Schreiber, E.; Carlisle, M., 1.5 Diffusion Experiments/DOSY. In *User Guide: Liquids NMR*, Steele, D., Ed. Varian, Inc.: Palo Alto, California, 2001; pp 40-67; (b) Cohen, Y.; Avram, L.; Frish, L., *Angew. Chem. Int. Ed.* **2005,** *44*, 520-554; (c) Berger, S.; Braun, S., *200 and More NMR Experiments A Practical Course*. Wiley-VCH: Weinheim, 2004; p 467-469.
8. (a) McCreery, R. L., *Chem. Rev.* **2008,** *108*, 2646-2687; (b) Hunt DuVall, S.; McCreery, R. L., *J. Am. Chem. Soc.* **2000,** *122*, 6759-6764.
9. Fielding, L., *Tetrahedron* **2000,** *56*, 6151-6170.
10. (a) Cougnon, C.; Gohier, F.; Belanger, D.; Mauzeroll, J., *Angew. Chem. Int. Ed.* **2009,** *48*, 4006-4008; (b) Allongue, P.; Delamar, M.; Desbat, B.; Fagebaume, O.; Hitmi, R.; Pinson, J.; Saveant, J.-M., *J. Am. Chem. Soc.* **1997,** *119*, 201-207.
11. Brown, J. S.; Lesutis, H. P.; Lamb, D. R.; Bush, D.; Chandler, K.; West, B. L.; Liotta, C. L.; Eckert, C. A.; Schiraldi, D.; Hurley, J. S., *Ind. Eng. Chem. Res.* **199,** *38*, 3622-3627.
12. Guillorn, M. A.; McKnight, T. E.; Melecho, A.; Merkulov, V. I.; Britt, P. F.; Austin, D. W.; Lowndes, D. H.; Simpson, M. L., *J. App. Phys.* **2002,** *91*, 3824-3828.

13. Gritzner, G.; Kuta, J., *Electrochim. Acta* **1984,** *29*, 869-873.
14. Stejskal, E. O., Tanner, J.E., *J. Chem. Phys.* **1965,** *42*, 288-292.
15. Sun, H.; Chen, W.; Kaifer, A. E., *Organometallics* **2006,** *25*, 1828-1830.
16. Connors, K. A., *Binding Constants, The Measurement of Molecular Complex Stability*. John Wiley and Sons: New York, 1987.
17. Izutsu, K., *Acid-Base Dissociation Constants in Dipolar Aprotic Solvents*. Blackwell Scientific Publications: London, 1990.
18. (a) Chambers, J. Q., Electrochemistry of Quinones. In *The Chemistry of Quinoid Compounds*, Patai, S.; Rappoport, Z., Eds. John Wiley and Sons: New York, 1988; Vol. 2, pp 719 - 758; (b) Costentin, C., *Chem. Rev.* **2008,** *108*, 2145-2179; (c) Eggins, B. R.; Chambers, J. Q., *J. Electrochem. Soc.* **1970,** *117*, 186-192; (d) Laviron, E., *J. Electroanal. Chem.* **1984,** *164*, 213-227; (e) Parker, V. D., *Chem. Comm.* **1969**, 716-717; (f) Parker, V. D., *Electrochim. Acta* **1973,** *18*, 519-524; (g) Stallings, M. D.; Morrison, M. M.; Sawyer, D. T., *Inorg. Chem.* **1981,** *20*, 2655-2660.
19. (a) Lehmann, M. W.; Evans, D. H., *Anal. Chem.* **1999,** *71*, 1947-1950; (b) Wipf, D. O.; Wehmeyer, K. R.; Wightman, R. M., *J. Org. Chem.* **1986,** *51*, 4760-4764.
20. Baranton, S.; Belanger, D., *J. Phys. Chem. B* **2005,** *109*, 24401-24410.
21. (a) Saby, C.; Ortiz, B.; Champagne, G. Y.; Belanger, D., *Langmuir* **1997,** *13*, 6805-6813; (b) McDermott, M. T.; Kariuki, J. K., *Langmuir* **2001,** *17*, 5947-5951.
22. Briggs, D.; Seah, M. P., *Practical Surface Analysis: Auger and X-ray photoelectron spectroscopy*. John Wiley & Sons: Chichester, UK, 1990; Vol. 1.
23. McDermott, M. T.; Kariuki, J. K., *Langmuir* **1999,** *15*, 6534-6540.
24. (a) Yang, G.; Liu, B.; Dong, S., *J. Electroanal. Chem.* **2005,** *585*, 301-305; (b) Leroux, Y. R.; Fei, H.; Noel, J. M.; Roux, C.; Hapiot, P., *J. Am. Chem. Soc.* **2010,** *132*, 14039-14041; (c) Hunt DuVall, S.; McCreery, R. L., *Anal. Chem.* **1999,** *71*, 4594-4602.
25. McCreery, R. L., *Chem. Rev.* **2008,** *108*, 2646-2687.

Appendix 2:

I. Diffusion coefficients of GSH, $IrCl_6^{2-}/IrCl_6^{3-}$ and the buffers components.

II. Derivation of rate law expressions for stepwise pathways 1 and 3 (Scheme 2.4).

III. Parameters used in digital simulations of cyclic voltammograms.

IV. References

I. Diffusion coefficients of GSH, $IrCl_6^{2-}/IrCl_6^{3-}$ and the buffers components.

Species	Diffusion Coefficient/ 10^6 cm^2 s^{-1}
GSH	$(5.13 \pm 0.05)^a$
$IrCl_6^{2-}/IrCl_6^{3-}$	$(7.0 \pm 1.0)^b$
$H_2PO_4^-$	9.59^c
HPO_4^{2-}	7.59^c
$malate^{1-}$/ $malate^{2-}$	7.83^c
$succinate^{1-}$/ $succinate^{2-}$	7.83^c
$citrate^{2-}$ / $citrate^{3-}$	6.23^c
$maleate^{1-}$/ $maleate^{2-}$	8.24^c

Table 2.S1 Diffusion coefficient of all species represented in Scheme 2.3 used to simulate the cyclic voltammetry of GSH in the presence of $IrCl_6^{2-}/IrCl_6^{3-}$ and the different Brönsted bases B.

[a] Determined by Pulsed Gradient Echo (PGE) ^1H NMR as described in the experimental section; the diffusion coefficient of all the glutathione derived species (i.e. G$^{\bullet}$, GG and G" in Scheme 2.3) was assumed to be the same as that of glutathione (G in Scheme 2.3). [b] Estimated though digital simulation of cyclic voltammograms of aqueous solutions of 1.0 mM K_3IrCl_6 alone. [c] Obtained from the CRC Handbook of Chemistry and Physics; the same diffusion coefficient was assumed for all deprotonation states of malic, succinic, citric and maleic species.[1]

II. Rate law derivations for stepwise pathways

A. Stepwise 1 PT-ET

PCET

$$GSH + B \underset{k_{-PT1}}{\overset{k_{PT1}}{\rightleftharpoons}} GS^- + BH^+ \quad \text{2.S1}$$

$$GS^- + IrCl_6^{2-} \xrightarrow{k_{ET1}} GS^\bullet + IrCl_6^{3-} \quad \text{2.S2}$$

$$GS^\bullet + GS^\bullet \xrightarrow{fast} GSSG \quad \text{2.S3}$$

If the PCET is rate determining, the production rate of GSSG is controlled by how fast $GS^\bullet$ is generated, therefore:

$$Rate = \frac{d[GSSG]}{dt} = -\frac{d[GS^\bullet]}{2dt} \quad \text{2.S4}$$

$$\frac{d[GS^\bullet]}{dt} = k_{ET1}\,[GS^-][IrCl_6^{2-}] \quad \text{2.S5}$$

Assuming GS^- is an intermediate obeying the steady state approximation then:

$$\frac{d[GS^-]}{dt} = k_{PT1}\,[GSH][B] - k_{-PT1}\,[GS^-][BH^+] - k_{ET1}\,[GS^-][IrCl_6^{2-}] = 0 \quad \text{2.S6}$$

Solving for $[GS^-]$

$$[GS^-] = \frac{k_{PT1}\,[GSH][B]}{k_{-PT1}\,[BH^+] + k_{ET1}\,[IrCl_6^{2-}]} \quad \text{2.S7}$$

Replacing in 2.S5 and 2.S4

$$Rate_1 = \frac{k_{PT1}\,k_{ET1}\,[B]\,[GSH][IrCl_6^{2-}]}{k_{-PT1}\,[BH^+] + k_{ET1}\,[IrCl_6^{2-}]} \quad \text{2.S8}$$

Defining k_{obs1} as:

$$k_{obs1} = \frac{k_{PT1}\,k_{ET1}\,[B]}{k_{-PT1}\,[BH^+] + k_{ET1}\,[IrCl_6^{2-}]} \quad \text{2.S9}$$

$$Rate_1 = k_{obs1}\,[GSH][IrCl_6^{2-}] \quad \text{2.S10}$$

B. Stepwise 3 ET-PT

$$\text{PCET}\begin{cases} \text{GSH} + \text{IrCl}_6^{2-} \underset{k_{-ET3}}{\overset{k_{ET3}}{\rightleftharpoons}} \text{GSH}^{\bullet+} + \text{IrCl}_6^{3-} & \text{2.S11} \\ \text{GSH}^{\bullet+} + \text{B} \xrightarrow{k_{PT3}} \text{GS}^{\bullet} + \text{BH}^{+} & \text{2.S12} \end{cases}$$

$$\text{GS}^{\bullet} + \text{GS}^{\bullet} \xrightarrow{\text{fast}} \text{GSSG} \qquad \text{2.S13}$$

If the PCET is rate determining, the production rate of GSSG is controlled by how fast $GS^{\bullet}$ is generated, therefore:

$$\text{Rate} = \frac{d[\text{GSSG}]}{dt} = -\frac{d[\text{GS}^{\bullet}]}{2dt} \qquad \text{2.S14}$$

$$\frac{d[\text{GS}^{\bullet}]}{dt} = k_{PT3}\,[\text{GSH}^{\bullet+}][\text{B}] \qquad \text{2.S15}$$

Assuming $GSH^{\bullet+}$ is an intermediate obeying the steady state approximation then:

$$\frac{d[\text{GSH}^{\bullet+}]}{dt} = k_{ET3}\,[\text{GSH}][\text{IrCl}_6^{2-}] - k_{-ET3}\,[\text{GSH}^{\bullet+}][\text{IrCl}_6^{3-}] - k_{PT3}\,[\text{GSH}^{\bullet+}][\text{B}] = 0 \qquad \text{2.S16}$$

Solving for $[GSH^{\bullet+}]$

$$[\text{GSH}^{\bullet+}] = \frac{k_{ET3}\,[\text{GSH}][\text{IrCl}_6^{2-}]}{k_{-ET3}\,[\text{IrCl}_6^{3-}] + k_{PT3}\,[\text{B}]} \qquad \text{2.S17}$$

Replacing in 2.S15 and 2.S14

$$\text{Rate}_3 = \frac{k_{PT3}\,k_{ET3}\,[\text{B}]\,[\text{GSH}][\text{IrCl}_6^{2-}]}{k_{-ET3}\,[\text{IrCl}_6^{3-}] + k_{PT3}\,[\text{B}]} \qquad \text{2.S18}$$

Defining k_{obs3} as:

$$k_{obs3} = \frac{k_{PT3}\,k_{ET3}\,[\text{B}]}{k_{-ET3}\,[\text{IrCl}_6^{3-}] + k_{PT3}\,[\text{B}]} \qquad \text{2.S19}$$

$$\text{Rate}_3 = k_{obs3}\,[\text{GSH}][\text{IrCl}_6^{2-}] \qquad \text{2.S20}$$

III. Parameters used in digital simulations of cyclic voltammograms.

The following are the electrochemical and kinetic parameters that best fitted the experimental voltammetry. Since CVs run at various scan rates were simulated, here we present the average of the estimated electrochemical and kinetic parameters. Also, the forward rate constant k_f for the reaction between glutathione G and $IrCl_6^{2-}$ is the same k_{obs} introduced in Scheme 2.3.

1.0 mM K_3IrCl_6 + 3.0 mM GSH + 35 mM phosphate buffer pH 4.0 + 1.0 M NaCl			
Electrochemical Reactions	**E**	**k_s**	**α**
$IrCl_6^{2-} + e^- = IrCl_6^{3-}$	0.7263	0.1	0.5
$G^{\bullet} + e- = G$	0.8560	1×10^{-6}	0.5
Chemical Reactions	**K**	**k_f**	**k_b**
$IrCl_6^{2-} + G = IrCl_6^{3-} + G^{\bullet}$	$(6.44\pm0.03) \times 10^{-3}$	$(1.1\pm0.3) \times 10^{3}$	$(1.67\pm0.04) \times 10^{5}$
$IrCl_6^{2-} + G^{\bullet} = IrCl_6^{3-} + G''$	1.0×10^{11}	1.0×10^{5}	1.0×10^{-6}
$G^{\bullet} + G^{\bullet} = GG$	1×10^{9}	5×10^{8}	0.5
$IrCl_6^{2-} = P$	NA	NA	NA

1.0 mM K_3IrCl_6 + 3.0 mM GSH + 35 mM phosphate buffer pH 5.0 + 1.0 M NaCl			
Electrochemical Reactions	**E**	**k_s**	**α**
$IrCl_6^{2-} + e^- = IrCl_6^{3-}$	0.7234	0.05	0.5
$G^{\bullet} + e- = G$	0.7969	1×10^{-6}	0.5
Chemical Reactions	**K**	**k_f**	**k_b**
$IrCl_6^{2-} + G = IrCl_6^{3-} + G^{\bullet}$	$(5.72\pm0.02) \times 10^{-2}$	$(1.7\pm0.3) \times 10^{3}$	$(3.0\pm0.6) \times 10^{4}$
$IrCl_6^{2-} + G^{\bullet} = IrCl_6^{3-} + G''$	1.0×10^{11}	$(1.1\pm0.3) \times 10^{5}$	$(1.1\pm0.3) \times 10^{-6}$
$G^{\bullet} + G^{\bullet} = GG$	1×10^{9}	5×10^{8}	0.5
$IrCl_6^{2-} = P$	NA	NA	NA

1.0 mM K_3IrCl_6 + 3.0 mM GSH + 35 mM phosphate buffer pH 6.0 + 1.0 M NaCl			
Electrochemical Reactions	**E**	**k_s**	**α**
$IrCl_6^{2-} + e^- = IrCl_6^{3-}$	0.7225	0.1	0.5
$G^{\bullet} + e- = G$	0.7378	1×10^{-6}	0.5
Chemical Reactions	**K**	**k_f**	**k_b**
$IrCl_6^{2-} + G = IrCl_6^{3-} + G^{\bullet}$	$(5.50\pm0.04) \times 10^{-1}$	$(2.3\pm0.3) \times 10^{4}$	$(4.2\pm0.6) \times 10^{4}$
$IrCl_6^{2-} + G^{\bullet} = IrCl_6^{3-} + G''$	1.0×10^{11}	$(5.4\pm1.0) \times 10^{6}$	$(5.4\pm1.0) \times 10^{-5}$
$G^{\bullet} + G^{\bullet} = GG$	1×10^{9}	5×10^{8}	0.5
$IrCl_6^{2-} = P$	30.0	1.53×10^{-2}	5.10×10^{-4}

1.0 mM K_3IrCl_6 + 3.0 mM GSH + 35 mM phosphate buffer pH 7.2 + 1.0 M NaCl			
Electrochemical Reactions	**E**	**k_s**	**α**
$IrCl_6^{2-} + e^- = IrCl_6^{3-}$	0.7214	0.1	0.5
$G^{\bullet} + e- = G$	0.6675	1.00×10^{-4}	0.5
Chemical Reactions	**K**	**k_f**	**k_b**
$IrCl_6^{2-} + G = IrCl_6^{3-} + G^{\bullet}$	8.16±0.09	$(1.2\pm0.1) \times 10^{5}$	$(1.4\pm0.2) \times 10^{4}$
$IrCl_6^{2-} + G^{\bullet} = IrCl_6^{3-} + G''$	1.0×10^{11}	$(9.0\pm0.9) \times 10^{6}$	$(9.0\pm0.9) \times 10^{-5}$
$G^{\bullet} + G^{\bullet} = GG$	1×10^{9}	5×10^{8}	0.5
$IrCl_6^{2-} = P$	36.7	1.53×10^{-2}	4.17×10^{-4}

1.0 mM K_3IrCl_6 + 3.0 mM GSH + 35 mM phosphate buffer pH 8.0 + 1.0 M NaCl			
Electrochemical Reactions	**E**	**k_s**	**α**
$IrCl_6^{2-} + e^- = IrCl_6^{3-}$	0.7261	0.1	0.5
$G^{\bullet} + e- = G$	0.6241	1.00×10^{-4}	0.5
Chemical Reactions	**K**	**k_f**	**k_b**
$IrCl_6^{2-} + G = IrCl_6^{3-} + G^{\bullet}$	$(5.3\pm0.1) \times 10^{1}$	$(1.8\pm0.1) \times 10^{5}$	$(3.4\pm0.3) \times 10^{3}$
$IrCl_6^{2-} + G^{\bullet} = IrCl_6^{3-} + G''$	1.0×10^{10}	$(6.0\pm1.0) \times 10^{6}$	$(6.0\pm1.0) \times 10^{-4}$
$G^{\bullet} + G^{\bullet} = GG$	1×10^{9}	5×10^{8}	0.5
$IrCl_6^{2-} = P$	36.7	1.53×10^{-2}	4.17×10^{-4}

1.0 mM K_3IrCl_6 + 3.0 mM GSH + 35 mM phosphate buffer pH 9.0 + 1.0 M NaCl			
Electrochemical Reactions	**E**	**k_s**	**α**
$IrCl_6^{2-} + e^- = IrCl_6^{3-}$	0.7275	0.1	0.5
$G^{\bullet} + e- = G$	0.5884	1.00×10^{-4}	0.5
Chemical Reactions	**K**	**k_f**	**k_b**
$IrCl_6^{2-} + G = IrCl_6^{3-} + G^{\bullet}$	$(2.24\pm0.02) \times 10^{2}$	$(2.55\pm0.07) \times 10^{5}$	$(1.14\pm0.03) \times 10^{3}$
$IrCl_6^{2-} + G^{\bullet} = IrCl_6^{3-} + G''$	1.0×10^{10}	$(7.9\pm0.6) \times 10^{6}$	$(7.9\pm0.6) \times 10^{-4}$
$G^{\bullet} + G^{\bullet} = GG$	9×10^{8}	5×10^{8}	0.6
$IrCl_6^{2-} = P$	43.5	1.53×10^{-2}	3.51×10^{-4}

1.0 mM K_3IrCl_6 + 3.0 mM GSH + 5.0 mM phosphate buffer pH 7.0 + 1.0 M NaCl			
Electrochemical Reactions	**E**	**k_s**	**α**
$IrCl_6^{2-} + e^- = IrCl_6^{3-}$	0.7308	0.1	0.5
$G^{\bullet} + e- = G$	0.6791	1.00×10^{-5}	0.5
Chemical Reactions	**K**	**k_f**	**k_b**
$IrCl_6^{2-} + G = IrCl_6^{3-} + G^{\bullet}$	7.48±0.03	$(4.3\pm0.7) \times 10^{4}$	$(5.7\pm0.9) \times 10^{3}$
$IrCl_6^{2-} + G^{\bullet} = IrCl_6^{3-} + G''$	8.0×10^{13}	$(3.0\pm1.0) \times 10^{6}$	$(3.7\pm1.5) \times 10^{-8}$
$G^{\bullet} + G^{\bullet} = GG$	1×10^{9}	5×10^{8}	0.5
$IrCl_6^{2-} = P$	80.0	1.53×10^{-2}	1.91×10^{-4}

1.0 mM K_3IrCl_6 + 3.0 mM GSH + 10 mM phosphate buffer pH 7.0 + 1.0 M NaCl			
Electrochemical Reactions	**E**	**k_s**	**α**
$IrCl_6^{2-} + e^- = IrCl_6^{3-}$	0.7307	0.1	0.5
$G^{\bullet} + e- = G$	0.6791	1.00×10^{-5}	0.5
Chemical Reactions	**K**	**k_f**	**k_b**
$IrCl_6^{2-} + G = IrCl_6^{3-} + G^{\bullet}$	7.46±0.01	$(6.2\pm0.8) \times 10^{4}$	$(8.3\pm1.0) \times 10^{3}$
$IrCl_6^{2-} + G^{\bullet} = IrCl_6^{3-} + G''$	1.0×10^{11}	$(6.1\pm0.8) \times 10^{6}$	$(6.1\pm0.8) \times 10^{-5}$
$G^{\bullet} + G^{\bullet} = GG$	1×10^{9}	5×10^{8}	0.5
$IrCl_6^{2-} = P$	80.0	1.53×10^{-2}	1.91×10^{-4}

1.0 mM K_3IrCl_6 + 3.0 mM GSH + 25 mM phosphate buffer pH 7.0 + 1.0 M NaCl			
Electrochemical Reactions	**E**	**k_s**	**α**
$IrCl_6^{2-} + e^- = IrCl_6^{3-}$	0.7256	0.1	0.5
$G^{\bullet} + e- = G$	0.6791	1.00×10^{-5}	0.5
Chemical Reactions	**K**	**k_f**	**k_b**
$IrCl_6^{2-} + G = IrCl_6^{3-} + G^{\bullet}$	6.10±0.06	$(1.2\pm0.2) \times 10^{5}$	$(2.0\pm0.3) \times 10^{4}$
$IrCl_6^{2-} + G^{\bullet} = IrCl_6^{3-} + G''$	1.0×10^{11}	$(1.11\pm0.08) \times 10^{7}$	$(1.11\pm0.08) \times 10^{-4}$
$G^{\bullet} + G^{\bullet} = GG$	9×10^{8}	5×10^{8}	0.6
$IrCl_6^{2-} = P$	52.0	1.53×10^{-2}	2.94×10^{-4}

1.0 mM K_3IrCl_6 + 3.0 mM GSH + 35 mM phosphate buffer pH 7.0 + 1.0 M NaCl			
Electrochemical Reactions	**E**	**k_s**	**α**
$IrCl_6^{2-} + e^- = IrCl_6^{3-}$	0.7300	0.1	0.5
$G^{\bullet} + e- = G$	0.6791	1.00×10^{-5}	0.5
Chemical Reactions	**K**	**k_f**	**k_b**
$IrCl_6^{2-} + G = IrCl_6^{3-} + G^{\bullet}$	7.3±0.1	$(1.6\pm0.3) \times 10^{5}$	$(2.2\pm0.4) \times 10^{4}$
$IrCl_6^{2-} + G^{\bullet} = IrCl_6^{3-} + G''$	1.0×10^{11}	$(1.53\pm0.06) \times 10^{7}$	$(1.53\pm0.06) \times 10^{-4}$
$G^{\bullet} + G^{\bullet} = GG$	1×10^{9}	5×10^{8}	0.5
$IrCl_6^{2-} = P$	80.0	1.53×10^{-2}	1.91×10^{-4}

1.0 mM K_3IrCl_6 + 3.0 mM GSH + 50 mM phosphate buffer pH 7.0 + 1.0 M NaCl			
Electrochemical Reactions	**E**	**k_s**	**α**
$IrCl_6^{2-} + e^- = IrCl_6^{3-}$	0.7294	0.1	0.5
$G^{\bullet} + e- = G$	0.6791	1.00×10^{-5}	0.5
Chemical Reactions	**K**	**k_f**	**k_b**
$IrCl_6^{2-} + G = IrCl_6^{3-} + G^{\bullet}$	7.16±0.06	$(1.8\pm0.4) \times 10^{5}$	$(2.4\pm0.6) \times 10^{4}$
$IrCl_6^{2-} + G^{\bullet} = IrCl_6^{3-} + G''$	1.0×10^{11}	$(1.6\pm0.1) \times 10^{7}$	$(1.6\pm0.1) \times 10^{-4}$
$G^{\bullet} + G^{\bullet} = GG$	1×10^{9}	5×10^{8}	0.5
$IrCl_6^{2-} = P$	80.0	1.53×10^{-2}	1.91×10^{-4}

1.0 mM K_3IrCl_6 + 3.0 mM GSH + 100 mM phosphate buffer pH 7.0 + 1.0 M NaCl			
Electrochemical Reactions	**E**	**k_s**	**α**
$IrCl_6^{2-} + e^- = IrCl_6^{3-}$	0.7284	0.1	0.5
$G^{\bullet} + e- = G$	0.6791	1.00×10^{-5}	0.5
Chemical Reactions	**K**	**k_f**	**k_b**
$IrCl_6^{2-} + G = IrCl_6^{3-} + G^{\bullet}$	6.81±0.04	$(2.3±0.2) \times 10^{5}$	$(3.3±0.3) \times 10^{4}$
$IrCl_6^{2-} + G^{\bullet} = IrCl_6^{3-} + G''$	1.0×10^{11}	$(1.83±0.09) \times 10^{7}$	$(1.83±0.09) \times 10^{-4}$
$G^{\bullet} + G^{\bullet} = GG$	1×10^{9}	5×10^{8}	0.5
$IrCl_6^{2-} = P$	80.0	1.53×10^{-2}	1.91×10^{-4}

1.0 mM K_3IrCl_6 + 3.0 mM GSH + 200 mM phosphate buffer pH 7.0 + 1.0 M NaCl			
Electrochemical Reactions	**E**	**k_s**	**α**
$IrCl_6^{2-} + e^- = IrCl_6^{3-}$	0.7141	0.1	0.5
$G^{\bullet} + e- = G$	0.6791	1.00×10^{-5}	0.5
Chemical Reactions	**K**	**k_f**	**k_b**
$IrCl_6^{2-} + G = IrCl_6^{3-} + G^{\bullet}$	3.91±0.07	$(2.56±0.02) \times 10^{5}$	$(6.6±0.2) \times 10^{4}$
$IrCl_6^{2-} + G^{\bullet} = IrCl_6^{3-} + G''$	1.0×10^{11}	$(6.0±1.0) \times 10^{6}$	$(6.0±1.0) \times 10^{-5}$
$G^{\bullet} + G^{\bullet} = GG$	1×10^{9}	5×10^{8}	0.5
$IrCl_6^{2-} = P$	80.0	1.53×10^{-2}	1.91×10^{-4}

1.0 mM K_3IrCl_6 + 3.0 mM GSH + 5.0 mM malic buffer pH 5.1 + 1.0 M NaCl			
Electrochemical Reactions	**E**	**k_s**	**α**
$IrCl_6^{2-} + e^- = IrCl_6^{3-}$	0.7302	0.1	0.5
$G^{\bullet} + e- = G$	0.7904	1.0×10^{-6}	0.5
Chemical Reactions	**K**	**k_f**	**k_b**
$IrCl_6^{2-} + G = IrCl_6^{3-} + G^{\bullet}$	$(9.60±0.07) \times 10^{-2}$	$(1.6±0.2) \times 10^{3}$	$(1.7±0.2) \times 10^{4}$
$IrCl_6^{2-} + G^{\bullet} = IrCl_6^{3-} + G''$	1.0×10^{11}	$(4.4±0.5) \times 10^{5}$	$(4.4±0.5) \times 10^{-6}$
$G^{\bullet} + G^{\bullet} = GG$	1×10^{10}	5×10^{8}	0.05
$IrCl_6^{2-} = P$	NA	NA	NA

1.0 mM K_3IrCl_6 + 3.0 mM GSH + 5.0 mM succinic buffer pH 5.6 + 1.0 M NaCl			
Electrochemical Reactions	**E**	**k_s**	**α**
$IrCl_6^{2-} + e^- = IrCl_6^{3-}$	0.7261	0.1	0.5
$G^{\bullet} + e- = G$	0.7590	1.0×10^{-6}	0.5
Chemical Reactions	**K**	**k_f**	**k_b**
$IrCl_6^{2-} + G = IrCl_6^{3-} + G^{\bullet}$	$(2.78±0.06) \times 10^{-1}$	$(3.1±0.4) \times 10^{3}$	$(1.1±0.1) \times 10^{4}$
$IrCl_6^{2-} + G^{\bullet} = IrCl_6^{3-} + G''$	1.0×10^{11}	$(6.2±0.6) \times 10^{5}$	$(6.2±0.6) \times 10^{-6}$
$G^{\bullet} + G^{\bullet} = GG$	1×10^{10}	5×10^{8}	0.05
$IrCl_6^{2-} = P$	NA	NA	NA

1.0 mM K_3IrCl_6 + 3.0 mM GSH + 5.0 mM maleic buffer pH 6.2 + 1.0 M NaCl			
Electrochemical Reactions	**E**	**k_s**	**α**
$IrCl_6^{2-} + e^- = IrCl_6^{3-}$	0.7248	0.1	0.5
$G^{\bullet} + e- = G$	0.7260	1.0×10^{-6}	0.5
Chemical Reactions	**K**	**k_f**	**k_b**
$IrCl_6^{2-} + G = IrCl_6^{3-} + G^{\bullet}$	$(9.5\pm0.2) \times 10^{-1}$	$(5.4\pm0.8) \times 10^{3}$	$(5.6\pm0.9) \times 10^{3}$
$IrCl_6^{2-} + G^{\bullet} = IrCl_6^{3-} + G''$	1.0×10^{11}	$(3.130\pm0.002) \times 10^{4}$	$(3.130\pm0.002) \times 10^{-7}$
$G^{\bullet} + G^{\bullet} = GG$	1×10^{10}	5×10^{8}	0.05
$IrCl_6^{2-} = P$	NA	NA	NA

1.0 mM K_3IrCl_6 + 3.0 mM GSH + 5.0 mM citrate buffer pH 6.4 + 1.0 M NaCl			
Electrochemical Reactions	**E**	**k_s**	**α**
$IrCl_6^{2-} + e^- = IrCl_6^{3-}$	0.7272	0.1	0.5
$G^{\bullet} + e- = G$	0.7142	0.50×10^{-6}	0.5
Chemical Reactions	**K**	**k_f**	**k_b**
$IrCl_6^{2-} + G = IrCl_6^{3-} + G^{\bullet}$	1.66±0.03	$(4.3\pm0.4) \times 10^{3}$	$(2.6\pm0.3) \times 10^{3}$
$IrCl_6^{2-} + G^{\bullet} = IrCl_6^{3-} + G''$	1.0×10^{11}	$(1.4\pm0.1) \times 10^{6}$	$(1.4\pm0.1) \times 10^{-5}$
$G^{\bullet} + G^{\bullet} = GG$	1×10^{9}	5×10^{8}	0.5
$IrCl_6^{2-} = P$	NA	NA	NA

1.0 mM K_3IrCl_6 + 3.0 mM GSH + 5.0 mM phosphate buffer pH 7.2 + 1.0 M NaCl			
Electrochemical Reactions	**E**	**k_s**	**α**
$IrCl_6^{2-} + e^- = IrCl_6^{3-}$	0.7285	0.1	0.5
$G^{\bullet} + e- = G$	0.6675	1.0×10^{-6}	0.5
Chemical Reactions	**K**	**k_f**	**k_b**
$IrCl_6^{2-} + G = IrCl_6^{3-} + G^{\bullet}$	$(1.07\pm0.02) \times 10^{1}$	$(4.2\pm0.9) \times 10^{4}$	$(3.9\pm0.9) \times 10^{3}$
$IrCl_6^{2-} + G^{\bullet} = IrCl_6^{3-} + G''$	3.0×10^{13}	$(9\pm3) \times 10^{5}$	$(3\pm1) \times 10^{-8}$
$G^{\bullet} + G^{\bullet} = GG$	1×10^{9}	5×10^{8}	0.5
$IrCl_6^{2-} = P$	1.00×10^{2}	1.53×10^{-2}	1.53×10^{-3}

1.0 mM K_3IrCl_6 + 3.0 mM GSH + 35 mM malic buffer pH 5.1 + 1.0 M NaCl			
Electrochemical Reactions	**E**	**k_s**	**α**
$IrCl_6^{2-} + e^- = IrCl_6^{3-}$	0.7245	0.1	0.5
$G^{\bullet} + e- = G$	0.7904	1.0×10^{-6}	0.5
Chemical Reactions	**K**	**k_f**	**k_b**
$IrCl_6^{2-} + G = IrCl_6^{3-} + G^{\bullet}$	$(7.2\pm0.2) \times 10^{-2}$	$(5.0\pm0.2) \times 10^{3}$	$(6.5\pm0.1) \times 10^{4}$
$IrCl_6^{2-} + G^{\bullet} = IrCl_6^{3-} + G''$	1.0×10^{11}	$(4.2\pm0.5) \times 10^{6}$	$(4.2\pm0.5) \times 10^{-5}$
$G^{\bullet} + G^{\bullet} = GG$	1×10^{9}	5×10^{8}	0.5
$IrCl_6^{2-} = P$	NA	NA	NA

1.0 mM K_3IrCl_6 + 3.0 mM GSH + 35 mM succinic buffer pH 5.6 + 1.0 M NaCl			
Electrochemical Reactions	**E**	**k_s**	**α**
$IrCl_6^{2-} + e^- = IrCl_6^{3-}$	0.7319	0.1	0.5
$G^{\bullet} + e- = G$	0.7590	8.0×10^{-7}	0.5
Chemical Reactions	**K**	**k_f**	**k_b**
$IrCl_6^{2-} + G = IrCl_6^{3-} + G^{\bullet}$	$(3.46\pm0.05) \times 10^{-1}$	$(1.3\pm0.1) \times 10^{4}$	$(3.8\pm0.5) \times 10^{4}$
$IrCl_6^{2-} + G^{\bullet} = IrCl_6^{3-} + G''$	1.0×10^{11}	$(6.5\pm0.8) \times 10^{6}$	$(6.5\pm0.8) \times 10^{-5}$
$G^{\bullet} + G^{\bullet} = GG$	1×10^{10}	5×10^{8}	0.05
$IrCl_6^{2-} = P$	NA	NA	NA

1.0 mM K_3IrCl_6 + 3.0 mM GSH + 35 mM maleic buffer pH 6.2 + 1.0 M NaCl			
Electrochemical Reactions	**E**	**k_s**	**α**
$IrCl_6^{2-} + e^- = IrCl_6^{3-}$	0.7361	0.1	0.5
$G^{\bullet} + e- = G$	0.7259	1.0×10^{-6}	0.5
Chemical Reactions	**K**	**k_f**	**k_b**
$IrCl_6^{2-} + G = IrCl_6^{3-} + G^{\bullet}$	1.45±0.05	$(4.1\pm0.5) \times 10^{4}$	$(2.8\pm0.4) \times 10^{4}$
$IrCl_6^{2-} + G^{\bullet} = IrCl_6^{3-} + G''$	1.0×10^{11}	$(5.2\pm0.6) \times 10^{6}$	$(5.2\pm0.6) \times 10^{-5}$
$G^{\bullet} + G^{\bullet} = GG$	1×10^{9}	5×10^{8}	0.5
$IrCl_6^{2-} = P$	NA	NA	NA

1.0 mM K_3IrCl_6 + 3.0 mM GSH + 35 mM citrate buffer pH 6.4 + 1.0 M NaCl			
Electrochemical Reactions	**E**	**k_s**	**α**
$IrCl_6^{2-} + e^- = IrCl_6^{3-}$	0.7354	0.1	0.5
$G^{\bullet} + e- = G$	0.7142	8.0×10^{-7}	0.5
Chemical Reactions	**K**	**k_f**	**k_b**
$IrCl_6^{2-} + G = IrCl_6^{3-} + G^{\bullet}$	2.3±0.2	$(3.7\pm0.5) \times 10^{4}$	$(1.6\pm0.3) \times 10^{4}$
$IrCl_6^{2-} + G^{\bullet} = IrCl_6^{3-} + G''$	1.0×10^{11}	$(5.4\pm0.5) \times 10^{6}$	$(5.4\pm0.5) \times 10^{-5}$
$G^{\bullet} + G^{\bullet} = GG$	8×10^{8}	5×10^{8}	0.6
$IrCl_6^{2-} = P$	NA	NA	NA

1.0 mM K_3IrCl_6 + 3.0 mM GSH + 35 mM phosphate buffer pH 7.2 + 1.0 M NaCl			
Electrochemical Reactions	**E**	**k_s**	**α**
$IrCl_6^{2-} + e^- = IrCl_6^{3-}$	0.7226	0.1	0.5
$G^{\bullet} + e- = G$	0.6675	1.0×10^{-5}	0.5
Chemical Reactions	**K**	**k_f**	**k_b**
$IrCl_6^{2-} + G = IrCl_6^{3-} + G^{\bullet}$	8.5±0.1	$(1.5\pm0.2) \times 10^{5}$	$(1.7\pm0.2) \times 10^{4}$
$IrCl_6^{2-} + G^{\bullet} = IrCl_6^{3-} + G''$	1.0×10^{11}	$(9.7\pm1.0) \times 10^{6}$	$(9.7\pm1.0) \times 10^{-5}$
$G^{\bullet} + G^{\bullet} = GG$	1×10^{9}	5×10^{8}	0.5
$IrCl_6^{2-} = P$	1.00×10^{2}	1.53×10^{-2}	1.53×10^{-3}

IV. References

1. "Ionic Conductivity and Diffusion at Infinite Dilution". In *CRC Handbook of Chemistry and Physics (Internet Version 2011)*, 91st ed.; Haynes, W. M., Ed. CRC Press/ Taylor and Francis: Boca Raton, FL, 2011.
2. Anslyn, E. V.; Dougherty, D. A., *Modern Physical Organic Chemistry*. University Science Books: 2006; p 1095.

Appendix 3:

I. Diffusion coefficients of GSH, metal complexes and buffers components.

II. Slope and R^2 of the Marcus plots (RTF^{-1} lnk_{obs2} vs. $E_{1/2}$) for the electron transfer from glutathione radical ($G^{\bullet}$) to metal complexes.

III. Parameters used in digital simulations of cyclic voltammograms.

i. Simulations of CV experiments done to obtain Marcus plots.

ii. Simulations of CV experiments done to obtain Brönsted plots.

I. Diffusion coefficients of GSH, metal complexes and buffers components.

Species	Diffusion Coefficient/ 10^6 cm^2 s^{-1}
GSH	$(5.13 \pm 0.05)^a$
$IrCl_6^{2-}/IrCl_6^{3-}$	$(7.0 \pm 1.0)^b$
$Fe(phen)_3^{3+}/Fe(phen)_3^{2+}$	$(3.1 \pm 0.1)^b$
$Fe(bpy)_3^{3+}/Fe(bpy)_3^{2+}$	$(2.9 \pm 0.1)^b$
$Mo(CN)_8^{3-}/Mo(CN)_8^{4-}$	$(2.82 \pm 0.04)^b$
$H_2PO_4^-$	9.59^c
HPO_4^{2-}	7.59^c
$malate^{1-}$/ $malate^{2-}$	7.83^c
$succinate^{1-}$/ $succinate^{2-}$	7.83^c
$citrate^{2-}$ / $citrate^{3-}$	6.23^c
$maleate^{1-}$/ $maleate^{2-}$	8.24^c

Table 3.S1. Diffusion coefficient of all species represented in Scheme 3.1 used to simulate the cyclic voltammetry of GSH in the presence of different metal complexes and Brönsted bases B.

[a] Determined by Pulsed Gradient Echo (PGE) ^1H NMR as described in the experimental section; the diffusion coefficient of all the glutathione derived species (i.e. G$^{\bullet}$, GG and G" in Scheme 3.1) was assumed to be the same as that of glutathione (G in Scheme 3.1). [b] Estimated though digital simulation of cyclic voltammograms of aqueous solutions of 1.0 mM of metal complex alone. [c] Obtained from the CRC Handbook of Chemistry and Physics; the same diffusion coefficient was assumed for all deprotonation states of malic, succinic, citric and maleic species.

II. Marcus plots (RTF^{-1} lnk_{obs2} vs. $E_{1/2}$) for the electron transfer from glutathione radical ($G^{\bullet}$) to metal complexes.

Table 3.S2. Slope and R^2 of the Marcus plots (RTF^{-1} lnk_{obs2} vs. $E_{1/2}$) for the electron transfer from glutathione radical ($G^{\bullet}$) to metal complexes.

Buffer	**Buffer Concentration/ mM**	**Slope**	**R^2**
Phosphate pH 7.0	10	NA	NA
	50	0.31 ± 0.03	0.9857
	100	0.31 ± 0.05	0.9574
Histidine pH 6.5	5-50	NA	NA

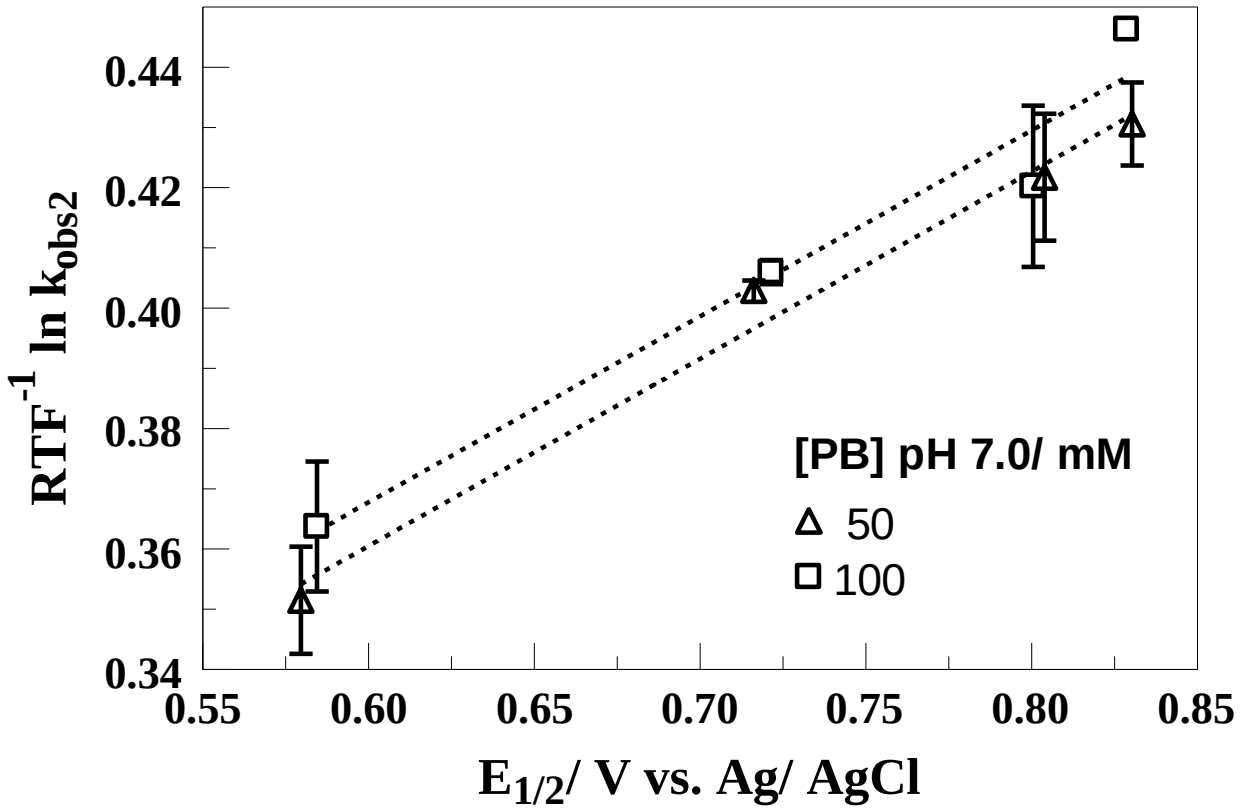

Figure 3.S1. $RTF^{-1} \ln k_{obs2}$ vs. $E_{1/2}$ of the mediator, at varying concentrations of phosphate buffer pH 7.0; k_{obs2} is the observed rate constant for the oxidation of $GS^{\cdot}$ by each mediator estimated through digital simulation of CVs run at various scan rates. The mediators, in increasing order of $E_{1/2}$, are $[Mo(CN)_8]^{4-/3-}$, $[IrCl_6]^{2-/3-}$, $[Fe(bpy)_3]^{3+/2+}$ and $[Fe(phen)_3]^{3+/2+}$.

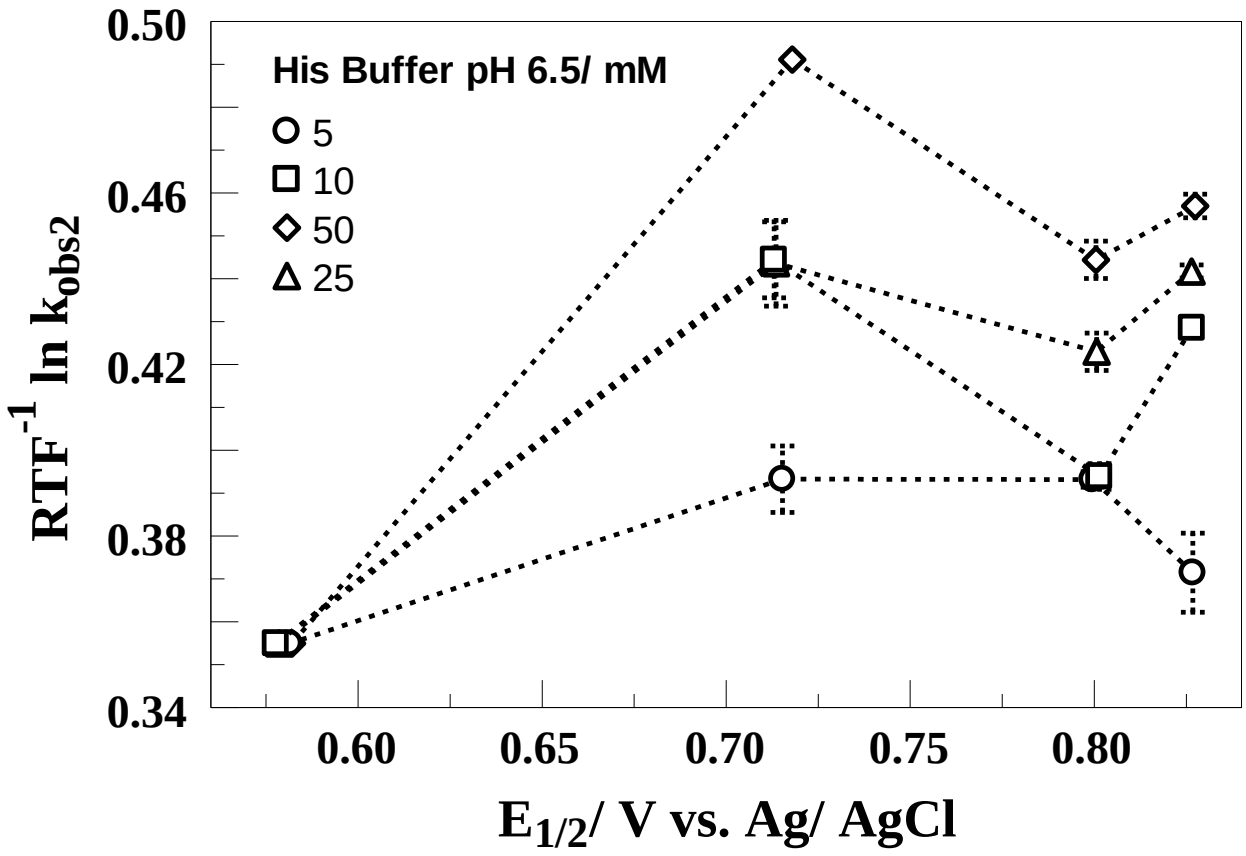

Figure 3.S2. $RTF^{-1} \ln k_{obs2}$ vs. $E_{1/2}$ of the mediator, at varying concentrations of histidine buffer pH 6.5; k_{obs2} is the observed rate constant for the oxidation of $GS^{\cdot}$ by each mediator estimated through digital simulation of CVs run at various scan rates. The mediators, in increasing order of $E_{1/2}$, are $[Mo(CN)_8]^{4-/3-}$, $[IrCl_6]^{2-/3-}$, $[Fe(bpy)_3]^{3+/2+}$ and $[Fe(phen)_3]^{3+/2+}$.

III. Parameters used in digital simulations of cyclic voltammograms.

The following are the electrochemical and kinetic parameters that best fitted the experimental voltammetry. Since CVs run at various scan rates were simulated, here we present the average of the estimated electrochemical and kinetic parameters. Also, the forward rate constant k_f for the reaction between glutathione G and the respective metal complex ($M^{(n+1)+}$) is the same k_{obs} introduced in Scheme 3.1.

i. Simulations of CV experiments done to obtain Marcus plots:

1.0 mM $Fe(phen)_3SO_4$ + 1.0 mM GSH + 10 mM phosphate buffer pH 7.0 + 1.0 M NaCl

Electrochemical Reactions	**E**	**k_s**	**α**
$Fe(phen)_3^{3+} + e^- = Fe(phen)_3^{2+}$	0.8279	0.1	0.5
$G^{\bullet} + e^- = G$	0.6791	2.5×10^{-4}	0.5
Chemical Reactions	**K**	**k_f**	**k_b**
$Fe(phen)_3^{3+} + G = Fe(phen)_3^{2+} + G^{\bullet}$	$(3.3\pm0.1) \times 10^{2}$	$(2.9\pm0.2) \times 10^{6}$	$(8.9\pm0.5) \times 10^{3}$
$Fe(phen)_3^{3+} + G^{\bullet} = Fe(phen)_3^{2+} + G''$	1.0×10^{11}	$(3.7\pm0.3) \times 10^{6}$	$(3.7\pm0.3) \times 10^{-5}$
$G^{\bullet} + G^{\bullet} = GG$	$(7.2\pm0.4) \times 10^{8}$	$(1.1\pm0.2) \times 10^{9}$	1.5±0.3
$Fe(phen)_3^{3+} = P$	1.00×10^{7}	2.21×10^{-2}	2.21×10^{-9}

1.0 mM $Fe(phen)_3SO_4$ + 1.0 mM GSH + 50 mM phosphate buffer pH 7.0 + 1.0 M NaCl

Electrochemical Reactions	**E**	**k_s**	**α**
$Fe(phen)_3^{3+} + e^- = Fe(phen)_3^{2+}$	0.8303	0.1	0.5
$G^{\bullet} + e^- = G$	0.6791	2.0×10^{-4}	0.5
Chemical Reactions	**K**	**k_f**	**k_b**
$Fe(phen)_3^{3+} + G = Fe(phen)_3^{2+} + G^{\bullet}$	$(3.7\pm0.1) \times 10^{2}$	$(9.8\pm0.6) \times 10^{6}$	$(2.69\pm0.08) \times 10^{4}$
$Fe(phen)_3^{3+} + G^{\bullet} = Fe(phen)_3^{2+} + G''$	1.0×10^{11}	$(1.9\pm0.5) \times 10^{7}$	$(1.9\pm0.5) \times 10^{-4}$
$G^{\bullet} + G^{\bullet} = GG$	$(8\pm1) \times 10^{8}$	1.0×10^{9}	(1.3±0.2)
$Fe(phen)_3^{3+} = P$	1.00×10^{7}	2.21×10^{-2}	2.21×10^{-9}

1.0 mM $Fe(phen)_3SO_4$ + 1.0 mM GSH + 100 mM phosphate buffer pH 7.0 + 1.0 M NaCl

Electrochemical Reactions	**E**	**k_s**	**α**
$Fe(phen)_3^{3+} + e^- = Fe(phen)_3^{2+}$	0.8287	0.1	0.5
$G^{\bullet} + e^- = G$	0.6791	2.0×10^{-4}	0.5
Chemical Reactions	**K**	**k_f**	**k_b**
$Fe(phen)_3^{3+} + G = Fe(phen)_3^{2+} + G^{\bullet}$	$(3.41\pm0.02) \times 10^{2}$	$(2.3\pm0.1) \times 10^{7}$	$(6.6\pm0.3) \times 10^{4}$
$Fe(phen)_3^{3+} + G^{\bullet} = Fe(phen)_3^{2+} + G''$	1.0×10^{11}	3.5×10^{7}	3.5×10^{-4}
$G^{\bullet} + G^{\bullet} = GG$	7.0×10^{8}	$(1.1\pm0.2) \times 10^{9}$	(1.6±0.4)
$Fe(phen)_3^{3+} = P$	1.00×10^{7}	2.21×10^{-2}	2.21×10^{-9}

1.0 mM $Fe(bpy)_3SO_4$ + 1.0 mM GSH + 10 mM phosphate buffer pH 7.0 + 1.0 M NaCl

Electrochemical Reactions	**E**	**k_s**	**α**
$Fe(bpy)_3^{3+} + e^- = Fe(bpy)_3^{2+}$	0.8066	0.1	0.5
$G^\bullet + e- = G$	0.6791	3.0×10^{-4}	0.5
Chemical Reactions	**K**	**k_f**	**k_b**
$Fe(bpy)_3^{3+} + G = Fe(bpy)_3^{2+} + G^\bullet$	$(1.40\pm0.09) \times 10^{2}$	$(6\pm1) \times 10^{5}$	$(4.3\pm0.7) \times 10^{3}$
$Fe(bpy)_3^{3+} + G^\bullet = Fe(bpy)_3^{2+} + G''$	1.0×10^{11}	1.0×10^{6}	1.0×10^{-5}
$G^\bullet + G^\bullet = GG$	$(9.6\pm0.9) \times 10^{8}$	1.0×10^{9}	1.0 ± 0.1
$Fe(bpy)_3^{3+} = P$	1.00×10^{7}	2.21×10^{-2}	2.21×10^{-9}

1.0 mM $Fe(bpy)_3SO_4$ + 1.0 mM GSH + 50 mM phosphate buffer pH 7.0 + 1.0 M NaCl

Electrochemical Reactions	**E**	**k_s**	**α**
$Fe(bpy)_3^{3+} + e^- = Fe(bpy)_3^{2+}$	0.8039	0.1	0.5
$G^\bullet + e- = G$	0.6791	2.0×10^{-4}	0.5
Chemical Reactions	**K**	**k_f**	**k_b**
$Fe(bpy)_3^{3+} + G = Fe(bpy)_3^{2+} + G^\bullet$	$(1.30\pm0.02) \times 10^{2}$	$(7\pm1) \times 10^{6}$	$(5.2\pm0.7) \times 10^{4}$
$Fe(bpy)_3^{3+} + G^\bullet = Fe(bpy)_3^{2+} + G''$	1.0×10^{11}	$(1.4\pm0.6) \times 10^{7}$	$(1.4\pm0.6) \times 10^{-4}$
$G^\bullet + G^\bullet = GG$	1.0×10^{9}	$(1.1\pm0.2) \times 10^{9}$	1.1 ± 0.2
$Fe(bpy)_3^{3+} = P$	1.00×10^{7}	2.21×10^{-2}	2.21×10^{-9}

1.0 mM $Fe(bpy)_3SO_4$ + 1.0 mM GSH + 100 mM phosphate buffer pH 7.0 + 1.0 M NaCl

Electrochemical Reactions	**E**	**k_s**	**α**
$Fe(bpy)_3^{3+} + e^- = Fe(bpy)_3^{2+}$	0.8004	0.1	0.5
$G^\bullet + e- = G$	0.6791	2.6×10^{-4}	0.5
Chemical Reactions	**K**	**k_f**	**k_b**
$Fe(bpy)_3^{3+} + G = Fe(bpy)_3^{2+} + G^\bullet$	$(1.12\pm0.02) \times 10^{2}$	$(1.02\pm0.05) \times 10^{7}$	$(9.1\pm0.4) \times 10^{4}$
$Fe(bpy)_3^{3+} + G^\bullet = Fe(bpy)_3^{2+} + G''$	1.0×10^{11}	$(1.3\pm0.7) \times 10^{7}$	$(1.3\pm0.7) \times 10^{-4}$
$G^\bullet + G^\bullet = GG$	$(6.8\pm0.5) \times 10^{8}$	$(1.1\pm0.2) \times 10^{9}$	1.7 ± 0.3
$Fe(bpy)_3^{3+} = P$	1.00×10^{7}	2.21×10^{-2}	2.21×10^{-9}

1.0 mM K_3IrCl_6 + 1.0 mM GSH + 10 mM phosphate buffer pH 7.0 + 1.0 M NaCl

Electrochemical Reactions	**E**	**k_s**	**α**
$IrCl_6^{2-} + e^- = IrCl_6^{3-}$	0.7170	0.1	0.5
$G^\bullet + e- = G$	0.6791	1.0×10^{-5}	0.5
Chemical Reactions	**K**	**k_f**	**k_b**
$IrCl_6^{2-} + G = IrCl_6^{3-} + G^\bullet$	4.4 ± 0.1	$(1.4\pm0.3) \times 10^{5}$	$(3.3\pm0.9) \times 10^{4}$
$IrCl_6^{2-} + G^\bullet = IrCl_6^{3-} + G''$	1.0×10^{11}	$(1.1\pm0.1) \times 10^{7}$	$(1.1\pm0.1) \times 10^{-4}$
$G^\bullet + G^\bullet = GG$	6.0×10^{8}	1.0×10^{9}	1.7
$IrCl_6^{2-} = P$	7.00×10^{1}	1.56×10^{-2}	2.23×10^{-4}

1.0 mM K_3IrCl_6 + 1.0 mM GSH + 50 mM phosphate buffer pH 7.0 + 1.0 M NaCl

Electrochemical Reactions	**E**	**k_s**	**α**
$IrCl_6^{2-} + e^- = IrCl_6^{3-}$	0.7162	0.1	0.5
$G^{\bullet} + e- = G$	0.6791	1.0×10^{-5}	0.5
Chemical Reactions	**K**	**k_f**	**k_b**
$IrCl_6^{2-} + G = IrCl_6^{3-} + G^{\bullet}$	4.2±0.1	$(2.7\pm0.3) \times 10^5$	$(6.4\pm0.9) \times 10^4$
$IrCl_6^{2-} + G^{\bullet} = IrCl_6^{3-} + G''$	1.0×10^{11}	$(6.5\pm0.4) \times 10^6$	$(6.5\pm0.4) \times 10^{-5}$
$G^{\bullet} + G^{\bullet} = GG$	6.0×10^8	1.0×10^9	1.7
$IrCl_6^{2-} = P$	7.00×10^1	1.56×10^{-2}	2.23×10^{-4}

1.0 mM K_3IrCl_6 + 1.0 mM GSH + 100 mM phosphate buffer pH 7.0 + 1.0 M NaCl

Electrochemical Reactions	**E**	**k_s**	**α**
$IrCl_6^{2-} + e^- = IrCl_6^{3-}$	0.7242	0.1	0.5
$G^{\bullet} + e- = G$	0.6791	1.0×10^{-5}	0.5
Chemical Reactions	**K**	**k_f**	**k_b**
$IrCl_6^{2-} + G = IrCl_6^{3-} + G^{\bullet}$	5.75±0.06	$(9.7\pm0.7) \times 10^5$	$(1.7\pm0.1) \times 10^5$
$IrCl_6^{2-} + G^{\bullet} = IrCl_6^{3-} + G''$	1.0×10^{11}	$(7.3\pm0.6) \times 10^6$	$(7.3\pm0.6) \times 10^{-5}$
$G^{\bullet} + G^{\bullet} = GG$	6.0×10^8	1.0×10^9	1.7
$IrCl_6^{2-} = P$	1.00×10^2	1.56×10^{-2}	1.56×10^{-4}

1.0 mM $K_4Mo(CN)_8$ + 1.0 mM GSH + 10 mM phosphate buffer pH 7.0 + 1.0 M NaCl

Electrochemical Reactions	**E**	**k_s**	**α**
$Mo(CN)_8^{4-} + e^- = Mo(CN)_8^{3-}$	0.5861	0.04	0.5
$G^{\bullet} + e- = G$	0.6791	1.0×10^{-5}	0.5
Chemical Reactions	**K**	**k_f**	**k_b**
$Mo(CN)_8^{4-} + G = Mo(CN)_8^{3-} + G^{\bullet}$	$(2.69\pm0.02) \times 10^{-2}$	$(8.2\pm0.2) \times 10^3$	$(3.04\pm0.09) \times 10^5$
$Mo(CN)_8^{4-} + G^{\bullet} = Mo(CN)_8^{3-} + G''$	1.0×10^5	1.0×10^6	1.0×10^1
$G^{\bullet} + G^{\bullet} = GG$	1.0×10^{10}	1.0×10^9	0.10
$Mo(CN)_8^{4-} = P$	1.00×10^4	1.00×10^{-2}	1.00×10^{-6}

1.0 mM $K_4Mo(CN)_8$ + 1.0 mM GSH + 50 mM phosphate buffer pH 7.0 + 1.0 M NaCl

Electrochemical Reactions	**E**	**k_s**	**α**
$Mo(CN)_8^{4-} + e^- = Mo(CN)_8^{3-}$	0.5796	0.04	0.5
$G^{\bullet} + e- = G$	0.6791	1.0×10^{-5}	0.5
Chemical Reactions	**K**	**k_f**	**k_b**
$Mo(CN)_8^{4-} + G = Mo(CN)_8^{3-} + G^{\bullet}$	$(2.08\pm0.06) \times 10^{-2}$	$(7.7\pm0.4) \times 10^3$	$(3.7\pm0.3) \times 10^5$
$Mo(CN)_8^{4-} + G^{\bullet} = Mo(CN)_8^{3-} + G''$	1×10^5	$(9\pm2) \times 10^5$	9±2
$G^{\bullet} + G^{\bullet} = GG$	1.0×10^{10}	1.0×10^9	0.10
$Mo(CN)_8^{4-} = P$	1.00×10^4	1.00×10^{-2}	1.00×10^{-6}

1.0 mM $K_4Mo(CN)_8$ + 1.0 mM GSH + 100 mM phosphate buffer pH 7.0 + 1.0 M NaCl

Electrochemical Reactions	**E**	**k_s**	**α**
$Mo(CN)_8^{4-} + e^- = Mo(CN)_8^{3-}$	0.5845	0.04	0.5
$G^{\bullet} + e^- = G$	0.6791	1.0×10^{-5}	0.5
Chemical Reactions	**K**	**k_f**	**k_b**
$Mo(CN)_8^{4-} + G = Mo(CN)_8^{3-} + G^{\bullet}$	$(2.52\pm0.02) \times 10^{-2}$	$(2.6\pm0.6) \times 10^{4}$	$(1.1\pm0.2) \times 10^{6}$
$Mo(CN)_8^{4-} + G^{\bullet} = Mo(CN)_8^{3-} + G''$	1.0×10^{5}	$(1.4\pm0.6) \times 10^{6}$	1.4 ± 0.6
$G^{\bullet} + G^{\bullet} = GG$	1.0×10^{10}	1.0×10^{9}	0.10
$Mo(CN)_8^{4-} = P$	1.00×10^{4}	1.00×10^{-2}	1.00×10^{-6}

1.0 mM $Fe(phen)_3SO_4$ + 1.0 mM GSH + 5.0 mM histidine buffer pH 6.5 + 1.0 M NaCl

Electrochemical Reactions	**E**	**k_s**	**α**
$Fe(phen)_3^{3+} + e^- = Fe(phen)_3^{2+}$	0.8268	0.1	0.5
$G^{\bullet} + e^- = G$	NA	NA	NA
Chemical Reactions	**K**	**k_f**	**k_b**
$Fe(phen)_3^{3+} + G = Fe(phen)_3^{2+} + G^{\bullet}$	$(1.01\pm0.01) \times 10^{2}$	$(1.4\pm0.3) \times 10^{5}$	$(1.4\pm0.3) \times 10^{3}$
$Fe(phen)_3^{3+} + G^{\bullet} = Fe(phen)_3^{2+} + G''$	1.0×10^{11}	$(1.9\pm0.6) \times 10^{6}$	$(1.9\pm0.6) \times 10^{-5}$
$G^{\bullet} + G^{\bullet} = GG$	3.0×10^{8}	1.0×10^{9}	3.3
$Fe(phen)_3^{3+} = P$	1.00×10^{7}	2.21×10^{-2}	2.21×10^{-9}

1.0 mM $Fe(phen)_3SO_4$ + 1.0 mM GSH + 10 mM histidine buffer pH 6.5 + 1.0 M NaCl

Electrochemical Reactions	**E**	**k_s**	**α**
$Fe(phen)_3^{3+} + e^- = Fe(phen)_3^{2+}$	0.8266	0.1	0.5
$G^{\bullet} + e^- = G$	NA	NA	NA
Chemical Reactions	**K**	**k_f**	**k_b**
$Fe(phen)_3^{3+} + G = Fe(phen)_3^{2+} + G^{\bullet}$	$(9.9\pm0.3) \times 10^{1}$	$(6.02\pm0.05) \times 10^{5}$	$(6.1\pm0.2) \times 10^{3}$
$Fe(phen)_3^{3+} + G^{\bullet} = Fe(phen)_3^{2+} + G''$	1.0×10^{11}	1.8×10^{7}	1.8×10^{-4}
$G^{\bullet} + G^{\bullet} = GG$	3.0×10^{8}	1.0×10^{9}	3.3
$Fe(phen)_3^{3+} = P$	1.00×10^{7}	2.21×10^{-2}	2.21×10^{-9}

1.0 mM $Fe(phen)_3SO_4$ + 1.0 mM GSH + 25 mM histidine buffer pH 6.5 + 1.0 M NaCl

Electrochemical Reactions	**E**	**k_s**	**α**
$Fe(phen)_3^{3+} + e^- = Fe(phen)_3^{2+}$	0.8265	0.1	0.5
$G^{\bullet} + e^- = G$	NA	NA	NA
Chemical Reactions	**K**	**k_f**	**k_b**
$Fe(phen)_3^{3+} + G = Fe(phen)_3^{2+} + G^{\bullet}$	$(9.9\pm0.2) \times 10^{1}$	$(1.9\pm0.1) \times 10^{6}$	$(1.9\pm0.2) \times 10^{4}$
$Fe(phen)_3^{3+} + G^{\bullet} = Fe(phen)_3^{2+} + G''$	1.0×10^{11}	$(2.9\pm0.2) \times 10^{7}$	$(2.9\pm0.2) \times 10^{-4}$
$G^{\bullet} + G^{\bullet} = GG$	$(3.4\pm0.7) \times 10^{8}$	1.0×10^{9}	3.0 ± 0.5
$Fe(phen)_3^{3+} = P$	1.00×10^{7}	2.21×10^{-2}	2.21×10^{-9}

1.0 mM $Fe(phen)_3SO_4$ + 1.0 mM GSH + 50 mM histidine buffer pH 6.5 + 1.0 M NaCl

Electrochemical Reactions	**E**	**k_s**	**α**
$Fe(phen)_3^{3+} + e^- = Fe(phen)_3^{2+}$	0.8275	0.1	0.5
$G^{\bullet} + e^- = G$	NA	NA	NA
Chemical Reactions	**K**	**k_f**	**k_b**
$Fe(phen)_3^{3+} + G = Fe(phen)_3^{2+} + G^{\bullet}$	1.0×10^2	$(3.0\pm0.2) \times 10^6$	$2.8\pm0.2 \times 10^4$
$Fe(phen)_3^{3+} + G^{\bullet} = Fe(phen)_3^{2+} + G''$	1.0×10^{11}	$(5.3\pm0.6) \times 10^7$	$(5.3\pm0.6) \times 10^{-4}$
$G^{\bullet} + G^{\bullet} = GG$	3.0×10^8	1.0×10^9	3.3
$Fe(phen)_3^{3+} = P$	1.00×10^7	2.21×10^{-2}	2.21×10^{-9}

1.0 mM $Fe(bpy)_3SO_4$ + 1.0 mM GSH + 5.0 mM histidine buffer pH 6.5 + 1.0 M NaCl

Electrochemical Reactions	**E**	**k_s**	**α**
$Fe(bpy)_3^{3+} + e^- = Fe(bpy)_3^{2+}$	0.7996	0.1	0.5
$G^{\bullet} + e^- = G$	NA	NA	NA
Chemical Reactions	**K**	**k_f**	**k_b**
$Fe(bpy)_3^{3+} + G = Fe(bpy)_3^{2+} + G^{\bullet}$	3.7×10^1	$(1.3\pm0.2) \times 10^5$	$(3.5\pm0.5) \times 10^3$
$Fe(bpy)_3^{3+} + G^{\bullet} = Fe(bpy)_3^{2+} + G''$	1.0×10^{11}	$(4.4\pm0.3) \times 10^6$	$(4.4\pm0.3) \times 10^{-5}$
$G^{\bullet} + G^{\bullet} = GG$	3.0×10^8	1.0×10^9	3.3
$Fe(bpy)_3^{3+} = P$	1.00×10^7	2.21×10^{-2}	2.21×10^{-9}

1.0 mM $Fe(bpy)_3SO_4$ + 1.0 mM GSH + 10 mM histidine buffer pH 6.5 + 1.0 M NaCl

Electrochemical Reactions	**E**	**k_s**	**α**
$Fe(bpy)_3^{3+} + e^- = Fe(bpy)_3^{2+}$	0.8015	0.1	0.5
$G^{\bullet} + e^- = G$	NA	NA	NA
Chemical Reactions	**K**	**k_f**	**k_b**
$Fe(bpy)_3^{3+} + G = Fe(bpy)_3^{2+} + G^{\bullet}$	$(3.74\pm0.04) \times 10^1$	$(4.6\pm0.2) \times 10^5$	$(1.24\pm0.06) \times 10^4$
$Fe(bpy)_3^{3+} + G^{\bullet} = Fe(bpy)_3^{2+} + G''$	1.0×10^{11}	$(4.5\pm0.5) \times 10^6$	$(4.5\pm0.5) \times 10^{-5}$
$G^{\bullet} + G^{\bullet} = GG$	7.0×10^8	1.0×10^9	1.4
$Fe(bpy)_3^{3+} = P$	1.00×10^7	2.21×10^{-2}	2.21×10^{-9}

1.0 mM $Fe(bpy)_3SO_4$ + 1.0 mM GSH + 25 mM histidine buffer pH 6.5 + 1.0 M NaCl

Electrochemical Reactions	**E**	**k_s**	**α**
$Fe(bpy)_3^{3+} + e^- = Fe(bpy)_3^{2+}$	0.8007	0.1	0.5
$G^{\bullet} + e^- = G$	NA	NA	NA
Chemical Reactions	**K**	**k_f**	**k_b**
$Fe(bpy)_3^{3+} + G = Fe(bpy)_3^{2+} + G^{\bullet}$	$(3.60\pm0.01) \times 10^1$	$(1.41\pm0.08) \times 10^6$	$(3.9\pm0.3) \times 10^4$
$Fe(bpy)_3^{3+} + G^{\bullet} = Fe(bpy)_3^{2+} + G''$	1.0×10^{11}	$(1.4\pm0.2) \times 10^7$	$(1.4\pm0.2) \times 10^{-4}$
$G^{\bullet} + G^{\bullet} = GG$	$(7.5\pm1.0) \times 10^8$	1.0×10^9	(1.3 ± 0.2)
$Fe(bpy)_3^{3+} = P$	1.00×10^7	2.21×10^{-2}	2.21×10^{-9}

1.0 mM $Fe(bpy)_3SO_4$ + 1.0 mM GSH + 50 mM histidine buffer pH 6.5 + 1.0 M NaCl

Electrochemical Reactions	**E**	**k_s**	**α**
$Fe(bpy)_3^{3+} + e^- = Fe(bpy)_3^{2+}$	0.8005	0.1	0.5
$G^{\bullet} + e- = G$	NA	NA	NA
Chemical Reactions	**K**	**k_f**	**k_b**
$Fe(bpy)_3^{3+} + G = Fe(bpy)_3^{2+} + G^{\bullet}$	$(3.6\pm0.1) \times 10^1$	$(1.9\pm0.2) \times 10^6$	$(5.1\pm0.3) \times 10^4$
$Fe(bpy)_3^{3+} + G^{\bullet} = Fe(bpy)_3^{2+} + G''$	1.0×10^{11}	$(3.2\pm0.5) \times 10^7$	$(3.2\pm0.5) \times 10^{-4}$
$G^{\bullet} + G^{\bullet} = GG$	3.0×10^8	1.0×10^9	3.3
$Fe(bpy)_3^{3+} = P$	1.00×10^7	2.21×10^{-2}	2.21×10^{-9}

1.0 mM K_3IrCl_6 + 1.0 mM GSH + 5.0 mM histidine buffer pH 6.5 + 1.0 M NaCl

Electrochemical Reactions	**E**	**k_s**	**α**
$IrCl_6^{2-} + e^- = IrCl_6^{3-}$	0.715	0.1	0.5
$G^{\bullet} + e- = G$	NA	NA	NA
Chemical Reactions	**K**	**k_f**	**k_b**
$IrCl_6^{2-} + G = IrCl_6^{3-} + G^{\bullet}$	1.31±0.06	$(4.0\pm0.6) \times 10^4$	$(3.0\pm0.6) \times 10^4$
$IrCl_6^{2-} + G^{\bullet} = IrCl_6^{3-} + G''$	1.0×10^{11}	$(4\pm1) \times 10^6$	$(4\pm1) \times 10^{-5}$
$G^{\bullet} + G^{\bullet} = GG$	7.0×10^8	1.0×10^9	1.4
$IrCl_6^{2-} = P$	NA	NA	NA

1.0 mM K_3IrCl_6 + 1.0 mM GSH + 10 mM histidine buffer pH 6.5 + 1.0 M NaCl

Electrochemical Reactions	**E**	**k_s**	**α**
$IrCl_6^{2-} + e^- = IrCl_6^{3-}$	0.713	0.1	0.5
$G^{\bullet} + e- = G$	NA	NA	NA
Chemical Reactions	**K**	**k_f**	**k_b**
$IrCl_6^{2-} + G = IrCl_6^{3-} + G^{\bullet}$	1.2±0.1	$(5\pm1) \times 10^4$	$(4\pm1) \times 10^4$
$IrCl_6^{2-} + G^{\bullet} = IrCl_6^{3-} + G''$	1.0×10^{11}	$(3\pm1) \times 10^7$	$(3\pm1) \times 10^{-4}$
$G^{\bullet} + G^{\bullet} = GG$	7.0×10^8	1.0×10^9	1.4
$IrCl_6^{2-} = P$	1.0×10^7	5.8×10^{-2}	5.8×10^{-9}

1.0 mM K_3IrCl_6 + 1.0 mM GSH + 25 mM histidine buffer pH 6.5 + 1.0 M NaCl

Electrochemical Reactions	**E**	**k_s**	**α**
$IrCl_6^{2-} + e^- = IrCl_6^{3-}$	0.714	0.1	0.5
$G^{\bullet} + e- = G$	NA	NA	NA
Chemical Reactions	**K**	**k_f**	**k_b**
$IrCl_6^{2-} + G = IrCl_6^{3-} + G^{\bullet}$	1.19±0.03	$(4.1\pm0.2) \times 10^4$	$(3.5\pm0.2) \times 10^4$
$IrCl_6^{2-} + G^{\bullet} = IrCl_6^{3-} + G''$	1.0×10^{11}	$(3\pm1) \times 10^7$	$(3\pm1) \times 10^{-4}$
$G^{\bullet} + G^{\bullet} = GG$	7.0×10^8	1.0×10^9	1.4
$IrCl_6^{2-} = P$	1.0×10^7	5.8×10^{-2}	5.8×10^{-9}

1.0 mM K_3IrCl_6 + 1.0 mM GSH + 50 mM histidine buffer pH 6.5 + 1.0 M NaCl

Electrochemical Reactions	**E**	**k_s**	**α**
$IrCl_6^{2-} + e^- = IrCl_6^{3-}$	0.7180	0.1	0.5
$G^{\bullet} + e- = G$	NA	NA	NA
Chemical Reactions	**K**	**k_f**	**k_b**
$IrCl_6^{2-} + G = IrCl_6^{3-} + G^{\bullet}$	1.45±0.01	(6.00±0.01) x 10^4	(4.15±0.02) x 10^4
$IrCl_6^{2-} + G^{\bullet} = IrCl_6^{3-} + G''$	1.0 x 10^{11}	2.0 x 10^8	2.0 x 10^{-3}
$G^{\bullet} + G^{\bullet} = GG$	7.0 x 10^8	1.0 x 10^9	1.4
$IrCl_6^{2-} = P$	1.0 x 10^7	5.8 x 10^{-2}	5.8 x 10^{-9}

1.0 mM $K_4Mo(CN)_8$ + 1.0 mM GSH + 5.0 mM histidine buffer pH 6.5 + 1.0 M NaCl

Electrochemical Reactions	**E**	**k_s**	**α**
$Mo(CN)_8^{4-} + e^- = Mo(CN)_8^{3-}$	0.581	0.05	0.5
$G^{\bullet} + e- = G$	NA	NA	NA
Chemical Reactions	**K**	**k_f**	**k_b**
$Mo(CN)_8^{4-} + G = Mo(CN)_8^{3-} + G^{\bullet}$	(7.2±0.5) x 10^{-3}	(2±1) x 10^3	(3±1) x 10^5
$Mo(CN)_8^{4-} + G^{\bullet} = Mo(CN)_8^{3-} + G''$	1.0 x 10^5	1.0 x 10^6	1.0 x 10^1
$G^{\bullet} + G^{\bullet} = GG$	1.0 x 10^{10}	1.0 x 10^9	0.10
$Mo(CN)_8^{4-} = P$	1.00 x 10^4	1.00 x 10^{-2}	1.00 x 10^{-6}

1.0 mM $K_4Mo(CN)_8$ + 1.0 mM GSH + 10 mM histidine buffer pH 6.5 + 1.0 M NaCl

Electrochemical Reactions	**E**	**k_s**	**α**
$Mo(CN)_8^{4-} + e^- = Mo(CN)_8^{3-}$	0.578	0.05	0.5
$G^{\bullet} + e- = G$	NA	NA	NA
Chemical Reactions	**K**	**k_f**	**k_b**
$Mo(CN)_8^{4-} + G = Mo(CN)_8^{3-} + G^{\bullet}$	(6.5±0.1) x 10^{-3}	(3.3±0.9) x 10^3	(5±1) x 10^5
$Mo(CN)_8^{4-} + G^{\bullet} = Mo(CN)_8^{3-} + G''$	1.0 x 10^5	1.0 x 10^6	1.0 x 10^1
$G^{\bullet} + G^{\bullet} = GG$	1.0 x 10^{10}	1.0 x 10^9	0.10
$Mo(CN)_8^{4-} = P$	1.00 x 10^4	1.00 x 10^{-2}	1.00 x 10^{-6}

1.0 mM $K_4Mo(CN)_8$ + 1.0 mM GSH + 25 mM histidine buffer pH 6.5 + 1.0 M NaCl

Electrochemical Reactions	**E**	**k_s**	**α**
$Mo(CN)_8^{4-} + e^- = Mo(CN)_8^{3-}$	0.5785	0.05	0.5
$G^{\bullet} + e- = G$	NA	NA	NA
Chemical Reactions	**K**	**k_f**	**k_b**
$Mo(CN)_8^{4-} + G = Mo(CN)_8^{3-} + G^{\bullet}$	(6.4±0.2) x 10^{-3}	(4.6±0.8) x 10^3	(7±1) x10^5
$Mo(CN)_8^{4-} + G^{\bullet} = Mo(CN)_8^{3-} + G''$	1.0 x 10^5	1.0 x 10^6	1.0 x 10^1
$G^{\bullet} + G^{\bullet} = GG$	1.0 x 10^{10}	1.0 x 10^9	0.10
$Mo(CN)_8^{4-} = P$	1.00 x 10^4	1.00 x 10^{-2}	1.00 x 10^{-6}

1.0 mM $K_4Mo(CN)_8$ + 1.0 mM GSH + 50 mM histidine buffer pH 6.5 + 1.0 M NaCl

Electrochemical Reactions	**E**	**k_s**	**α**
$Mo(CN)_8^{4-} + e^- = Mo(CN)_8^{3-}$	0.5821	0.05	0.5
$G^{\bullet} + e^- = G$	NA	NA	NA
Chemical Reactions	**K**	**k_f**	**k_b**
$Mo(CN)_8^{4-} + G = Mo(CN)_8^{3-} + G^{\bullet}$	$(7.38\pm0.03) \times 10^{-3}$	$(4.6\pm0.2) \times 10^{3}$	$(6.3\pm0.2) \times 10^{5}$
$Mo(CN)_8^{4-} + G^{\bullet} = Mo(CN)_8^{3-} + G''$	1.0×10^{5}	1.0×10^{6}	1.0×10^{1}
$G^{\bullet} + G^{\bullet} = GG$	1.0×10^{10}	1.0×10^{9}	0.10
$Mo(CN)_8^{4-} = P$	1.00×10^{4}	1.00×10^{-2}	1.00×10^{-6}

ii. Simulations of CV experiments done to obtain Brönsted plots:

1.0 mM $K_4Mo(CN)_8$ + 1.0 mM GSH + 50 mM malic buffer pH 5.1 + 1.0 M NaCl

Electrochemical Reactions	**E**	**k_s**	**α**
$Mo(CN)_8^{4-} + e^- = Mo(CN)_8^{3-}$	0.5831	0.1	0.5
$G^{\bullet} + e^- = G$	NA	NA	NA
Chemical Reactions	**K**	**k_f**	**k_b**
$Mo(CN)_8^{4-} + G = Mo(CN)_8^{3-} + G^{\bullet}$	$(3.13\pm0.01) \times 10^{-3}$	$(1.1\pm0.1) \times 10^{3}$	$(3.5\pm0.5) \times 10^{5}$
$Mo(CN)_8^{4-} + G^{\bullet} = Mo(CN)_8^{3-} + G''$	NA	NA	NA
$G^{\bullet} + G^{\bullet} = GG$	1.0×10^{10}	1.0×10^{9}	0.10
$Mo(CN)_8^{4-} = P$	1.00×10^{4}	1.00×10^{-2}	1.00×10^{-6}

1.0 mM $K_4Mo(CN)_8$ + 1.0 mM GSH + 50 mM succinic buffer pH 5.6 + 1.0 M NaCl

Electrochemical Reactions	**E**	**k_s**	**α**
$Mo(CN)_8^{4-} + e^- = Mo(CN)_8^{3-}$	0.5880	0.05	0.5
$G^{\bullet} + e^- = G$	NA	NA	NA
Chemical Reactions	**K**	**k_f**	**k_b**
$Mo(CN)_8^{4-} + G = Mo(CN)_8^{3-} + G^{\bullet}$	$(1.287\pm0.01) \times 10^{-3}$	$(1.6\pm0.2) \times 10^{3}$	$(1.2\pm0.2) \times 10^{6}$
$Mo(CN)_8^{4-} + G^{\bullet} = Mo(CN)_8^{3-} + G''$	NA	NA	NA
$G^{\bullet} + G^{\bullet} = GG$	1.0×10^{10}	1.0×10^{9}	0.10
$Mo(CN)_8^{4-} = P$	1.00×10^{4}	1.00×10^{-2}	1.00×10^{-6}

1.0 mM $K_4Mo(CN)_8$ + 1.0 mM GSH + 50 mM maleic buffer pH 6.2 + 1.0 M NaCl

Electrochemical Reactions	**E**	**k_s**	**α**
$Mo(CN)_8^{4-} + e^- = Mo(CN)_8^{3-}$	0.5837	0.05	0.5
$G^{\bullet} + e^- = G$	NA	NA	NA
Chemical Reactions	**K**	**k_f**	**k_b**
$Mo(CN)_8^{4-} + G = Mo(CN)_8^{3-} + G^{\bullet}$	$(4.03\pm0.07) \times 10^{-3}$	$(3.2\pm0.5) \times 10^{3}$	$(8\pm1) \times 10^{5}$
$Mo(CN)_8^{4-} + G^{\bullet} = Mo(CN)_8^{3-} + G''$	1×10^{5}	$(8\pm2) \times 10^{5}$	8±2
$G^{\bullet} + G^{\bullet} = GG$	1.0×10^{10}	1.0×10^{9}	0.10
$Mo(CN)_8^{4-} = P$	1.00×10^{4}	1.00×10^{-2}	1.00×10^{-6}

1.0 mM $K_4Mo(CN)_8$ + 1.0 mM GSH + 50 mM histidine buffer pH 6.5 + 1.0 M NaCl

Electrochemical Reactions	**E**	**k_s**	**α**
$Mo(CN)_8^{4-} + e^- = Mo(CN)_8^{3-}$	0.5821	0.05	0.5
$G^{\bullet} + e^- = G$	NA	NA	NA
Chemical Reactions	**K**	**k_f**	**k_b**
$Mo(CN)_8^{4-} + G = Mo(CN)_8^{3-} + G^{\bullet}$	$(7.38\pm0.03) \times 10^{-3}$	$(4.6\pm0.2) \times 10^{3}$	$(6.3\pm0.2) \times 10^{5}$
$Mo(CN)_8^{4-} + G^{\bullet} = Mo(CN)_8^{3-} + G''$	1.0×10^{5}	1.0×10^{6}	1.0×10^{1}
$G^{\bullet} + G^{\bullet} = GG$	1.0×10^{10}	1.0×10^{9}	0.10
$Mo(CN)_8^{4-} = P$	1.00×10^{4}	1.00×10^{-2}	1.00×10^{-6}

1.0 mM $K_4Mo(CN)_8$ + 1.0 mM GSH + 50 mM phosphate buffer pH 7.0 + 1.0 M NaCl

Electrochemical Reactions	**E**	**k_s**	**α**
$Mo(CN)_8^{4-} + e^- = Mo(CN)_8^{3-}$	0.5796	0.04	0.5
$G^{\bullet} + e^- = G$	0.6791	1.0×10^{-5}	0.5
Chemical Reactions	**K**	**k_f**	**k_b**
$Mo(CN)_8^{4-} + G = Mo(CN)_8^{3-} + G^{\bullet}$	$(2.08\pm0.06) \times 10^{-2}$	$(7.7\pm0.4) \times 10^{3}$	$(3.7\pm0.3) \times 10^{5}$
$Mo(CN)_8^{4-} + G^{\bullet} = Mo(CN)_8^{3-} + G''$	1×10^{5}	$(9\pm2) \times 10^{5}$	9 ± 2
$G^{\bullet} + G^{\bullet} = GG$	1.0×10^{10}	1.0×10^{9}	0.10
$Mo(CN)_8^{4-} = P$	1.00×10^{4}	1.00×10^{-2}	1.00×10^{-6}

1.0 mM $Fe(phen)_3SO_4$ + 1.0 mM GSH + 50 mM malic buffer pH 5.1 + 1.0 M NaCl

Electrochemical Reactions	**E**	**k_s**	**α**
$Fe(phen)_3^{3+} + e^- = Fe(phen)_3^{2+}$	0.8259	0.1	0.5
$G^{\bullet} + e^- = G$	NA	NA	NA
Chemical Reactions	**K**	**k_f**	**k_b**
$Fe(phen)_3^{3+} + G = Fe(phen)_3^{2+} + G^{\bullet}$	3.98 ± 0.02	$(1.10\pm0.01) \times 10^{5}$	$(2.76\pm0.01) \times 10^{4}$
$Fe(phen)_3^{3+} + G^{\bullet} = Fe(phen)_3^{2+} + G''$	1.00×10^{11}	$(4.25\pm0.07) \times 10^{7}$	$(4.25\pm0.07) \times 10^{-4}$
$G^{\bullet} + G^{\bullet} = GG$	7.0×10^{8}	1.0×10^{9}	1.4
$Fe(phen)_3^{3+} = P$	1.00×10^{7}	2.21×10^{-2}	2.21×10^{-9}

1.0 mM $Fe(phen)_3SO_4$ + 1.0 mM GSH + 50 mM succinic buffer pH 5.6 + 1.0 M NaCl

Electrochemical Reactions	**E**	**k_s**	**α**
$Fe(phen)_3^{3+} + e^- = Fe(phen)_3^{2+}$	0.8251	0.1	0.5
$G^{\bullet} + e^- = G$	NA	NA	NA
Chemical Reactions	**K**	**k_f**	**k_b**
$Fe(phen)_3^{3+} + G = Fe(phen)_3^{2+} + G^{\bullet}$	$(1.31\pm0.01) \times 10^{1}$	$(4.6\pm0.1) \times 10^{5}$	$(3.52\pm0.08) \times 10^{4}$
$Fe(phen)_3^{3+} + G^{\bullet} = Fe(phen)_3^{2+} + G''$	1.0×10^{11}	$(1.2\pm0.2) \times 10^{7}$	$(1.2\pm0.2) \times 10^{-4}$
$G^{\bullet} + G^{\bullet} = GG$	7.0×10^{8}	1.0×10^{9}	1.4
$Fe(phen)_3^{3+} = P$	1.00×10^{7}	2.21×10^{-2}	2.21×10^{-9}

1.0 mM $Fe(phen)_3SO_4$ + 1.0 mM GSH + 50 mM maleic buffer pH 6.2 + 1.0 M NaCl

Electrochemical Reactions	**E**	**k_s**	**α**
$Fe(phen)_3^{3+} + e^- = Fe(phen)_3^{2+}$	0.8268	0.1	0.5
$G^{\bullet} + e^- = G$	NA	NA	NA
Chemical Reactions	**K**	**k_f**	**k_b**
$Fe(phen)_3^{3+} + G = Fe(phen)_3^{2+} + G^{\bullet}$	$(5.1\pm0.3) \times 10^1$	$(1.3\pm0.1) \times 10^6$	$(2.50\pm0.06) \times 10^4$
$Fe(phen)_3^{3+} + G^{\bullet} = Fe(phen)_3^{2+} + G''$	1.0×10^{11}	$(4\pm1) \times 10^7$	$(4\pm1) \times 10^{-4}$
$G^{\bullet} + G^{\bullet} = GG$	7.0×10^8	1.0×10^9	1.4
$Fe(phen)_3^{3+} = P$	1.00×10^7	2.21×10^{-2}	2.21×10^{-9}

1.0 mM $Fe(phen)_3SO_4$ + 1.0 mM GSH + 50 mM histidine buffer pH 6.5 + 1.0 M NaCl

Electrochemical Reactions	**E**	**k_s**	**α**
$Fe(phen)_3^{3+} + e^- = Fe(phen)_3^{2+}$	0.8275	0.1	0.5
$G^{\bullet} + e^- = G$	NA	NA	NA
Chemical Reactions	**K**	**k_f**	**k_b**
$Fe(phen)_3^{3+} + G = Fe(phen)_3^{2+} + G^{\bullet}$	1.0×10^2	$(3.0\pm0.2) \times 10^6$	$2.8\pm0.2 \times 10^4$
$Fe(phen)_3^{3+} + G^{\bullet} = Fe(phen)_3^{2+} + G''$	1.0×10^{11}	$(5.3\pm0.6) \times 10^7$	$(5.3\pm0.6) \times 10^{-4}$
$G^{\bullet} + G^{\bullet} = GG$	3.0×10^8	1.0×10^9	3.3
$Fe(phen)_3^{3+} = P$	1.00×10^7	2.21×10^{-2}	2.21×10^{-9}

1.0 mM $Fe(phen)_3SO_4$ + 1.0 mM GSH + 50 mM phosphate buffer pH 7.0 + 1.0 M NaCl

Electrochemical Reactions	**E**	**k_s**	**α**
$Fe(phen)_3^{3+} + e^- = Fe(phen)_3^{2+}$	0.8303	0.1	0.5
$G^{\bullet} + e^- = G$	0.6791	2.0×10^{-4}	0.5
Chemical Reactions	**K**	**k_f**	**k_b**
$Fe(phen)_3^{3+} + G = Fe(phen)_3^{2+} + G^{\bullet}$	$(3.7\pm0.1) \times 10^2$	$(9.8\pm0.6) \times 10^6$	$(2.69\pm0.08) \times 10^4$
$Fe(phen)_3^{3+} + G^{\bullet} = Fe(phen)_3^{2+} + G''$	1.0×10^{11}	$(1.9\pm0.5) \times 10^7$	$(1.9\pm0.5) \times 10^{-4}$
$G^{\bullet} + G^{\bullet} = GG$	$(8\pm1) \times 10^8$	1.0×10^9	(1.3 ± 0.2)
$Fe(phen)_3^{3+} = P$	1.00×10^7	2.21×10^{-2}	2.21×10^{-9}

Appendix 4:

I. Information regarding parameters in PGE-^{1}H-NMR experiments, an example of the data obtained and control experiments

II. Diffusion coefficients for the phthalates as function of their concentration by ^{1}H-NMR at 25 °C and plot for the determination of the stoichiometry of 1,4-H_2Q with HP^-.

III. Voltammetry and simulations not displayed in the text,

- **a. Voltammetric measurements used to determine mechanism of oxidation of 1,4-H_2Q in the presence of HP^- and P^{2-}**
- **b. Comparison of 5.0 mM 1,4-H_2Q + 20 mM P^{2-} Voltammetry to that of 5.0 mM 1,4-Q alone in MeCN**
- **c. Voltammetry and simulations of 1,4-H_2Q with HP^- and P^{2-} with fitting parameters.**

IV. References

I. Information regarding parameters in PGE-^{1}H-NMR experiments, an example of the data obtained and control experiments

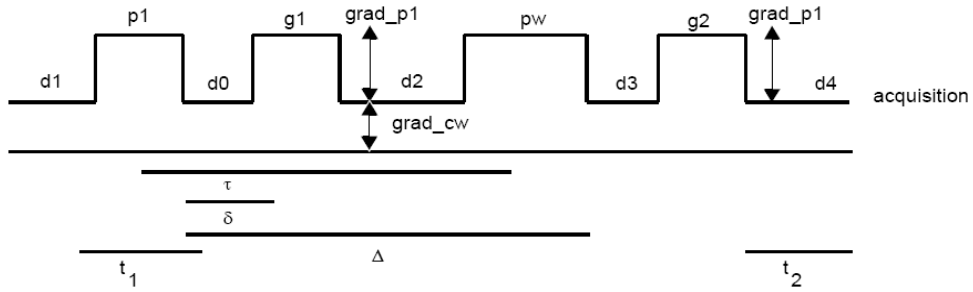

Figure 4.S1 Pulse sequence of the PGE-^{1}H-NMR technique on a Varian NMR.[1]

Values and important information regarding the PGE-NMR sequence were (using the notation from the pulse sequence, Figure 4.S1): δ = 1 ms, while Δ = varied depending on sample and pw (180°) value (generally ~73 ms), applied gradient range (*grad_p1* and *grad_p2*) was 20-30 G cm^{-1} in 10 steps. The delay times were d1 = 2.000 s, d0 = d3 = 0.001 s, and d2 = d4 = 0.020 s. The parameter *grad_cw* was kept at 0 G cm^{-1}, as this parameter is typically used in DOSY experiments.[1] Also, the parameter *tramp* (on Varian PGE-NMR) programs remained at 0 s throughout the collection of the PGE arrays. Furthermore, these experiments were not conducted in the *stimulated* mode (also known as, Pulsed Gradient Stimulated Echo (PGSE)), and therefore "*n*" was the input for this parameter, indicating *no*.[1] Figure 4.S2 gives an example of the graphical analysis and PGE spectra obtained upon performing a PGE-^{1}H-NMR experiment on the HDO peak in 100 % D_2O.

To determine whether ion pairing is responsible for the noted changes in diffusion NMR, experiments with 1,4-QH_2 with 10.0 mM and 200 mM $TBAPF_6$ (same as supporting electrolyte concentration in CV experiments) were performed. The diffusion coefficient (D) of 1,4-QH_2 in 10.0 mM $TBAPF_6$ was 2.83x10^{-5} cm^2 s^{-1} (+1.4% change), while the D of 1,4-QH_2 in 200 mM

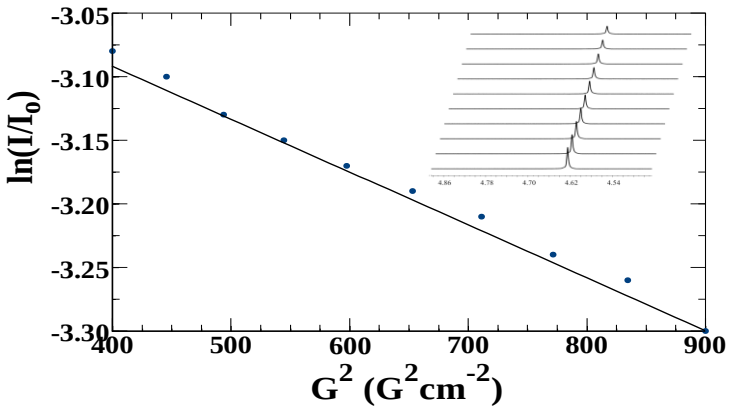

Figure 4.S2 Example of graphical analysis of the PGE-^{1}H-NMR spectra of the HDO peak in D_2O.

$TBAPF_6$ was 2.60x10^{-5} cm^2 s^{-1} (-6.8%). A similar experiment was also performed using 10 mM tetrabutylammonium perchlorate ($TBAClO_4$), which gave a D of 2.75 x 10^{-5} cm^2 s^{-1} (-1.4%). All of these values were corrected for changes in viscosity between light acetonitrile containing 200 mM $TBAPF_6$ and heavy acetonitrile-d_3 without supporting electrolyte.[2] However, a new correction for the diffusion experiment performed with 200 mM $TBAPF_6$ had to be made, by determining the viscosity of light and heavy acetonitrile containing 200 mM $TBAPF_6$. The correction factor was found to be 1.08, and was used to correct the above stated value for the D value of 1,4-QH_2 with 200 mM $TBAPF_6$.

II. Diffusion coefficients for the phthalates as function of the concentration of phthalate concentration by ^{1}H-NMR at 25 °C and plot of 1,4-H_2Q diffusion coefficient as a function of phthalate concentration.

Table 4.S1 Diffusion coefficients for the phthalates as function of phthalate concentration by ^{1}H-NMR at 25 °C

Base	D x 10^{-5} (cm^2 s^{-1})		
	No base added	10 mM of base	20 mM of base
H_2P	2.16 ± 0.08	-	-
HP^-	2.21 ± 0.06	2.27 ± 0.08	2.09 ± 0.07
P^{2-}	1.51± 0.06	1.22 ± 0.01	1.40 ± 0.05

To determine the stoichiometry, diffusion molar ratio analyses are performed. These analyses are analogous to those performed using fast-exchange ^{1}H-NMR peaks to determine the binding stoichiometry and ultimately the association constants. However, in this case, the diffusion coefficient of the host (1,4-H_2Q) is measured while the concentration of the guest (HP^- and P^{2-}) is varied. The determination of the stoichiometry is made via the noted inflection point in the plot of the diffusion coefficient of the host (D_{H2Q}, diffusion coefficient of 1,4-H_2Q) as a function of the guest concentration, as is represented in Figure 4.S3. The inflection point in Figure 4.3 for 1,4-H_2Q with HP^- occurs roughly at 10.0 mM HP^-, while that of 1,4-H_2Q with P^{2-} occurs at 5.0 mM P^{2-}. Based on this information, the stoichiometry of 1,4-H_2Q with HP^- is 2:1, while that of

1,4-H_2Q with P^{2-} is 1:1. The association constants could not be determined from this data because the molecular size and the diffusion coefficients of 1,4-H_2Q and the phthalate species are roughly equivalent. When using such analyses to determine the association constants it is best to have one species that is significantly larger, so that the influence on binding will have a negligible impact on the diffusion coefficient.[3, 4]

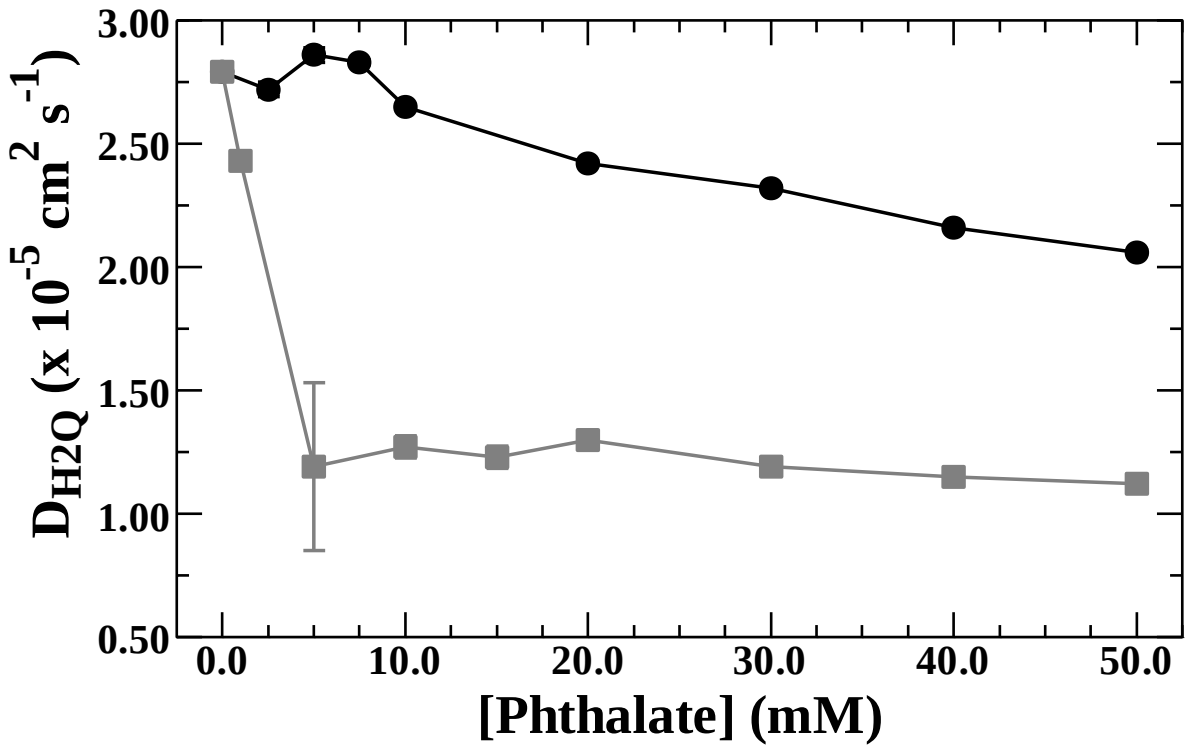

Figure 4.S3 Plot of 1,4-H_2Q diffusion coefficient (D_{H2Q}) as a function of HP^- (black circles) and P^{2-} (grey squares) concentrations. Lines do not represent a fitting.

III. Voltammetry and simulations not displayed in the text,

a. Voltammetric measurements used to determine mechanism of oxidation of 1,4-H_2Q in the presence of HP^- and P^{2-}

Table 4.S2 Voltammetric measurements recorded from multiple voltammograms at various scan rates of 1,4-H_2Q in the presence of 20 mM of HP^- or P^{2-}.

Base	$\partial Ep/\partial \log \nu$ (V/decade, Peak I_a')	$\partial Ep/\partial \log \nu$ (V/decade, Peak II_a)	$\partial Ep/\partial \log \nu$ (V/decade, Peak I_c')	$\partial Ep/\partial \log \nu$ (V/decade, Peak II_c)	$E_p - E_{p/2}$ (V, peak I_a')	$E_p - E_{p/2}$ (V, peak II_a)	$E_p - E_{p/2}$ (V, peak I_c')	$E_p - E_{p/2}$ (V, peak II_c)
HP^-	0.0402 ± 0.0005	-	-0.0985 ± 0.005	-	0.1060 ± 0.003	-	0.1532 ± 0.0005	-
P^{2-}	0.0389 ± 0.01	0.1221 ± 0.001	-0.005 ± 0.001	-0.1379 ± 0.04	0.0781 ± 0.004	0.0520 ± 0.001	-0.0601 ± 0.0006	-0.1001 ± 0.005

The above values assist in the determination of the mechanism of oxidation and/or reduction. A transition from a situation where the chemical step is the rate determining step to a situation where electron transfer is the rate determining step can be derived from the values of $(E_p - E_{p/2})$ and $\partial E_p / \partial \log \nu$, where E_p is the peak potential, $E_{p/2}$ is the potential where the current is equal to half the peak current and ν is the scan rate of the CV experiment. This transition is characterized by an increase of $(E_p - E_{p/2})$ from 0.0475 to 0.095 V and an increase in $\partial E_p / \partial \log \nu$ from 0.0296 to 0.0592 V/decade, for a two electron process at 25 ^oC.[5-7] The values of $\partial E_p / \partial \log \nu$ and $(E_p - E_{p/2})$ determined for the oxidation of 1,4-$H_2Q(HP)^-$, represented by peak I_a' (Figure 4.1A) at 0.0402 and 0.106 V, are relatively close to the theoretical values that describe an ECEC process. Therefore, with 20 mM HP^- the oxidation of 1,4-H_2Q can be described as an ECEC process. However, the same cannot be said for the reduction scan of 1,4-H_2Q with 20 mM HP^-,

since these values are larger than those studied in theory. The values of $\partial E_p / \partial \log \nu$ and ($E_p - E_{p/2}$) determined for the oxidation of 1,4-H_2Q with 20 mM P^{2-} were all greater than the values evaluated by this theory. Therefore, it is difficult to determine the sequence of ET's and PT's taking place for this reaction.

b. Comparison of 1,4-H_2Q with 20 mM P^{2-} Voltammetry to that of 1,4-Q alone in MeCN

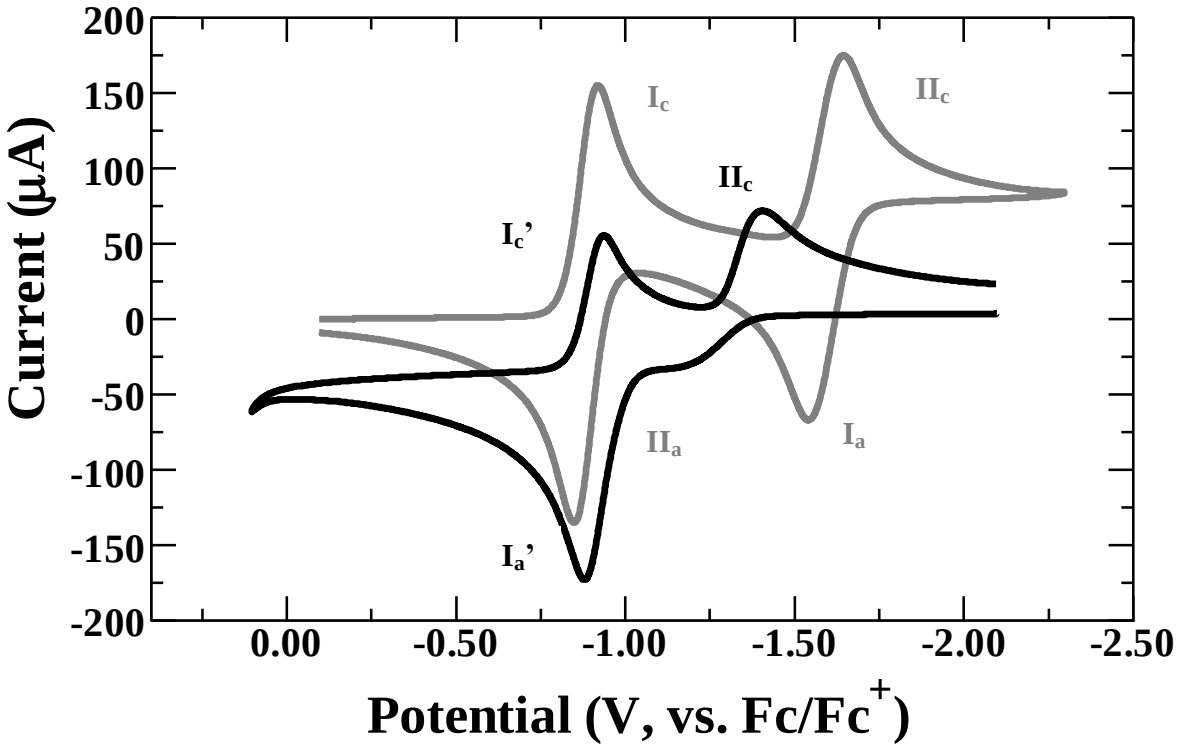

Figure 4.2 CV response of 5.0 mM 1,4-H_2Q with 20 mM P^{2-} (black line) and 5.0 mM 1,4-Q alone in MeCN with 0.2 M $TBAPF_6$ as supporting electrolyte.

Figure 4.2 displays the voltammetry of 1,4-H_2Q with 20 mM P^{2-} overlaid with the CV of 1,4-Q alone in MeCN. The notation denoting the peaks of the voltammogram of 1,4-H_2Q with 20 mM P^{2-} are the same as those in the text. The notation denoting the peaks of the CV response for 1,4-Q alone, however are not related to those in the text and are given in grey text in Figure 4.2. The

oxidation peak (I_a') for 1,4-H_2Q with 20 mM P^{2-} has a similar peak potential ($E_{pa,Ia'}$ = -0.879 V) to that of peak II_a for 1,4-Q ($E_{pa,\ IIa}$ = -0.849 V). Likewise, the first reduction peak for the CV response of 1,4-H_2Q with 20 mM P^{2-} (peak I_c') has a similar peak potential ($E_{pa,\ Ic'}$ = -0.938 V) to the first reduction peak (I_c) of 1,4-Q alone (-0.920 V). However, the second reduction peak for 1,4-H_2Q with 20 mM P^{2-} (II_c) is significantly positive ($E_{pc,\ IIc}$ = -1.405 V) relative to that found for 1,4-Q alone ($E_{pc,\ IIc}$ = -1.643 V). None of the peak potentials are significantly different at 10 mM P^{2-} added, with the exception of peak II_c, which is found at significantly more positive potentials, $E_{pc,\ IIc}$ = -1.314 V. Such a difference in peak potentials between 10 and 20 mM P^{2-}, indicates that the complex being formed is very negatively charged, such as that proposed to be formed in the text after reduction of 1,4-$Q^{\cdot-}$ to form 1,4-Q^{2-} (equation 19), 1,4-H_2Q complexed by one P^{2-} molecule, 1,4- $HQ(P)^{3-}$. Therefore, if larger concentrations were added, you should see an even greater shift to more negative potentials, which is essentially the opposite effect noted by Gupta *et. al.*[8]

c. Voltammetry and simulations of 1,4-H_2Q with the HP^- and P^{2-} with fitting parameters

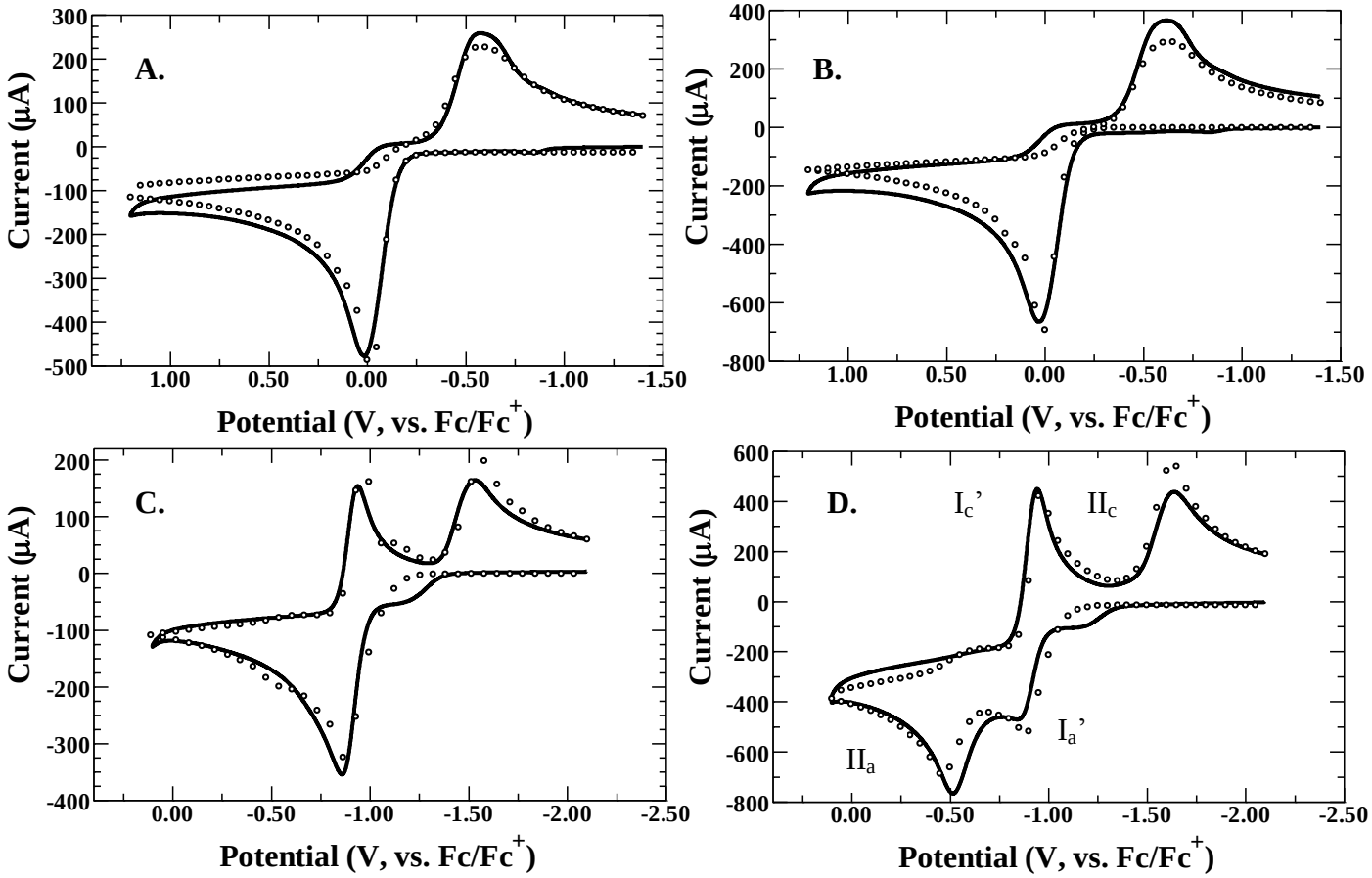

Figure 4.S4 CV responses (lines) and simulations (circles) of 5.0 mM 1,4-H_2Q with 20 mM HP^- at A.) 0.5 and B.) 1 V s^{-1}. CV responses (lines) and simulations (circles) of 5.0 mM 1,4-H_2Q with 20 mM P^{2-} at C.) 0.5 and D.) 5 V s^{-1}. CV's were recorded in 0.2 M $TBAPF_6$.

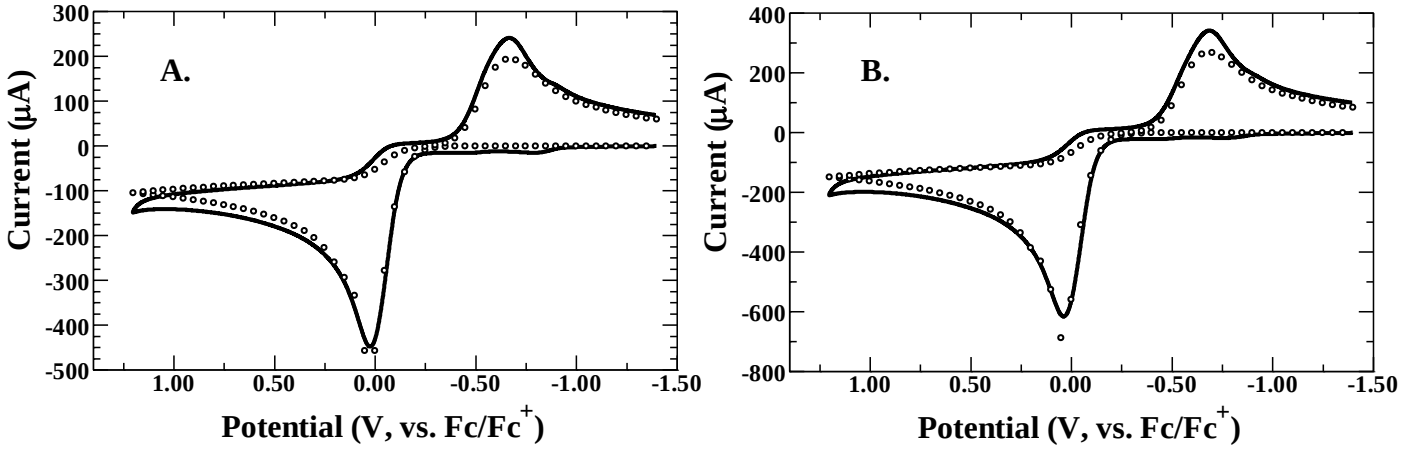

Figure 4.S5 CV responses (lines) and simulations (circles) of 5.0 mM 1,4-H_2Q with 30 mM HP^- at A.) 0.5 and B.) 1 V s^{-1}.

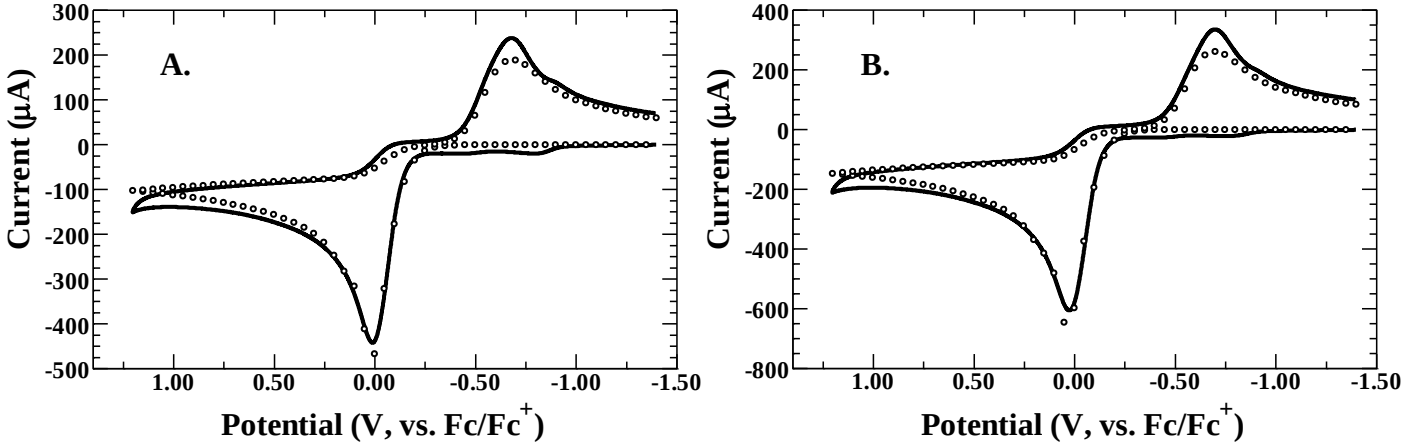

Figure 4.S6 CV responses (lines) and simulations (circles) of 5.0 mM 1,4-H_2Q with 40 mM HP^- at A.) 0.5 and B.) 1 V s^{-1}.

Tables of the fitting parameters for Scheme 4.2, 1,4-H_2Q with HP^-

1,4-H_2Q/Phthalate Concentration	5.0 mM 1,4-H_2Q/20.0 mM HP^-			5.0 mM 1,4-H_2Q/30.0 mM HP^-		
Electrochemical Reactions	E^o	α	k_s	E^o	α	k_s
$H_2Q(HP)_2^{2-} \rightleftharpoons H_2Q^{+\cdot}(HP)_2^{2-} + e^-$	-0.216	0.5	0.012	-0.241	0.5	0.009
$HQ^{\cdot}(HP)^- \rightleftharpoons HQ^+(HP)^- + e^-$	-0.165	0.5	0.0026	-0.195	0.5	0.0007
$Q + e^- \rightleftharpoons Q^{\cdot -}$	-0.901	0.5	0.05	-0.901	0.5	0.051
Chemical Reactions	K	k_f	k_b	K	k_f	k_b
$H_2Q + HP^- \rightleftharpoons H_2Q(HP)^-$	36	1.0×10^8	2.8×10^6	36	1.0×10^8	2.8×10^6
$H_2Q(HP)^- + HP^- \rightleftharpoons H_2Q(HP)_2^{2-}$	3	1.0×10^8	3.3×10^7	3	1.0×10^8	3.3×10^7
$H_2Q^{+\cdot}(HP)_2^{2-} \rightleftharpoons HQ^{\cdot}(HP)^- + H_2P$	2	1.0×10^9	5.0×10^8	2	1.0×10^9	5.0×10^8
$HQ^+(HP)^- \rightleftharpoons Q + H_2P$	0.1	1.0×10^9	1.0×10^{10}	0.1	1.0×10^9	1.0×10^{10}
$HQ^{\cdot}(HP)^- + HQ^{\cdot}(HP)^- \rightleftharpoons Q + H_2Q(HP)_2^{2-}$	0.0069	5.0×10^5	7.3×10^7	0.0083	5.0×10^5	6.0×10^7
$H_2P + HP^- \rightleftharpoons H_3P_2^-$	89	5.0×10^9	5.6×10^7	89	5.0×10^9	5.6×10^7
$Q^{\cdot -} + H_3P_2^- \rightleftharpoons HQ^{\cdot}(HP)^- + H_2P$	2.7×10^{13}	1.0×10^8	3.6×10^{-6}	8.5×10^{12}	1.0×10^8	1.2×10^{-5}

1,4-H_2Q/Phthalate Concentration	5.0 mM 1,4-H_2Q/40.0 mM HP^-		
Electrochemical Reactions	E^o	α	k_s
$H_2Q(HP)_2^{2-} \rightleftharpoons H_2Q^{+\cdot}(HP)_2^{2-} + e^-$	-0.241	0.5	0.009
$HQ^{\cdot}(HP)^- \rightleftharpoons HQ^+(HP)^- + e^-$	-0.195	0.5	0.0007
$Q + e^- \rightleftharpoons Q^{\cdot -}$	-0.901	0.5	0.051
Chemical Reactions	K	k_f	k_b
$H_2Q + HP^- \rightleftharpoons H_2Q(HP)^-$	36	1.0×10^8	2.8×10^6
$H_2Q(HP)^- + HP^- \rightleftharpoons H_2Q(HP)_2^{2-}$	3	1.0×10^8	3.3×10^7
$H_2Q^{+\cdot}(HP)_2^{2-} \rightleftharpoons HQ^{\cdot}(HP)^- + H_2P$	2	1.0×10^9	5.0×10^8
$HQ^+(HP)^- \rightleftharpoons Q + H_2P$	0.1	1.0×10^9	1.0×10^{10}
$HQ^{\cdot}(HP)^- + HQ^{\cdot}(HP)^- \rightleftharpoons Q + H_2Q(HP)_2^{2-}$	0.0083	5.0×10^5	6.0×10^7
$H_2P + HP^- \rightleftharpoons H_3P_2^-$	89	5.0×10^9	5.6×10^7
$Q^{\cdot -} + H_3P_2^- \rightleftharpoons HQ^{\cdot}(HP)^- + H_2P$	8.5×10^{12}	1.0×10^8	1.2×10^{-5}

Table of the fitting parameters for Scheme 4.3, 1,4-H_2Q with P^{2-}

1,4-H_2Q/Phthalate Concentration	5.0 mM 1,4-H_2Q/20.0 mM P^{2-}		
Electrochemical Reactions	E^o	α	k_s
$HQ(P)^{3-} \rightleftharpoons HQ^{\cdot}(P)^{2-} + e^-$	-1.246	0.5	$(7.2 \pm 3) \times 10^{-5}$
$HQ^{\cdot}(P)^{2-} \rightleftharpoons HQ(P)^- + e^-$	-0.916	0.5	1.0×10^{-5}
$Q + e^- \rightleftharpoons Q^{\cdot-}$	-0.916	0.5	1
$Q^{\cdot-} + e^- \rightleftharpoons Q^{2-}$	-1.376	0.5	0.008
Chemical Reactions	K	k_f	k_b
$H_2Q + P^{2-} \rightleftharpoons HQ^- + HP^-$	3981	1.0×10^8	2.5×10^4
$HQ^- + P^{2-} \rightleftharpoons HQ(P)^{3-}$	100	1.0×10^4	100
$HQ^{\cdot}(P)^{2-} \rightleftharpoons Q^{\cdot-} + HP^-$	0.007	12	1700
$HQ(P)^- \rightleftharpoons Q + HP^-$	0.007	300	4.3×10^4
$Q^{2-} + HP^- \rightleftharpoons HQ(P)^{3-}$	2.2×10^4	1.0×10^8	4400
$HQ^{\cdot}(P)^{2-} + Q^{\cdot-} \rightleftharpoons Q + HQ(P)^{3-}$	2.6×10^{-6}	0.053	2.0×10^4

IV. References

1. Schreiber, E.; Carlisle, M., 1.5 Diffusion Experiments/DOSY. In *User Guide: Liquids NMR*, Steele, D., Ed. Varian, Inc.: Palo Alto, California, 2001; pp 40-67.
2. Sun, H.; Chen, W.; Kaifer, A. E. *Organometallics* **2006,** 25, 1828-1830.
3. Cohen, Y.; Avram, L.; Frish, L. *Angew. Chem. Int. Ed.* **2005,** 44, 520-554.
4. Fielding, L. *Tetrahedron* **2000,** 56, 6151-6170.
5. Nadjo, L.; Saveant, J.-M. *J. Electroanal. Chem.* **1973,** 48, 113-145.
6. Saveant, J.-M., Electron Transfer, Bond Breaking and Bond Formation. In *Advances in Physical Organic Chemistry*, Tidwell, T. T., Ed. Academic Press: New York, 2000; Vol. 35, pp 117-192.
7. Saveant, J.-M., *Elements of Molecular and Biomolecular Electrochemistry: An Electrochemical Approach to Electron Transfer Chemistry*. Wiley: New York, 2006.
8. Gupta, N.; Linschitz, H. *J. Am. Chem. Soc.* **1997,** 119, 6384-6391.
9. Bard, A. J.; Faulkner, L. R., *Electrochemical Methods: Fundamentals and Applications*. 2 ed.; John Wiley & Sons: New York, 2001.
10. Lehmann, M. W.; Evans, D. H. *Anal. Chem.* **1999,** 71, (10), 1947-1950.
11. Wipf, D. O.; Wehmeyer, K. R.; Wightman, R. M. *J. Org. Chem.* **1986,** 51, 4760-4764.
12. Izutsu, K., *Acid-Base Dissociation Constants in Dipolar Aprotic Solvents*. Blackwell Scientific Publications: London, 1990.

Vita

Jonnathan Medina-Ramos was born on January 16, 1984, in Santiago de Cali, Colombia. He graduated from Antonio Jose Camacho High School in 2000 and received his degree in Chemistry from the Universidad del Valle in 2006, both in Santiago de Cali city. Subsequently, he worked as a high school chemistry teacher in the same city for about a year before joining the chemistry PhD program at Virginia Commonwealth University in January of 2008. He received a PhD in chemistry from Virginia Commonwealth University in December of 2012.